



HAL
open science

Strengthening of corroded reinforced concrete (RC) beams with near surface mounted (NSM) technique using carbon fiber polymer (CFRP) rods: an experimental and finite element (FE) modelling study

Belal Almassri

► **To cite this version:**

Belal Almassri. Strengthening of corroded reinforced concrete (RC) beams with near surface mounted (NSM) technique using carbon fiber polymer (CFRP) rods: an experimental and finite element (FE) modelling study. Civil Engineering. INSA de Toulouse, 2015. English. NNT: 2015ISAT0009. tel-01195812

HAL Id: tel-01195812

<https://theses.hal.science/tel-01195812>

Submitted on 8 Sep 2015

HAL is a multi-disciplinary open access archive for the deposit and dissemination of scientific research documents, whether they are published or not. The documents may come from teaching and research institutions in France or abroad, or from public or private research centers.

L'archive ouverte pluridisciplinaire **HAL**, est destinée au dépôt et à la diffusion de documents scientifiques de niveau recherche, publiés ou non, émanant des établissements d'enseignement et de recherche français ou étrangers, des laboratoires publics ou privés.



THÈSE

En vue de l'obtention du

DOCTORAT DE L'UNIVERSITÉ DE TOULOUSE

Délivré par *l'institut national des sciences appliquées de Toulouse (INSA de Toulouse)*

Présentée et soutenue par

Belal ALMASSRI

Le 04/06/2015

Titre :

*Réparation ou renforcement des poutres en béton armé corrodées ou non par l'insertion de joncs de carbone dans la surface du béton (NSM technique):
Etude expérimentale et modélisation par éléments finis*

JURY

<i>Emmanuel FERRIER</i>	<i>Rapporteur</i>	Professeur, Université de Lyon 1
<i>Dario CORONELLI</i>	<i>Rapporteur</i>	Professeur associé, Politecnico di Milano
<i>Jean-Paul BALAYSSAC</i>	<i>Examineur</i>	Professeur, INSA de Toulouse
<i>Abdelouahab KHELIL</i>	<i>Examineur</i>	Professeur, Université de Lorraine
<i>Raoul FRANCOIS</i>	<i>Examineur</i>	Professeur, INSA de Toulouse
<i>Firas AL MAHMOUD</i>	<i>Examineur</i>	Maître de conférences, Université de Lorraine

Ecole doctorale et spécialité : *MEGEP : Génie civil*

Unité de recherche : *Laboratoire Matériaux des Constructions de Toulouse LMDC*

Directeur(s) de Thèse : *M. Raoul François et M. Firas Al Mahmoud*

Rapporteurs : *M. Emmanuel Ferrier et M. Dario Coronelli*

Auteur: Belal ALMASSRI

Titre: Réparation ou renforcement de poutres en béton armé corrodées ou non par joncs de carbone mis en place dans des engravures de surface du béton (NSM CFRP technique) : expérimentation et modélisation éléments finis

Thèse de doctorat de l'institut national des sciences appliquées de Toulouse (INSA Toulouse)

Spécialité : Génie Civil

Résumé:

Cette thèse s'intéresse à l'efficacité des renforcements par matériaux composites à base de fibres carbone (CFRP : Carbon Fiber Reinforced Polymer) par la technique NSM (Near Surface Mounted ; réalisation d'engravures sur la surface du béton) pour requalifier les structures corrodées. Elle est composée d'une partie expérimentale et d'une partie modélisation par la méthode des Eléments Finis (EF). La technique NSM consiste à réaliser des engravures sur la surface du béton où sont insérés les joncs de carbone rendus adhérents par remplissage d'une résine époxy. Les éléments étudiés dans cette thèse sont des poutres en béton armé naturellement corrodées pendant 28 années d'exposition à un environnement salin. Dans cette thèse, nous nous intéressons aux modes de rupture et à la capacité portante à la fois : en flexion et à l'effort tranchant. Le degré de corrosion a été mesuré par la méthode de perte de masses locales après la fin des essais mécaniques sur les barres longitudinales ainsi que sur les cadres d'effort tranchant.

La première partie présente les résultats expérimentaux obtenus sur une poutre corrodée et une poutre témoin réparée ou renforcée en flexion par un jonc de carbone de 6 mm de diamètre inséré dans la surface tendue par la technique NSM. Les essais ont pour objectif d'étudier la capacité portante, la flèche à la ruine, la rigidité en flexion et le mode de ruine des deux poutres afin de vérifier l'efficacité du renforcement ou de la réparation. Les résultats font apparaître un nouveau mode de ruine pour la poutre corrodée renforcée par séparation du béton d'enrobage, liée à la fissuration induite par la corrosion. Néanmoins, la réparation par jonc de carbone permet de restituer la capacité portante initiale (avant la corrosion) et permet de restaurer une ductilité suffisante.

La seconde partie présente les résultats expérimentaux obtenus sur des poutres courtes permettant de mettre en avant la résistance vis à vis de l'effort tranchant. A partir des poutres longues testées dans la première partie, deux poutres courtes corrodées et deux poutres courtes témoins sont extraites. Une poutre courte corrodée et une poutre témoin sont réparées

ou renforcées en flexion et une poutre corrodée et une poutre témoin sont en plus réparées ou renforcées vis-à-vis à l'effort tranchant par des jonses de carbone de 6 mm de diamètre par la technique NSM. L'éventuel glissement des armatures longitudinales sur les appuis a été mesuré durant les essais de flexion 3 points. Les résultats expérimentaux montrent que la corrosion des armatures longitudinales et la corrosion des cadres d'effort tranchant n'affectent pas le mode de ruine et modifient très peu les capacités portantes. La réparation vis-à-vis de l'effort tranchant avec la technique NSM change le mode de ruine de la formation d'une fissure diagonale due au glissement des barres d'acier tendues, à la formation d'une large fissure de flexion à mi-travée suivie de l'écrasement du béton comprimé. Même en présence de corrosion et avec ou sans renforcement vis-à-vis de l'effort tranchant, le ratio entre la portée de l'effort tranchant « a » et la hauteur effective de la poutre « d » (a/d) reste un paramètre majeur influant sur le comportement mécanique.

La troisième partie s'intéresse à la modélisation par la méthode de modélisation par EF du comportement global en flexion. Une première approche 2D est élaborée avec le code FEMIX développé à l'Université de Minho par le professeur Barros. Cinq poutres sont modélisées : 3 corrodées dont une réparée par la technique NSM et 2 témoins dont une renforcée par la technique NSM. La modélisation par EF donne de bons résultats sauf dans le cas de la poutre corrodée réparée dont le mode de ruine est non conventionnel (séparation du béton d'enrobage). Une approche 3D utilisant le logiciel ABAQUS a alors permis de modéliser ce mode de ruine particulier.

La quatrième et dernière partie est consacrée à l'étude numérique des poutres courtes. Quatre poutres sont modélisées : 2 corrodées réparées dont une réparée vis-à-vis de l'effort tranchant et 2 témoins renforcées dont une renforcée vis-à-vis de l'effort tranchant. La modélisation par EF est faite en 3D en utilisant le code FEMIX. Les résultats numériques reproduisent correctement les aspects importants du comportement force-flèche ainsi que les modes de fissuration à la ruine pour les poutres réparées vis-à-vis de l'effort tranchant ou non.

Mots clés : poutres, béton armé, corrosion, réparation, renforcement, fibres de carbone, ductilité, flexion, effort tranchant, flèche, rigidité Eléments Finis, FEMIX, ABAQUS.

Author: Belal ALMASSRI

Title: Strengthening of corroded reinforced concrete (RC) beams with near surface mounted (NSM) technique using carbon fiber polymer (CFRP) rods; an experimental and finite element (FE) modelling study

PhD thesis at l'institut national des sciences appliquées de Toulouse (INSA Toulouse)

Speciality: Civil Engineering

Abstract:

The thesis is composed of an experimental and Finite Element Modeling (FEM) study, investigating the effectiveness of the (Near Surface Mounted CFRP rods technique (NSM)) on the corroded RC beams. In the NSM technique, the CFRP rods are placed inside pre-cut grooves and are bonded to the concrete with epoxy adhesive. The thesis studies the failure modes and the mechanical performance of the corroded RC beams due to steel corrosion and finally, the prediction of the mechanical behaviour of the repaired corroded RC beams using nonlinear models based on FE numerical modelling. The corroded RC beams studied here in this study were exposed to natural corrosion for more than 28 years.

The first part includes experimental results which were obtained on two beams: (one corroded and one control beams, both are 3 metres long) repaired or strengthened in bending with one 6-mm-diameter NSM CFRP rod. The beams were tested in a three-point bending test up to failure. Overall stiffness was studied. Ultimate capacity, ductility and failure modes were also reviewed. Finally some comparisons were made between repaired and non-repaired beams in order to assess the effectiveness of the NSM technique. The experimental results showed that the NSM technique improved the overall characteristics (ultimate load capacity and stiffness) of the control and corroded beams and allowed sufficient ductility to be restored in repaired corroded elements, thus restoring the safety margin, despite a non-conventional failure mode with the separation of the concrete cover that occurred in the corroded beam due to corrosion products.

The second part discusses the experimental results of two short corroded beams, which were tested under three-point bending until failure, along with two short control beams of the same characteristics (age, length and cross-section). One RC corroded deep beam was repaired in bending and the other one was repaired in both bending and shear with NSM CFRP rods. After the beams had been tested up to failure, the main steel bars and the stirrups were extracted from the beams and the loss of mass was measured and plotted for both the longitudinal and transverse reinforcement. The slip of tensile reinforcement at the end of the

beams was also measured during the tests. The effect of corrosion and the effect of repairing with CFRP NSM rods in bending and shear on the behaviour of deep beams are discussed. Experimental results showed that both corroded and control deep beams repaired only in bending failed due to shear failure mode(diagonal tension failure), while corroded and control beams repaired in both bending and shear failed due to concrete crushing. The test results also showed that the corrosion of both longitudinal and transversal reinforcement hardly modified the mechanical response of deep beams. Even in presence of corrosion and repairing with NSM CFRP rods, the ratio between the shear span “a” and the effective depth “d” (a/d ratio) appears to be a major parameter.

The third part shows experimental results and numerical modelling results of 2D finite element model using the FEMIX computer code were obtained on five, 3-metre-long beams: three corroded RC beams and two control beams. Two beams, one corroded and one control were repaired or strengthened in bending with NSM CFRP rod and were then tested in three-point bending up to failure. The FE numerical modelling results from FEMIX were compatible with the experimental ones except for the repaired corroded beam, for which a three-dimensional model using the commercial software ABAQUS was required. Finally some comparisons were made between the experimental and FE numerical modelling results obtained using ABAQUS in order to study the specific failure mode of the corroded beam, which occurred by the separation of concrete cover.

Finally, the last part presents 3D numerical modelling results in terms of load-deflection curves, and failure modes for 4 short corroded beams: two corroded beams and two control beams, half of the beams were let repaired or strengthened in bending only with NSM CFRP rods while the others were repaired or strengthened in both bending and shear with NSM technique. Results showed that the FE model was able to capture the main aspects of the experimental load-deflection curves of the RC beams, moreover it has presented the experimental failure modes and FE numerical modelling crack patterns and both gave similar results for both shear-repaired and non-shear repaired beams, three dimensional crack patterns were produced for shear-repaired beams in order to investigate the splitting cracks occurred at the middle of the beams and near the support.

Keywords: RC beams, corrosion, repair, strengthening, NSM CFRP rods, ductility, bending, shear, deflection, stiffness, Finite Element, FEMIX, ABAQUS.

A three-year journey in France was tough without meeting you. To my mother, I couldn't have done this without your prayers and support. Thank you for everything

Acknowledgment

The present work was mainly developed at the laboratory of materials and durability of construction LMDC, INSA de Toulouse, the University of Toulouse, France.

This research was carried out under the supervision of Mr. Raoul Francois (Full professor at the University of Toulouse, France) and Mr. Firas Al Mahmoud (Assistant professor at the University of Lorraine, France), I would specially like to express the deepest appreciation to their support, useful directions, their advice and their friendship.

I express my gratitude to Mr. Joaquim Barros (Full professor at the University of Minho, Portugal) for welcoming me in an international academic mobility in his team.

I would like to thank Mr. Emmanuel Ferrier and Mr. Dario Coronelli for accepting to be the reviewers of my thesis. I am thankful for any advice and suggestions from all the jury members.

The financial support provided by the French Government which was directed during the three years by the CampusFrance, is gratefully acknowledged. My special thanks go to the Academic Cooperation Division in the French Consulate in Jerusalem for selecting me to this program.

I would also like to thank Mr. Gilles Escadeillas (The head of the LMDC) for welcoming me at the LMDC. Many thanks go to all of the academic staff, the technicians and my colleagues for helping and supporting me during my thesis.

My deepest appreciation goes to Amjad Kreit, not only as a research mate but also as a friend since day one in Toulouse, thanks a lot for all of the support, help, guidance and unforgettable moments.

Finally, my sincere gratitude goes to my family in Palestine, in particular to my mother, my sister Samah, my four brothers: Imad, Alaa, Mohammed and Fayez for their love and infinite support.

Table of contents

Table of contents	I
List of figures	V
List of Tables.....	IX
I. Résumé long en français	1
Bibliographie.....	22
II. General Introduction.....	25
References	31
Chapter 1	32
Flexural strengthening of corroded RC beams with NSM CFRP rods, an experimental part.....	32
Introduction	32
Mechanical behaviour of corroded RC beams strengthened by NSM CFRP rods.....	33
1.1 Introduction	34
1.2 Experimental programme	36
1.2.1 Material properties	39
1.2.1.1 Concrete properties.....	39
1.2.1.2 Characteristics of steel bars, CFRP bars and filling material	39
1.2.2 Repair technique.....	41
1.2.3 Cracking maps of corroded beam A1CL3-R and control beam A1T-R.....	41
1.3 Experimental results.....	43
1.3.1 Mechanical properties of corroded steel bars	43
1.3.2 Yielding moment and ultimate strength	43
1.3.3 Failure modes	44
1.3.4 Losses of diameter due to corrosion for tensile steel bars and steel stirrups in corroded beam A1CL3-R.....	45
1.3.5 Ultimate capacity.....	48
1.3.6 Ultimate deflection	49
1.3.7 Percentage increase in the yielding capacity for beams repaired with NSM FRP rods.....	51
1.3.8 Effect of corrosion on both yielding and ultimate capacity.....	52
1.3.9 Stiffness of beams	53
1.3.10 Ductility.....	53
1.3.11 Failure modes	54
1.4 Conclusions	55
1.5 References	56
1.6 Appendix: classical RC calculations	59

Conclusions	60
Chapter 2	61
Shear strengthening of corroded RC beams with NSM CFRP rods, an experimental part	61
Introduction	61
Behaviour of corroded shear-critical Reinforced Concrete beams repaired with NSM CFRP rods	62
2.1 Introduction	63
2.2 Experimental program: specimens, test setup, monitoring system and material properties.....	65
2.2.1 Experimental procedure.....	65
2.2.2 Material properties	67
2.2.2.1 Concrete properties.....	67
2.2.2.2 Characteristics of steel bars, CFRP bars and filling material	68
2.2.3 Repair technique with NSM against bending and shear forces	69
2.2.4 Instrumentation of beams	72
2.3 Experimental results.....	73
2.3.1 Losses of diameter due to corrosion for tensile steel bars and steel stirrups in corroded beams A1CL3-B and A1CL3-SB	73
2.3.2 Ultimate load capacity and failure modes	75
2.3.3 Slip measurements.....	79
2.3.4 Effect of corrosion.....	80
2.3.5 Effect of NSM CFRP repair on the ultimate load capacity	81
2.3.6 Effect of a/d ratio on the shear strength.....	82
2.4 Conclusions	84
2.5 References	85
Conclusions	88
Chapter 3	89
Flexural strengthening of corroded RC beams with NSM CFRP rods, a finite element modelling part	89
Introduction	89
Behaviour of corroded Reinforced Concrete beams repaired with NSM CFRP rods, Experimental and Finite Element Study	90
3.1 Introduction	91
3.2 Experimental programme	93
3.2.1 Material properties	93
3.2.1.1 Concrete properties.....	93
3.2.1.2 Characterization of steel Bars, CFRP Bars and filling material	94
3.2.2 NSM repair technique	96

3.3 Experimental results	97
3.3.1 Corrosion damage of the steel bars in corroded beam A1CL3-R.....	97
3.3.2 Response in bending for both corroded and non-corroded repaired beams	98
3.3.3 Failure modes	98
3.4 Numerical modelling.....	99
3.4.1 Concrete properties.....	99
3.4.2 CFRP rods	100
3.4.3 Steel reinforcement properties.....	101
3.4.4 Modelling of RC beams	102
3.4.4.1 Corroded RC beams	103
3.4.4.2 Results for all beams	104
3.4.5 Three-dimensional model for RC beam A1CL3-R	105
3.4.5.1 Concrete properties.....	105
3.4.5.2 Steel properties	107
3.4.5.3 CFRP rods and filling material.....	107
3.4.5.4 Simulation of corrosion cracks	108
3.4.6 FEM numerical model.....	109
3.4.6.1 General description.....	109
3.4.6.2 Meshing and step size increments	109
3.4.7 FEM results of 3D model	110
3.4.7.1 Ultimate load capacity and failure mode of RC beam A1CL3-R.....	110
3.5 Conclusions	111
3.6 Acknowledgements	112
3.7 References	112
Conclusions	115
Chapter 4	116
Shear strengthening of corroded RC beams with NSM CFRP rods, a finite element modelling part.	116
Introduction	116
A FEM-based model to study the behaviour of corroded RC beams shear repaired by NSM CFRP rods technique	117
4.1 Introduction	118
4.2 Experimental programme	119
4.2.1 Experimental procedure.....	119
4.2.2 Main experimental results	120
4.2.2.1 Corrosion results.....	120
4.2.2.2 Ultimate load capacity and modes of failure	123

4.3 Numerical model	125
4.3.1 Concrete Properties	125
4.3.1.1 Fracture mode I for concrete “tension softening of concrete”	125
4.3.1.2 Fracture mode II for concrete “Shear softening of concrete”	126
4.3.2 Steel properties	126
4.3.3 CFRP properties	128
4.3.4 Modelling of RC beams bending and shear repaired with NSM CFRP rods (A1CL3-SB and A1T-SB)	128
4.3.4.1 Modelling of corroded RC beam A1CL3-SB	129
4.3.5 Modelling of RC beams non-shear repaired with NSM CFRP rods (A1CL3-B, A2CL2-A and A1T-B)	129
4.4 Numerical modelling results.....	130
4.4.1 Load-deflection curves and failure modes for RC beams non-shear repaired with NSM CFRP rods (A1CL3-B, A2CL2-A and A1T-B)	130
4.4.2 Load-deflection curves and failure modes for RC beams shear repaired with NSM CFRP rods (A1CL3-SB and A1T-SB).....	132
4.5 Conclusions	135
4.6 References	137
Conclusions	140
General Conclusion	141
Scientific Production	143
References	144

List of figures

Figure I- 1 vue schématique de la chambre à brouillard salin et de la conservation des poutres	7
Figure I- 2 plan de ferrailage des poutres de type A. Toutes les dimensions sont en mm	8
Figure I- 3 comparaison entre les réponses en flexion 3 points des différentes poutres (A2T, A2TI, A1T-R, A2CL3, A1CL3-R and A2CL1).....	9
Figure I- 4 faciès de rupture des deux poutres réparées en flexion par la technique NSM	10
Figure I- 5 schéma de découpe des poutres longues A1CL3-R et A1T permettant d'obtenir 4 poutres courtes (A1CL3-B , A1CL3-SB, A1T-B, A1T-SB) correspondant aux extrémités peu sollicitées lors de la flexion	11
Figure I- 6 Vue de la réparation vis à vis de l'effort tranchant et de l'instrumentation permettant de mesurer le glissement des armatures longitudinales sur appuis	12
Figure I- 7 modes de ruine des quatre poutres courtes	12
Figure I- 8 influence du ratio a/d sur la capacité portante des poutres	14
Figure I- 9 comparaison entre les résultats expérimentaux et la modélisation EF 2D utilisant le code FEMIX	15
Figure I- 10 Modèle éléments finis pour la simulation des poutres renforcées par la technique NSM. 15	
Figure I- 11 Fissures de corrosion obtenues expérimentalement et modélisation correspondante avec ABAQUS	16
Figure I- 12 loi de comportement de l'acier en traction : non corrodé (a) ; corrodé (b)	17
Figure I- 13 Comparaison entre le comportement expérimental et les modélisations faites avec ABAQUS : R1 sans introduction de la fissure de corrosion; R2 avec introduction de la fissure de corrosion.....	17
Figure I- 14 visualisation du mode de rupture par separation du béton d'enrobage reproduit par ABAQUS : modèle R2.....	18
Figure I- 15 modélisation EF de la pouter courte renforcée au cisaillement par les joncs de carbone engravés à 45°	18
Figure I- 16 Comparaison entre les résultats expérimentaux et les simulations EF pour les poutres réparées vis à vis de l'effort tranchant A1CL3-SB et A1T-SB	19
Figure I- 17 Comparaison entre les résultats expérimentaux et les simulations EF pour les poutres non réparées vis à vis du cisaillement A1CL3-B et A1T-B	20
Figure I- 18 faciès de fissuration obtenus par EF pour les poutres non renforcées vis à vis de l'effort tranchant A1CL3-B et A1T-B (en rose les fissures complètement ouvertes, en rouge celles qui s'ouvrent, en bleu les fissures qui se ré-ouvrent, en vert celles qui se ferment et en bleu foncé celles qui sont fermées)	20
Figure I- 19 (a) faciès de fissuration obtenus par EF pour les poutres renforcées vis à vis de l'effort tranchant (en rose les fissures complètement ouvertes, en rouge celles qui s'ouvrent, en bleu les fissures qui se ré-ouvrent, en vert celles qui se ferment et en bleu foncé celles qui sont fermées).....	21
Figure I- 19 (b) faciès de fissuration obtenus par EF pour les poutres renforcées vis à vis de l'effort tranchant dans les plans x-z & y-z (en rose les fissures complètement ouvertes, en rouge celles qui s'ouvrent, en bleu les fissures qui se ré-ouvrent, en vert celles qui se ferment et en bleu foncé celles qui sont fermées).	201
Figure II - 1 Installation of NSM CFRP rod into the concrete surface (8).....	26
Figure II - 2 Classical failure modes of RC beams strengthened with NSM CFRP rods (9)	27
Figure 1 - 1 The climate accelerated aggressive environment system	37
Figure 1 - 2 Reinforcement layout for Type A beams. Dimensions are in mm	38
Figure 1 - 3 Stress-strain diagrams for steel and CFRP bars.....	40
Figure 1 - 4 Installation of CFRP rod into concrete surface.....	41

Figure 1 - 5 A1CL3-R cracking map after 20 kN loading.....	42
Figure 1 - 6 A1T-R cracking map after 20 kN loading	42
Figure 1 - 7 Non-corroded bar (a) Vs Corroded bar (corrosion pits) (b).....	43
Figure 1 - 8 Bending moment versus deflection	44
Figure 1 - 9 Beams after failure.....	44
Figure 1 - 10 Corrosion cracks appear in the concrete cover from the steel part closest to the tensile surface exposed to chloride	45
Figure 1 - 11 Corrosion damage along re-bars according to the location in the beams (top or bottom).....	45
Figure 1 - 12 Diameter loss percentages vs. position along the corroded beam A1CL3-R	46
Figure 1 - 13 Parts of beam A1CL3-R	46
Figure 1 - 14 Corrosion in steel stirrups of A1CL3-R.....	47
Figure 1 - 15 Comparisons of moment capacity (A2T, A2TI, A1T-R, A2CL3, A1CL3-R and A2CL1 (8,9)).....	49
Figure 1 - 16 Deflection (mm) for beams at failure	50
Figure 1 - 17 Yielding capacity increase.....	51
Figure 1 - 18 Stiffness ratio for repaired beams	53
Figure 1 - 19 Ductility index chart	54
Figure 1 - 20 Force equilibrium and strain compatibility for RC beams.....	59
Figure 2 - 1 The climate accelerated aggressive environment system	65
Figure 2 - 2 Reinforcement layout of type A beams. Dimensions are in mm	67
Figure 2 - 3 Stress-strain diagrams for steel and CFRP bars.....	69
Figure 2 - 4 Installation of CFRP rod in concrete surface.....	69
Figure 2 - 5 Parts of corroded and control beam	70
Figure 2 - 6 Moment-deflection curves for A1CL3-R and A1T-R	70
Figure 2 - 7 Modes of failure and damages of two full span beams A1CL3-R and A1T-R.....	71
Figure 2 - 8 Shear repair configuration for A1CL3-SB and A1T-SB (Dimensions in mm)	71
Figure 2 - 9 Beams instrumentation for a) full span beams and b) short beams	72
Figure 2 - 10 Short span beams instrumentation	73
Figure 2 - 11 Diameter loss percentages of longitudinal tensile steel bars	74
Figure 2 - 12 Parts of corroded beam A1CL3-R	74
Figure 2 - 13 Corrosion in steel stirrups of corroded beam A1CL3-R.....	75
Figure 2 - 14 Load-deflection curves for all beams.....	75
Figure 2 - 15 Failure modes for all beams tested	77
Figure 2 - 16 Yielding capacity values for all beams	78
Figure 2 - 17 Steel layouts inside the four beams.....	78
Figure 2 - 18 Slip measurements for all beams	79
Figure 2 - 19 Effect of corrosion on yielding load capacity of beams repaired in shear.....	81
Figure 2 - 20 a/d ratio effect on the shear strength of beams	83
Figure 3 - 1 Reinforcement layout of type A beams. Dimensions are in mm	93
Figure 3 - 2 Tensile stress-strain curves for steel and CFRP rods (Corroded and control steel bar curves are average results of 2 tested specimens in each case).....	95
Figure 3 - 3 Installation of CFRP rod in concrete surface.....	96
Figure 3 - 4 Concrete surfaces after installation of the CFRP rod.....	96
Figure 3 - 5 Average cross-section loss percentages in corroded beam A1CL3-R.	97
Figure 3 - 6 Moment-deflection curves for beams A1CL3-R and A1T-R tested experimentally	98
Figure 3 - 7 Experimental failure modes.....	99
Figure 3 - 8 Tension softening diagram for concrete	100

Figure 3 - 9 Ductility factor ($\epsilon_{\text{corroded}}/\epsilon_u$) for steel bars versus corrosion, from Dang & Francois (31)	101
Figure 3 - 10 uniaxial constitutive model for non-corroded rebar	101
Figure 3 - 11 Geometry in (mm), mesh, loading and support conditions for non-strengthened beams with NSM CFRP	102
Figure 3 - 12 Geometry, mesh, loading and support conditions for strengthened beams with NSM CFRP	103
Figure 3 - 13 corrosion pits in tensile steel bars of corroded RC beam	103
Figure 3 - 14 Load Deflection curves for all beams using FEMIX	104
Figure 3 - 15 2D crack failure pattern using FEMIX	105
Figure 3 - 16 Drucker-Prager failure criterion in stress space (32)	107
Figure 3 - 17 Tension softening of concrete	107
Figure 3 - 18 Corrosion-induced cracks appear in the concrete cover from the steel part closest to the tensioned surface exposed to chloride for type "A" beams (Almassri et al.(13))	108
Figure 3 - 19 Cracks created at concrete cover plane of corroded beam in (mm)	109
Figure 3 - 20 Boundary conditions, steel skeleton and meshing of beam model	109
Figure 3 - 21 Experimental curves vs. 3D FE Model moment-deflection curves obtained with Abaqus for RC beam A1CL3-R	110
Figure 3 - 22 Mode of failure obtained for corroded RC beam A1CL3-R by 3D FE model using Abaqus	111
Figure 4 - 1 Reinforcement layout all beams. Dimensions are in mm	120
Figure 4 - 2 Diameter loss percentages of longitudinal tensile steel bars for corroded beams	121
Figure 4 - 3 Stirrups numbers of corroded beams (a) A1CL3-R (b) A2CL2-A	121
Figure 4 - 4 Stirrups corrosion maps (a) diameter in mm for A1CL3-R (b) diameter loss % in A2CL2-A	122
Figure 4 - 5 Load-deflection curves for all beams	123
Figure 4 - 6 Experimental modes of failure for all tested beams	124
Figure 4 - 7 Tensile steel bars slip occurred in non-shear repaired beams A1T-SB and A1CL3-SB ..	124
Figure 4 - 8 RC fracture mode I "tri-linear tension softening diagram"	125
Figure 4 - 9 RC fracture mode II "linear shear softening diagram"	126
Figure 4 - 10 uniaxial constitutive model of non-corroded steel bars	127
Figure 4 - 11 uniaxial constitutive model of corroded steel bars	127
Figure 4 - 12 The boundary conditions of the 3D model in an isometric plane in GiD-FEMIX	128
Figure 4 - 13 Geometry in (mm), mesh, loading and support conditions in x-y plane for shear repaired beams with NSM CFRP rods	129
Figure 4 - 14 Geometry in (mm), mesh, loading and support conditions in x-y plane for non-shear-repaired beams with NSM CFRP rods	130
Figure 4 - 15 Experimental vs FE numerical model load-deflection curves for non-shear-repaired beams A1CL3-B , A2CL2-A and A1T-B	131
Figure 4 - 16 FE crack pattern of the non-shear-repaired beams (in pink colour: crack completely open; in red colour: crack in the opening process; in cyan colour: crack in the reopening process; green colour: crack in the closing process; in blue colour: closed crack)	131
Figure 4 - 17 maximum strain values in the steel bars for the non-shear repaired beam A1CL3-B ...	132
Figure 4 - 18 Experimental vs FE numerical model load-deflection curves for shear-repaired beams A1CL3-SB and A1T-SB	133
Figure 4 - 19 FE crack patterns of the shear repaired beams in x-y plane (in pink colour: crack completely open; in red colour: crack in the opening process; in cyan colour: crack in the reopening process; green colour: crack in the closing process; in blue colour: closed crack)	133

Figure 4 - 20 FE crack patterns of the shear repaired beams in x-z & y-z planes (in pink colour: crack completely open; in red colour: crack in the opening process; in cyan colour: crack in the reopening process; green colour: crack in the closing process; in blue colour: closed crack). 134

Figure 4 - 21 (a) Section parallel to the crack plane for the theory of the failure mode proposed by Bianco et al. 24. (b) Splitting cracks at the bottom of the shear repaired beams A1CL3-SB and A1T-SB. (c) Splitting cracks at the edge of the shear repaired beams A1CL3-SB and A1T-SB 135

List of Tables

Table 1 - 1 Concrete mix and cement chemical composition.....	39
Table 1 - 2 Mechanical characteristics of the concrete at 27 years (average of 3 tests).....	39
Table 1 - 3 Effective mechanical properties of steel bars (calculated from the residual cross-section).....	39
Table 1 - 4 Characteristics of CFRP rods.....	40
Table 1 - 5 Filling material properties.....	40
Table 1 - 6 Experimental results for all beams.....	50
Table 1 - 7 Calculated values of (Yielding moment) M_y	52
Table 1 - 8 Comparison of loss of cross sections against the loss of ultimate and yielding experimental values.....	52
Table 1 - 9 Ductility index values.....	54
Table 1 - 10 Summary of calculated values of moment.....	59
Table 2 - 1 The climate accelerated aggressive environment system.....	66
Table 2 - 2 Concrete mix.....	68
Table 2 - 3 Mechanical characteristics of the concrete at 27 years (average of 3 tests).....	68
Table 2 - 4 Effective mechanical properties of steel bars (calculated from the residual cross-section).....	68
Table 2 - 5 Characteristics of CFRP rods.....	68
Table 2 - 6 Filling material properties.....	69
Table 2 - 7 Repair plan for all beams.....	72
Table 2 - 8 Summary of NSM CFRP repair effect for repaired and non-repaired beams.....	82
Table 2 - 9 Effect of shear repair with NSM for control beams.....	82
Table 2 - 10 Effect of shear repair with NSM for corroded beams.....	82
Table 3 - 1 Mechanical characteristics of the concrete at 27 years (average values of 3 tests).....	94
Table 3 - 2 Average values of steel bar properties.....	94
Table 3 - 3 CFRP rod characteristics.....	95
Table 3 - 4 Filling material properties according to the manufacturer.....	95
Table 3 - 5 concrete properties used in FEMIX simulation analysis.....	100
Table 3 - 6 FEM vs. Experimental results for A1CL3-R using Abaqus.....	110
Table 4 - 1 Concrete properties.....	125
Table 4 - 2 Average values of steel bars properties.....	127
Table 4 - 3 CFRP rods characteristics.....	128

I. Résumé long en français

Le Béton Armé est encore le matériau de construction le plus utilisé dans le monde depuis son développement au cours du 20^{ème} siècle. Le béton est un matériau durable et une protection efficace pour les armatures en raison du pH élevé de sa solution interstitielle, de sa bonne adhérence avec les armatures qui permet un fonctionnement complémentaire des deux matériaux. Cette protection peut être remise en cause dans le cas où le béton d'enrobage est carbonaté ou pollué par les chlorures, ce qui conduit à la corrosion des armatures. La corrosion des armatures du béton armé est dommageable pour le fonctionnement pérenne des structures. La corrosion des armatures a plusieurs conséquences. Premièrement, une réduction de la section des armatures responsable d'une diminution de capacité portante, deuxièmement une perte de ductilité pouvant donner d'une rupture fragile du béton armé. Troisièmement, les produits de corrosion qui sont expansifs induisent une fissuration du béton d'enrobage qui modifie l'adhérence entre armature et béton et ainsi affecte la rigidité flexionnelle des éléments de béton armé (1-3).

L'endommagement des armatures par la corrosion est très difficile à évaluer in-situ et les méthodes non destructives (CND) ne permettent pas aujourd'hui de déterminer la perte de section des armatures. Au contraire, les méthodes destructives permettent d'avoir une information sur le degré de corrosion bien que les mesures de pertes de section soient rendus délicates par l'hétérogénéité intrinsèque de la dégradation par corrosion (4). Les conséquences mécaniques de la corrosion ont été largement étudiées ces dernières décennies. Bien que non représentatives de la corrosion naturelle, les études utilisant une corrosion accélérée sous champ électriques (5,6) sont les plus utilisées en raison de la rapidité de l'intensité de la corrosion obtenue. La corrosion accélérée en ambiance agressive (7-9) qui est similaire à la corrosion naturelle a été utilisée moins fréquemment. L'ensemble des études montrent que la perte de capacité portante est liée à la perte maximale de section d'armatures dans les zones les plus sollicitées : entre 0,7% à 1% de perte de capacité portante pour une perte de section d'armatures de 1%.

La corrosion naturelle des armatures conduit à une réduction importante de l'élongation de l'acier à rupture, ce qui induit un changement dans le mode de rupture des éléments en béton armé, d'une rupture classique ductile par excès de compression du béton après allongement plastique des armatures, à une rupture fragile des aciers corrodés accompagnée d'une réduction importante de la flèche maximale à rupture. Par exemple, Khan et al. (7) ont trouvé

une réduction de 53% de la flèche à rupture de poutres corrodées à long terme en comparaison avec des poutres témoins du même âge pour seulement une réduction de 17% en terme de capacité portante correspondant à une perte de section maximale de 21,5% dans la section la plus sollicitée. Dang et François (8) ont trouvé également que la réduction de capacité portante d'une poutre corrodée pendant 27 ans était de 26% par rapport à une poutre témoin du même âge mais de 47% en terme de flèche à rupture, ce qui confirme que la perte de ductilité du béton armé due à la corrosion est le problème majeur de la requalification des structures corrodées vis-à-vis des règles de dimensionnement proposées par les différents standards.

Récemment, les renforcements à base de fibres de carbone (FRP) ont progressivement remplacé ceux en aciers pour le renforcement des structures en béton armé (12,13). L'accroissement de ce mode de renforcement s'explique par plusieurs bénéfices : poids réduit, processus d'installation aisé et rapide, haute résistance mécanique et disponibilité en différentes dimensions et géométries (14). La technique la plus répandue est basée sur le collage de feuilles de FRP sur la surface des éléments à renforcer connue sous le nom d'EBR (externally bonded reinforcement). Les derniers résultats de recherche sur cette technique montrent que les hautes résistances mécaniques des FRP ne peuvent pas être utilisées complètement en raison de rupture d'adhérence prématurée au niveau du collage (15, 16). D'autres études montrent également que la technique EBR est sensible aux variations de température et que son efficacité peut être réduite à la fois en cas de basses ou hautes températures. Enfin, la technique EBR est sensible également aux dégradations de surfaces accidentelles, d'origine mécanique ou non.

Une nouvelle technique de renforcement a émergé plus récemment appelée NSM pour Near Surface Mounted reinforcement. Cette technique est basée sur l'enfouissement dans des engravures réalisées à la surface du béton, d'armatures en fibres de carbone (CFRP) ou de verre (GRFP). La technique NSM est en fait apparue dans les années 40 où les armatures en acier de renforcement étaient implantées dans des engravures faites à la surface du béton et enrobées de mortier. De nos jours, les armatures en fibres de carbone (joncs de carbone) ou rubans de carbone sont utilisées et le matériau de remplissage est une résine epoxy.

Les modes de rupture des éléments de béton armé renforcés par la technique NSM varient de la dégradation du renforcement (arrachement du jonc ou sa rupture) jusqu'à une rupture conventionnelle par écrasement du béton comprimé en fonction du ratio entre la section du

renforcement en CFRP et la section de béton ainsi que la longueur du renforcement par rapport à la portée (17). Une étude précédente (18) a montré que le renforcement de poutres en béton armé par la technique NSM peut conduire à des modes de rupture non conventionnels comme la séparation du béton d'enrobage.

L'utilisation de la technique NSM pour réparer et renforcer des structures endommagées par la corrosion des armatures est très récente et peu de chercheurs ont pour l'instant travaillé dans ce domaine. Kreit et al. (18) ont montré que la technique NSM permet de restaurer la capacité portante initiale d'une poutre corrodée avec 36 % de perte de section dans la section la plus sollicitée en flexion. Cependant, le caractère fragile ou ductile ainsi que la restauration de la flèche maximale à la rupture d'éléments en béton armé corrodés n'ont pas encore été étudiés.

L'utilisation de la technique NSM avec des joncs de carbone (CFRP) a donné des résultats encourageants pour le renforcement vis-à-vis de l'effort tranchant de poutres endommagées et susceptibles de périr à l'effort tranchant. De Lorenzis et Nanni (19) ont montré que la technique NSM pouvait accroître la résistance à l'effort tranchant, en particulier 106% d'augmentation de la résistance a été mesurée par rapport à l'absence de cadres d'effort tranchant internes. Une augmentation significative a été également trouvée pour des poutres sous dimensionnées vis-à-vis de l'effort tranchant. Islam (20) a testé 4 poutres en béton armé : une poutre témoin avec un renforcement classique vis-à-vis du tranchant et 3 autres poutres qui ont été renforcées à l'effort tranchant avec des joncs de carbone par la technique NSM, pour lesquelles une augmentation de la capacité portante de 17 à 25% a été mesurée.

Quelques chercheurs (21) ont utilisé des renforcements sous forme de rubans de tissu de CFRP insérés dans les engravures par la technique NSM à la place des joncs de carbone en comparaison avec les renforcements classiques par tissus collés sur la surface extérieure (EBR) et ils ont trouvés que les rubans de tissus insérées par la technique NSM permettaient une plus grande capacité portante après la formation des fissures d'effort tranchant, ainsi qu'une optimisation du fonctionnement du CFRP puisque les contraintes de traction mesurées dans les rubans de tissus engravés étaient largement supérieure à celle mesurées sur les tissus collés en surface.

De Lorenzis et al. (22) ont suggéré quelques méthodes pour accroître la résistance à l'effort tranchant de poutres en Té renforcées en diminuant la distance entre les joncs de carbone insérés par la technique NSM et en augmentant leur longueur d'ancrage par insertion

également dans la membrure de la poutre en T_e. Ils ont indiqué que la diminution de la distance entre les joncs de carbone conduit à une augmentation significative de la résistance à l'effort tranchant. Une inclinaison des joncs de carbone de 45° augmente également la résistance vis-à-vis de l'effort tranchant, ce qui est cohérent avec les résultats de Barros et al. (23) obtenus sur des rubans de carbone inclinés qui apparaissaient plus efficaces que les rubans verticaux. De Lorenzis et Nanni (19) ont observé deux modes de rupture différents pour les poutres réparées vis-à-vis de l'effort tranchant par la technique NSM. Le premier est la rupture d'adhérence entre les joncs et le béton et le second est la séparation du béton d'enrobage le long des armatures longitudinales. Ils en ont déduit que si le premier mode de rupture (perte d'adhérence) pouvait être évité en inclinant les joncs de carbone, le second mode (séparation du béton d'enrobage) était alors celui qui contrôlait l'augmentation de la capacité portante. Un autre mode de rupture observé (24) était la séparation complète du béton d'enrobage sur le côté de la section parallèlement aux cadres d'effort tranchant internes.

Une recherche précédente (25) a étudié la prédiction de la performance de structures en béton armé renforcées par la technique NSM, sur la base de calcul non-linéaires utilisant la méthode des éléments finis. La modélisation utilisant le code commercial ANSYS a montré l'effet prépondérant du diamètre du jonc de carbone sur la rigidité en flexion et la capacité portante de poutres renforcées par la technique NSM, ainsi l'utilisation d'un jonc de diamètre 16 mm accroît de 83.6% la capacité portante en comparaison avec un jonc de 6 mm de diamètre.

Le code de calcul FEMIX basé sur la Méthode des Eléments Finis (MEF), a été utilisé par de nombreux chercheurs pour simuler le comportement de poutres BA renforcées par des rubans de carbone insérées par la technique NSM. Sena Cruz et al. (26) ont montré que la colle epoxy a un effet négligeable sur le comportement global, et que le faciès de fissuration ainsi que les courbes chargement-flèches obtenues numériquement étaient semblables aux résultats expérimentaux. Le code de calcul ABAQUS basé sur la MEF, a été utilisé de nombreuses fois pour simuler le comportement de poutre en BA. Ainsi Lundqvist et al. (27) ont étudié la longueur d'ancrage des joncs en carbone pour éviter une rupture prématurée, et Radfar et al. (28) ont étudié la mode rupture en « boîte de conserve » (Peeling-off) pour des poutres renforcées par des tissus de carbone externes (EBR). Une autre étude de Kang et al. (29) a utilisé ABAQUS pour étudier l'influence de la profondeur de l'engravure réalisée pour insérer des rubans de tissus carbone sur la capacité portante. Il n'y a pas aujourd'hui d'études réalisées pour modéliser par la MEF, le comportement mécanique des structures en BA corrodées et réparées par la technique NSM.

Suryanto et al. (30) ont indiqué qu'il était indispensable de prendre en compte le comportement post-pic adoucissant de la loi de comportement contrainte –déformation en cisaillement du béton pour arriver à modéliser correctement l'endommagement réel obtenu sur le béton pendant la phase de fissuration. Récemment, un modèle multidirectionnel de fissuration diffuse a été implémenté par Barros et al. (31) dans le but de simuler le comportement en flexion et à l'effort tranchant de poutres BA renforcées par des matériaux composites en fibres de carbone (CFRP). Barros et al. (23) ont étudié les limitations de l'utilisation des rubans de tissus carbone engravés pour le renforcement à l'effort tranchant en prenant en compte la fissuration du béton sur lequel s'attachent les rubans de renforcement. Nanni et al. (32) ont prédit la contribution du système de renforcement NSM sur la résistance à l'effort tranchant mais cette modélisation était basée uniquement sur un mode de rupture par perte d'adhérence des rubans de tissus engravés. Malheureusement, la séparation de béton d'enrobage sur lequel sont insérés les rubans de tissus de carbone est bien plus fréquente (22,23). Bianco et al. (33) ont développé une approche analytique capable de prédire le comportement de rubans de carbone engravés par la technique NSM sur la résistance à l'effort tranchant basée sur différents modes possibles de rupture : perte d'adhérence, rupture de cônes de béton en traction autour du renforcement, couplage entre la perte d'adhérence et une rupture superficielle du béton, rupture en traction du ruban de carbone.

La plupart des études concernant le comportement des structures corrodées est basée sur l'utilisation d'un courant imposé qui transforme les armatures en anodes. Ce phénomène n'a rien à voir avec la corrosion réelle dans le béton armé qui est une corrosion non uniforme. Très peu d'études ont été conduites sur la base d'une corrosion naturelle ou d'une corrosion accélérée via des conditions environnementales sévères telles que des cycles humidification-séchage. En conséquence, il n'y a pratiquement pas d'études sur la réparation par des matériaux composites de structures corrodées naturellement et celles qui existent sont consacrées à l'étude du comportement vis-à-vis de la flexion. Il n'y a donc pas d'études concernant la réparation au tranchant de structures corrodées naturellement.

Les objectifs de cette thèse sont ainsi :

Premièrement, étudier l'efficacité de la réparation utilisant des joncs de carbone par la technique NSM sur le comportement mécanique en flexion et à l'effort tranchant de poutres BA naturellement corrodées;

Deuxièmement, implémenter une modélisation numérique basée sur la méthode des éléments finis, pour simuler le comportement non-linéaire des poutres en BA corrodées réparées par la technique NSM en termes de charge de plastification, capacité ultime et modes de rupture.

La thèse est ainsi composée de quatre chapitres, chaque chapitre étant organisé autour d'un article scientifique publié dans un journal international ou en cours d'évaluation par les pairs.

Le premier chapitre s'intéresse au comportement après réparation de deux poutres en béton armé (une poutre corrodée naturellement et une poutre témoin du même âge) renforcées vis-à-vis de la flexion par un jonc de carbone engravé par la technique NSM et testées en flexion 3 points jusqu'à la rupture. Par ailleurs, sont aussi présentés : les propriétés mécaniques des armatures en traction après corrosion, les performances des poutres réparées en terme de charge de plastification, charge de rupture, flèche à rupture et mode de ruine. La carte de corrosion des armatures longitudinales et transversales est établie pour la poutre corrodée ainsi que les performances mécaniques résiduelles en traction des armatures corrodées. Pour établir la carte de corrosion, les produits de corrosion ont été retirés des armatures en utilisant une solution de Clarke (ISO 8407) et la section résiduelle d'acier a été mesurée en utilisant deux méthodes : une mesure du diamètre résiduel direct par l'intermédiaire d'un pied à coulisse, une mesure indirecte par perte de masse de petit morceaux d'armatures obtenus par sciage et dont la longueur est adaptée au faciès de corrosion. Pour la seconde méthode la dimension des échantillons d'armatures variait autour de 1 à 2 cm et la pesée s'est effectuée avec une balance de précision 0.001g. La masse de référence a été établie à partir des armatures extraites de la poutre témoin non corrodée. Les deux méthodes ont été utilisées pour calculer le diamètre résiduel des barres d'armatures le long de la poutre. En effet, des études précédentes ont montré que le faciès de corrosion naturelle était très variable le long du périmètre des armatures et que la forme complexe de la section résiduelle ne pouvait pas être rendue par une mesure d'un diamètre minimal résiduel obtenu par le pied à coulisse. De plus, le calcul de la section basé sur un diamètre résiduel majore fortement la perte de section réelle. Dans ce chapitre sont également discuté l'efficacité de la technique NSM ainsi que la restauration d'une ductilité suffisante et l'évolution de la raideur en flexion.

Les poutres testées dans ce chapitre et dans les chapitres suivants font parties d'un programme expérimental engagé en 1984 au Laboratoire de Génie Civil (nom précédent du LMDC créé en 1989) de l'INSA et l'Université Toulouse 3 dont le but initial était de comprendre le rôle du chargement mécanique et des fissures induites sur le processus de corrosion d'éléments de

structures en béton armé. Ce programme à long terme consistait en la réalisation d'un ensemble de 72 poutres en béton armé de dimension 3000x280x150 mm, 36 étant conservées sous deux niveaux de chargement différents dans un environnement salin et les 36 autres servant de poutres témoins car étant soumises à des effets différés comparables tels que le fluage et le vieillissement. De nombreuses études ont été réalisées sur ces poutres depuis la fin des années 80 pour évaluer le processus de corrosion en présence de fissures, la pénétration des chlorures et les changements dans le comportement mécanique induits par la corrosion. L'environnement de corrosion accélérée (mais comparable à une corrosion naturelle) consistait à une exposition à un brouillard salin à base d'eau salée à 35g/l de NaCl (figure I-1). Après 6 années de conservation, les poutres ont été exposées à des cycles d'humidification-séchage pour accélérer le processus de corrosion :

- 0-6 ans : pulvérisation continue du brouillard salin dans les conditions du laboratoire (20°C)
- 6-9 ans : cycle de pulvérisation d'une semaine et de séchage naturel d'une semaine dans les conditions du laboratoire (20°C)
- 9-19 ans : cycle de pulvérisation d'une semaine et de séchage naturel d'une semaine mais la chambre environnementale ayant été transférée à l'extérieur, les poutres sont exposées aux températures naturelles variant en moyenne mensuelle entre 5.1°C et 21.3 °C
- 19-27 ans : les cycles ont été stoppés, les poutres restant dans la chambre environnementale
- Depuis 27 ans : reprise des cycles avec 2 jours de pulvérisation et 12 jours de séchage.

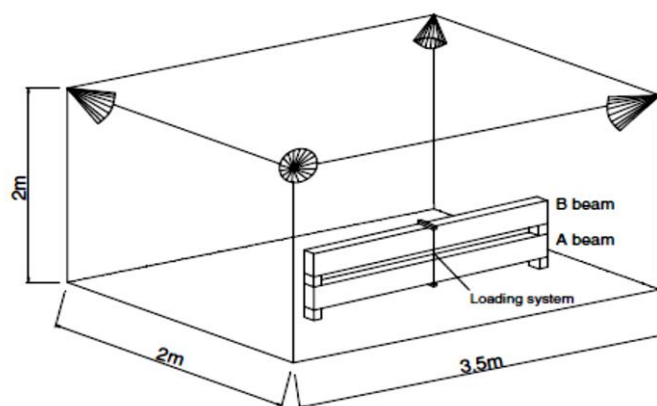


Figure I- 1 vue schématique de la chambre à brouillard salin et de la conservation des poutres

La corrosion obtenue par l'exposition au brouillard salin et les cycles d'humidification séchage est très proche de celle observable en conditions naturelles en termes de distribution de la corrosion le long des armatures ou du périmètre, de type de corrosion (non uniforme) et des oxydes formés. Il est très important pour réaliser des prédictions de durée de vie des structures d'avoir accès à de telles dégradations naturelles (36) plutôt que d'utiliser des résultats obtenus à très court terme en appliquant un courant électrique continu ou en ajoutant des chlorures pendant le gâchage du béton (37,38). Les poutres étaient séparées en deux groupes intitulés A et B correspondant à deux différents ferraillements mais le même type d'acier HA (limite élastique 500 MPa). Les poutres A et B avaient un enrobage respectif de 40 et 10 mm qui correspondaient respectivement au moment du coulage à l'enrobage minimum pour une exposition à un environnement très agressif (par exemple les chlorures marin) et l'enrobage minimum pour une exposition à un environnement non-agressif. Les poutres étaient sollicitées en flexion 3 points en accouplant une poutre de type A avec une poutre de type B. Deux niveaux de sollicitations ont été appliqués : le niveau 1 correspondant au dimensionnement à l'ELS en fissuration très préjudiciable et le niveau 2 correspondant au dimensionnement à l'ELU. Le chargement résultant était ainsi de $M_{ser1}=13.5$ kN.m pour les poutres de type 1 (A1) et $M_{ser2}=21$ kN.m pour les poutres de type 2 (A2). Toutes les poutres étudiées dans cette thèse sont de type A : une corrodée A1CL3-R et une témoin A1T-R et des poutres non réparées (A2CL1, A2CL3, A2T et A2TI) testées précédemment par Khan et Dang dans leur thèses. La figure I-2 montre le plan de ferraillement des poutres de type A sujet de cette thèse.

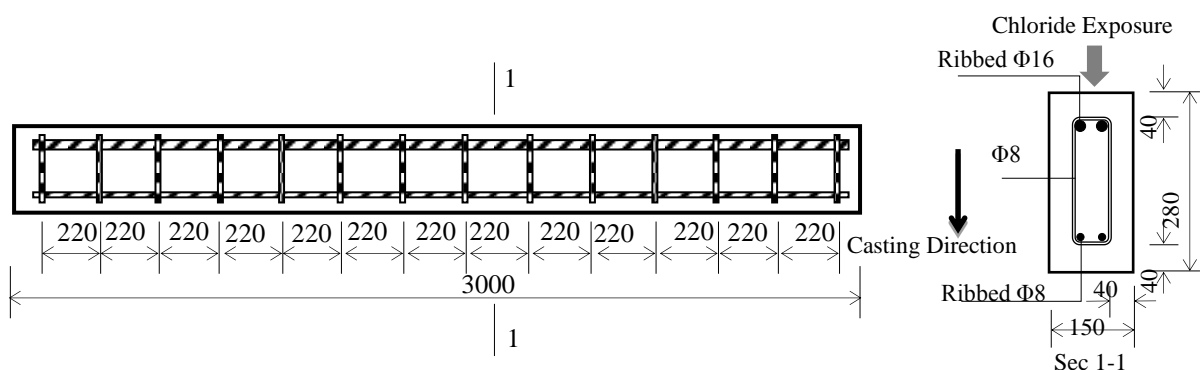


Figure I- 2 plan de ferraillement des poutres de type A. Toutes les dimensions sont en mm

Les résultats expérimentaux présentés dans ce premier chapitre ont été obtenus sur les deux poutres A1CL3-R et A1T-R âgées de 28 ans, réparées par un jonc de carbone de diamètre 6 mm tout le long de la face supérieure de la poutre par rapport au sens de coulage. En effet, pendant la conservation en ambiance agressive ou dans le labo, en raison du chargement

mécanique par couplage de deux poutres A et B, la face tendue des poutres de type A correspondait à la face supérieure et les poutres A ont été coulées dans cette configuration pour faciliter leur mise en œuvre. Les poutres ont été testées en flexion 3 points avant et après le renforcement par la technique NSM afin d'évaluer le changement dans les raideurs en flexion. Les cartes de fissuration résultant du processus de corrosion ont également été tracées avant la réparation. Après réparation, les deux poutres ont été testées jusqu'à rupture. Les résultats expérimentaux ont montré que la technique NSM est capable de restaurer la capacité initiale d'une poutre significativement dégradée par une corrosion à long terme. La figure I-3 montre les comparaisons entre les poutres témoins réparées ou non et les poutres corrodées réparées ou non. L'insertion d'un jonc de carbone de 6 mm par la technique NSM dans une poutre témoin (A1T-R) augmente significativement sa capacité ultime (A2T et A2TI). La poutre corrodée réparée (A1CL3-R) qui présente une perte de diamètre maximale de 38% retrouve une capacité portante au moins égale à celle des poutres témoins non réparées et une capacité portante significativement supérieure à celle des poutres corrodées non-réparées A2CL1 et A2CL3 avec un accroissement du moment de 17 kN.m et 11 kN.m respectivement.

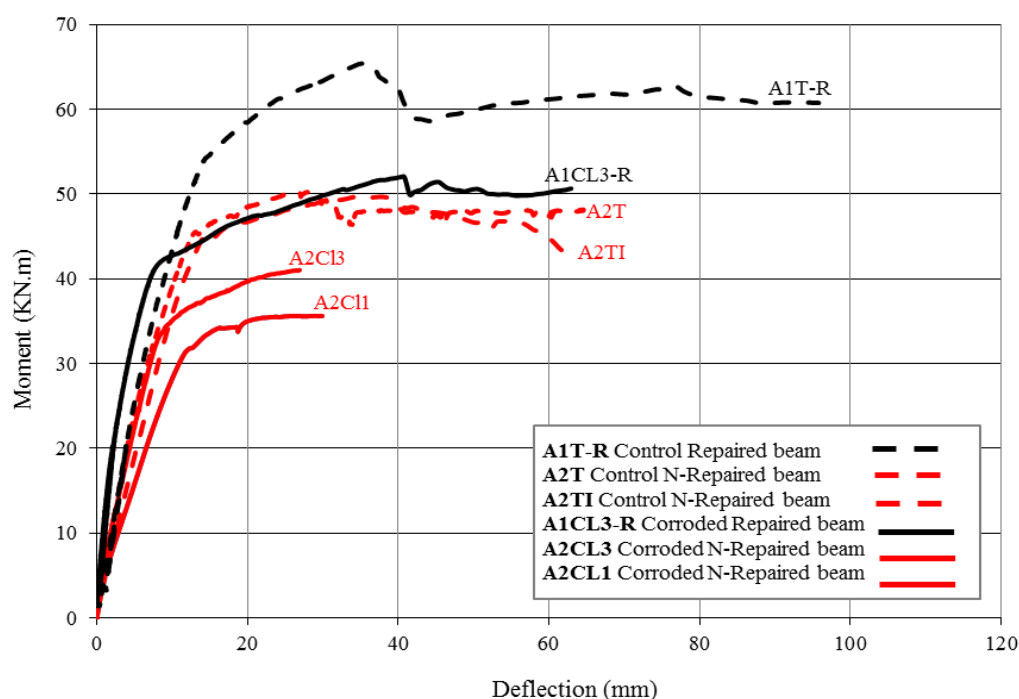


Figure I- 3 comparaison entre les réponses en flexion 3 points des différentes poutres (A2T, A2TI, A1T-R, A2CL3, A1CL3-R and A2CL1)

L'efficacité de la réparation par la technique NSM d'une poutre corrodée peut être limitée par l'apparition d'un nouveau mode de rupture qui est la séparation du béton d'enrobage au

niveau des fissures de corrosion. Le mode de ruine obtenu sur la poutre corrodée réparée (A1CL3-R) (figure I-4) est différent de celui obtenu sur les poutres corrodées non réparées (A2CL1 et A2CL3) qui ont péri par une rupture fragile des armatures tendues au niveau de piqures de corrosion sévères. La rupture de la poutre corrodée réparée (A1CL3-R) intervient suivant un mode non-conventionnel dû à l'existence d'un plan de rupture généré par les fissures de corrosion. Ce plan de rupture est parallèle à la surface tendue du béton mais situé au niveau des armatures tendues.

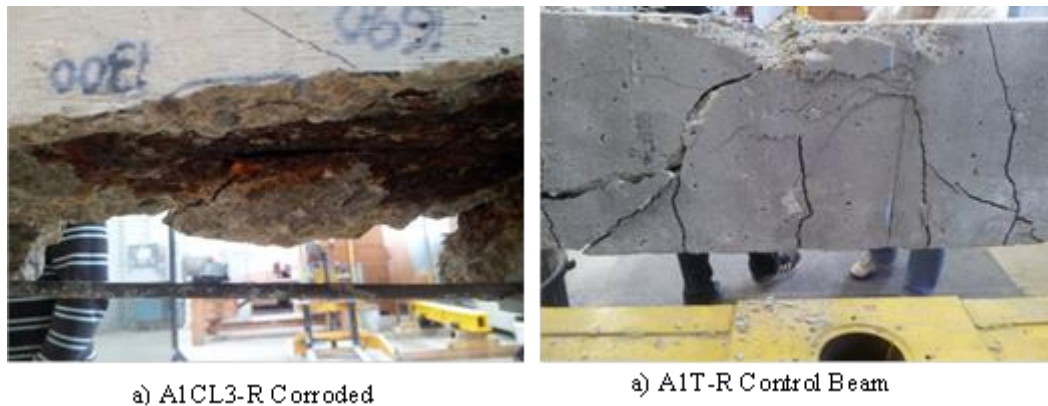


Figure I- 4 faciès de rupture des deux poutres réparées en flexion par la technique NSM

On a également constaté que la réparation par la technique NSM avait permis d'augmenter légèrement la raideur en flexion des deux poutres réparées (corrodée ou témoin). De plus, la réparation permet également d'augmenter la valeur de la flèche maximale à rupture par rapport aux poutres non réparées. Ce résultat est important car il permet de montrer que la réparation par la technique NSM permet de restaurer une ductilité suffisante (2.8 fois supérieur à celle de la poutre corrodée non réparée) qui était perdue en raison du caractère fragile du comportement des aciers corrodés en traction. Finalement, on constate que 1% de perte de section des armatures due à la corrosion correspond à 1% de perte de la charge de plastification. Le pourcentage est différent pour la capacité portante car le mode de rupture est différent.

Le second chapitre s'intéresse au comportement mécanique en flexion 3 points après réparation de quatre poutres courtes (2 corrodées et 2 témoins) qui sont réparées ou renforcées par des joncs de carbone insérés par la technique NSM en flexion mais également vis-à-vis de l'effort tranchant pour deux d'entre elles. Les quatre poutres courtes sont obtenues par sciage en trois parties des deux poutres longues (A1CL3-R et A1T-R) étudiées au chapitre 1. La partie centrale endommagée lors des essais de flexion présentés au chapitre 1 est éliminée et il reste les deux extrémités de longueur 800 mm peu sollicitées lors de la flexion (figure I-5).

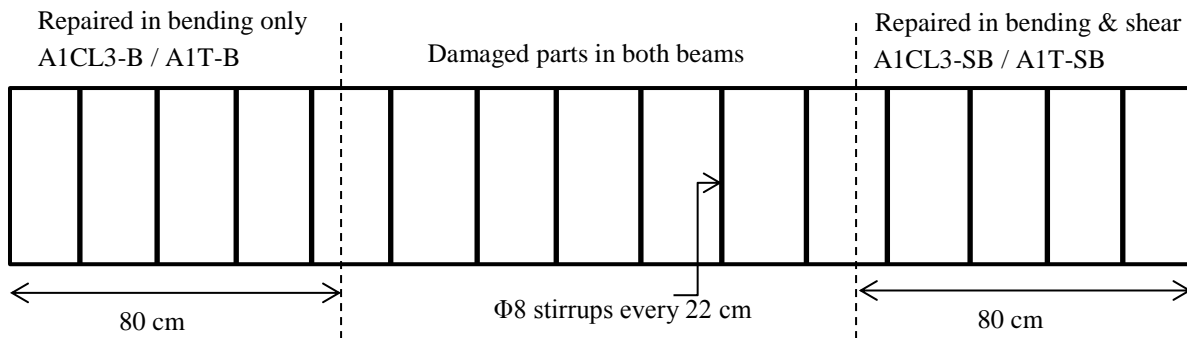


Figure I- 5 schéma de découpe des poutres longues A1CL3-R et A1T permettant d'obtenir 4 poutres courtes (A1CL3-B , A1CL3-SB, A1T-B, A1T-SB) correspondant aux extrémités peu sollicitées lors de la flexion

Par ailleurs, les résultats expérimentaux obtenus sur ces quatre poutres courtes (résistance à l'effort tranchant, capacité portante, mode de rupture) sont comparés avec des poutres courtes similaires mais non réparées ou renforcées testées lors des thèses de Khan et Dang. Cette comparaison permet de discuter l'effet du renforcement par NSM sur le comportement des poutres courtes. Finalement, l'influence du ratio (a/d) entre la portée au tranchant (a) et la hauteur effective de la section (d) sur la résistance à l'effort tranchant est discutée.

L'utilisation de poutres courtes permet un comportement en flexion plus critique vis-à-vis de l'effort tranchant. Compte tenu du fait que les poutres courtes sont extraites des poutres longues renforcées ou réparées vis-à-vis de la flexion et testées au premier chapitre, nous avons choisi de conserver le renforcement NSM le long de la face « tendue » des poutres. Les poutres courtes obtenues ainsi sont nommées A1CL3-B et A1T-B correspondant respectivement à la poutre corrodée et à la poutre témoin du même âge. Les deux autres poutres courtes ont fait l'objet d'un renforcement vis-à-vis de l'effort tranchant en insérant par la technique NSM quatre joncs de carbone sur chaque face latérale de la poutre courte : deux de chaque côté espacés de 10 cm. Pour une meilleure résistance vis-à-vis de l'effort tranchant, les joncs de carbone sont inclinés de 45° pour être perpendiculaires aux fissures dues à l'effort tranchant lors de la flexion 3 points.

Après que les quatre poutres aient été testées en flexion 3 points jusqu'à rupture, les armatures ont été extraites des poutres corrodées et témoins pour les mesures du degré de corrosion et les essais de traction pour établir la loi de comportement des aciers.

Les poutres courtes testées ne possèdent pas d'ancrage particulier des armatures longitudinales à leurs extrémités. Une perte de capacité d'ancrage est donc envisageable au cours des essais. Nous avons donc mesuré le glissement des barres longitudinales en utilisant

des LVDT (linear variable differential transducers) installés à chaque extrémité de barres. Un autre LVDT a été utilisé pour mesurer la flèche à mi-portée (figure I-6).

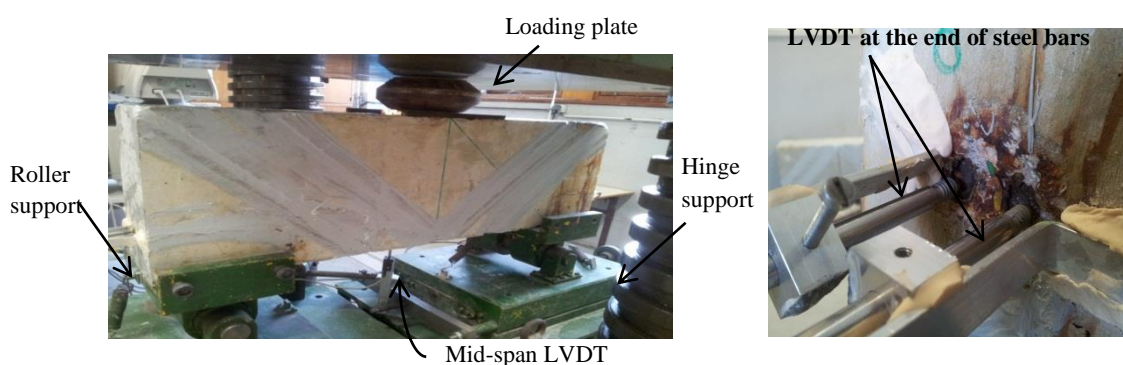


Figure I- 6 Vue de la réparation vis à vis de l'effort tranchant et de l'instrumentation permettant de mesurer le glissement des armatures longitudinales sur appuis

Les résultats expérimentaux montrent que le mode de rupture obtenu pour les poutres non renforcées vis à vis de l'effort tranchant (poutre corrodée A1CL3-B et témoin A1T-B) a été par la formation d'une fissure inclinée de cisaillement d'effort tranchant, alors que les poutres renforcées vis-à-vis de l'effort tranchant (poutre corrodée A1CL3-SB et témoin A1T-SB) ont montrés un mode de rupture différent par excès de compression sur la fibre comprimée précédée de la formation de fissures de flexion largement ouvertes à mi-portée comme le montre la figure I-7.



Figure I- 7 modes de ruine des quatre poutres courtes

Les fissures diagonales d'effort tranchant apparaissent toujours du même côté des poutres courtes quel que soit le degré d'endommagement dû à la corrosion à cause de la différence de longueur d'ancrage entre les deux extrémités des poutres courtes. En effet, les poutres courtes

ont été obtenues par sciage et un côté correspond donc à la face sciée et l'autre extrémité correspond à la face de coffrage. Les armatures longitudinales atteignent donc la face coupée alors qu'il y a quelques mm entre l'extrémité des armatures longitudinales et la face coffrée : cela conduit à une différence de longueur d'ancrage sur appuis. En conséquence, la rupture à l'effort tranchant apparaît systématiquement du côté de la face coffrée.

Il a été constaté que le glissement des armatures longitudinales est réduit dans le cas des poutres corrodées, ce qui peut paraître comme un résultat surprenant puisqu'il y a des fissures de corrosion longeant les armatures longitudinales près des appuis. Cependant le confinement apporté à la fois par les cadres d'effort tranchant et par la réaction d'appuis qui a tendance à refermer les fissures de corrosion permet d'expliquer cette meilleure adhérence des barres corrodées par rapport aux barres non corrodées.

En conséquence, la perte d'adhérence au niveau de l'ancrage est la cause de la rupture de la poutre témoin non réparée vis-à-vis de l'effort tranchant, ce qui n'est pas le cas de la poutre corrodée non réparée vis-à-vis du tranchant.

Le comportement des poutres corrodées est influencé par la corrosion des armatures mais cet effet est lié au mode de ruine : pour la poutre réparée vis-à-vis de l'effort tranchant (A1CL3-SB), c'est la corrosion à mi-portée qui est à considérer pour évaluer le changement de charge de plastification alors que pour la poutre non réparée vis-à-vis de l'effort tranchant (A1CL3-B), c'est la corrosion au niveau de la fissure diagonale de cisaillement.

On constate également que la réparation vis-à-vis de l'effort tranchant par la technique NSM en insérant des joncs inclinés à 45° permet de réduire très significativement le glissement des armatures longitudinales sur appuis.

On ne constate pas d'effet significatif de la réparation vis-à-vis de l'effort tranchant de la poutre corrodée dans le cas d'un ratio (a/d) plus petit que 2 (figure I-8). Même en présence de corrosion des armatures et avec un renforcement vis-à-vis de l'effort tranchant et du moment de flexion, on constate qu'il y a toujours un comportement fortement influencé par le rapport (a/d) avec une transition entre un comportement piloté par la flexion ou le cisaillement aux alentours de 2.5-3

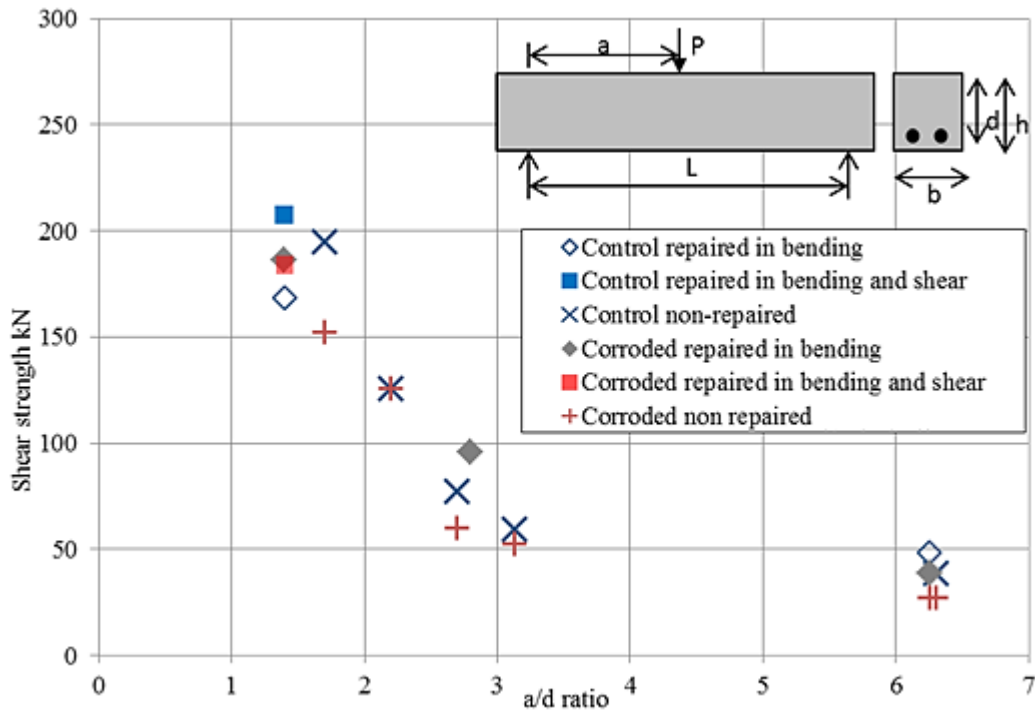


Figure I- 8 influence du ratio a/d sur la capacité portante des poutres

Le troisième chapitre s'intéresse à la mise en œuvre d'un modèle éléments finis non-linéaire pour simuler le comportement des poutres longues réparées ou renforcées (présentées au chapitre 1) par la technique NSM. Une première approche est réalisée en 2D en utilisant le code de calcul FEMIX pour simuler 5 poutres dont les deux du premier chapitre, les trois autres sont des poutres testées lors des thèses de Khan et Dang.

La modélisation réalisée avec FEMIX permet de modéliser de façon correcte le comportement des quatre poutres (figure I-9) (A1T-R, A2T, A2CL3, A2CL1) mais pas celui de la poutre A1CL3-R en terme de flèche ultime à rupture qui est largement sous-évaluée par le modèle EF. La raison est principalement due au fait d'un mode de rupture particulier due aux fissures de corrosion : la séparation du béton d'enrobage.

Pour cette raison, une modélisation 3D est réalisée en utilisant le code de calcul ABAQUS.

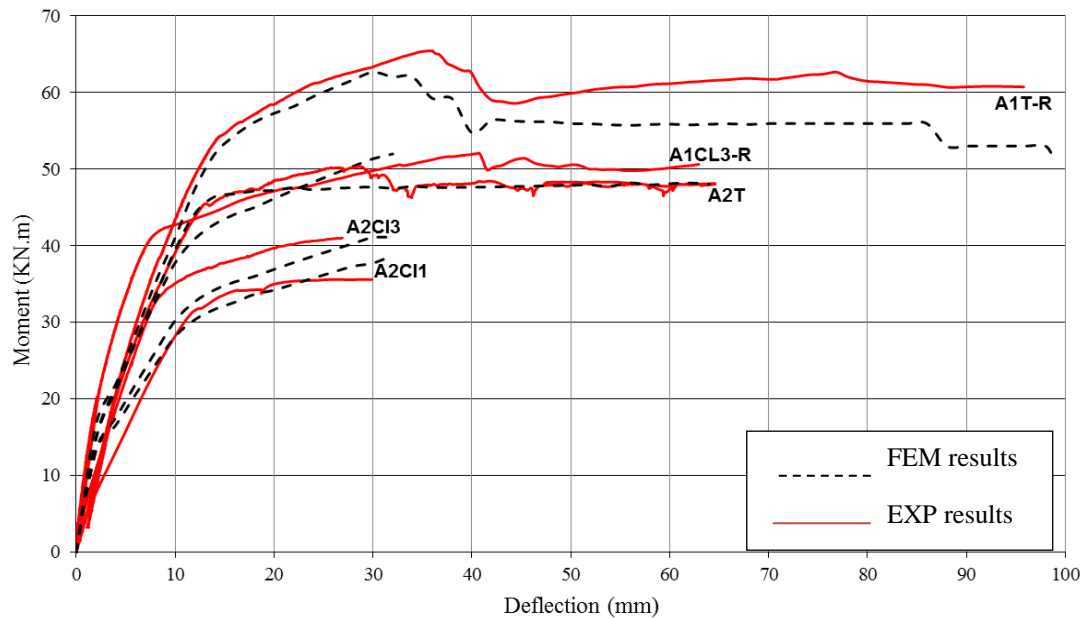


Figure I- 9 comparaison entre les résultats expérimentaux et la modélisation EF 2D utilisant le code FEMIX

Pour la modélisation 2D utilisant FEMIX, le béton a été modélisé en utilisant des éléments à 8 nœuds en formulation contrainte plane. Les armatures et les joncs de carbone ont été simulés en utilisant des éléments linéaires à 3 nœuds de type « cable ». Pour ce modèle, les armatures et les joncs sont supposés parfaitement adhérent au béton (figure I-10). Il s’agit bien sûr d’une hypothèse forte mais l’idée est de simuler dans un premier temps les charges ultimes et la flèche ultime et pas la rigidité en flexion. La corrosion des armatures a été simulée en réduisant la section des armatures de façon uniforme en considérant le degré de corrosion expérimental mesuré à mi-portée des poutres simulées. La corrosion des cadres d’effort tranchant n’a pas été considérée car elle n’intervient pas sur la résistance en flexion.

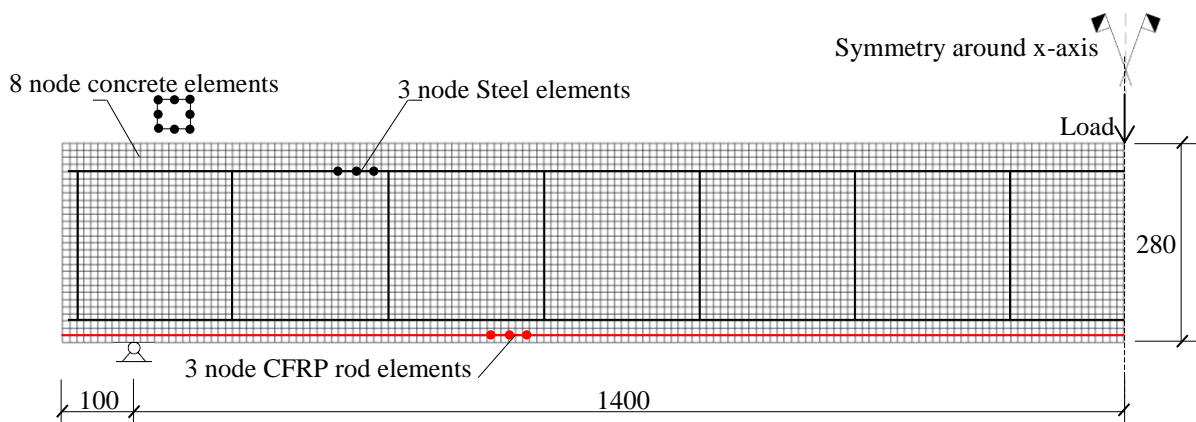


Figure I- 10 Modèle éléments finis pour la simulation des poutres renforcées par la technique NSM

Pour la modélisation 3D utilisant ABAQUS, le béton et le matériau de remplissage des engravures (résine epoxy) ont été modélisés en utilisant des éléments 3D massifs. Les armatures en acier et le jonc de carbone ont été modélisé sous forme d'éléments linéaire de type « treillis ». Les plaques d'appuis ainsi que la plaque de chargement en acier ont également été modélisées sous forme d'éléments 3D massifs mais avec une limite élastique très supérieure à celle de l'acier d'armature pour éviter leur plastification dans le calcul.

Le comportement plastique du béton en compression a été modélisé via un critère de Drucker-Prager avec un comportement d'érouissage différent en traction qu'en compression. Les fissures de corrosion dans la poutre A1CL3-R sont supposées être la cause de la rupture non conventionnelle de la poutre en flexion. Pour cette raison, la surface plane correspondant aux fissures de corrosion a été modélisée en utilisant un outil spécifique d'ABAQUS : « crack tool in interaction section ». Pour ce faire, nous avons séparé le modèle EF en plusieurs parties pour ne définir un plan de fissuration que sur la longueur correspondant aux résultats expérimentaux (figure I-11). La fissure horizontale ainsi définie avec ABAQUS est initialement fermée mais peut s'ouvrir pendant le chargement. Comme pour la modélisation avec FEMIX, la corrosion a été prise en compte uniquement sur les armatures longitudinales en réduisant la section de 20% qui correspond au degré de corrosion maximal atteint à mi-portée de la poutre.

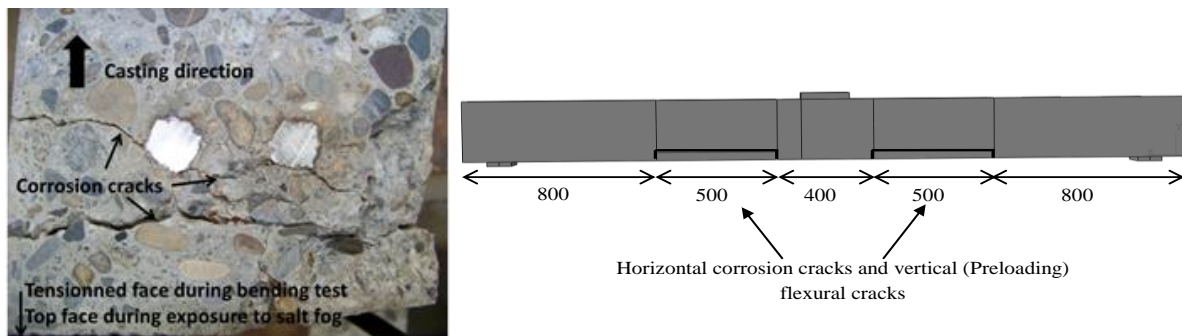


Figure I- 11 Fissures de corrosion obtenues expérimentalement et modélisation correspondante avec ABAQUS

Les résultats expérimentaux ont montré que la réparation avec le technique NSM de la poutre corrodée a permis d'éviter la rupture fragile prématurée des armatures tendues corrodées qui est le mode de rupture des poutres corrodées non réparées. Cependant cela n'est pas suffisant pour retrouver la ductilité des poutres renforcées non corrodées en raison de l'apparition d'un nouveau mode de rupture non-conventionnel par séparation du béton d'enrobage au niveau du plan des fissures de corrosion. La modélisation 2D utilisant le code FEMIX a permis de

reproduire les aspects principaux du comportement des différentes poutres modélisées : charge de plastification, charge ultime.

L'analyse menée avec FEMIX permet également de visualiser la diminution de la flèche maximale à rupture des poutres corrodées non réparées due à la prise en compte d'une loi de comportement de l'acier modifiée par la corrosion avec une rupture fragile pour une déformation maximale à rupture réduite de 50% (figure I-12).

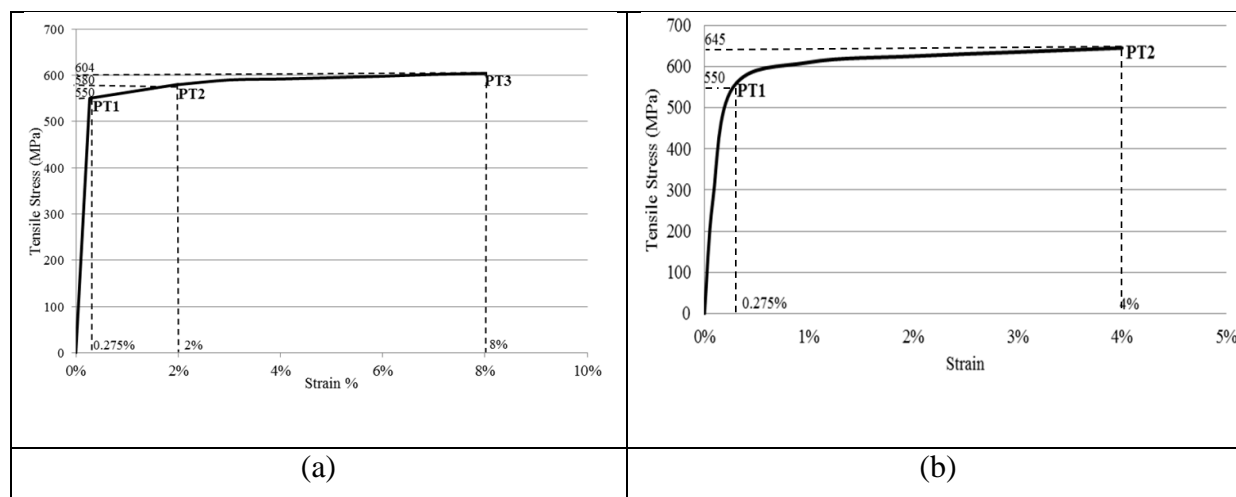


Figure I- 12 loi de comportement de l'acier en traction : non corrodé (a) ; corrodé (b)

L'analyse menée par FEMIX ne montre pas que la réparation par un jonc de carbone suivant la technique NSM peut restaurer la ductilité de la poutre en flexion perdue à cause de la corrosion de l'acier et sa rupture fragile. De plus, ce résultat n'est pas corroboré par l'expérience qui fait apparaître un nouveau mode de rupture. Il a donc été nécessaire de réaliser un nouveau modèle 3D avec ABAQUS pour mettre en évidence ce phénomène. Ainsi les figures I-13 et I-14 montrent que l'introduction d'un défaut tel que la fissuration du béton d'enrobage en raison du développement de la corrosion permet de retrouver les résultats expérimentaux.

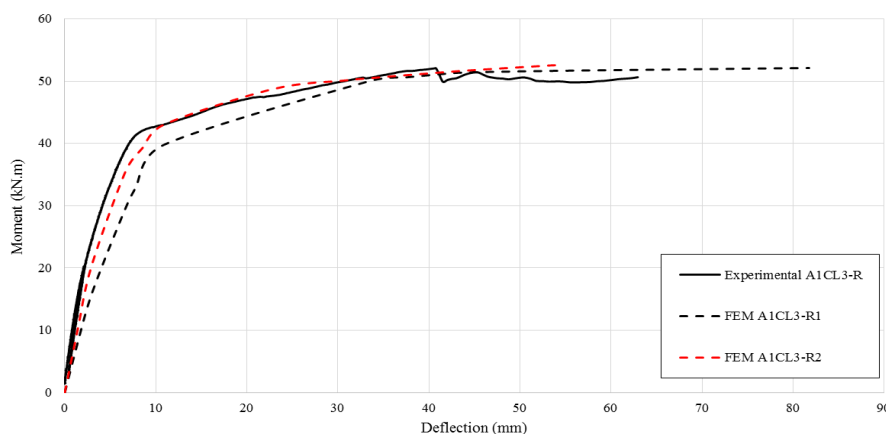


Figure I- 13 Comparaison entre le comportement expérimental et les modélisations faites avec ABAQUS : R1 sans introduction de la fissure de corrosion; R2 avec introduction de la fissure de corrosion

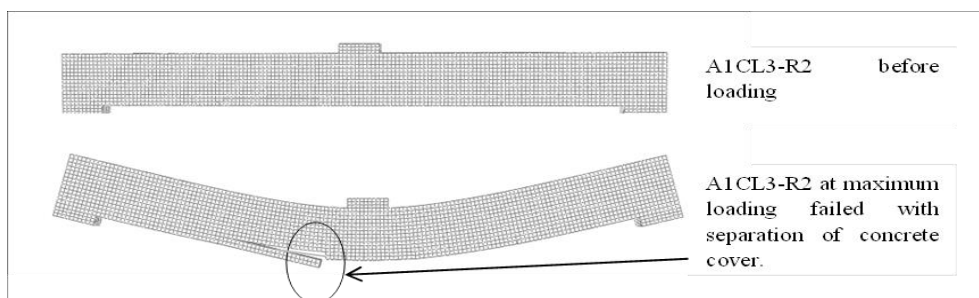


Figure I- 14 visualisation du mode de rupture par separation du béton d'enrobage reproduit par ABAQUS : modèle R2

Le quatrième chapitre s'intéresse à la mise en œuvre d'un modèle éléments finis non-linéaire pour simuler le comportement des poutres courtes réparées ou renforcées (présentées au chapitre 2) par la technique NSM en flexion et en cisaillement. Les simulations sont réalisées en utilisant le code de calcul FEMIX. Les poutres courtes renforcées au cisaillement ont été équipées de jonc de carbone engravé dans la face latérale des poutres par une résine epoxy à haute adhérence.

La modélisation est basée sur une approche multidirectionnelle de la fissuration diffuse afin de reproduire le comportement vis-à-vis de l'effort tranchant. L'aspect le plus important de ce modèle constitutif est l'utilisation d'un effet adoucissant du béton dans le cas de la formation de fissures en mode II capable donc de prendre en compte le développement des fissures de cisaillement d'effort tranchant. Le modèle est réalisé en contraintes planes (figure I-15).

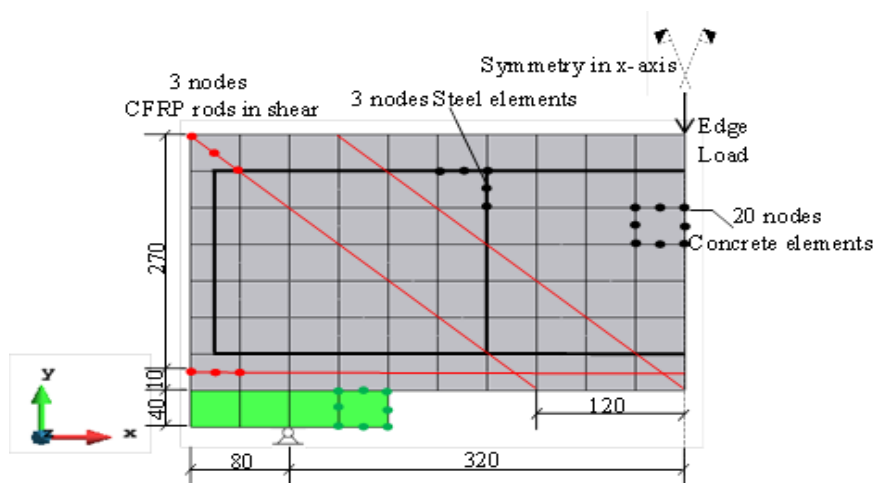


Figure I- 15 modélisation EF de la poutre courte renforcée au cisaillement par les joncs de carbone engravés à 45°

Les éléments finis utilisés pour simuler le béton sont des éléments quadratiques solides à 20 nœuds. Les armatures sont des éléments linéaires à 3 nœuds avec une loi de comportement

élasto-plastique et les joncs de carbone sont eux considérés parfaitement élastiques linéaires jusqu'à rupture. La résine epoxy n'est pas modélisée car des études précédentes ont montré qu'elle avait un effet négligeable sur la réponse globale des poutres renforcées par la technique NSM. Pour éviter les problèmes de convergence due à un chargement concentré sur un point du maillage, un chargement sur la frontière a été utilisé pour le calcul. De plus l'accroissement de ce chargement a été contrôlé en déplacement à partir d'un point situé au milieu de la poutre.

La corrosion des armatures longitudinales tendues a été prise en compte comme étant une réduction uniforme de la section d'armatures de 12% car c'est celle qui a été mesuré expérimentalement à mi-portée de la poutre corrodée A1CL3-SB là où s'est ouverte une large fissure de flexion. En revanche, pour l'autre poutre corrodée A1CL3-B, aucune réduction de section n'a été considérée pour le calcul EF en raison du fait que la rupture expérimentale a eu lieu par ouverture d'une large fissure diagonale à un endroit où la corrosion était inexistante.

Les résultats de la simulation numérique montrent une bonne corrélation avec ceux obtenus lors des essais de flexion en termes de raideur et charge de plastification. Néanmoins, il n'a pas été possible de reproduire le comportement total en flexion pour des problèmes de convergence numérique liés à la formation de la fissuration dans le calcul numérique.

Pour les poutres réparées vis-à-vis de l'effort tranchant A1CL3-SB et A1T-SB, les résultats expérimentaux et numériques font apparaître une baisse de charge de plastification de 12% qui est cohérent avec l'intensité de la corrosion également de 12% au milieu de la poutre corrodée (figure I-16).

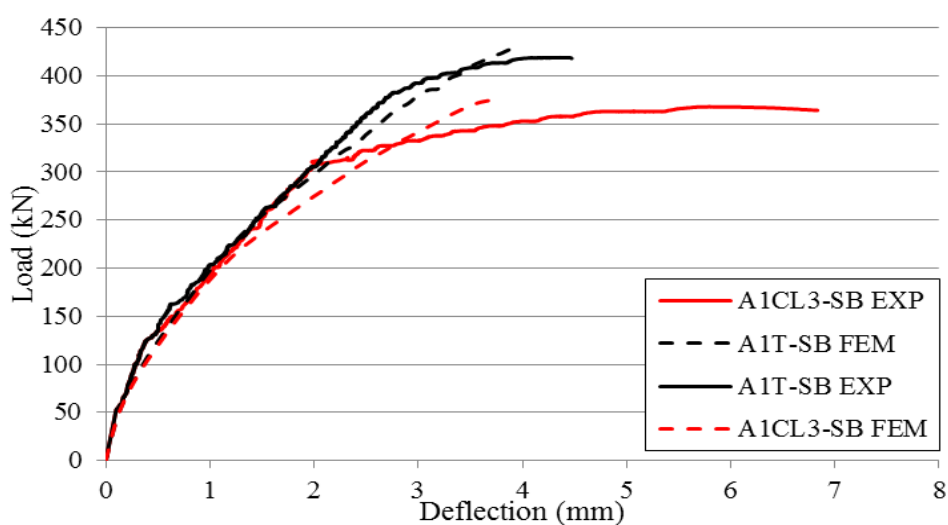


Figure I- 16 Comparaison entre les résultats expérimentaux et les simulations EF pour les poutres réparées vis à vis de l'effort tranchant A1CL3-SB et A1T-SB

Pour les poutres non renforcées vis-à-vis de l'effort tranchant A1CL3-B et A1T-B, on ne constate pas de changement de charge de plastification puisqu'il n'y a pas de corrosion significative à l'endroit où se produisent les fissures les plus ouvertes (figure I-17).

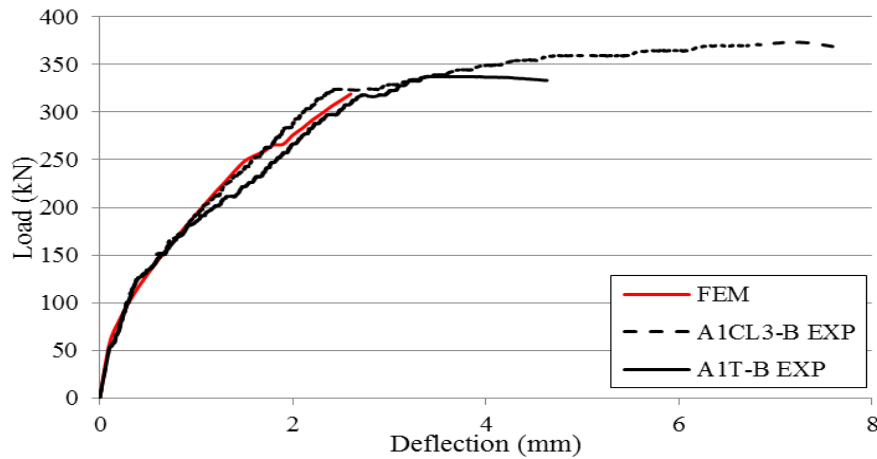


Figure I- 17 Comparaison entre les résultats expérimentaux et les simulations EF pour les poutres non réparées vis à vis du cisaillement A1CL3-B et A1T-B

Les faciès de fissuration ont été obtenus pour le modèle numérique dans les 3 plans de l'espace. Dans le cas des poutres non renforcées vis-à-vis de l'effort tranchant, on retrouve des fissures diagonales qui s'ouvrent (figure I-18), ce qui est cohérent avec les résultats expérimentaux.

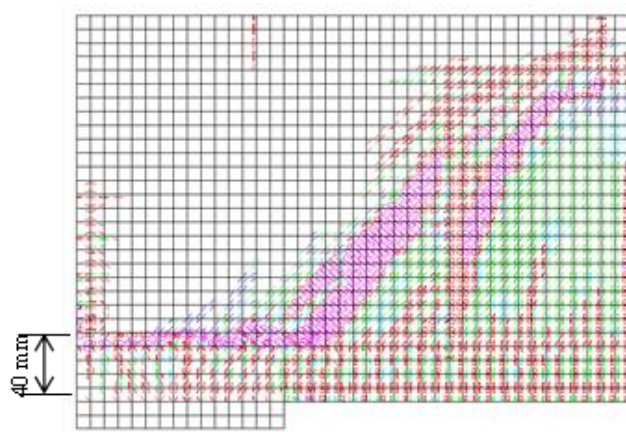


Figure I- 18 faciès de fissuration obtenus par EF pour les poutres non renforcées vis à vis de l'effort tranchant A1CL3-B et A1T-B (en rose les fissures complètement ouvertes, en rouge celles qui s'ouvrent, en bleu les fissures qui se ré-ouvrent, en vert celles qui se ferment et en bleu foncé celles qui sont fermées)

Pour les poutres renforcées vis à vis de l'effort tranchant, les faciès de fissuration obtenus par le calcul EF montre bien le changement de mode de rupture des deux poutres qui correspond à la création de larges fissures au milieu de la poutre au lieu de fissures diagonales au niveau des appuis (figure I-19a). De plus, le modèle EF reproduit bien également les faciès de

fissuration obtenus sur les poutres réparées vis-à-vis de l'effort tranchant avec des fissures s'ouvrant également le long de la surface inférieure de la poutre et jusqu'aux appuis (figure I-19b).

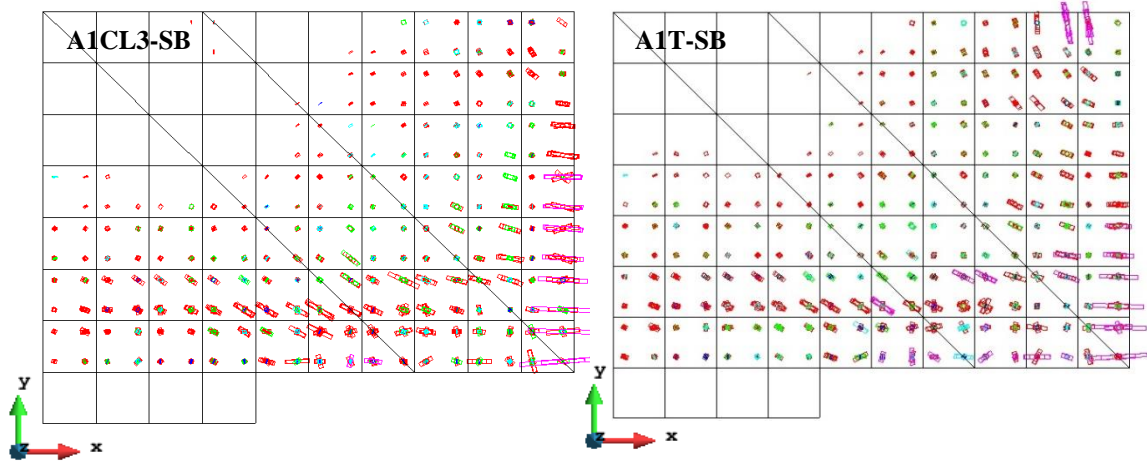


Figure I- 19 (a) faciès de fissuration obtenus par EF pour les poutres renforcées vis à vis de l'effort tranchant (en rose les fissures complètement ouvertes, en rouge celles qui s'ouvrent, en bleu les fissures qui se ré-ouvrent, en vert celles qui se ferment et en bleu foncé celles qui sont fermées).

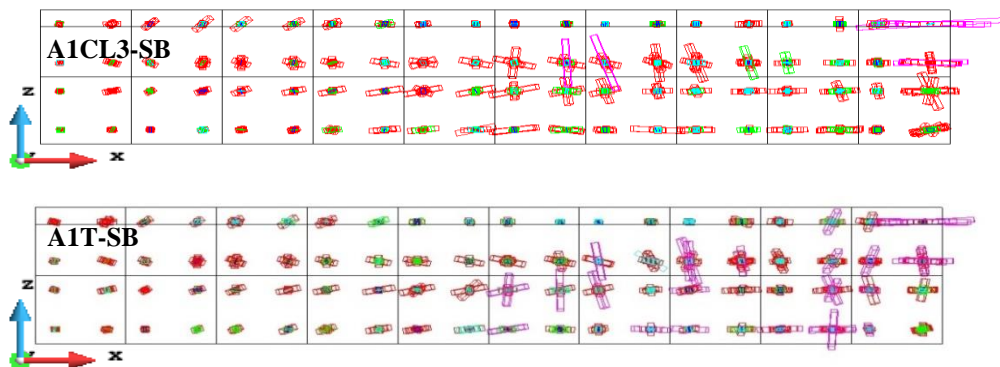


Figure I- 19 (b) faciès de fissuration obtenus par EF pour les poutres renforcées vis à vis de l'effort tranchant dans les plans x-z & y-z (en rose les fissures complètement ouvertes, en rouge celles qui s'ouvrent, en bleu les fissures qui se ré-ouvrent, en vert celles qui se ferment et en bleu foncé celles qui sont fermées).

Il semble ainsi que la technique NSM pourrait être une voie efficace pour la réparation des poutres dégradées par corrosion des armatures. Cependant, l'apparition de nouveaux modes de rupture non-conventionnels méritent une attention particulière et de réaliser des investigations complémentaires pour pouvoir proposer une méthode de réparation faible et complète.

La prise en compte d'une adhérence non-parfaite pour modéliser les glissements aux niveaux des appuis ainsi que le comportement de l'adhérence en présence de corrosion est également une perspective nécessaire des travaux de cette thèse.

Bibliographie

1. Al-Sulaimani G, Kaleemullah M, Basunbul I. Rasheeduzzafar,(1990)“Influence of corrosion and cracking on bond behaviour and strength of reinforced concrete members” ACI Structural Journal, 87 (2), 220-231. ASTM G1. 1990;
2. Andrade C, Alonso C, Garcia D, Rodriguez J. Remaining lifetime of reinforced concrete structures: Effect of corrosion on the mechanical properties of the steel. 1991;
3. Cairns J, Plizzari GA, Du Y, Law DW, Franzoni C. Mechanical properties of corrosion-damaged reinforcement. ACI Mater J. 2005;102(4).
4. François R, Khan I, Dang V. Impact of corrosion on mechanical properties of steel embedded in 27-year-old corroded reinforced concrete beams. Mater Struct. 2013 Jun 1;46(6):899–910.
5. Torres-Acosta AA, Navarro-Gutierrez S, Terán-Guillén J. Residual flexure capacity of corroded reinforced concrete beams. Eng Struct. 2007;29(6):1145–52.
6. Malumbela G, Moyo P, Alexander M. A step towards standardising accelerated corrosion tests on laboratory reinforced concrete specimens. J South Afr Inst Civ Eng. 2012;54(2):78–85.
7. Khan I, François R, Castel A. Structural performance of a 26-year-old corroded reinforced concrete beam. Eur J Environ Civ Eng. 2012;16(3-4):440–9.
8. Dang VH, François R. Influence of long-term corrosion in chloride environment on mechanical behaviour of RC beam. Eng Struct. 2013;48:558–68.
9. Zhu W, François R. Corrosion of the reinforcement and its influence on the residual structural performance of a 26-year-old corroded RC beam. Constr Build Mater. 2014;51:461–72.
10. François R, Khan I, Dang VH. Impact of corrosion on mechanical properties of steel embedded in 27-year-old corroded reinforced concrete beams. Mater Struct. 2013;46(6):899–910.
11. Almusallam AA. Effect of degree of corrosion on the properties of reinforcing steel bars. Constr Build Mater. 2001;15(8):361–8.
12. FIB, Bond of reinforcement in concrete, Bulletin No. 10, The international federation for structural concrete FIB, state of the art report prepared by task group Bond models, 2000, lausanne, switzerland, 427 pp.
13. ACI , Guide for the Design and Construction of Externally Bonded FRP Systems for Strengthening Concrete Structures, 440.2R 02 American Concrete Institute ACI,committe 440, 2002, 45 pp.
14. FIB, technical report bulletin 14, “Externally bonded FRP reinforcement for RC structures”, The international federation for structural concrete FIB, published in Europe (fib, CEB-FIP, 2001).

15. Bilotta A, Ceroni F, Di Ludovico M, Nigro E, Pecce M, Manfredi G. Bond efficiency of EBR and NSM FRP systems for strengthening concrete members. *J Compos Constr.* 2011;15(5):757–72.
16. Nguyen DM, Chan TK, Cheong HK. Brittle failure and bond development length of CFRP-concrete beams. *J Compos Constr.* 2001;5(1):12–7.
17. Al-Mahmoud F, Castel A, François R, Tourneur C. Strengthening of RC members with near-surface mounted CFRP rods. *Compos Struct.* 2009;91(2):138–47.
18. Kreit A, Al-Mahmoud F, Castel A, François R. Repairing corroded RC beam with near-surface mounted CFRP rods. *Mater Struct.* 2011;44(7):1205–17.
19. De Lorenzis L, Nanni A. Shear strengthening of reinforced concrete beams with near-surface mounted fiber-reinforced polymer rods. *ACI Struct J.* 2001;98(1).
20. Islam AA. Effects of NSM CFRP bars in shear strengthening of concrete members. *ASCE*; 2009. p. 1–14.
21. Dias SJ, Barros JA. Performance of reinforced concrete T beams strengthened in shear with NSM CFRP laminates. *Eng Struct.* 2010;32(2):373–84.
22. De Lorenzis L, Nanni A, La Tegola A. Flexural and shear strengthening of reinforced concrete structures with near surface mounted FRP rods. 2000. p. 521–8.
23. Barros JA, Baghi H, Dias SJ, Ventura-Gouveia A. A FEM-based model to predict the behaviour of RC beams shear strengthened according to the NSM technique. *Eng Struct.* 2013;56:1192–206.
24. Rizzo A, De Lorenzis L. Behavior and capacity of RC beams strengthened in shear with NSM FRP reinforcement. *Constr Build Mater.* 2009;23(4):1555–67.
25. Hawileh RA. Nonlinear finite element modeling of RC beams strengthened with NSM FRP rods. *Constr Build Mater.* 2012;27(1):461–71.
26. Sena Cruz JM, Barros JA, Gettu R, Azevedo ÁF. Bond behavior of near-surface mounted CFRP laminate strips under monotonic and cyclic loading. *J Compos Constr.* 2006;10(4):295–303.
27. Lundqvist J, Nordin H, Täljsten B, Olofsson T. Numerical analysis of concrete beams strengthened with CFRP-A study of anchorage lengths. 2005. p. 247–54.
28. Radfar S, Foret G, Saeedi N, Sab K. Simulation of concrete cover separation failure in FRP plated RC beams. *Constr Build Mater.* 2012;37:791–800.
29. Kang J-Y, Park Y-H, Park J-S, You Y-J, Jung W-T. Analytical evaluation of RC beams strengthened with near surface mounted CFRP laminates. *ACI Spec Publ.* 2005;230.
30. Suryanto B, Nagai K, Maekawa K. Modeling and analysis of shear-critical ECC members with anisotropic stress and strain fields. *J Adv Concr Technol.* 2010;8(2):239–58.

31. Barros JA, Costa IG, Ventura-Gouveia A. CFRP flexural and shear strengthening technique for RC beams: experimental and numerical research. *Adv Struct Eng.* 2011;14(3):551–71.
32. Nanni A, Di Ludovico M, Parretti R. Shear strengthening of a PC bridge girder with NSM CFRP rectangular bars. *Adv Struct Eng.* 2004;7(4):297–309.
33. Bianco V, Barros JA, Monti G. A new approach for modelling the NSM shear strengthening contribution in reinforced concrete beams. 2007;
34. Castel A, François R, Arliguie G. Mechanical behaviour of corroded reinforced concrete beams—Part 1: experimental study of corroded beams. *Mater Struct.* 2000;33(9):539–44.
35. Vidal T, Castel A, François R. Corrosion process and structural performance of a 17 year old reinforced concrete beam stored in chloride environment. *Cem Concr Res.* 2007;37(11):1551–61.
36. Poursae A, Hansson C. Potential pitfalls in assessing chloride-induced corrosion of steel in concrete. *Cem Concr Res.* 2009;39(5):391–400.
37. Otieno M, Beushausen H, Alexander M. Prediction of corrosion rate in reinforced concrete structures—a critical review and preliminary results. *Mater Corros.* 2012;63(9):777–90.
38. Yuan Y, Ji Y, Shah SP. Comparison of two accelerated corrosion techniques for concrete structures. *ACI Struct J.* 2007;104(3).

II. General Introduction

Reinforced concrete is considered as relatively new construction material developed and used extensively only since the 20th century. Concrete is a durable material and a protective environment for the embedding steel as it protects it with a dense covering material and allows it to function effectively as reinforcement. It is an ideal environment for steel but if the chloride ions from de-icing salts or sea water penetrate into the concrete through the cracks and pores reaching the steel bars surface causing steel corrosion.

Corrosion leads to cross-sectional loss of the steel bars which can be reflected on the mechanical behaviour of the RC structures in terms of yielding capacity, ultimate capacity and ultimate deflection. Moreover, the corrosion will lead to volume increase and will cause cracks in the concrete. Additionally the corrosion will decrease the bond strength between the steel re-bars and the concrete interface (1–3). The mechanical behaviour of the corroded RC beams were studied by different researchers, most of the studies showed that the corrosion can significantly affect the ultimate capacity of the RC structures and can lead to the early premature failure of the steel reinforcements.

Recently, fiber reinforced polymer materials (FRP) have progressively replaced conventional concrete and steel in the strengthening of the RC structures (4,5), in the last years the significant and increasing need of FRP to be used in structural strengthening and repair is due to the main following advantages: low weight, not time consuming in terms of installation process, high tensile strength and the availability in different sizes and geometry shapes (4).

The most common strengthening technique is based on the application of the FRP on the surface of the elements to be strengthened as externally bonded reinforcement (EBR) technique. The last research results on the EBR technique showed that this technique cannot fully exploit the high tensile strength of the FRP material due to the early debonding (6,7). Moreover, the EBR technique is exposed to the accidents and the mechanical damages.

A new strengthening technique called Near Surface Mounted (NSM) FRP reinforcement is one of the promising techniques, the NSM technique is based on bonding glass (GFRP) or carbon (CFRP) into pre-cut grooves in the concrete cover of the RC elements need to be strengthened or repaired. The NSM technique started to be used in strengthening or repairing the RC structures in 1940s; the re-bars were used at that time to be inserted into the grooves

and then the filled with the cement mortar, nowadays the FRP rods/strips replaced the re-bars and the epoxy adhesive material replaced the cement mortar.

Usually the following main steps are followed to implement the NSM CFRP rods technique (see Fig. II-1):

- Open two cuts into the concrete cover using a special saw-cut machine.
- Clean the remaining concrete lug using a hammer and hand chisel.
- Use the compressed air to clean the remaining dust and rubbles.
- Prepare the epoxy adhesive material according to the manufacturers recommendations.
- Fill the groove with half of the quantity of the epoxy adhesive material then insert the CFRP rod in it.
- Turn the CFRP rod into the groove to be covered in all faces.
- Fill the rest of the quantity of the epoxy adhesive material into the groove in order to ensure no voids. Finally, level the groove's surface.

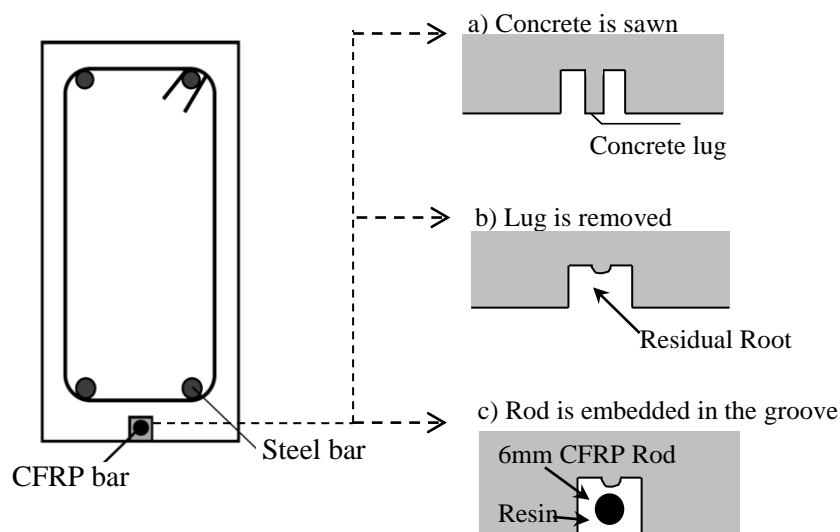


Figure II - 1 Installation of NSM CFRP rod into the concrete surface (8)

The failure modes for RC members strengthened with NSM CFRP rods technique vary from degradation of the strengthening system (pull-out or rupture of the CFRP rod) to compressive concrete crushing (see Fig. II-2), some previous studies showed that strengthening of the RC members with NSM CFRP rods may lead to new non-conventional modes of failure such as the splitting of the concrete cover.

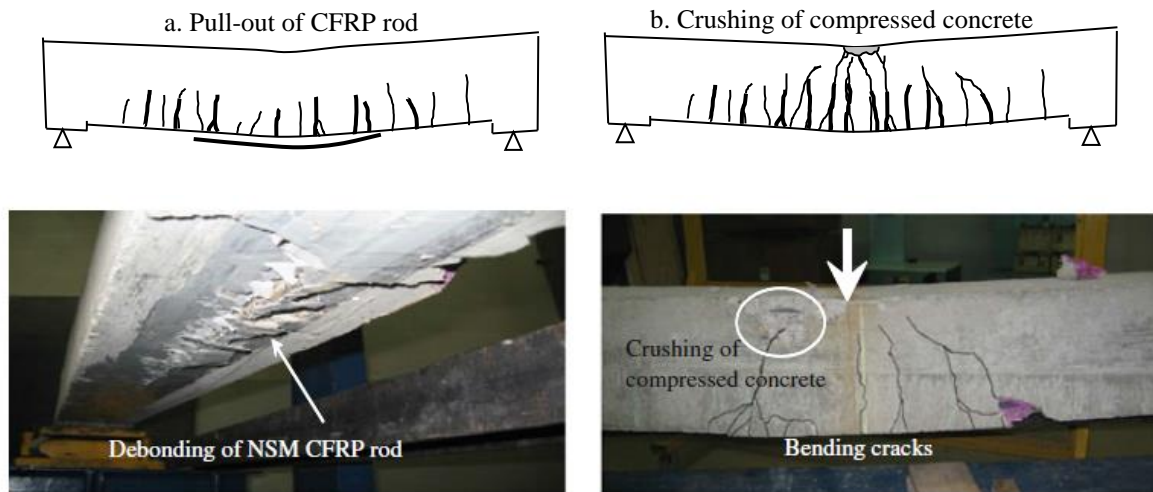


Figure II - 2 Classical failure modes of RC beams strengthened with NSM CFRP rods (9)

Different testing programs were carried out by previous studies in order to assess the shear capacity increase that could be obtained by using the NSM CFRP reinforcement technique, the results showed that the NSM technique could be promising in increasing the shear capacity of the RC beams, some studies were giving some suggestions throughout decreasing the space between the CFRP rods and inclining the rods by 45 degrees to be perpendicular to the shear cracks. Very limited studies focused on the steel corrosion effect on the shear capacity of the RC beams as most of the literature was dealing with the flexural behaviour. While no studies were found on corroded RC beams repaired with NSM CFRP technique in shear.

Most of the available studies on corrosion are based on the accelerating corrosion system using anodic current to the rebar. Few studies were conducted to study the mechanical behaviour of the naturally corroded RC structures and very few studies were dealing with the effectiveness of the repair techniques on those structures.

In the present study the following research methodology was applied. The research is composed of experimental and Finite Element Modeling (FEM) study.

The main two objectives of this study are:

- To study the effectiveness of the NSM CFRP rods technique on the mechanical performance of the naturally corroded RC beams in both shear and bending aspects, including the serviceability aspects, e.g. ultimate deflection and ductility.

- To implement numerical models based on the FEM simulation analysis, in order to simulate the non-linear behaviour of the corroded RC structures repaired with NSM CFRP rods in terms of yielding capacity, ultimate capacity, ultimate deflection and failure modes.

The RC beams used here in this study were exposed to natural corrosion for more than 28 years. The corrosion resulted from a natural process: chloride induced corrosion, without any accelerated process such as impressed current. The resulting corrosion was very scattered from one bar to another and from one section to another, this experimental program aimed at understanding the mechanical behaviour of the corroded RC beams.

The thesis is composed of four chapters; each chapter was organized as research paper which is either published or under the journal review. Those papers are kept in their original journal format in this thesis therefore; there are some repetitions in some sections, e.g. the experimental context, the beams conservation etc.

Chapter 1 aims at studying the post repair performance of two RC beams strengthened with NSM CFRP rods in bending (one corroded beam and one control beam) all are tested in 3-points loading test up to failure. Moreover, it studies the mechanical properties of the corroded steel bars, the experimental results of the RC beams in terms of yielding capacity, ultimate capacity, ultimate deflection and failure modes. The corrosion maps for corroded steel bars and steel stirrups are shown in this chapter for the corroded beam and the corrosion effects on the yielding and ultimate capacity are also presented. The effectiveness of the NSM CFRP rods technique on the RC beams in terms of ductility and beams stiffness are also discussed.

Chapter 2 aims at studying the post repair performance of four short span RC beams, half of those beams are repaired or strengthened with NSM CFRP rods in bending and shear while others are kept repaired or strengthened in bending only (two corroded beams and two control beams) all are tested in three points loading test up to failure. Moreover, it compares the experimental results (shear capacity, yielding capacity and failure modes) with other results obtained from similar but non-repaired beams with NSM, the experimental slip results of the tensile steel bars in the four short beams also was presented in this chapter in comparison with other slip results obtained from similar short non-repaired beams. The NSM effect on shear capacity is discussed. Finally, the effect of span to section depth (effective ratio) (a/d) of the beam on the shear strength is presented.

Chapter 3 aims at implementing non-linear finite element models for the repaired RC beams with NSM CFRP rods in bending (shown in chapter 1) using the FE computer code FEMIX, while more investigation is presented also using another FE commercial software ABAQUS, other non-repaired RC beams are also discussed, all beams are tested in three-points loading test up to failure. Moreover, it compares the experimental results (ultimate capacity, yielding capacity and failure modes) with FE results obtained for repaired and non-repaired RC beams with NSM, the FE models also study the crack patterns and some special failure mode obtained from the experimental results. Finally, the NSM effect is discussed using the FE models.

Chapter 4 aims at implementing non-linear finite element models for the short span RC beams repaired with NSM CFRP rods in shear (shown in chapter 2) using the FE computer code FEMIX. Moreover, it compares the experimental results (ultimate capacity, yielding capacity and modes of failure) with FE results obtained for repaired and non-repaired RC beams with NSM technique in shear. Finally, the FE models investigate the corrosion effect and NSM effect on the shear capacity of the RC beams.

Because of its efficiency, NSM technique could be a promising way to repair RC structures damaged by corrosion. For RC beams repaired in bending, the NSM technique was able to increase the ultimate load capacity of a corroded beam that has suffered considerable damage and allowed it to reach to the ultimate capacity of the control beam (non-corroded one), it also increased both ductility and stiffness of the repaired RC beams and restored sufficient amount of ductility. Nevertheless, the appearance of new non-conventional failure mode needs more investigation to propose a relevant method of design furnishing safe design provisions.

For RC beams repaired in shear, the NSM technique was able to change the failure mode for the shear repaired RC beams from diagonal tension failure to concrete crushing failure. The corrosion of both longitudinal and transversal reinforcement hardly modified the mechanical response of deep beams. Even in presence of corrosion and repairing with NSM CFRP rods, the ratio between the shear span “a” and the effective depth “d” (a/d ratio) appears to be a major parameter.

For RC beams repaired in bending with NSM, the two-dimensional FEM analysis using FEMIX captured the main aspects observed in the experimental tests, while three-dimensional FEM analysis using ABAQUS was able to predict both load-bearing capacity and ultimate deflection reduction due to corrosion if the crack plane induced by corrosion was taken into account in the model. While for RC beams repaired in shear with NSM, the computer code

FEMIX was able to capture the load-deflection curves and failure modes for both repaired and non-repaired RC beams. The effectiveness level of the NSM technique in shear repairing was limited by the semi conical effect of each NSM CFRP rod contribution which led to splitting cracks happened at the middle of the RC beams strengthened in shear.

More investigations are also required in the field of FE modelling of corrosion damaged RC structures repaired with NSM, especially in terms of corrosion simulation along the steel bars and bond-slip relationship between concrete and corroded steel.

References

1. Al-Sulaimani G, Kaleemullah M, Basunbul I. Rasheeduzzafar,(1990)“Influence of corrosion and cracking on bond behaviour and strength of reinforced concrete members” *ACI Structural Journal*, 87 (2), 220-231. ASTM G1. 1990;
2. Andrade C, Alonso C, Garcia D, Rodriguez J. Remaining lifetime of reinforced concrete structures: Effect of corrosion on the mechanical properties of the steel. 1991;
3. Cairns J, Plizzari GA, Du Y, Law DW, Franzoni C. Mechanical properties of corrosion-damaged reinforcement. *ACI Mater J*. 2005;102(4).
4. FIB, technical report bulletin 14, “Externally bonded FRP reinforcement for RC structures”, The international federation for structural concrete FIB, published in Europe (fib, CEB-FIP, 2001).
5. ACI , Guide for the Design and Construction of Externally Bonded FRP Systems for Strengthening Concrete Structures, 440.2R 02 American Concrete Institute ACI,committe 440, 2002, 45 pp.
6. Bilotta A, Ceroni F, Di Ludovico M, Nigro E, Pecce M, Manfredi G. Bond efficiency of EBR and NSM FRP systems for strengthening concrete members. *J Compos Constr*. 2011;15(5):757–72.
7. Nguyen DM, Chan TK, Cheong HK. Brittle failure and bond development length of CFRP-concrete beams. *J Compos Constr*. 2001;5(1):12–7.
8. Kreit A, Al-Mahmoud F, Castel A, François R. Repairing corroded RC beam with near-surface mounted CFRP rods. *Mater Struct*. 2011;44(7):1205–17.
9. Kreit A. Prolongation de la durée de vie des hôpitaux, PhD thesis at l’Institut National des Sciences Appliquees de Toulouse, France. 2012.

Chapter 1

Flexural strengthening of corroded RC beams with NSM CFRP rods, an experimental part

Introduction

This chapter aims at studying the post repair performance of two RC beams strengthened with NSM CFRP rods in bending, one is corroded beam A1CL3 and one is control A1T, both beams were 29 years-old, they were part of long-term corrosion program was carried out in the LMDC (laboratory of materials and durability of constructions), the series of full-scale RC beams were casted and stored in a chloride environment in order to improve the knowledge about the corrosion process of the reinforcing steel bars as well as to study the mechanical properties of corroded RC beams. This chapter presents the experimental results of the two beams repaired in bending with NSM technique using one 6mm diameter CFRP rod (both beams were noted with “R” letter due to bending repair with NSM) and then tested in 3-points loading tests up to failure, the experimental results of the corroded repaired beam A1CL3-R were compared to the control repaired beam A1T-R and also to similar non-repaired RC beams; corroded RC beams: A2CL3 (26 years-old tested by Khan et al. (8)) and A2CL1 (27 years-old tested by Dang and François (9)), and control RC beams: A2TI and A2T tested by (8) and (9) respectively.

The cracking maps were drawn for both beams (A1CL3-R and A1T-R), which were then tested until failure, the moment-deflection curves were recorded for both beams. The corrosion distribution and diameter losses of the steel bars were studied. In order to assess the effectiveness of the NSM CFRP rods technique, the ultimate capacity and the ultimate deflection values of the repaired RC beams (the corroded A1CL3-R and the control A1T-R) were compared to other non-repaired RC beams (the corroded A2CL3, A2CL1 and the control A2T, A2TI). The NSM effect on the yielding capacity, ductility and stiffness of the repaired RC beams was also discussed. Moreover, it shows the difference in the failure modes of the repaired RC beams from the non-repaired RC beams especially for the corroded RC beam.

Mechanical behaviour of corroded RC beams strengthened by NSM CFRP rods

Belal ALMASSRI (1), Amjad KREIT (1), Firas AL MAHMOUD (2), Raoul FRANCOIS (1)

(1) *Université de Toulouse; UPS, INSA, LMDC (Laboratoire Matériaux et Durabilité des Constructions), France*

(2) *Institut Jean Lamour, CP2S, Nancy Université, UPVM, CNRS, IUT NB, 54601 Villers-lès-Nancy, France*

Keywords: corrosion, repair, RC beams, NSM rods, deflection, stiffness.

ABSTRACT

Corrosion of steel in reinforced concrete leads to several major defects. Firstly, a reduction in the cross-sectional area of the reinforcement and in its ductility results in premature bar failure. Secondly, the expansion of the corrosion products causes concrete cracking and steel–concrete bond deterioration and also affects the bending stiffness of the reinforced concrete members, causing a reduction in the overall load-bearing capacity of the reinforced concrete beams. This paper investigates the validity of a repair technique using Near Surface Mounted (NSM) carbon-fibre-reinforced polymer (CFRP) rods to restore the mechanical performance of corrosion-damaged RC beams. In the NSM technique, the CFRP rods are placed inside pre-cut grooves and are bonded to the concrete with epoxy adhesive.

Experimental results were obtained on two beams: (a corroded beam that had been exposed to natural corrosion for 25 years and a control beam, both are 3 metres long) repaired in bending only. Both beams were repaired with one 6-mm-diameter NSM CFRP rod. The beams were tested in a three-point bending test up to failure. Overall stiffness and crack maps before and after the repair were studied. Ultimate capacity, ductility and failure mode were also reviewed. Finally some comparisons were made between repaired and non-repaired beams in order to assess the effectiveness of the NSM technique. The experimental results showed that the NSM technique improved the overall characteristics (ultimate load capacity and stiffness) of the control and corroded beams and allowed sufficient ductility to be restored in repaired corroded elements, thus restoring the safety margin, despite a non-classical mode of failure with the separation of the concrete cover that occurred in the corroded beam due to corrosion products.

1.1 Introduction

Corrosion of reinforcing steel is still a very necessary area of study for infrastructure built of reinforced concrete. The cost of rehabilitating corroded RC structures worldwide exceeds \$1.8 trillion per year (1). The corrosion of steel bars in the RC elements leads to many major defects. Firstly, the corrosion of steel bars leads to a reduction in the cross sectional area of the steel reinforcement and a significant reduction in its ductility, which leads to early failure of the steel bars. Secondly, the corrosion products increase the volume of the bars and set up internal pressure that leads to the cracking of the RC elements and bonding problems between the steel bars and the concrete, and also affect the bending stiffness of the RC elements (2–4). The damage due to corrosion is difficult to evaluate and NDT methods do not permit the loss of cross-section to be determined. In contrast, destructive methods give information on the loss of cross-section but the results are largely scattered due to the heterogeneity of the corrosion pattern (5)

The consequences of corrosion on the residual mechanical properties of RC elements have been widely studied in recent decades. Experimental studies using electrically accelerated corrosion (6,7) or climate accelerated processes (8–10) have shown that the loss of load-bearing capacity is related to the maximum loss of cross-section: from 0.7% to 1.1% of loss in load-bearing capacity for 1% loss of cross-section. Corrosion of steel bars leads to a reduction in ultimate elongation (5,10,11); which induces a change in the failure mode of RC elements from classical ductile behaviour to brittle behaviour with a large reduction of ultimate deflection. For example, Khan et al. (8) recorded a total decrease of 53% in the ultimate deflection of a long-term corroded beam compared to a control beam, and a reduction of 17% was found in load bearing capacity while the average cross-sectional loss in the corroded beam was 21.5%. Dang and François (9) found that the mechanical performance after 27 years of corrosion was reduced in terms of both ultimate load capacity (26% loss of ultimate capacity in the corroded beam compared to the control beam) and ductility (47% loss of ductility in the corroded beam compared to the control beam). As a result, ductility would be the major problem in terms of the rehabilitation standards for corroded RC members.

To increase the service life of corroded reinforced concrete structures, it is necessary to repair and then to increase both load bearing and deformation capacity. During recent years, many researchers have studied how to strengthen the reinforced concrete elements using externally bonded fibre-reinforced polymer EBR (FRP) laminates (12–15). A new strengthening

technique called Near Surface Mounted (NSM) FRP reinforcement has attracted much research and practical applications. The NSM technique requires grooves to be cut in the concrete cover then the FRP reinforcement to be bonded to the concrete and, finally, the grooves to be filled with epoxy or cement grout. Bilotta et al. (16) showed that the tensile strength of FRP material used in the NSM technique was highly exploited and the debonding was delayed compared to the EBR technique. The NSM FRP rods technique is considered to have some other advantages compared with other strengthening techniques like EBR. De Lorenzis and Teng (17) mentioned some of those advantages. Firstly, NSM bars are protected by the concrete cover so they are less exposed to accidental damage like fire. Secondly, much less time and work is needed to fix and install the NSM FRP rods than in the EBR technique.

In several cases, the strengthening of RC members by NSM CFRP rods leads to non-conventional failure modes. For ordinary beams, the failure mode varies from rupture of tensile reinforcement to compressive concrete crushing and it depends on the ratio between the tensile strength of the reinforcement and the compressive strength of the concrete. But, for strengthened RC members, the failure mode varies from degradation of the strengthening system to compressive concrete crushing and depends on the ratio of a combination of CFRP cross-section and CFRP length to the concrete compressive strength (18).

Ductility is an important structural design parameter in most of design codes. In RC members, ductility is defined as the ratio of ultimate deformation to yield deformation and allows obtaining an indicator that could be used for warning before failure. Previous studies have observed a ductility reduction in RC beams as a result of corrosion of the tensile steel bars (19,20).

Badawi and Soudki (21) showed a slight reduction in ductility for RC beams strengthened with NSM CFRP rods. Their results also showed that the ductility of the NSM CFRP strengthened beams was reduced as the prestressing level of RC beams increased. The NSM technique could have a small effect on the ultimate elongation of RC members when a classical failure mode is obtained (18). On the other hand, it could lead to more brittle and less ductile state in cases of non-classical failure such as peeling-off, which was observed by Al Mahmoud et al. (22), De Lorenzis et al. (23) and Radfar et al. (24), or pull-out of the CFRP rod, which was observed by Al Mahmoud et al. (25), De Lorenzis and Nanni (26) and De Lorenzis et al. (27).

The use of the NSM technique with FRP rods to repair and to strengthen infrastructure damaged by steel corrosion is very recent and few researchers have studied the subject. Kreit et al. (28) showed that the NSM technique allowed the initial ultimate capacity to be recovered for corroded beams with a 36% loss of cross-section in the maximum bending area. Ductile or brittle failure and the recovery of the ultimate elongation of corroded repaired RC members with NSM FRP rods have not yet been studied.

To increase understanding of the failure modes and the mechanical performance of repaired corroded beams, an experimental work was undertaken to study the possibility of using a 6-mm-diameter NSM CFRP rod to repair a long-term naturally corroded RC beam and it was compared with a repaired control beam. The flexural capacity of the repaired beams was compared with that of non-repaired corroded beams. In a three point bending test, all beams were tested up to failure in order to study their overall bending moment-deflection behaviour, failure modes, stiffness properties and ultimate deflection. The corroded steel bars were extracted from the beams in order to study the corrosion while tensile tests were conducted in order to study the mechanical properties of the steel bars.

1.2 Experimental programme

An experimental programme was started at LMDC (Laboratory of Materials and Durability of Constructions) in 1984 with the aim of understanding the effects of steel corrosion on the structural behaviour of RC elements. This long-term programme consisted of casting a set of 72 RC beams of dimensions $3,000 \times 280 \times 150$ mm. Thirty-six of them were stored in a chloride environment under service load to measure the flexural cracks occurring during the corrosion process. Many experimental studies have been conducted on these beams to evaluate the development of corrosion cracking, to measure chloride content and to analyse the changes in mechanical behaviour (19,29). The other 36 beams were stored under the same mechanical load but in a non-aggressive environment to be used later as control beams to study the same long-term effects, such as creep and ageing of the concrete. The natural aggressive environment system consisted of salt fog spray (35 g/l of NaCl) (see Fig 1-1).

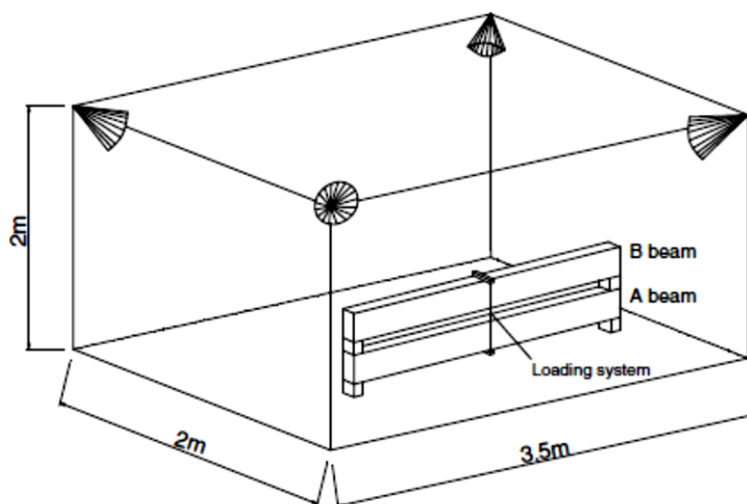


Figure 1 - 1 The climate accelerated aggressive environment system

After 6 years of storage, the beams were subjected to wetting–drying cycles in order to accelerate the corrosion process:

- 0–6 years: continuous spraying under laboratory conditions ($T=20^{\circ}\text{C}$);
- 6–9 years: cyclic spraying under laboratory conditions ($T=20^{\circ}\text{C}$), 1 week of spraying and 1 week of drying;
- 9–19 years: cyclic spraying, 1 week of spraying and 1 week of drying, but the confined room was transferred outside, so the beams were exposed to the outside temperature with monthly-average temperatures ranging from 5.1°C to 21.3°C .
- 19–27 years: cycles were stopped; the beams were still stored in the controlled room and exposed to the outside temperature.
- 27- present: cyclic spraying, 2 days of spraying and 12 days of drying.

The corrosion obtained in this climate-accelerated programme was very close to the corrosion observed under natural conditions in terms of corrosion distribution, corrosion type and oxides produced. It is very important for service life prediction of RC elements to have access to such natural degradation (30), rather than that resulting from the use of an applied current or a CaCl_2 admixture in the concrete (31,32). The beams were divided into two groups named type A and type B, which had different reinforcement layouts but the same reinforcing steel bar (yield strength = 500 MPa). Beams A and B had 40 mm and 10 mm of concrete cover respectively. According to French standards at the time of manufacturing (33), the 40 mm cover represents the minimum concrete cover in very aggressive environments (i.e. chloride aggression) and the 10 mm cover represents the minimum concrete cover in a non-aggressive

environment. The beams were loaded in three-point flexure by coupling a type A beam with a type B beam. Two loading values were applied: $M_{ser1}=14$ kN.m for beams referred to as A1 (A1CL3-R and A1T-R) and $M_{ser2}=21$ kN.m for beams referred to as A2 (A2CL1, A2CL3, A2T and A2TI), which had the same type and shape of reinforcement but different values of service loading. The beams studied in this paper are all type A beams; one corroded beam (A1CL3-R) and one control beam (A1T-R). Long-term corroded beams A2CL1, A2CL3, A2TI and A2T tested by (8,9) but not repaired were also used here for comparison. The control beam A1T-R was strengthened using the same method as the one used to repair the corroded beam A1CL3-R. The layout of the reinforcement is shown in Fig. 1-2. For these beams, M_{ser1} represented the maximum loading value for durability in an aggressive environment for the type A beam (serviceability limit-state requirements in an aggressive environment).

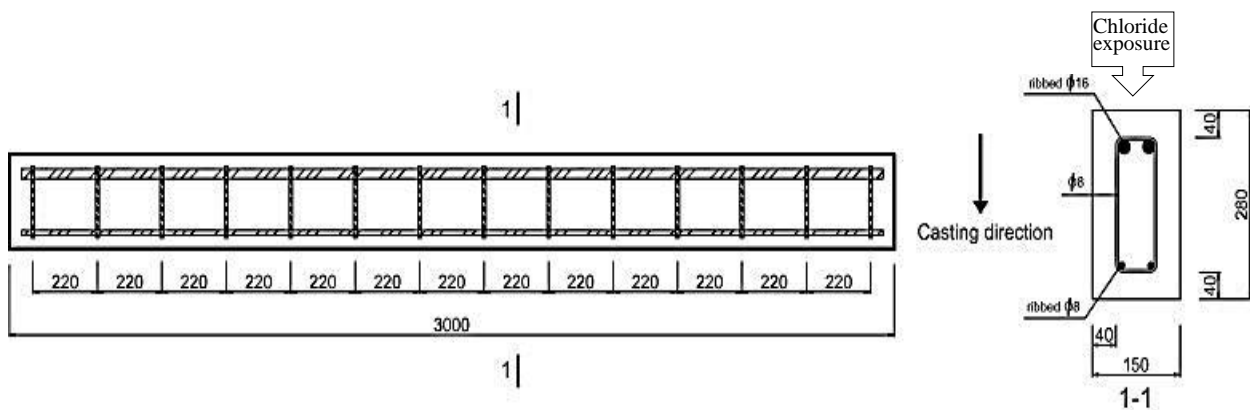


Figure 1 - 2 Reinforcement layout for Type A beams. Dimensions are in mm

1.2.1 Material properties

1.2.1.1 Concrete properties

The concrete mix is given in Table 1-1. The Water/Cement ratio was 0.5 but could be adjusted by changing the water quantity to obtain a constant workability of 7 cm in the slump test (slump class S2) in order to meet the most commonly specified consistence according to European Standard EN 206-1 (34). The average compression stress and the elastic modulus obtained on three cylindrical specimens ($\phi 11 \times 22$ cm) (according to (34)) were 45 MPa and 32 GPa respectively tested after 28 days. The tensile strength, measured using the splitting test, was 4.7 MPa. Water porosity was 15.2%. To measure concrete characteristics, cylindrical cores, 70×140 mm, were drilled out of both the corroded and control beams and tested in compression. Table 1-2 gives the results of these core tests.

Table 1 - 1 Concrete mix and cement chemical composition

Mix component	mm	kg/m ³
Rolled gravel (silica + limestone)	5/15	1 220
Sand	0/5	820
Portland cement: OPC HP		400
Water		200

Table 1 - 2 Mechanical characteristics of the concrete at 27 years (average of 3 tests)

Mechanical characteristics	A1CL3-R	A1T-R
Compression strength (MPa)	62.2	58.9
Elastic modulus (MPa)	33 700	29 700

1.2.1.2 Characteristics of steel bars, CFRP bars and filling material

The steel reinforcing bars were composed of natural S500 half-hard steels; ordinary ribbed reinforcing steel bars were used. The steel bar characteristics were measured after extracting the corroded bars from the corroded beam A1CL3-R and the results are shown in Table 1-3

Table 1 - 3 Effective mechanical properties of steel bars (calculated from the residual cross-section)

Specimen number	Yield		Ultimate	
	Strength(MPa)		Strength(MPa)	
		Avg		Avg
Specimen 1 corroded	570	578	708	710
Specimen 2 corroded	585		711	
Specimen 1 non-corroded	595	600	640	645
Specimen 2 non-corroded	605		649	

Al-Mahmoud et al., (35) measured the mechanical properties of CFRP rods through a test programme conducted on 3 specimens tested in axial tension. The CFRP rods showed brittle failure that started with splitting and ended with the failure of the rods as shown in figure 1-3. Table 1-4 shows the mechanical properties of the CFRP rods. In order to increase the bonding between the CFRP rods and the filling material, the rods were coated with 0.2/0.3 mm of surface sanding material which was sprinkled onto an epoxy paste applied to the surface of the rods.

Table 1 - 4 Characteristics of CFRP rods

Type of test	Ultimate strength (MPa)	Modulus of Elasticity (MPa)
Manufacturer's test	2300	150000
Laboratory test	1875	145900

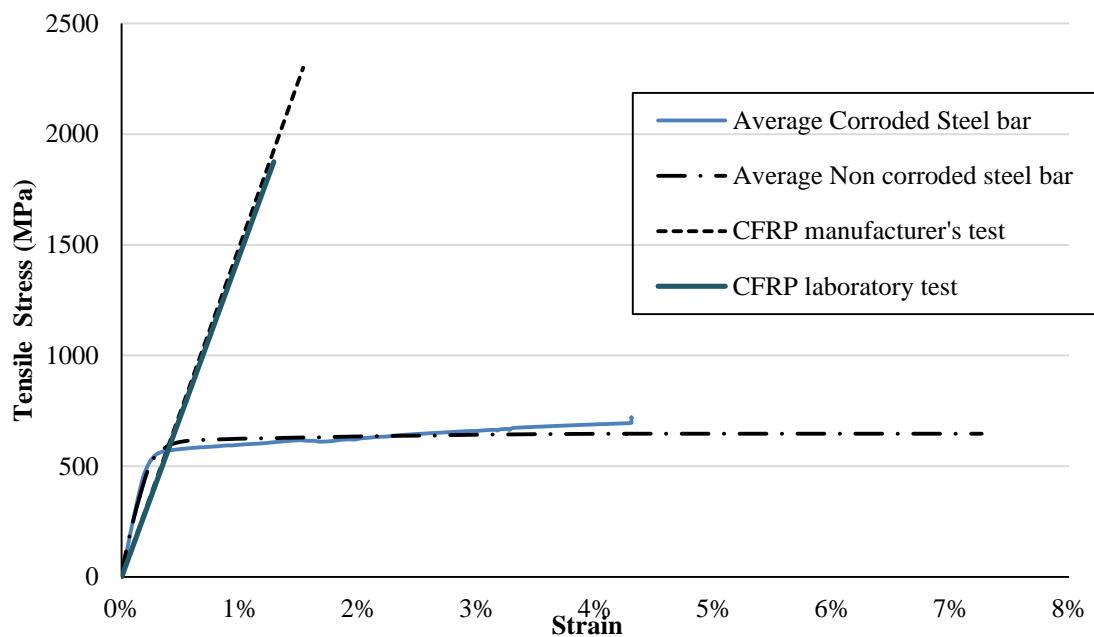


Figure 1 - 3 Stress-strain diagrams for steel and CFRP bars

Table 1-5 shows the characteristics of the filling material (epoxy paste) after 7 days (28):

Table 1 - 5 Filling material properties

Material	Compressive Strength (MPa)	Tensile Strength (MPa)	Elastic Modulus (MPa)
Epoxy	83	29.5	4900

1.2.2 Repair technique

The NSM CFRP rod was installed in the corroded beam A1CL3-R and in the control beam A1T-R by making two cuts in the concrete cover in the longitudinal direction at the tension side. A special concrete saw with a diamond blade was used.

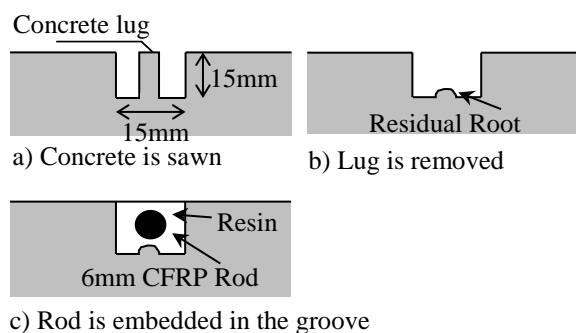


Figure 1 - 4 Installation of CFRP rod into concrete

The remaining concrete lug formed by the sawing was then removed using a hammer and hand chisel so that the lower surface became rough (Figure 1-4). The groove was airbrushed to remove dust, debris and fine particles so as to ensure proper bonding between the paste and the concrete. Then, the groove was half filled and the CFRP rod was placed inside it and pressed lightly. This forced the paste to flow around the CFRP rod. More paste was applied to fill the groove and the surface was levelled. As a result, the CFRP rod was placed in the middle of the cross-section in the tension area. The CFRP rod had a total length of 3000 mm and a diameter of 6 mm, which means that the repair was along the whole length of the beam. The groove was 15 mm deep and 15 mm wide (around twice the rod diameter). The two beams were tested 1 week after installation of the CFRP rod in order to ensure the maximum degree of adhesion between the concrete surface and the epoxy paste material.

1.2.3 Cracking maps of corroded beam A1CL3-R and control beam A1T-R

Figures 1-5 and 1-6 show the cracking maps of the beams A1CL3-R and A1T-R after 26 years. All the corrosion cracks were concentrated in the tension area of the concrete and their maximum width was found to be 1.8 mm. Only the width of longitudinal cracks was measured using a binocular lens. The transversal cracks were due to the initial and sustained loading during beam storage. Despite the cover being the same for tension and compression bars, long-term storage in the chloride environment induced mainly corrosion and corrosion cracks along the tension reinforcement.

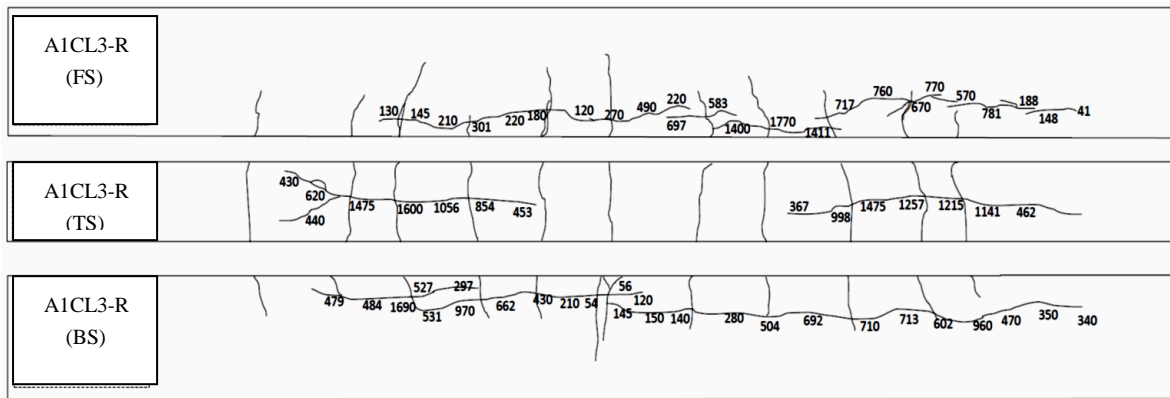
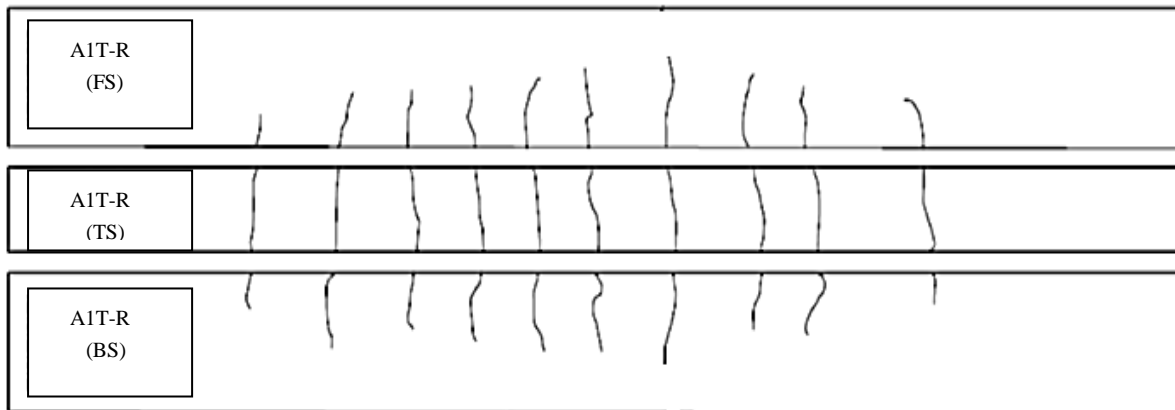


Figure 1 - 5 A1CL3-R cracking map after 20 kN loading



FS (Front Side), TS (Tensile Side), BS (Back Side)

Figure 1 - 6 A1T-R cracking map after 20 kN loading

Dang and Francois (9) and Khan et al. (8) explained this result to be a consequence of:

1. The difference in exposure between the tensile and compression faces; the tensile face was the upper horizontal face exposed directly to salt fog.
2. The casting direction: tension bars were also top bars according to the casting direction and exhibited some interface defects well known as top-bar effects.
3. The tensile face was cracked and the cracks in the upper surface exposed to chloride indicated the most aggressive environment (CEB-FIP model code).

1.3 Experimental results

1.3.1 Mechanical properties of corroded steel bars

Clark's solution ANSI/ASTM G1-72 was used to remove the corrosion from the surface of the steel bars, and then the effect of corrosion on the diameter loss of the steel reinforcement bars was measured using two different methods. The first used a vernier calliper just after cleaning and drying the steel bars and the second used the weight loss of the steel bar to calculate the diameter loss. The second method required the critical parts of corroded steel bars to be cut into small pieces 1-2 cm long and then weighed to an accuracy of 0.001g. A reference mass was measured on bars extracted from the control beam.

Both methods were used to evaluate the diameter loss of the corroded steel bars as some previous papers (5) had shown that the shape of corrosion damage was too complex to be measured only by the vernier calliper, which would give very conservative values of the diameter loss as the residual cross section varied widely around the disk as shown in figure 1-7.

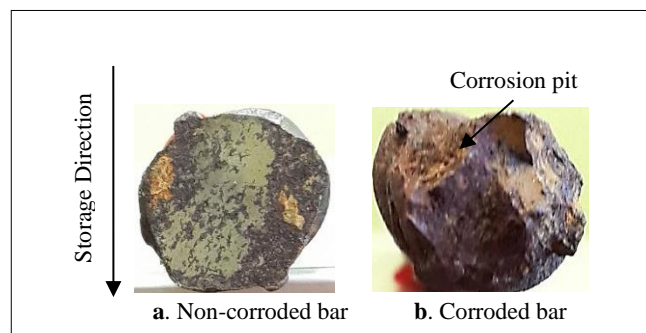


Figure 1 - 7 Non-corroded bar (a) Vs Corroded bar (corrosion pits)

1.3.2 Yielding moment and ultimate strength

Both the repaired corroded beam A1CL3-R and the repaired control beam A1T-R were tested using 3-point loading up to failure. Figure 1-8 shows the bending moment versus the deflection for the two beams. The yielding moment values for A1CL3-R and A1T-R were 41 kN.m and 53 kN.m, respectively, while the ultimate moment values were 52 kN.m and 66 kN.m respectively.

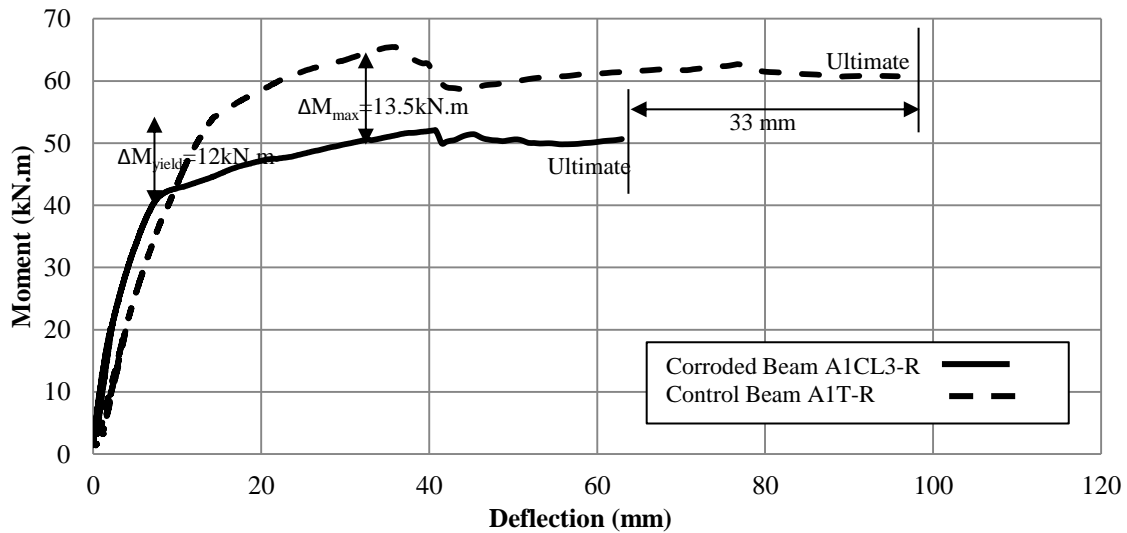


Figure 1 - 8 Bending moment versus deflection

1.3.3 Failure modes

The classical failure modes for RC beams occur either by concrete crushing or by the failure of the tensile steel bars. In the case of Type A beams, the failure of the control beam is normally due to steel bar yielding followed by concrete crushing (8). After strengthening, the failure mode of RC beams can be concrete crushing, pull-out of the FRP rods or peeling off as shown by Al-Mahmoud et al. (18). The failure mode observed for A1CL3-R was different from both the conventional and non-conventional failure modes found on repaired non-corroded beams. The failure mode of the repaired corroded beam A1CL3-R was the separation of the concrete cover as shown in Figure 1-9. The failure of the repaired control beam A1T-R occurred by the crushing of compressed concrete.



a) A1CL3-R Corroded Beam

a) A1T-R Control Beam

Figure 1 - 9 Beams after failure

It should be noted that the failure plane corresponding to the separation of the concrete cover was the plane of corrosion cracks as shown in Figure 1-10.

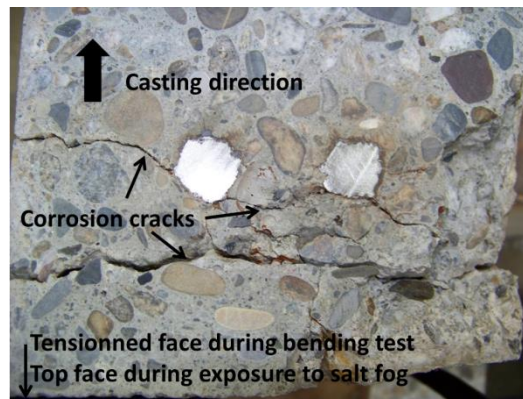


Figure 1 - 10 Corrosion cracks appear in the concrete cover from the steel part closest to the tensile surface exposed to chloride

1.3.4 Losses of diameter due to corrosion for tensile steel bars and steel stirrups in corroded beam A1CL3-R

The values of the diameter losses were calculated for both the Back Side (BS) and Front Side (FS) tensile steel bars, which were extracted from the corroded beam A1CL3-R just after the bending test. Figures 1-11 and 1-12 show the diameter losses against position along the whole length of the beam for BS and FS tensile steel bars. There is corrosion at the top of the bars close to the surface cover, which reflects the classical result for natural corrosion (31) and also at the bottom of the bars because of the effect of casting direction and bar location at the top of the beam, both of which induce poor interface quality (36,37).

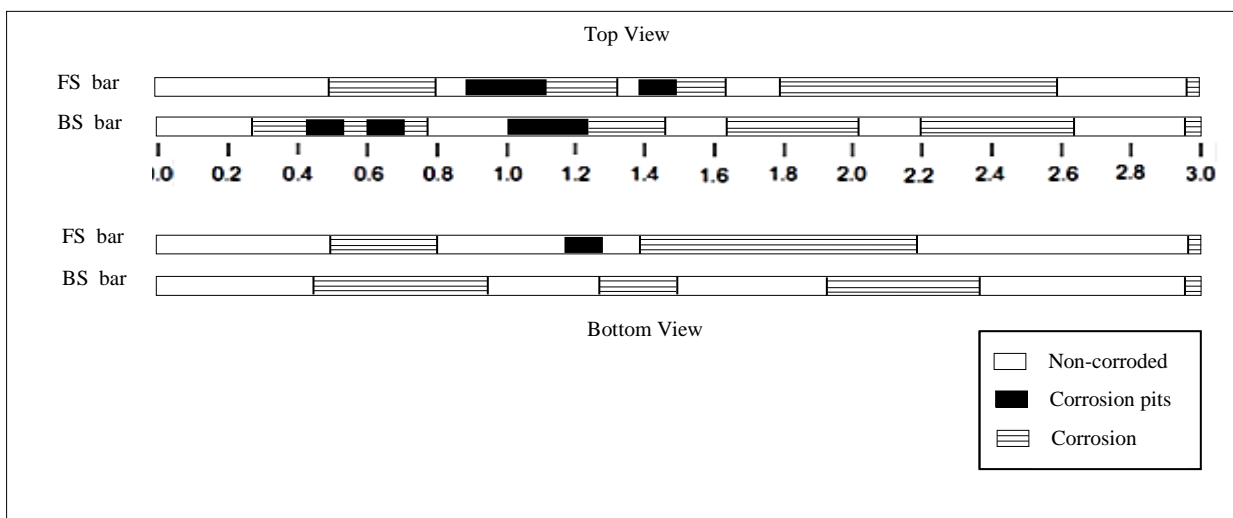


Figure 1 - 11 Corrosion damage along re-bars according to the location in the beams (top or bottom)

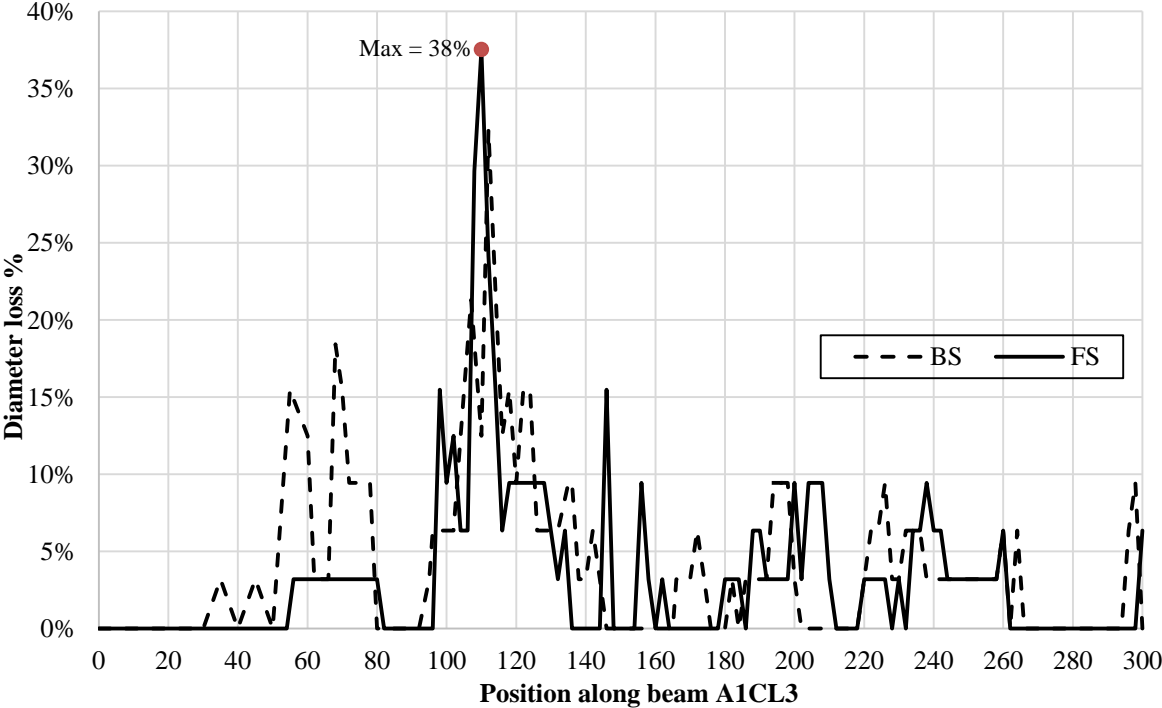


Figure 1 - 12 Diameter loss percentages vs. position along the corroded beam A1CL3-R

The steel stirrups were numbered regarding to their parts (the first number represents the part's number and the second number represents the stirrup's number) as shown in Figure 1-13:

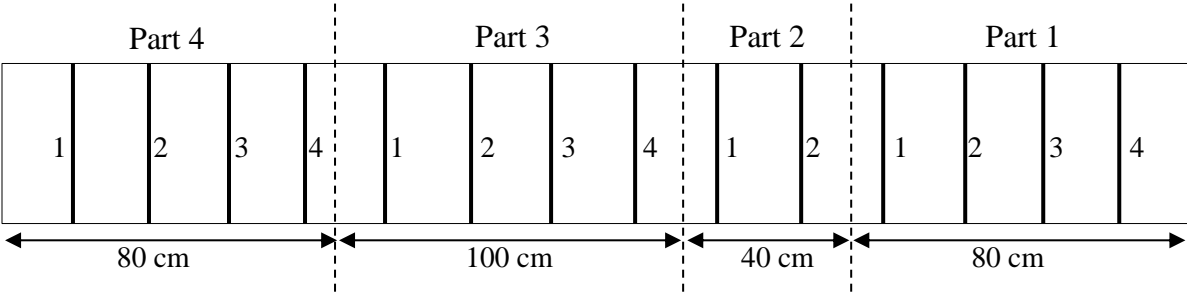


Figure 1 - 13 Parts of beam A1CL3-R

Figure 1-14 shows the locations of corrosion in the steel stirrups and the diameter values:

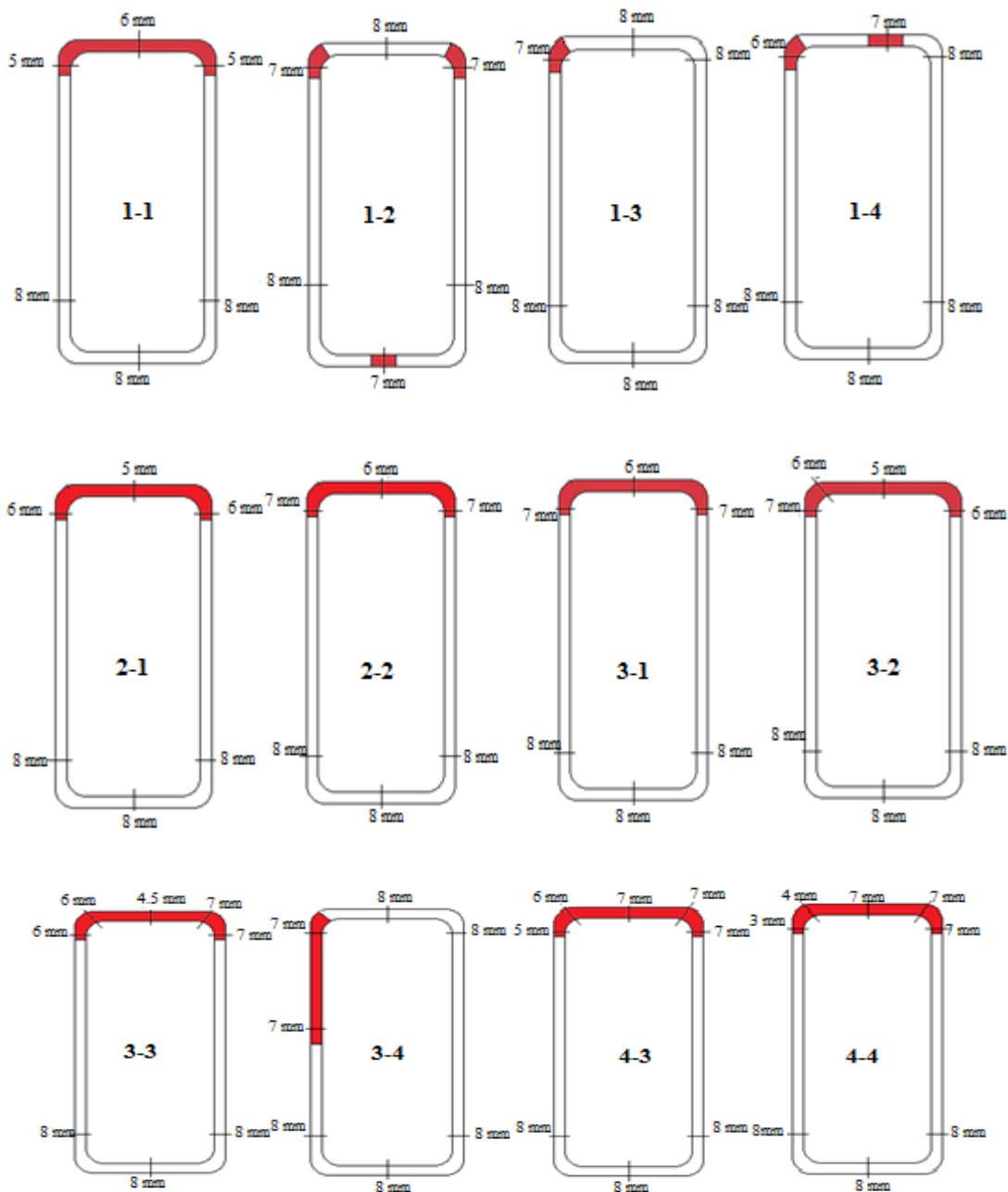


Figure 1 - 14 Corrosion in steel stirrups of A1CL3-R

It can be seen from figure 1-14 that the stirrup corrosion map is in good agreement with the longitudinal bars' corrosion map: parts of the stirrups in contact with compressive steel bars located at the bottom of the beam (according to casting direction) are not corroded, which agrees with the absence of corrosion in compressive longitudinal steel bars. On the other hand, parts of the stirrups in contact with tensile steel bars are corroded and, in some places, highly corroded, with 50% of cross-section loss. It should also be noted that there is no evidence of a difference in long-term corrosion damage of stirrups between those located near

the flexural cracks and those located in the non-cracked parts near the supports. This confirms that there is no relation between mechanical cracks and long-term corrosion for natural corrosion as described by Beeby (38) and François et al. (39).

There was no corrosion along the vertical parts of stirrups located near the flexural cracks or even in the non-cracked area which agrees with the long-term results presented by François et al. (39) and showing the beneficial effect of interface quality even in presence of cracks. The vertical surface here had a good interface quality and there was no mechanical damage or defects due to casting, such as bleeding.

1.3.5 Ultimate capacity

Table 1-6 and Figure 1-15 present the ultimate bending moment capacity for repaired corroded and control beams, in comparison with non-repaired corroded and control beams. For non-repaired corroded beams, the residual ultimate load capacity is correlated with the maximum loss of cross-section: beam A2CL3, with 33% max. diameter loss in tensile steel bars, shows a higher capacity than beam A2CL1 with 44% max. diameter loss in tensile steel bars. The results also show that the repaired corroded beam A1CL3-R (38% max. diameter loss in tensile steel bars) has higher ultimate bending moment capacity than either A2CL1 or A2CL3 with 17 kN.m and 11 kN.m respectively.

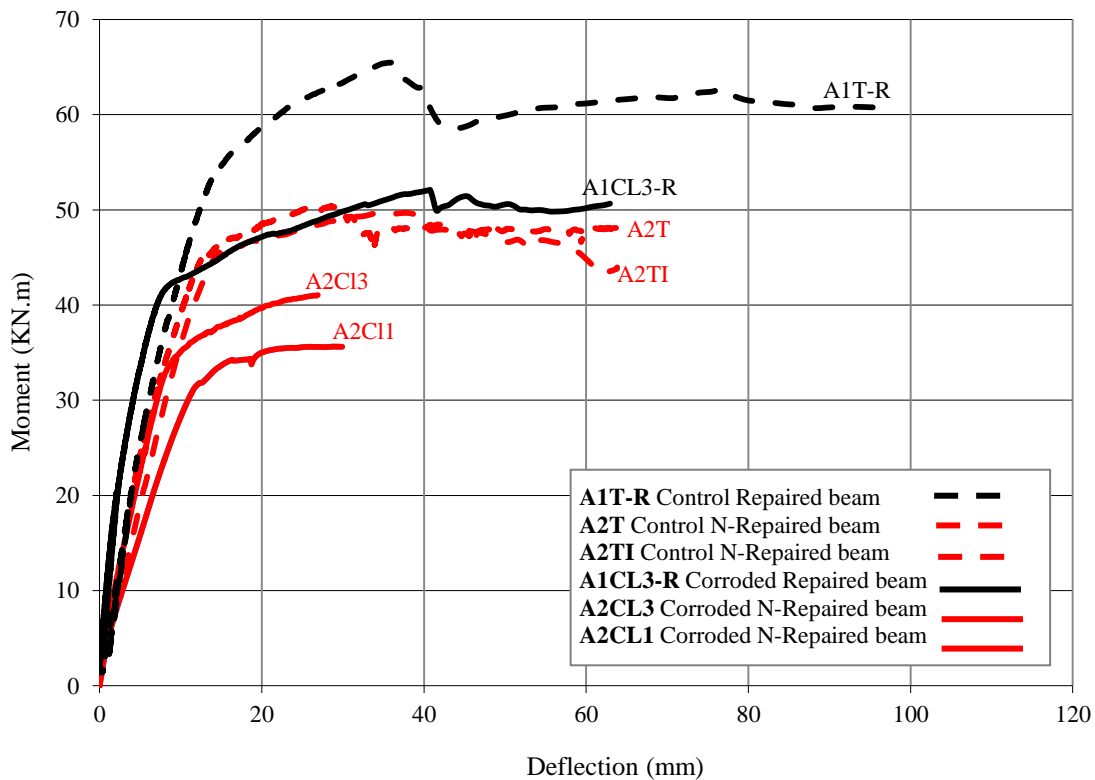


Figure 1 - 15 Comparisons of moment capacity (A2T, A2TI, A1T-R, A2CL3, A1CL3-R and A2CL1 (8,9))

Figure 1-15 also shows that both ultimate bending moment capacity and ultimate deflection of the control beam A1T-R (repaired using the NSM technique) were higher than the ultimate capacity of non-repaired control beams A2T or A2TI.

1.3.6 Ultimate deflection

Figure 1-16 presents the ultimate deflection values for corroded and control beams at failure points. The ultimate deflection value (93 mm) for repaired control beam A1T-R at the failure point was more than the ultimate deflection value for non-repaired control beams A2T (64 mm) and A2TI (64 mm). Results showed that the ultimate deflection value for repaired corroded beam A1CL3-R (63 mm) was higher than the ultimate deflection values for the corroded non-repaired beams A2CL3 and A2CL1 (28 mm and 30 mm respectively). On the other hand, the ultimate deflection for A1CL3 was almost the same as the ultimate deflection for non-repaired control beams A2T and A2TI. Thus, repairing the corroded beam with the NSM technique doubles the ultimate deflection value compared to that of non-repaired corroded beams while the NSM increases the ultimate deflection for control beams 1.5 times relative to the non-repaired beams.

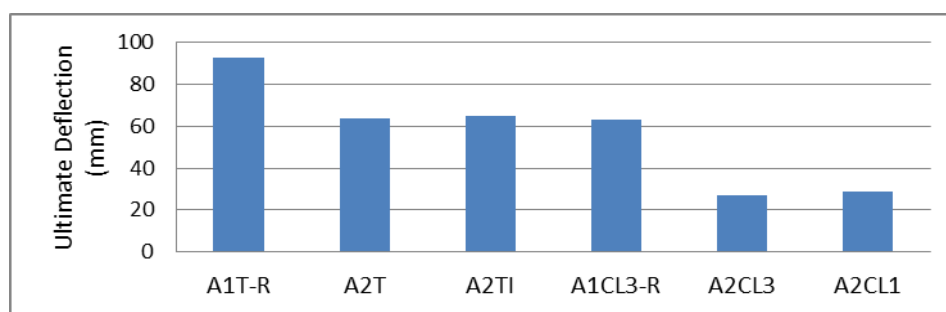


Figure 1 - 16 Deflection (mm) for beams at failure

Table 1 - 6 Experimental results for all beams

Beam	Description	Max diameter loss % (1)	Failure mode	Ultimate moment (kN.m)	Ultimate deflection (mm)	Ultimate Deflection loss % (2)	Ratio (2)/(1)
A1T-R	Repaired control beam	0	Concrete crushing	65.5	93	-	0
A1CL3-R	Repaired corroded beam	38	Separation of concrete cover	52.1	63	32*	0.84
A2T (Dang and François, (9))	Non-repaired control beam	0	Concrete crushing	50.9	64	-	0
A2TI (Khan et al, (8))	Non-repaired control beam	0	Concrete crushing	49.7	63.8	-	0
A2CL3 (Khan et al, (8))	Non-repaired corroded beam	33	Failure of corroded steel bar	40.9	28	56**	1.7
A2CL1 (Dang and François, (9))	Non-repaired corroded beam	44	Failure of corroded steel bar	35.6	29.9	53**	1.2

* Compared to control repaired beam A1T-R

** Compared to control non-repaired beam A2T

1.3.7 Percentage increase in the yielding capacity for beams repaired with NSM FRP rods

Figure 1-17 presents the theoretical percentage increase of the repaired beams (shown in Appendix) over the non-repaired beams of type A in terms of yielding capacity in comparison with experimental results. An increase of 19% (Table 1-7) was recorded in the repaired corroded beam A1CL3-R compared to the non-repaired one while an increase of 18% was found in the repaired control beam A1T-R compared to A2T (non-repaired control beam tested by Khan et al, (8)). The percentage of difference between the repaired corroded beam A1CL3-R and the repaired control beam A1T-R was 20.7% due to the loss of steel diameter in the corroded beam (20%) assumed at the middle of the beam. Table 1-7 presents the details of the increase in yielding capacity for the beams A1CL3-R and A1T-R.

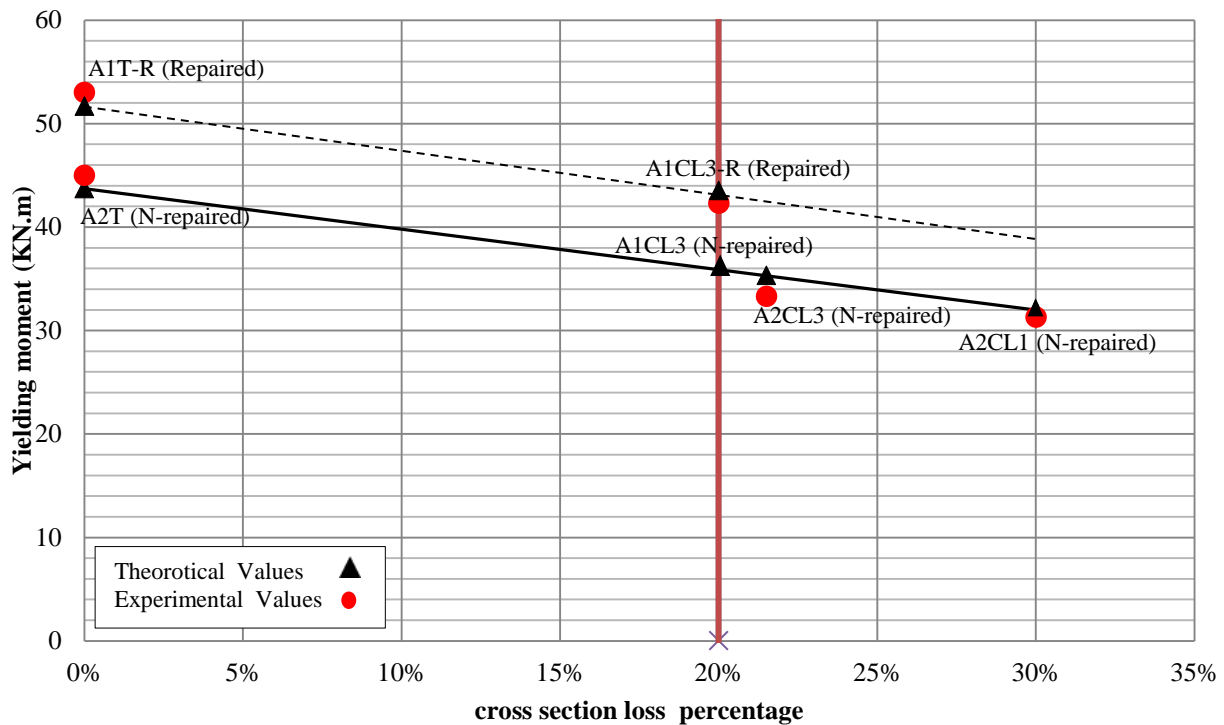


Figure 1 - 17 Yielding capacity increase

Table 1 - 7 Calculated values of (Yielding moment) M_y

Beam	M_y , repaired (kN.m)	M_y , non-repaired (kN.m)	Increase percentage
A1CL3-R	43.5	36.5	19
A1T-R	51.7	43.7	18

Figure 1-17 also shows the percentage increase in M_y of the corroded (non-repaired) beams (A2CL3 and A2CL1). If they were repaired with the same process they would have an increase of 18.9% and 18.8% respectively (almost the same increase for both beams as shown by the parallel lines in figure 1-17). This percentage of increase falls as the percentage of steel diameter loss decreases.

1.3.8 Effect of corrosion on both yielding and ultimate capacity

Table 1 - 8 Comparison of loss of cross sections against the loss of ultimate and yielding experimental values

Beam	Avg loss of cross section % at the middle (1)	Yielding capacity (kN.m)	Ultimate capacity (kN.m)	Loss of yielding capacity % (2)	Loss of ultimate capacity % (3)	(3)/(1) ratio	(2)/(1) ratio
A2T	0	45	50.9	0	0	0	0
A2CL3	21.5	32.5	40.9	27.8	19.6	0.7	1
A2CL1	30	31.3	35.6	30.4	34	1.1	1
A1T-R	0	53	65.5	0	0	0	0
A1CL3-R	20*	42.3	52.1	20.6	20.5	1	1

* Note: $M_y = 42.3$ kN.m meets 20% loss of cross section at the middle of the beam.

Table 1-8 shows that every 1% loss of cross section corresponds to 1% loss of yielding capacity, while there is more scatter in the case of the ultimate capacity as the failure mode varies for each beam (e.g. 1% loss of cross section corresponds to 0.7% loss of ultimate capacity for A2CL3 while it corresponds to 1.1% for A2CL1 and 1% for A1CL3-R).

1.3.9 Stiffness of beams

The two beams A1CL3-R and A1T-R were loaded with a 20 kN service load before starting the repair process. They were also tested with 20 kN after the repair with NSM. Figure 1-18 shows the values of the stiffness (the slope value before the yielding point is reached) for both beams before and after the repair process (stiffness ratio).

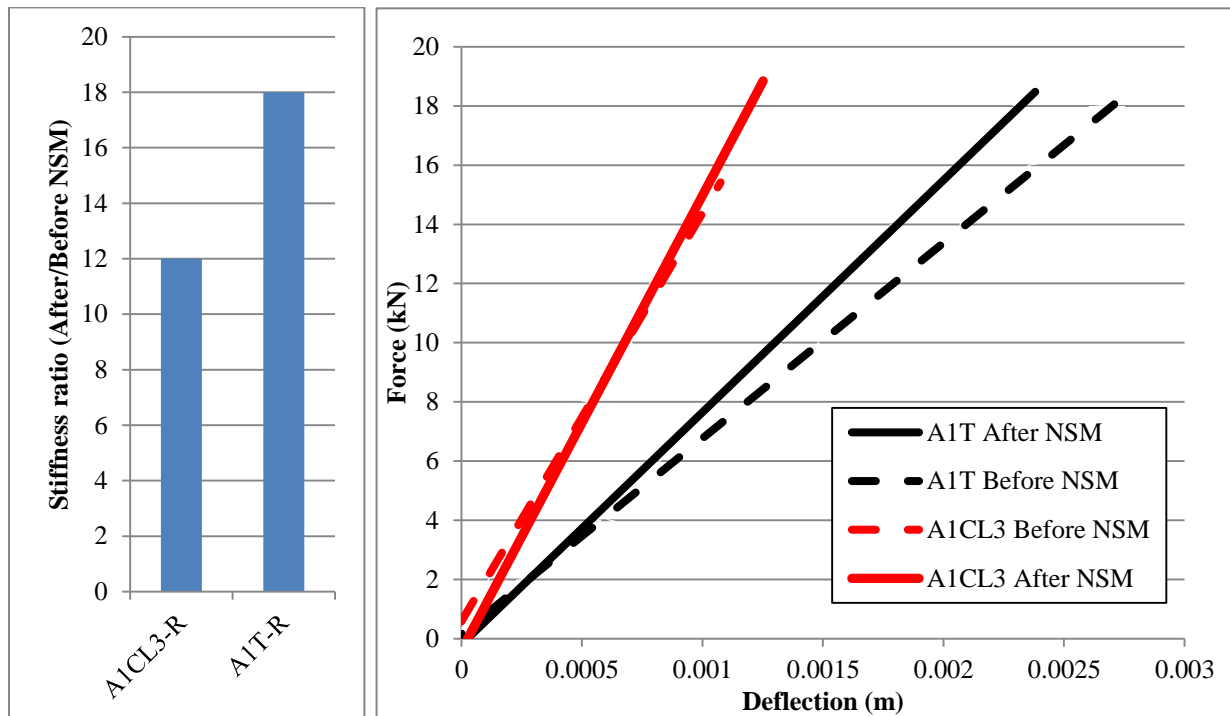


Figure 1 - 18 Stiffness ratio for repaired beams

The stiffness of cracked beams depends on the number of cracks and the crack spacing, and could be affected by the degree of corrosion. The repair process using 6-mm-diameter rods increased the stiffness of the two beams (A1CL3-R and A1T-R) before the yielding point with almost the same ratio: 12% and 18% respectively.

1.3.10 Ductility

Ductility is the ability of the structures to sustain large deformations without decrease in load resistance and it is necessary for RC beams to provide an early warning of failure. Ductility has generally been measured by a ratio called the ductility factor or index ($\Delta u/\Delta y$) corresponding to a deformation (such as curvature, deflection, rotation) at failure (Δu) divided by the corresponding value at yielding (Δy) (Classical definition by Badawi and Soudki (21)). Ductility index values are calculated and presented in table 1-9 and figure 1-19.

The ductility of corroded beams decreases 5 times for each 1% loss of cross section but this could be unacceptable for the safety of a corroded structure. The NSM technique allows the initial ductility of the beam before corrosion to be recovered as shown in figure 19.

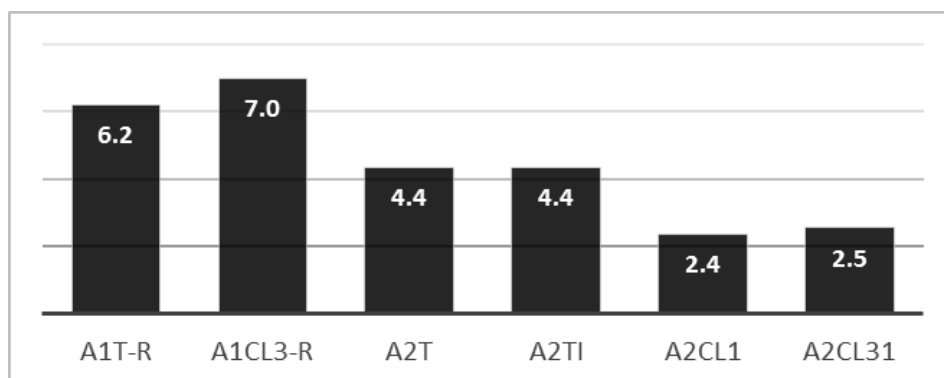


Figure 1 - 19 Ductility index chart

Table 1 - 9 Ductility index values

Beam	Ultimate deflection value (Δ_u) mm	Yielding deflection value (Δ_y) mm	Ductility Index
A1T-R	93	15	6.2
A1CL3-R	63	9	7.0
A2T	64	14.5	4.4
A2TI	63.8	14.5	4.4
A2CL1	29.9	12.5	2.4
A2CL3	28	11.2	2.5

1.3.11 Failure modes

The failure mode observed on repaired corroded beam A1CL3-R was different from those on non-repaired corroded beams A2CL1 and A2CL3, which failed by brittle failure of the tension steel bar at deep corrosion pits. Failure of repaired corroded beam A1CL3-R occurred by a non-conventional mode due to the existence of a rupture plane induced by corrosion cracks. This plane was parallel to the concrete tensile surface but located at steel bar level so it was easy to remove the concrete cover from the reinforcing skeleton. This failure mode was observed by Kreit et al. (28) for a corroded beam of type B with 1 cm of concrete cover repaired with a 6-mm NSM CFRP rod. On the other hand, the failure mode of repaired control beam A1T-R was classical: yielding of the steel bars was reached, followed by crushing of the compressive concrete. The use of transversal strengthening could be an option to avoid this

specific failure mode of separation of concrete cover (or spalling) induced by corrosion of the tensile reinforcement.

1.4 Conclusions

According to the experimental results found in this paper, the following conclusions can be drawn:

1. The NSM technique is able to increase the ultimate load capacity of a corroded beam that has suffered considerable damage and can allow it to reach to the ultimate capacity of the control beam.
2. The efficiency of the NSM technique in repairing corroded beams could be limited by the separation of concrete cover due to corrosion cracks.
3. The NSM technique slightly increases the stiffness of both repaired corroded and repaired control beams.
4. The NSM technique increases the ultimate deflection value for repaired control and corroded beams.
5. The NSM technique restores sufficient ductility (2.8 times that of the non-repaired corroded beams) after ductility loss due to the brittle behaviour of corroded RC beams because of steel corrosion.
6. If there is 1% cross section loss due to steel corrosion it will be reflected as a 1% loss in the yielding capacity value. The percentage is different for ultimate capacity as the mode of failure is not the same in each case: 1% increase due to NSM corresponds to 1% (dc/ds) increase in yielding moment.
7. Because of its efficiency, NSM technique could be a promising way to repair RC structures damaged by corrosion. Nevertheless, the appearance of a new non-conventional failure mode needs more investigation to propose a relevant method of design furnishing safe design provisions.

1.5 References

1. Schmitt G. Global needs for knowledge dissemination, research, and development in materials deterioration and corrosion control. World Corros Organ N Y. 2009.
2. Al-Sulaimani G, Kaleemullah M, Basunbul I. Rasheeduzzafar,(1990)“Influence of corrosion and cracking on bond behaviour and strength of reinforced concrete members” ACI Structural Journal, 87 (2), 220-231. (ASTM G1. 1990).
3. Andrade C, Alonso C, Garcia D, Rodriguez J. Remaining lifetime of reinforced concrete structures: effect of corrosion on the mechanical properties of the steel. In: Proceedings of the international conference on life prediction of corrodible structures. National Association of Corrosion Engineers, Cambridge, UK, 23–26 September; 1991. p. 12/1–11.
4. Cairns J, Plizzari GA, Du Y, Law DW, Franzoni C. Mechanical properties of corrosion-damaged reinforcement. ACI Mater J. 2005;102(4).
5. François R, Khan I, Dang VH. Impact of corrosion on mechanical properties of steel embedded in 27-year-old corroded reinforced concrete beams. Mater Struct. 2013;46(6):899–910.
6. Torres-Acosta AA, Navarro-Gutierrez S, Terán-Guillén J. Residual flexure capacity of corroded reinforced concrete beams. Eng Struct. 2007;29(6):1145–52.
7. Malumbela G, Moyo P, Alexander M. A step towards standardising accelerated corrosion tests on laboratory reinforced concrete specimens. J South Afr Inst Civ Eng. 2012;54(2):78–85.
8. Khan I, François R, Castel A. Structural performance of a 26-year-old corroded reinforced concrete beam. Eur J Environ Civ Eng. 2012;16(3-4):440–9.
9. Dang VH, François R. Influence of long-term corrosion in chloride environment on mechanical behaviour of RC beam. Eng Struct. 2013;48:558–68.
10. Zhu W, François R. Corrosion of the reinforcement and its influence on the residual structural performance of a 26-year-old corroded RC beam. Constr Build Mater. 2014;51:461–72.
11. Almusallam AA. Effect of degree of corrosion on the properties of reinforcing steel bars. Constr Build Mater. 2001;15(8):361–8.
12. Sherwood E, Soudki K. Confinement of Corrosion Cracking in Reinforced Concrete Beams Using Carbon Fiber Reinforced Polymer Laminates. ACI Spec Publ. 1999;188.
13. Soudki KA, Sherwood TG. Behaviour of reinforced concrete beams strengthened with carbon fibre reinforced polymer laminates subjected to corrosion damage. Can J Civ Eng. 2000;27(5):1005–10.
14. Steiner W. Strengthening of structures with CFRP strips. Canadian Society for Civil Engineers, Montreal, Quebec, Canada; 1996. p. 407–19.

15. Soudki K. FRP Repair of Corrosion-damaged Concrete Beams — Waterloo Experience. In: Pandey M, Xie W-C, Xu L, editors. *Advances in Engineering Structures, Mechanics & Construction* [Internet]. Springer Netherlands; 2006. p. 165–73. Available from: http://dx.doi.org/10.1007/1-4020-4891-2_14
16. Bilotta A, Ceroni F, Di Ludovico M, Nigro E, Pecce M, Manfredi G. Bond efficiency of EBR and NSM FRP systems for strengthening concrete members. *J Compos Constr.* 2011;15(5):757–72.
17. De Lorenzis L, Teng J. Near-surface mounted FRP reinforcement: An emerging technique for strengthening structures. *Compos Part B Eng.* 2007;38(2):119–43.
18. Al-Mahmoud F, Castel A, François R, Tourneur C. Strengthening of RC members with near-surface mounted CFRP rods. *Compos Struct.* 2009;91(2):138–47.
19. Castel A, François R, Arliguie G. Mechanical behaviour of corroded reinforced concrete beams—Part 1: experimental study of corroded beams. *Mater Struct.* 2000;33(9):539–44.
20. Du Y, Clark LA, Chan AH. Impact of reinforcement corrosion on ductile behavior of reinforced concrete beams. *ACI Struct J.* 2007;104(3).
21. Badawi M, Soudki K. Flexural strengthening of RC beams with prestressed NSM CFRP rods—experimental and analytical investigation. *Constr Build Mater.* 2009;23(10):3292–300.
22. Al-Mahmoud F, Castel A, François R, Tourneur C. RC beams strengthened with NSM CFRP rods and modeling of peeling-off failure. *Compos Struct.* 2010;92(8):1920–30.
23. De Lorenzis L, Micelli F, La Tegola A. Passive and active near surface mounted FRP rods for flexural strengthening of RC beams. 2002.
24. Radfar S, Foret G, Saeedi N, Sab K. Simulation of concrete cover separation failure in FRP plated RC beams. *Constr Build Mater.* 2012;37:791–800.
25. Al-Mahmoud F, Castel A, François R. Failure modes and failure mechanisms of RC members strengthened by NSM CFRP composites—Analysis of pull-out failure mode. *Compos Part B Eng.* 2012;43(4):1893–901.
26. De Lorenzis L, Nanni A. Bond between near-surface mounted fiber-reinforced polymer rods and concrete in structural strengthening. *ACI Struct J.* 2002;99(2).
27. De Lorenzis L, Nanni A, La Tegola A. Flexural and shear strengthening of reinforced concrete structures with near surface mounted FRP rods. 2000. p. 521–8.
28. Kreit A, Al-Mahmoud F, Castel A, François R. Repairing corroded RC beam with near-surface mounted CFRP rods. *Mater Struct.* 2011;44(7):1205–17.
29. Vidal T, Castel A, François R. Corrosion process and structural performance of a 17 year old reinforced concrete beam stored in chloride environment. *Cem Concr Res.* 2007;37(11):1551–61.

30. Poursaei A, Hansson C. Potential pitfalls in assessing chloride-induced corrosion of steel in concrete. *Cem Concr Res.* 2009;39(5):391–400.
31. Yuan Y, Ji Y, Shah SP. Comparison of two accelerated corrosion techniques for concrete structures. *ACI Struct J.* 2007;104(3).
32. Otieno M, Beushausen H, Alexander M. Prediction of corrosion rate in reinforced concrete structures—a critical review and preliminary results. *Mater Corros.* 2012;63(9):777–90.
33. French regulations for reinforced concrete structures. B.A.E.L. 1983.
34. EN 206-1. European standard, concrete – Part 1: specifications, performance, production and conformity. NF EN 206-1; April. 2004.
35. Al-Mahmoud F, Castel A, François R, Tourneur C. Effect of surface pre-conditioning on bond of carbon fibre reinforced polymer rods to concrete. *Cem Concr Compos.* 2007;29(9):677–89.
36. Horne A, Richardson I, Brydson R. Quantitative analysis of the microstructure of interfaces in steel reinforced concrete. *Cem Concr Res.* 2007;37(12):1613–23.
37. Soylev T, François R. Quality of steel–concrete interface and corrosion of reinforcing steel. *Cem Concr Res.* 2003;33(9):1407–15.
38. Beeby A. Concrete in the oceans: cracking and corrosion. Cement and Concrete Association; 1978.
39. R. François, A. Castel, T. Vidal, N.-A. Vu. Long term corrosion behavior of reinforced concrete structures in chloride environment. *J Phys IV Fr.* 2006 Nov;136:285–93.

1.6 Appendix: classical RC calculations

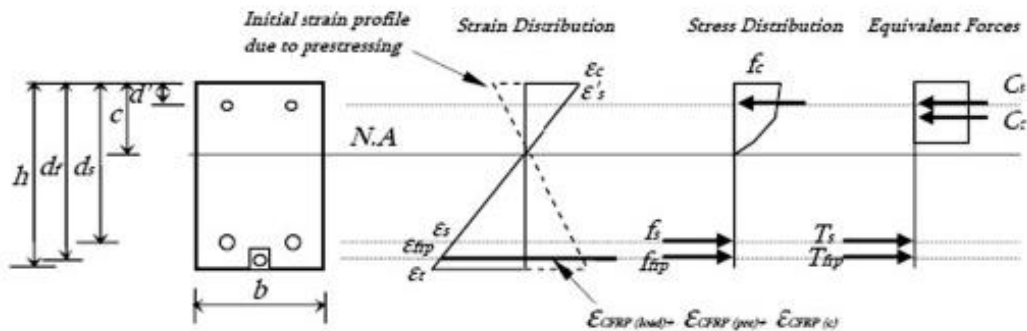


Figure 1 - 20 Force equilibrium and strain compatibility for RC beams

Table 1-10 presents the calculated moment values of the corroded beam A1CL3-R and the control beam A1T-R based on the classical mode of failure for RC beams by concrete crushing (Equations used in Almahmoud et al, 2009) as shown in figure 1-20.

Where b : width of beam; d_s : effective depth of beam; h : height of beam; f_y : yielding stress of steel bars; E_s : modulus of elasticity of steel bars; E_f : modulus of elasticity of FRP bars; A_s : cross sectional area of steel bars; A_f : cross sectional area of FRP bars.

The values used for the calculations were: for A1CL3-R ($b = 15$ cm, $h = 28$ cm, $d_s = 22.4$ cm, $E_s = 200$ GPa, $E_f = 150$ GPa, $A_s = 3.42$ cm², $A_f = 0.28$ cm², $f_y = 578$ MPa) and for A1T-R ($b = 15$ cm, $h = 28$ cm, $d_s = 22.4$ cm, $E_s = 214$ GPa, $E_f = 150$ GPa, $A_s = 4.02$ cm², $A_f = 0.28$ cm², $f_y = 600$ MPa). As mentioned before, the high degree of corrosion and the increase in shear stresses in the concrete cover prevented the beam from reaching the maximum theoretical value of the classical failure mode and it failed by the separation of the concrete cover. More studies need to be conducted on this new mode of failure in order to understand its mechanism.

Table 1 - 10 Summary of calculated values of moment

Beam	Yielding bending moment M_y (kN.m)		Ultimate bending moment M_y (kN.m)	
	Calculated	Experimental	Calculated	Experimental
A1CL3-R	43.5	42.3	63.4	52.1
A1T-R	51.7	53	68.4	65.5

Conclusions

The moment-deflection curves for all tested beams showed that the NSM technique increased the yielding moment capacity of the RC beams, an increase of 19% was recorded in the repaired corroded beam A1CL3-R compared to the non-repaired one while an increase of 18% was found in the repaired control beam A1T-R compared to A2T (non-repaired control beam). The NSM also increased the ultimate bending moment capacity for corroded beams as the repaired corroded beam A1CL3-R had higher ultimate capacity than either A2CL1 or A2CL3 (non-repaired corroded beams) with 17 kN.m and 11 kN.m respectively, the same effect occurred for the repaired control beam A1T-R which had higher ultimate capacity than the ultimate capacity of non-repaired control beams A2T or A2TI. The NSM technique also increased the ultimate deflection of the repaired RC beams, the ultimate deflection value (93 mm) for repaired control beam A1T-R at the failure point was more than the ultimate deflection value for non-repaired control beams A2T (64 mm) and A2TI (64 mm), as well as the ultimate deflection value for repaired corroded beam A1CL3-R (63 mm) was higher than the ultimate deflection values for the corroded non-repaired beams A2CL3 and A2CL1 (28 mm and 30 mm respectively).

The NSM repair technique using 6-mm-diameter rods slightly increased the stiffness of the two RC beams (A1CL3-R and A1T-R) before the yielding point with almost the same ratio: 12% and 18% respectively. The NSM also allowed the initial ductility of the corroded beam before corrosion to be recovered, as the ductility index for corroded repaired RC beams was found to be 7 while for non-repaired corroded beams the ductility index value was around 2.5 which mean that the NSM recovered almost 2.8 times that of the non-repaired corroded beams.

Finally, using the NSM as a repair technique for the corroded RC beams results of a new non-conventional failure mode which occurred in the repaired corroded RC beam A1CL3-R by the separation of concrete cover while the other beam A1T-R failed classically by the yielding of the steel bars followed by the crushing of the compressive concrete, the separation of concrete cover as mode of failure happened due to the existence of a rupture plane induced by corrosion cracks. More investigation regarding this new mode of failure is required as well as proposing transversal strengthening could be a solution which can prevent this premature mode of failure from happening.

Chapter 2

Shear strengthening of corroded RC beams with NSM CFRP rods, an experimental part

Introduction

This chapter aims at studying the post repair performance of four short span RC beams, after the corroded repaired RC beam A1CL3-R and the control repaired RC beam A1T-R have been tested up to failure and the bending behavior of the repaired RC beams with NSM was studied in chapter 1, the two beams were cut into small parts in order to extract the four edges (4 deep RC beams could be studied to highlight the shear behavior), while the middle parts of the two long beams were neglected as they were damaged due to the previous 3-points loading tests.

The four RC deep beams were one corroded beam A1CL3-SB and one control beam A1T-SB are repaired with NSM CFRP rods in bending and shear while the two others are kept repaired in bending only (one corroded A1CL3-B and one control A1T-B), four CFRP 6mm diameter rods were installed 10 cm apart on each side of each end of the short RC beams to be repaired in shear. All short beams are tested in three-points loading test up to failure. Linear variable differential transducers (LVDT) were fixed at either end of each steel bar of the short RC beams during the tests in order to measure the slip of the tensile steel bars; one more LVDT was fixed at the middle of the beam to measure the deflection.

It compares the load-deflection curves at the mid-span point for the repaired beams with other corroded non-repaired RC beams; A2CL2-A and A2CL2-B (extracted from the corroded beam A2CL2 (27 years-old), tested by Dang (36)), A2CL3-A and A2CL3-B (extracted from the corroded beam A2CL3 (26 years-old), tested by Khan et al. (12)), Control non-repaired RC beams beams; Control 1 and 2 tested by (Dang (36)) and A2T tested by Khan et al. (12).

The shear strengthening effect on the failure modes of the short RC beams was also discussed here throughout presenting the modes of failure for both shear-repaired and non-shear-repaired RC beams.

The NSM effect in shear strengthening on the tensile steel bars slip in the four short beams was presented in this chapter in comparison with other slip results obtained from similar short non-repaired beams, the corrosion distribution and diameter losses of the tensile steel bars were also presented. Finally, the effect of span to section depth (effective) ratio (a/d) of the beam on the shear strength is presented.

Behaviour of corroded shear-critical Reinforced Concrete beams repaired with NSM CFRP rods

Belal ALMASSRI (1), Amjad KREIT (1), Firas AL MAHMOUD (2), Raoul FRANCOIS (1)

(1) *Université de Toulouse; UPS, INSA, LMDC (Laboratoire Matériaux et Durabilité des Constructions), Toulouse, France*

(2) *Institut Jean Lamour, UMR 7198, CNRS, Université de Lorraine, Nancy, France*

Keywords: reinforced concrete, corrosion, repair, shear, carbon fibre.

ABSTRACT

This paper discusses the results of an experimental program designed to investigate the effect of repairing the RC corroded shear-critical deep beams with Near Surface Mounted (NSM) carbon fibre-reinforced polymer (CFRP) rods. A 28-year-old RC beam corroded by exposure to a chloride environment was cut into two small short-shear-span beams, or deep beams, which were tested under three-point bending until failure, along with a control beam of the same characteristics (age, length and cross-section). One RC corroded deep beam was repaired in bending and the other one was repaired in both bending and shear with NSM CFRP rods. Force-displacement curves were plotted for the corroded and control deep beams. After the beams had been tested up to failure, the main steel bars and the stirrups were extracted from the beams and the loss of mass was measured and plotted for both the longitudinal and transverse reinforcement. The slip of tensile reinforcement at the end of the beams was also measured during the tests.

The effect of corrosion and the effect of repairing with CFRP NSM rods in bending and shear on the behaviour of deep beams are discussed. Experimental results show that both corroded and control deep beams repaired only in bending failed due to shear mode of failure (diagonal tension failure), while corroded and control beams repaired in both bending and shear failed due to concrete crushing. The test results also showed that the corrosion of both longitudinal and transversal reinforcement hardly modified the mechanical response of deep beams. Even in presence of corrosion and repairing with NSM CFRP rods, the ratio between the shear span “a” and the effective depth “d” (a/d ratio) appears to be a major parameter.

2.1 Introduction

The cost of rehabilitating corroded RC structures worldwide exceeds \$1.8 trillion per year (1). Corrosion of the steel bars in the RC elements causes a reduction in the cross sectional area of the steel reinforcement and a significant reduction in its ductility, which leads to the early failure of steel bars (2,3). Most of the experimental research literature mainly focuses on the effect of steel corrosion on the flexural behaviour of reinforced concrete elements (4–7) and, so far, little research has concerned the effect of corrosion on the shear behaviour of corroded reinforced concrete beams. Accelerated corrosion tests were conducted on RC beams (8–10) in order to understand the effect of the corroded steel stirrups on the shear behaviour of RC beams. Instead of using impressed current induced corrosion, some studies (11,12) have aimed to assess the shear behaviour of naturally corroded RC beams. This work was based on a long-term programme in which the RC beams were stored in a chloride environment under service loads in order to obtain results that were closer to the real state of corroded structures.

The near surface mounted reinforcement technique (NSM) using carbon fibre reinforced polymer (CFRP) rods is a strengthening technique that has given encouraging results in repairing deteriorated RC beams that are likely to fail in a brittle shear failure mode. De Lorenzis and Nanni, (13) showed that the use of NSM FRP rods could improve the shear capacity of RC beams, a 106% increase in the shear strength being recorded in the absence of internal steel stirrups. A significant increase was also recorded for limited shear reinforced beams. Islam (14) tested four concrete beams: a control beam having typical shear steel reinforcement and three other beams that were strengthened in shear with CFRP bars using the NSM technique, for which a 17-25% increase in shear strength was found.

Rizzo and De Lorenzis, (15) carried out a testing program in order to assess the shear capacity increase that could be obtained by using the NSM FRP reinforcement technique, and made a comparison between the externally bonded U-wrapped laminates and the NSM technique. One side of each beam was reinforced strongly in shear with 10 mm diameter stirrups every 50 mm, while the other side was reinforced with a limited shear reinforcement using 6 mm diameter stirrups every 160 mm. The beams were simply supported and were tested with a four-point loading test. The beams strengthened with the NSM technique, both NSM round bars and NSM strips were used, an increase in the shear capacity of 16% was recorded for the beam strengthened with externally bonded U-wrapped laminate, while 45 degrees inclination of beams strengthened with NSM round bars and NSM strips gave 14 % and 9.4 % increase in the shear capacity over using the 90 degrees of U-wrapped laminate as strengthening

technique respectively. Dias and Barros, (16) also found that the NSM technique using CFRP laminates had advantages over the externally bonded reinforcement (EBR) technique in terms of maximum load-bearing capacity and load capacity after shear crack formation, and found much higher strain values in the CFRP rods, which means that the NSM technique makes better use of the tensile strength of the CFRP material.

De Lorenzis et al. (17) suggested some methods for increasing the shear capacity of the strengthened T-beams by decreasing the space between the FRP rods and increasing the anchorage length of the FRP rods in a T-beam that was also anchored to the flange. They mentioned that decreasing the space between the FRP rods which corresponds to an increase in the FRP material inside the RC beam will lead to an important increase in the shear capacity of the RC beam. They also mentioned that inclining the FRP rods at 45 degrees increased the shear capacity of the reinforced concrete elements, in agreement with the findings of Barros et al. (18) on inclined FRP laminates, which proved to be more effective than vertical laminates.

De Lorenzis and Nanni (13) observed two failure modes for beams repaired in shear with NSM FRP rods. The first was de-bonding of the FRP rods and the second was splitting of the concrete cover over the longitudinal steel bars. They concluded that, once failure by FRP rod de-bonding was prevented by using inclined rods rather than vertical ones, splitting of the concrete cover of the longitudinal steel reinforcement was the most important factor controlling the mode of failure. Another failure mode observed (15) was the splitting of the concrete cover side of all of the internal steel stirrups.

The present paper studies the post-repair performance of corroded short-span reinforced concrete beams repaired with the NSM FRP technique. Some of these beams were repaired in bending only and the others were repaired in bending and shear. All were tested statically in three-point loading up to failure. The failure modes and the mechanical performance of all beams were studied, and the shear capacity of the short-span corroded beams repaired in shear and bending was compared to that of similar non-repaired beams. The relationship between the shear strength of the RC beam and its span to section depth ratio was also studied and the slipping of the steel bars was measured for all beams during the loading tests. Finally, the corroded steel bars were extracted from the beams to study their corrosion and tensile tests were conducted to study their mechanical properties.

2.2 Experimental program: specimens, test setup, monitoring system and material properties

2.2.1 Experimental procedure

An experimental programme was started at LMDC (Laboratory of Materials and Durability of Constructions) in 1984 with the aim of understanding the effects of steel corrosion on the structural behaviour of RC elements. This long-term programme consisted of casting a set of 72 RC beams of dimensions $3,000 \times 280 \times 150$ mm. Thirty-six of them were stored in a chloride environment under service load to measure the flexural cracks occurring during the corrosion process. Many experimental studies have been conducted on these beams to evaluate the development of corrosion cracking, to measure chloride content and to analyse the changes in their mechanical behaviour (19,20). The other 36 beams were stored under the same mechanical load but in a non-aggressive environment to be used later as control beams in the study of long-term effects, such as creep and ageing of the concrete. The natural aggressive environment system consisted of salt fog spray (35 g/l of NaCl) (see Fig 2.1).

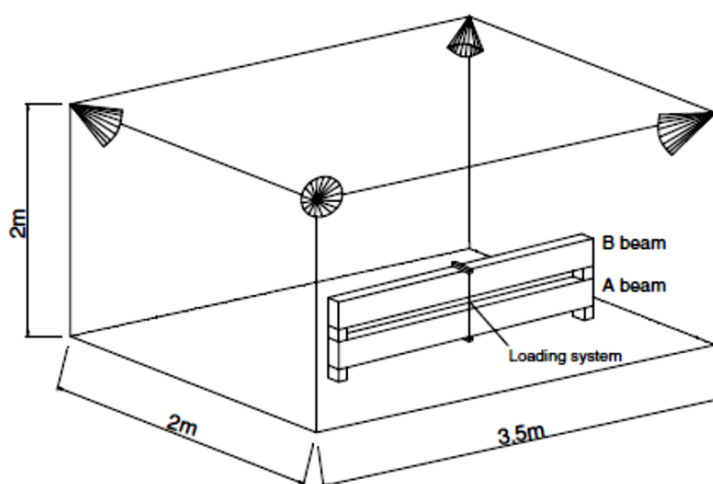


Figure 2 - 1 The climate accelerated aggressive environment system

For 9 years, the beams were under sustained loadings in chloride environment in the laboratory conditions so the temperature was controlled (around 20°C) while after 9 years the salt fog chamber was transferred outside so the temperature was not controlled and the beams were exposed to the outside temperature with monthly-average values ranging from 5.1°C to 21.3°C . The beams have been stored in the saline fog for 6 years; the corroded beams were transferred to wetting-drying cycles in order to accelerate the corrosion process (Table 2-1). The loading system was allowed to monitor the decrease of the force applied due to concrete creep, and then the load was re-adjusted periodically during the

first years. Moreover, a spring system of the loading device was allowed to accept some increase in beam deflection without affecting the load. Nevertheless, the loading device was kept in the aggressive environment and the monitoring system stopped giving load information after 6 years. After 19 years of storage, it was decided to perform mechanical tests on the beams, the loading system was removed. However, because of the high chloride content (21) and storage conditions, corrosion continued to propagate.

Table 2 - 1 The climate accelerated aggressive environment system

Years	Spraying State	Loading Conditions	Conservation conditions	Temperature
0-6	Continuous	Loaded	Confined room	20°C
6-9	WDC*	Loaded	Confined room	20°C
9-19	WDC*	Loaded	Open room	CSWF**
19-27	Stopped	Unloaded	Open room	CSWF**
27-present	WDC*	Unloaded	Open room	CSWF**

*WDC: wetting-drying cycles for one week respectively.

**CSWF: climate of south-west of France, ranging from 5.1 to 21.3°C average value per month.

The corrosion obtained in this climate-accelerated programme was very close to the corrosion observed under natural conditions in terms of corrosion distribution, corrosion type and oxides produced. The corrosion distribution was largely stochastic with a maximum corrosion pit to average corrosion ratio between 4 and 8. The hydroxyl-oxides played a significant role in the corrosion products. While for the three forms of the hydroxyl-oxides, Geothite was in considerable proportion, and then followed by Akaganeite. Lepidocrocite was relatively weaker. The content of Lepidocrocite was still higher than Magnetite (22,23). To predict the service life of RC elements, it is very important to have access to such natural degradation (24) rather than that resulting from the use of an applied current or a CaCl₂ admixture in the concrete (25,26). The beams were divided into two groups named type A and type B, which had different reinforcement layouts but the same reinforcing steel bar (yield strength = 500 MPa). Beams A and B had 40 mm and 10 mm of concrete cover respectively. According to French standards at the time of manufacturing (27), the 40 mm cover represents the minimum concrete cover in very aggressive environments (i.e. chloride aggression) and the 10 mm cover represents the minimum concrete cover in a non-aggressive environment. The beams were loaded in three-point flexure by coupling a type A beam with a type B beam. Two loading values were applied: M_{ser1}=13.5 kN.m for beams referred to as A1 (A1CL3-R and A1T-R); The loading value for type A2 beam was designed according to ultimate load limit state (ULS) in a non-aggressive environment while the loading value for type A1 beam was

designed according to serviceability limit state (SLS) requirements for steel corrosion in an aggressive chloride environment based on an indirect limitation of crack width using a tensile stress limitations of the steel bars (27). $M_{ser2}=21$ kN.m for beams referred to as A2 (A2CL1, A2CL3, A2T and A2TI), which had the same type and shape of reinforcement but different values of service loading. The beams studied in this paper are type A beams; one corroded beam (A1CL3-R) and one control beam (A1T-R). Long-term corroded beams A2CL1, A2CL3, A2TI and A2T tested by (21,28) but not repaired were also used here for comparison. The control beam A1T-R was strengthened using the same method as the one used to repair the corroded beam A1CL3-R. The layout of the reinforcement is shown in Fig. 2-2. The flexural and shear reinforcement ratios were equal to 1.2 and 0.2 % respectively. Flexural reinforcement ratio of 1.2% refers to an under reinforced beams state as for this case it is guaranteed that the crushing of concrete will not be reached “earlier” at smaller deformations. Figure 2-2 shows the steel distribution inside type A beams.

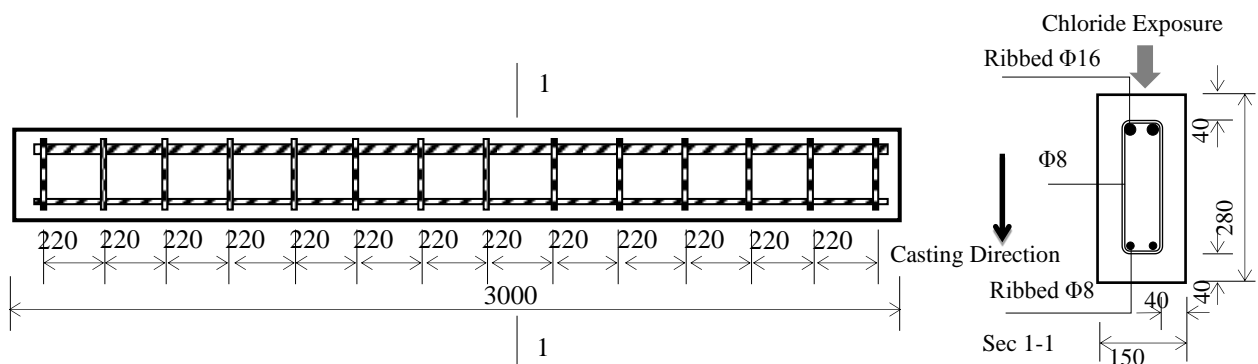


Figure 2 - 2 Reinforcement layout of type A beams. Dimensions are in mm

2.2.2 Material properties

2.2.2.1 Concrete properties

The concrete mix is given in Table 2-2. The Water/Cement ratio was 0.5 but could be adjusted by changing the water quantity to obtain a constant workability of 7 cm in the slump test (slump class S2) in order to meet the most commonly specified consistence according to European Standard EN 206-1 (29). The average compressive strength and the elastic modulus obtained according to European Standard NF EN 12390-2 (30) on three cylindrical specimens (diameter 11 cm \times height 22 cm) tested after 28 days were 45 MPa and 32 GPa respectively. The tensile strength, measured using the splitting test, was 4.7 MPa. Water porosity was 15.2% according to (31). To measure concrete characteristics, cylindrical cores 70 mm \times 140 mm, were drilled out of both the corroded and control beams and tested in compression. Table 2-3 gives the results of these core tests.

Table 2 - 2 Concrete mix

Mix component	mm	kg/m ³
Rolled gravel (silica + limestone)	5/15	1 220
Sand	0/5	820
Portland cement: OPC HP		400
Water		200

Table 2 - 3 Mechanical characteristics of the concrete at 27 years (average of 3 tests)

Mechanical characteristics	A1CL3-R	A1T-R
Compressive strength (MPa)	62.2	58.9
Elastic modulus (MPa)	33 700	29 700

2.2.2.2 Characteristics of steel bars, CFRP bars and filling material

The steel reinforcing bars were composed of natural S500 half-hard steels and were ordinary ribbed bars. The steel bar characteristics were measured after extracting the corroded bars from the corroded beam A1CL3-R and the results are shown in Table 2-4.

Table 2 - 4 Effective mechanical properties of steel bars (calculated from the residual cross-section)

Specimen Type	Yield Strength (MPa)	Ultimate Strength (MPa)	Yield Strain %	Elastic Modulus (GPa)
corroded	578	710	0.27	200
non-corroded	600	645	0.28	214

Al-Mahmoud et al. (32) measured the mechanical properties of CFRP rods through a test programme conducted on 3 specimens tested in axial tension. The CFRP rods showed brittle failure that started with splitting and ended with the failure of the rods as shown in figure 3. Table 2-5 shows the mechanical properties of the CFRP rods. In order to increase the bonding between the CFRP rods and the filling material, the rods were coated with 0.2/0.3 mm of surface sanding material, which was sprinkled onto an epoxy paste applied to the surface of the rods.

Table 2 - 5 Characteristics of CFRP rods

Type of test	Ultimate strength (MPa)	Modulus of Elasticity (MPa)
Manufacturer's test	2 300	150 000
Laboratory test	1 875	145 900

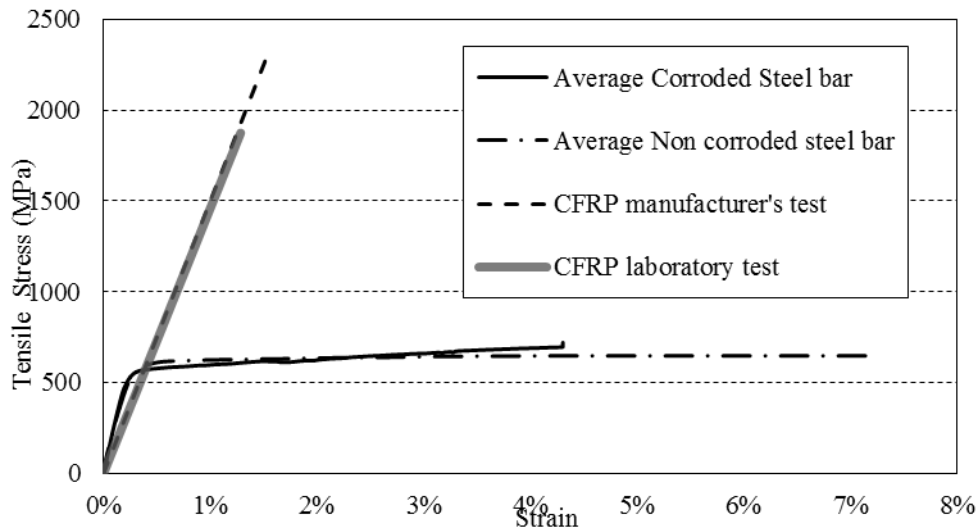


Figure 2 - 3 Stress-strain diagrams for steel and CFRP bars

Table 2-6 shows the characteristics of the filling material (epoxy paste) after 7 days according to the manufacturer’s specifications.

Table 2 - 6 Filling material properties

Material	Compressive Strength (MPa)	Tensile Strength (MPa)	Elastic Modulus (MPa)
Epoxy	83	29.5	4900

2.2.3 Repair technique with NSM against bending and shear forces

The NSM CFRP rod was installed in the corroded beam A1CL3-R and in the control beam A1T-R by making two cuts in the concrete cover in the longitudinal direction at the tension side. A special concrete saw with a diamond blade was used.

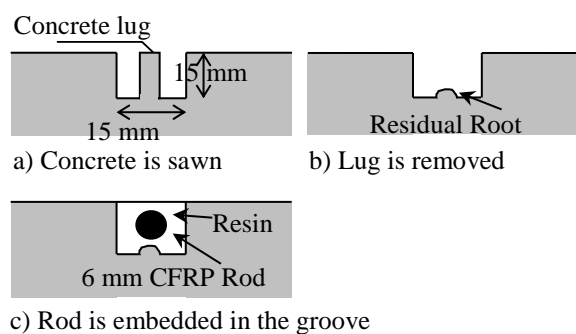


Figure 2 - 4 Installation of CFRP rod in concrete surface

The remaining concrete lug formed by the sawing was then removed using a hammer and hand chisel so that the lower surface became rough (Figure 2-4). The groove was airbrushed to remove dust, debris and fine particles so as to ensure proper bonding between the paste and the concrete. Then, the groove was half filled and the CFRP rod was positioned inside it and

pressed lightly. This forced the paste to flow around the CFRP rod. More paste was applied to fill the groove and the surface was levelled. As a result, the CFRP rod was placed in the middle of the cross-section in the tension area. The CFRP rod had a total length of 3000 mm and a diameter of 6 mm, which means that the repair was along the whole length of the beam. The groove was 15 mm deep and 15 mm wide (around 2.5 times the rod diameter) (33). Previous study was done by Al-Mahmoud et al (34) showed that FRP below supports and FRP away of the supports did not change the failure mode which was due to the pull-out of the CFRP rod. The two beams were tested one week after installation of the CFRP rod in order to ensure that the filling material reached its full strength.

After the two full span lengths of the corroded beam A1CL3-R and control beam A1T-R had been loaded up to failure, the four end parts (A1CL3-SB, A1CL3-B, A1T-SB and A1T-B) shown in figure 2-5 were extracted of the full span of the two beams. Figure 2-6 presents the moment-deflection curves for both full span beams A1CL3-R and A1T-R.

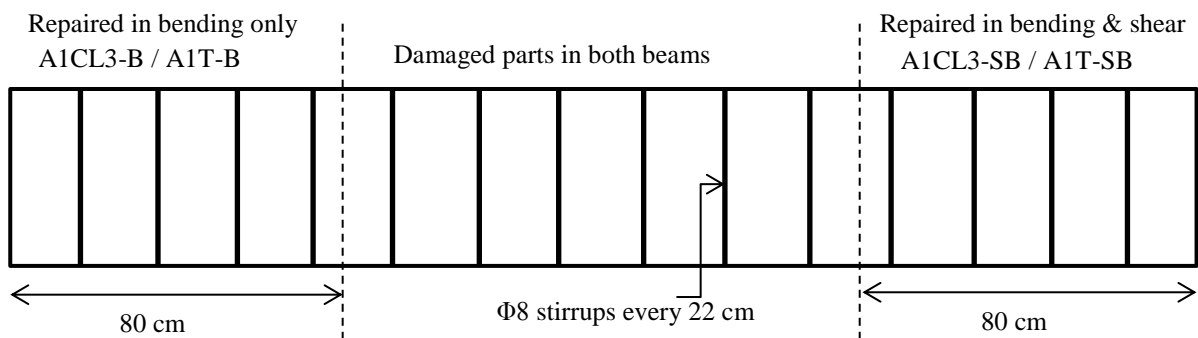


Figure 2 - 5 Parts of corroded and control beam

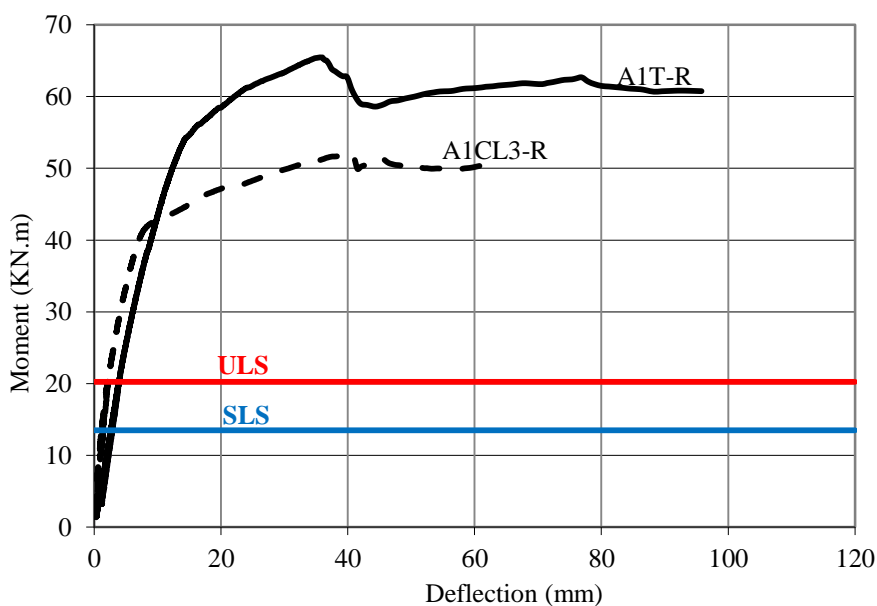


Figure 2 - 6 Moment-deflection curves for A1CL3-R and A1T-R

Figure 2-7 illustrates the failure of mode for both beams, the corroded A1CL3-R beam which failed due to separation of the concrete cover at the middle of the beam, and the control A1T-R beam which failed due to concrete crushing.



Figure 2 - 7 Modes of failure and damages of two full span beams A1CL3-R and A1T-R

The two left end parts (A1CL3-B and A1T-B) were re-repaired in bending only by replacing the cracked areas of the epoxy paste material with fresh epoxy paste of the same type while the two right end parts (A1CL3-SB and A1T-SB) were re-repaired in bending and in shear using the configuration shown in figure 2-8: four rods were installed 10 cm apart on each side of each end. In order to obtain better repair, the CFRP rods were inclined at 45 degrees so that they would be perpendicular to the shear cracks.

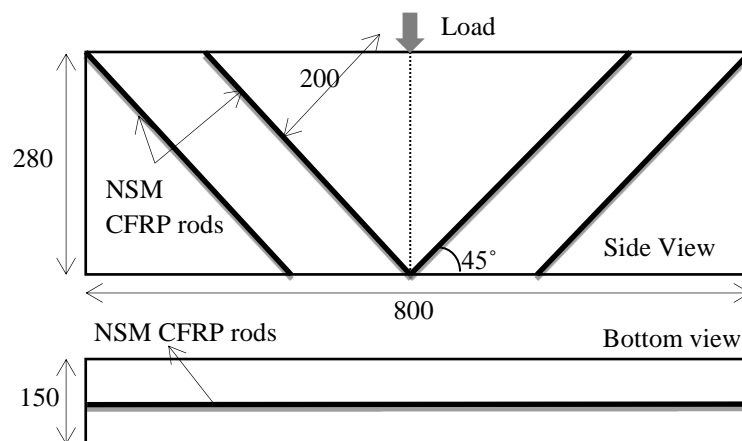


Figure 2 - 8 Shear repair configuration for A1CL3-SB and A1T-SB (Dimensions in mm)

Table 2 - 7 Repair plan for all beams

Beams	Dimensions $h \times b \times L$ mm	Corrosion status	Repair with CFRP NSM rods
A1CL3-B	280 × 150 × 800	Corroded	Bending -
A1CL3-SB	280 × 150 × 800	Corroded	Bending Shear
A1T-B	280 × 150 × 800	Non Corroded	Bending -
A1T-SB	280 × 150 × 800	Non Corroded	Bending Shear

2.2.4 Instrumentation of beams

In order to verify the anchorage between the longitudinal steel bars and the concrete during the loading process, the slip of the longitudinal steel bars was measured using linear variable differential transducers (LVDT) fixed at either end of each steel bar. One more LVDT was fixed at the mid-span to measure the deflection of the beam as shown in figure 2-9, 2-10.

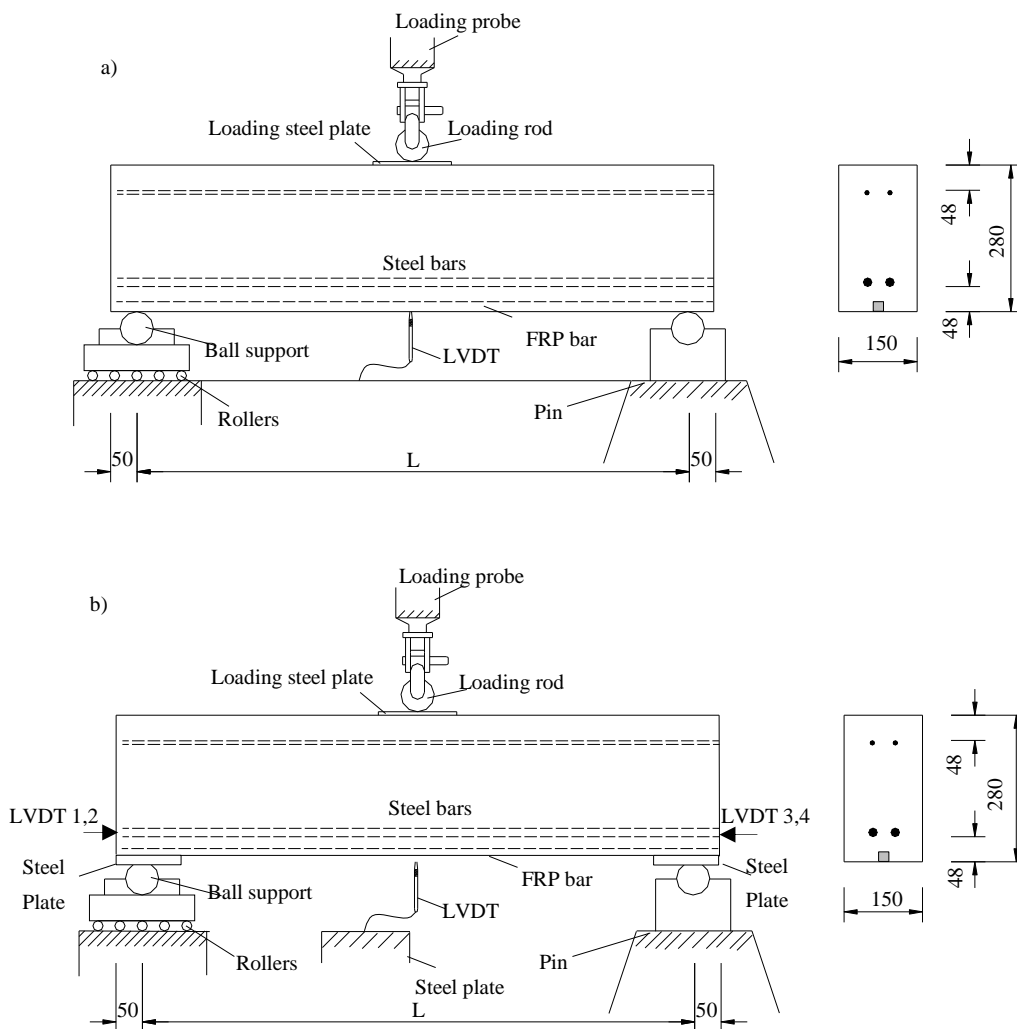


Figure 2 - 9 Beams instrumentation for a) full span beams and b) short beams

As shown in figure 2-9, the LVDT in testing the full span beams (A1CL3 and A1T) was installed at the middle of the beam-span on the same steel support plates as in this case no settlement will take place for both supports while the mid-span LVDT in testing the short beams (A1CL3-B, A1CL3-SB, A1T-B and A1T-SB) was installed on a separate steel plate which takes into account the supports settlement. LVDT at the end of steel bars were fixed on the concrete surface as shown in figure 2-10.

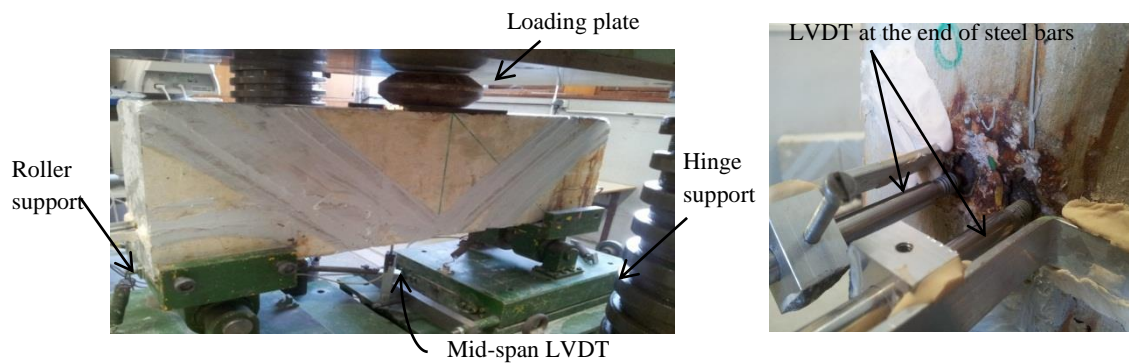


Figure 2 - 10 Short span beams instrumentation

2.3 Experimental results

2.3.1 Losses of diameter due to corrosion for tensile steel bars and steel stirrups in corroded beams A1CL3-B and A1CL3-SB

Clark's solution ANSI/ASTM G1-72 was used to remove the corrosion from the surface of the steel reinforcement bars and then the diameter loss of the bars due to corrosion was measured using two different methods: direct measurement with a vernier calliper just after the steel bars had been cleaned and dried, and measurement of the weight loss of the steel bar to calculate the diameter loss. The second method required the critical parts of corroded steel bars to be cut into small pieces 1-2 cm long, which were then weighed to an accuracy of 0.001g. A reference mass was measured on bars extracted from the control beam. Both methods were used to evaluate the diameter loss of the corroded steel bars as some previous papers (35) had shown that the shape of corrosion damage was too complex to be measured only by the vernier calliper.

The maximum diameter loss was found to be 18% at 28 cm away from the mid-span position of A1CL3-B, while 9 % diameter loss was found in A1CL3-SB at 20 cm away from mid span. Figure 2-11 presents the diameter loss percentage for tensile steel bars at all locations along the two corroded beams.

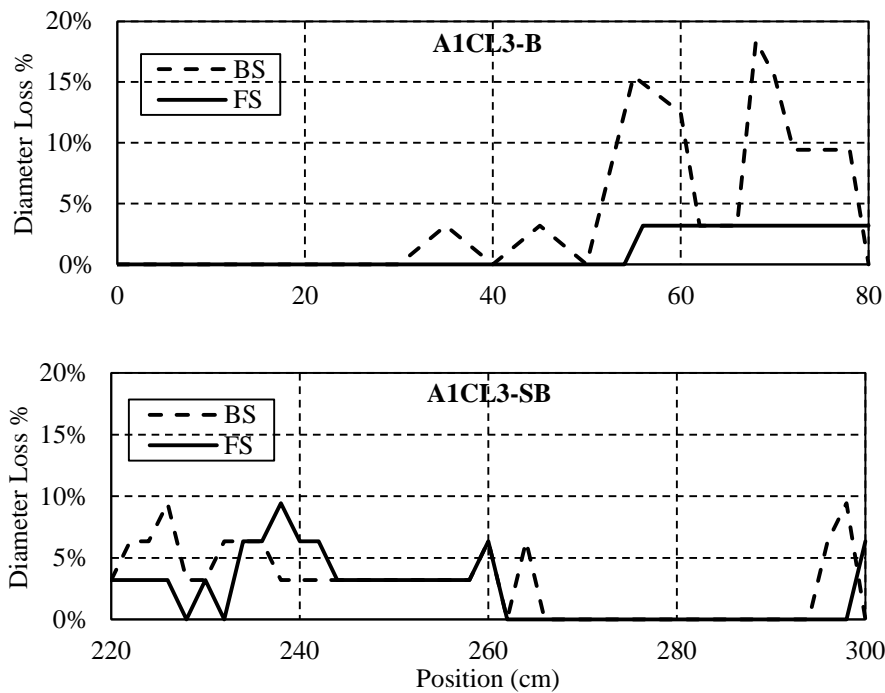


Figure 2 - 11 Diameter loss percentages of longitudinal tensile steel bars

The steel stirrups were numbered to indicate the part of the beam they came from and their position in that part (the first number represents the part of the beam and the second number represents the number of the stirrup) as shown in figure 2-12:

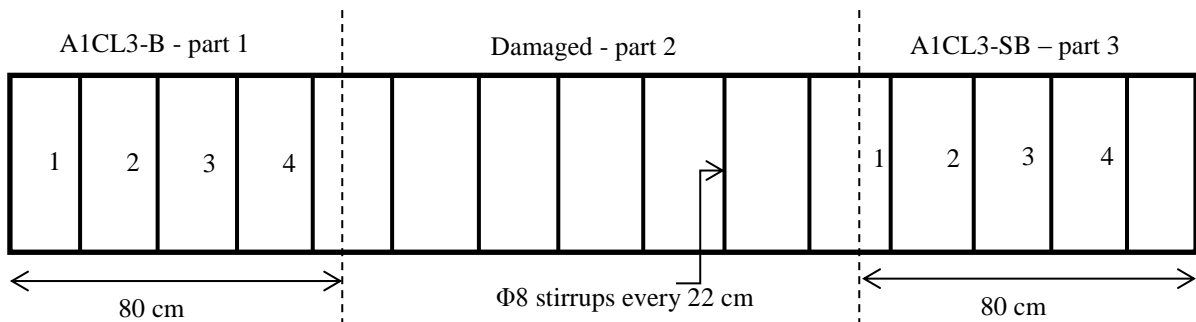


Figure 2 - 12 Parts of corroded beam A1CL3-R

Figure 2-13 shows the locations of corrosion in the steel stirrups and the diameter values. No corrosion was found at stirrups 1-1 and 1-2, the maximum diameter loss found in beam A1CL3-B was 63 % at stirrup 1-4 while the maximum loss in A1CL3-SB was 38 % at stirrup 3-1.

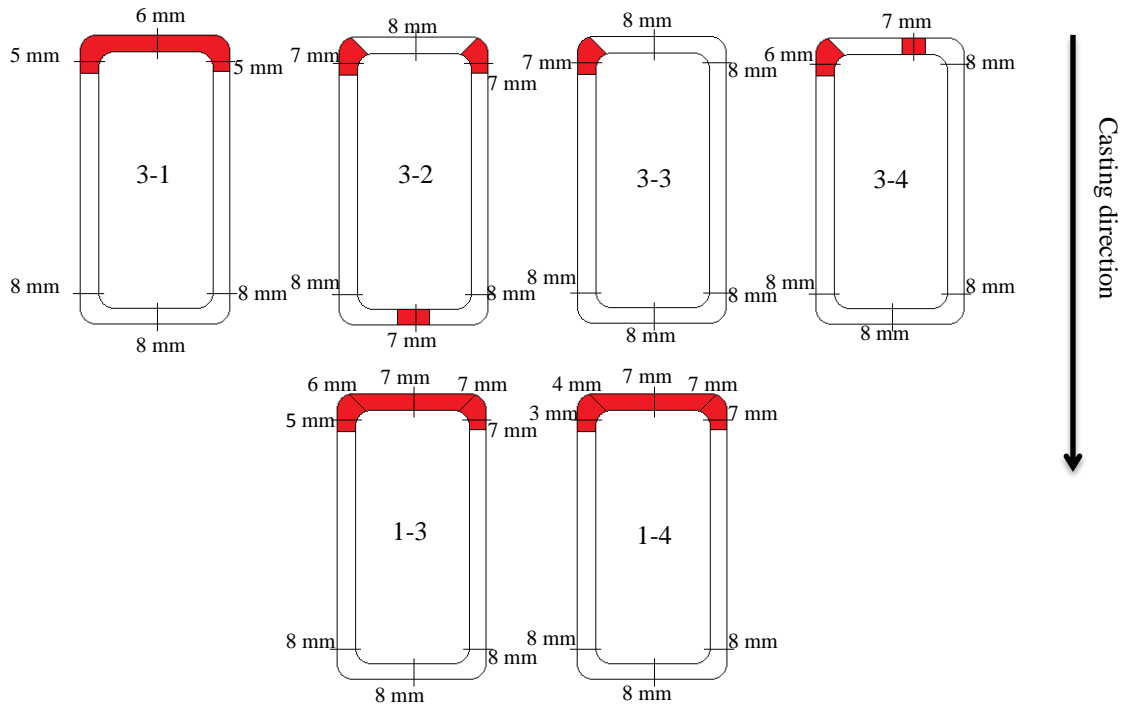


Figure 2 - 13 Corrosion in steel stirrups of corroded beam A1CL3-R

2.3.2 Ultimate load capacity and failure modes

Figure 2-14 shows the load-deflection curves at the mid-span point for all beams.

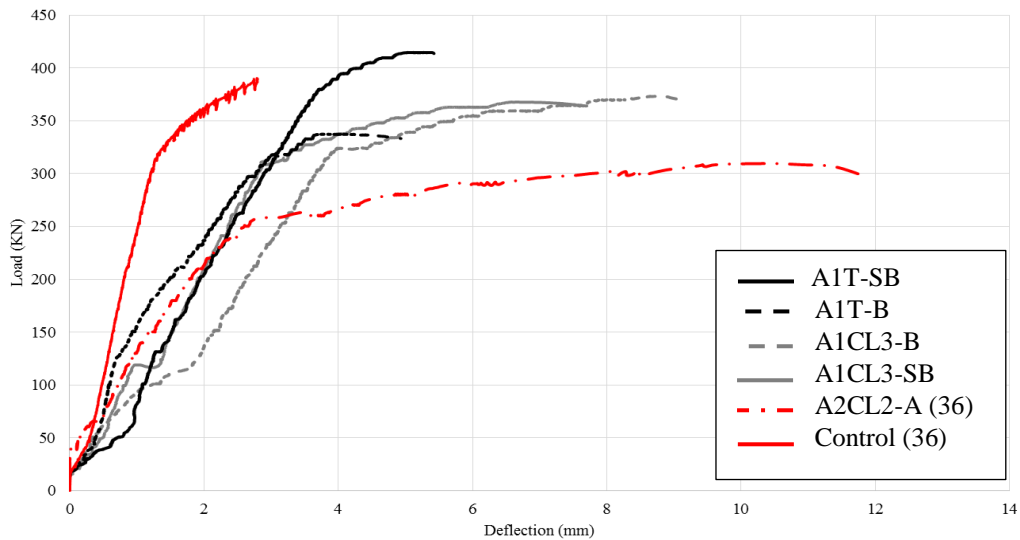


Figure 2 - 14 Load-deflection curves for all beams

The shear repaired control beam A1T-SB failed at 414.6 kN. This was larger than the ultimate load capacity of control beam A1T-B not repaired for shear, which failed at 337.4 kN. The ultimate load capacities of shear repaired corroded beam A1CL3-SB and the non-shear-repaired beam A1CL3-B were close to each other (367.8 kN and 373.3 kN respectively). Figure 2-14 also shows that the stiffness of shear-repaired beams A1T-SB and A1CL3-SB

was different from that of the non-shear-repaired beams A1T-B and A1CL3-B. The different cracking pattern, shown in figure 15, can explain this difference in stiffness. Figure 2-14 also presents the load-deflection curves for two similar non-repaired short span beams (75cm), one control and one corroded A2CL2-A, tested by Dang (36). Figure 2-14 also shows that both the control non-repaired beam tested by Dang (36) and the beam repaired in bending A1T-B have almost the same yielding capacity which reflects that the strengthening with NSM FRP rod in bending didn't increase the anchorage capacity for both beams as they failed with diagonal tension failure with slipping of tensile steel bars.

The same ultimate load capacity values were obtained for both beams A1T-B and A1CL3-B as there was no steel corrosion found at the end of beam A1CL3-B where diagonal crack appears (see Figure 2-11), the post-yielding deflection difference between both beams can be explained by the difference of the tensile steel bars slipping of both beams (Figure 2-18) as in case of A1CL3-B, the maximum slipping was only between 10%-20% of the maximum slipping of A1T-B.

As shown in figure 2-15, repairing against shear changed the mode of failure for the beams from diagonal tension failure to compression crushing of concrete, the shear repaired control and corroded beams (A1T-SB and A1CL3-SB) failed due to compression crushing of concrete while the non-shear-repaired corroded beam A1CL3-B, failed due to a combination of diagonal tension failure and compression crushing of the concrete. This was not the case for the non-shear-repaired control beam A1T-B, which failed due to diagonal tension failure induced by slipping of the tensile steel bars.

Shear strengthening leads to a change in failure mode from diagonal crack failure close to support due to slipping of re-bars at anchorage, to large flexural crack at mid span followed by concrete crushing. As a result, yielding of tension steel bars which occurred close to support for beams without shear strengthening move to mid-span for shear strengthening beams.

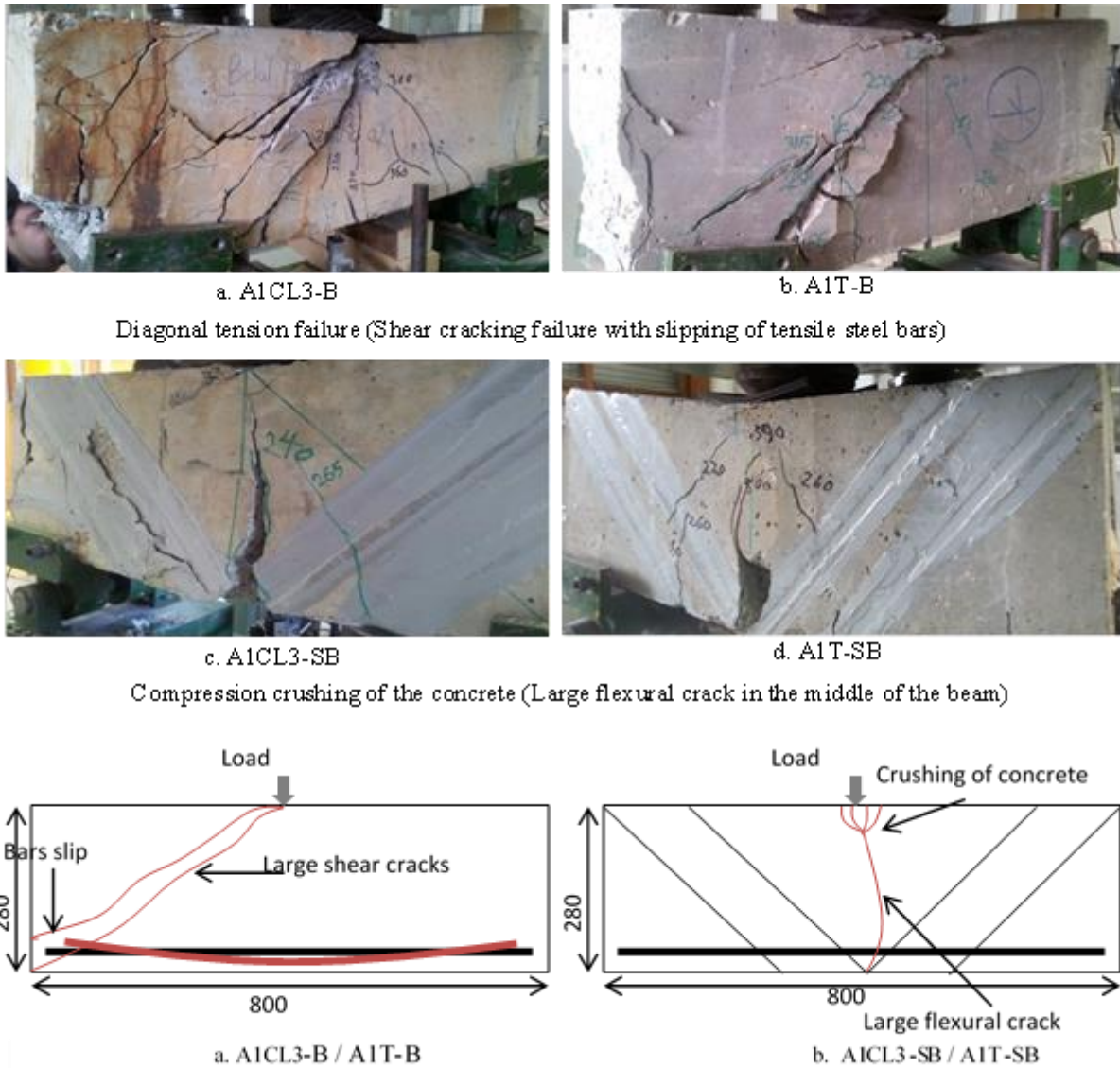


Figure 2 - 15 Failure modes for all beams tested

Figure 2-16 (a) shows the yielding load capacity values for beams non-repaired in shear with NSM FRP rods, all of the beams were failed due to diagonal tension crack failure with the slipping of tensile steel bars, the decrease in yielding capacity for A2CL2-A beam compared with the others refer to the 10 % loss in cross section due to corrosion which found in tensile steel bars at the edge of the beam (the same edge of diagonal tension failure) (36), while figure 2-16 (b) shows the difference in yielding capacity for the two beams repaired in shear with NSM FRP rods, the difference also happened due to the 6% loss in tensile steel bar diameter (figure 2-11) which meets 12 % loss in cross section at mid span.

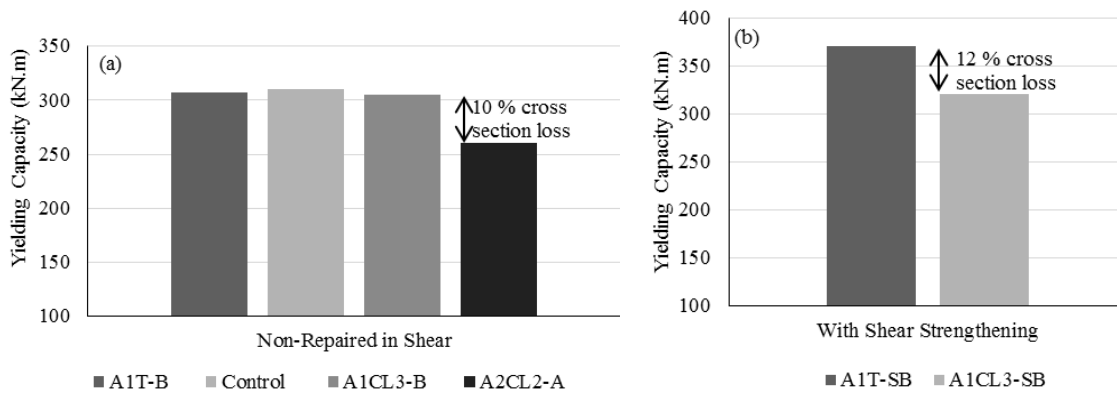


Figure 2 - 16 Yielding capacity values for all beams

Diagonal shear failure occurred always on the same side of the short beams whatever the corrosion damage because of the difference in anchorage length between both beam edges. Indeed, figure 2-17 presents the steel layout inside the four beams A1T-B, A1T-SB, A1CL3-B and A1CL3-SB, the load was located at the middle of each beam while the steel geometry is not symmetrical inside the beams as there is 2 cm at the edge of each full beam, the diagonal tension crack failure and the tensile steel bar slip happened in the NC edge as shown in figure 2-15.

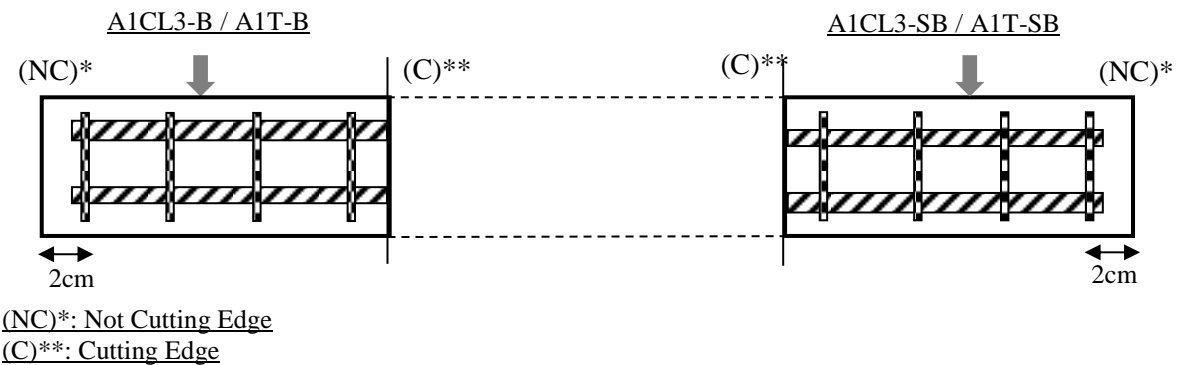


Figure 2 - 17 Steel layouts inside the four beams

2.3.3 Slip measurements

Figure 2-18 shows the slip measured for tensile steel bar ends in all tested beams.

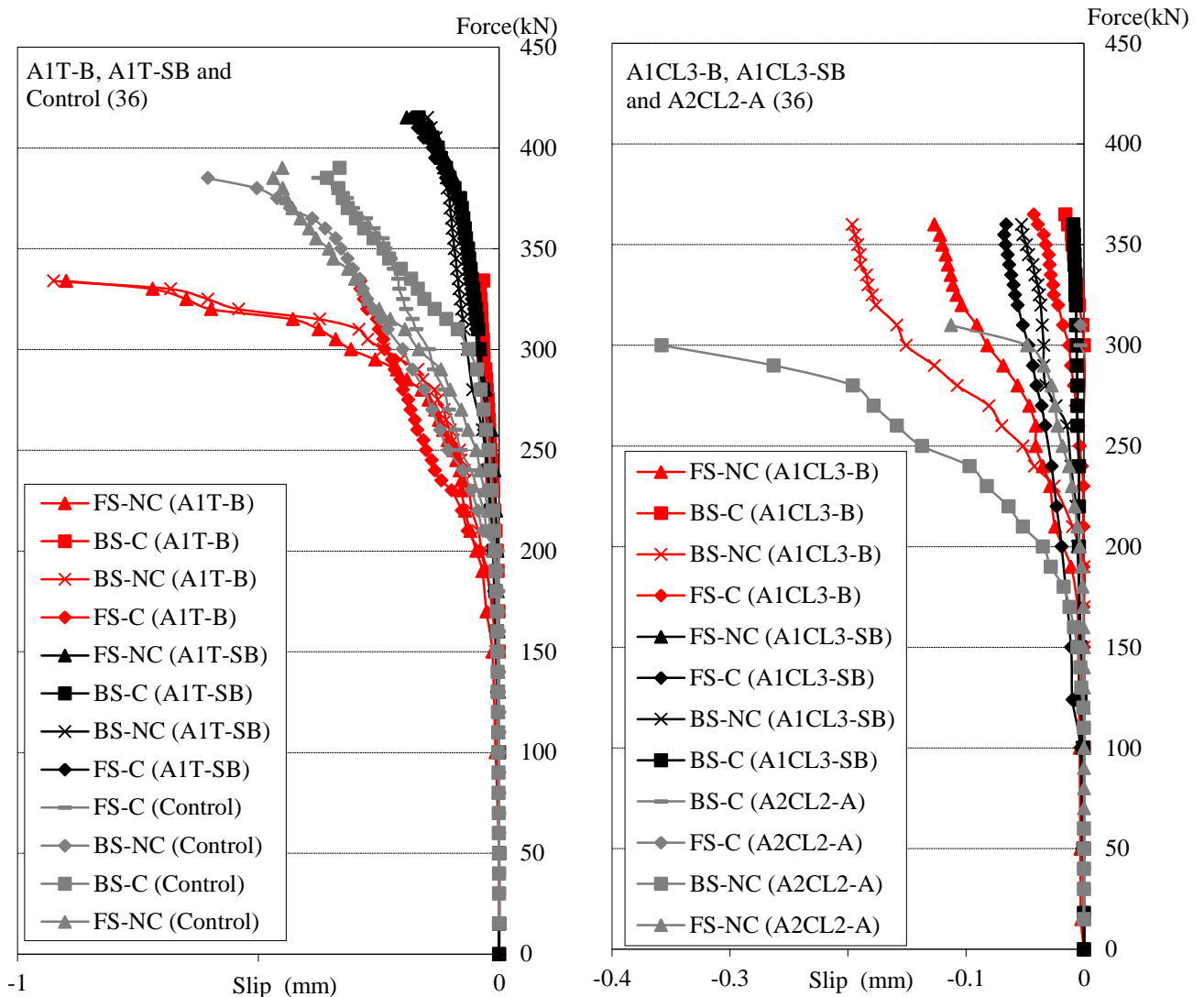


Figure 2 - 18 Slip measurements for all beams

The steel bars started to slip at 170 kN and 150 kN in the non-shear-repaired corroded beam (A1CL3-B) and control beam (A1T-B) respectively, while for beams A2CL3-A and A2CL3-B tested by Khan et al. (12), slipping started at 100 kN and 150 kN respectively. Figure 18 shows that, without shear repair, slipping of the tensile steel bars was greater in the case of non-corroded beam (A1T-B) than in the case of corroded beam (A1CL3-B), figure 18 also shows the slipping of the tensile steel bars for one control beam and one corroded beam A2CL2-A (non-repaired neither in bending nor in shear with NSM) tested by Dang (36). Moreover, failure of control beam (A1T-B) was a consequence of the re-bar slipping on the support. This result may appear surprising, as it is usually accepted that corrosion reduces the bond stress (37), it must be borne in mind that the natural corrosion process (38) confinement

due to both the corroded stirrups (39) and the reactive force on the support modify the bond capacity as shown by Cairns et al. (40). Moreover, natural corrosion of beam A1CL3-B did not lead to corrosion all around the perimeter of the re-bars and so did not result in the same change in bond strength as the accelerated corrosion induced by impressed current that is usually described in literature.

As shown in figure 2-18, which compares the shear-repaired beams A1T-SB and A1CL3-SB with beams A1T-B and A1CL3-B not repaired in shear and beams not repaired neither in bending nor in shear with NSM Dang (36), it is clear that repairing for shear with NSM CFRP rods significantly increased the anchorage capacity.

2.3.4 Effect of corrosion

The effect of corrosion on the shear resistance is a complicated area of study due to the variability in failure modes. In this section, the data of maximum corrosion damage was used for comparison in terms of load bearing capacity. Khan et al. (12) tested two beams (A2CL3-A and A2CL3-B) of the same type as those tested in this study but which were 1.15 meters long without any repair either in bending or in shear. The maximum loss in the cross sectional area of the steel was found to be 25% and 21% in longitudinal tensile steel bars, and 36% and 60% in the steel stirrups for A2CL3-A and A2CL3-B respectively. The re-bar diameter loss wasn't reflected by a significant change in the ultimate load capacity compared to the control beam (values shown in table 2-8). This agrees with the results found here, as the maximum load capacities for corroded beam A1CL3-B and control beam A1T-B were 373.3 kN and 337.4 kN respectively. The maximum diameter loss of longitudinal steel bars was 18% for beam A1CL3-B and 9% for A1CL3-SB. The diameter loss of the longitudinal steel bars at the middle of beam A1CL3-SB was 6%, which corresponds to 12% loss of cross section and matches the theoretical 46.2 kN (0.12×385) loss in the yielding capacity in comparison with A1T-SB. The loss in yielding capacity was found to be 50 kN experimentally, as shown in figure 2-19.

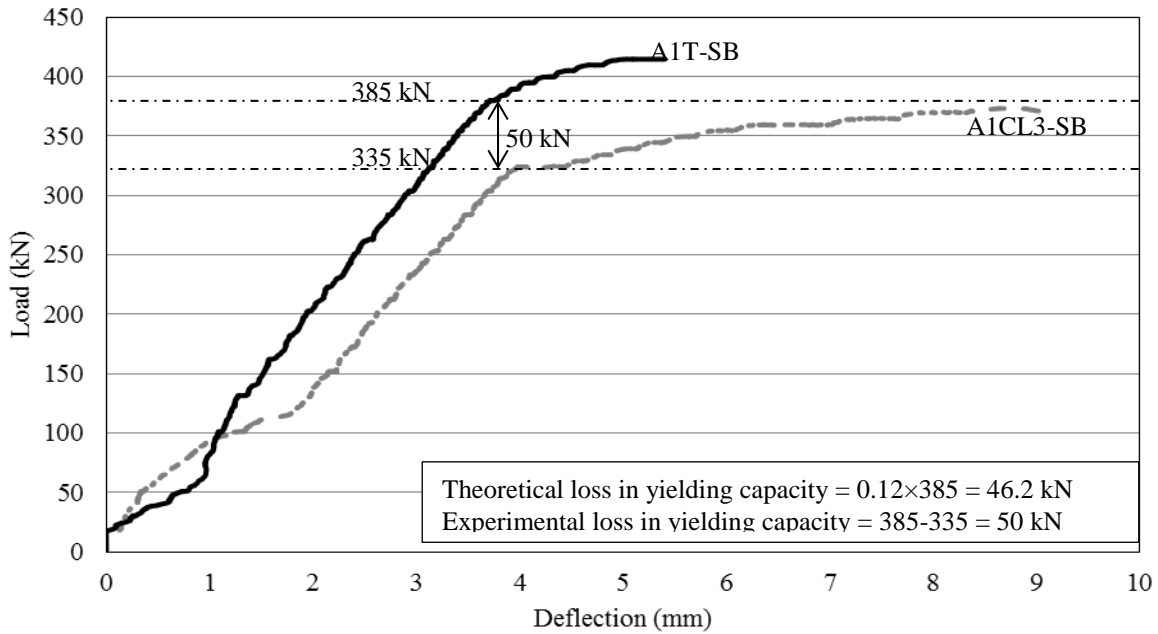


Figure 2 - 19 Effect of corrosion on yielding load capacity of beams repaired in shear

It is also noteworthy that the slipping of the steel bars that occurred in the corroded beam A1CL3-B was on the left side (not corroded) while, on the other side (corroded with 18 % of diameter loss), no slip was recorded, which agrees with findings on the control beam A1T-B as a great deal of slip was recorded in that beam despite the fact that it was not corroded. The same result found by Khan et al. (12) who recorded more steel bar slip in the control beam than in the corroded one.

2.3.5 Effect of NSM CFRP repair on the ultimate load capacity

A summary of test results for the CFRP repair on tested beams is presented in Tables 2-8, 2-9 and 2-10. In order to compare the ratio of shear span “a” to effective depth “d” (a/d ratio) for all beams, a dimensionless parameter k is introduced; it corresponds to the a/d ratio divided by the load capacity ratio assuming that for short span beams, the ultimate capacity is proportional to the span.

It is clear that the NSM repair in shear has a crucial effect on the load capacity of RC control beams, as the slip of tensile steel bars was reduced in this case. As shown in table 2-9, the non-repaired control beams gave a value of k less than 1 in comparison with control beam repaired in shear and bending with NSM (A1T-SB) which denotes the increase percentage in load capacity over the non-repaired control beams tested in (12) and (36). For corroded beams (table 2-10), the shear repair with NSM had no effect on load capacity for a/d greater than 2.7. On the other hand, there was no marked increase in the load capacity due to repair with NSM for corroded beams which had a/d values less than 2, which could be explained by the reduced importance of the bending effect of RC beams as the a/d values decreased.

Table 2 - 8 Summary of NSM CFRP repair effect for repaired and non-repaired beams

Beam	Type of repair	Max. Diameter loss in steel bars %	Ultimate Load (kN)	Failure mode
A1T-B	Bending	0	337	Diagonal tension failure & slip of tensile steel bars
A1T-SB	bending & shear	0	415	Compression crushing of the concrete
A1CL3-B	Bending	18	373	Diagonal tension failure & slip of tensile steel bars
A1CL3-SB	bending & shear	9	368	Compression crushing of the concrete
A2T(12)	Non	0	261	Diagonal tension failure
A2CL3A (12)	Non	25	230	Diagonal tension failure
A2CL3B (12)	Non	21	256	Diagonal tension failure

Table 2 - 9 Effect of shear repair with NSM for control beams

Beam	a/d ⁽¹⁾	Ultimate Load (kN)	Load capacity ratio (R1) (4/5)	a/d ratio(R2) (3/2)	k : (R2)/(R1)
A1T-SB	1.4 ⁽²⁾	415 ⁽⁴⁾	-	-	-
A2T(12)	2 ⁽³⁾	261 ⁽⁵⁾	1.59	1.43	0.90
Control 1 (36)	3.125 ⁽³⁾	119.2 ⁽⁵⁾	3.48	2.23	0.64
Control 2 (36)	2.7 ⁽³⁾	155 ⁽⁵⁾	2.68	1.93	0.72

Table 2 - 10 Effect of shear repair with NSM for corroded beams

Beam	a/d ⁽¹⁾	Ultimate Load (kN)	Load capacity ratio (R1) (4/5)	a/d ratio(R2) (3/2)	k : (R2)/(R1)
A1CL3-SB	1.4 ⁽²⁾	368 ⁽⁴⁾	-	-	-
A2CL3A (12)	2 ⁽³⁾	230 ⁽⁵⁾	1.60	1.43	0.89
A2CL3B (12)	2 ⁽³⁾	256 ⁽⁵⁾	1.44	1.43	0.99
A2CL1-A (36)	3.125 ⁽³⁾	110 ⁽⁵⁾	3.35	2.23	0.67
A2CL2-B (36)	2.7 ⁽³⁾	120 ⁽⁵⁾	3.07	1.93	0.63
A2CL2-A (36)	1.67 ⁽³⁾	310 ⁽⁵⁾	1.19	1.19	1

2.3.6 Effect of a/d ratio on the shear strength

Kani (41,42) was one of the first to study the effect of size for slender, deep beams. One important parameter having a crucial effect on the shear strength value is the span to section depth (effective) ratio (a/d) of the beam, for which Kani (41) found a transitional point of a/d ratio around 2.5-3. Below this point, the beams developed an arch action and had a considerable reserve of strength beyond the first cracking point. In this paper the a/d effect

was studied for the beams repaired with NSM by plotting the experimental values of shear strength for beams having different values of a/d , some of which were repaired with NSM in bending and shear, while others were repaired in bending only and the rest were non-repaired beams. The analytical load capacities using the classical bending theory have also been added to the graph as a reference (Figure 2-20).

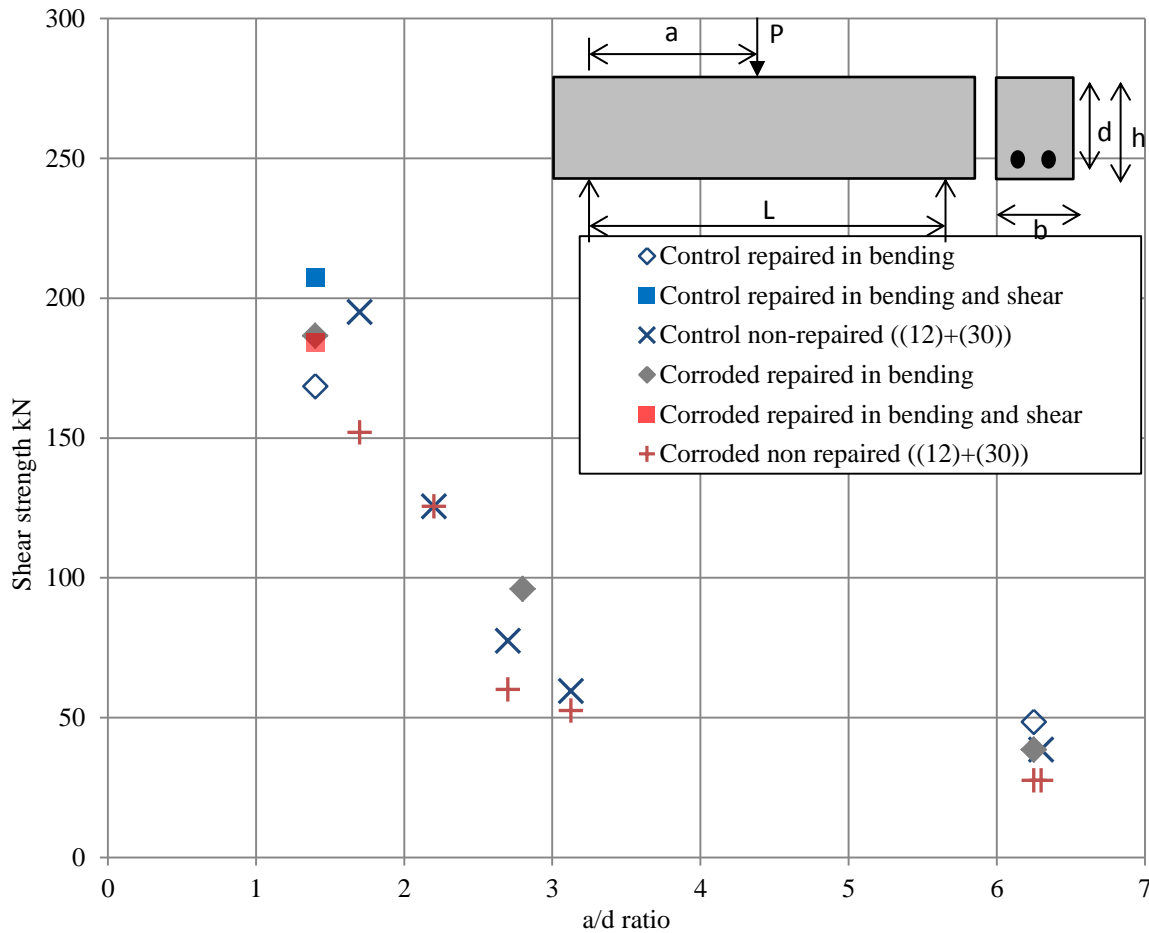


Figure 2 - 20 a/d ratio effect on the shear strength of beams

Figure 2-20 shows two general trends for the shear strength values; the first trend represent the deep beams (a/d less than 3) and the second represents the slender beams (a/d greater than 3). It is clear that the shear strength decreases for increasing a/d ratios and the reduction in shear strength is steeper than in the slender beams, in agreement with the result found by Higgins and Farrow (43). The a/d ratio is considered to be an important parameter for deep beams as the general trend found for such beams is far from the classical bending theory effect. By adding FRP in shear, not only the bonding anchorage but also the yielding capacity of the whole beam was increased. More also shown in Figure 2-20, the control beam repaired in shear gave higher value of shear strength than the non-repaired ones.

Shear resistance mechanism of non-strengthened and non-corroded elements is not totally clarified (44), shear is one of a few areas of research into fundamentals of the behaviour of concrete structures where contention remains amongst researchers. There is a continuing debate between researchers from a structures perspective and those from a materials or fracture mechanics perspective about the mechanisms that enable the force flow through a concrete member and across cracks) and so with corrosion and NSM strengthening, the complexity of the problems will increase significantly.

2.4 Conclusions

According to the results found in this paper, the following conclusions can be drawn:

1. The failure mode of all non-shear-repaired RC beams (corroded and control) was due to shear cracking while, for shear-repaired beams the failure mode changed to concrete crushing with a large flexural crack at the middle.
2. Corrosion reduced the slip of the tensile steel bars on the support as the pressure induced by the support closed the corrosion induced cracks. As a result, loss of anchorage which was the cause of failure for non-repaired control beams was not involved in the failure of non-repaired corroded beams.
3. Depending on the location of cracks induced by the load during the mechanical testing, the corrosion found in the vicinity of cracks led to a reduction in the yielding capacity of the corroded RC beam.
4. Repairing against shear using NSM FRP rods significantly decreased the maximum slip of the tensile steel bars for control RC beams.
5. No marked effect of shear repair with NSM was recorded on the load capacity of corroded beams having shear span to effective depth ratio values less than 2.
6. Even with reinforcement corrosion and use of repair CFRP rods in both bending and shear, there was still a change in mechanical response in bending for a/d ratios around 2.5-3, which is a transition zone between bending response and shear response.
7. Non-linear numerical models which are able to consider both corrosion damage and strengthening interventions with NSM are required in the future.

2.5 References

1. Schmitt G. Global needs for knowledge dissemination, research, and development in materials deterioration and corrosion control. *World Corros Organ N Y*. 2009.
2. Andrade C, Alonso C, Garcia D, Rodriguez J. Remaining lifetime of reinforced concrete structures: effect of corrosion on the mechanical properties of the steel. In: *Proceedings of the international conference on life prediction of corrodible structures*. National Association of Corrosion Engineers, Cambridge, UK, 23–26 September; 1991. p. 12/1–11.
3. Al-Sulaimani G, Kaleemullah M, Basunbul I. Rasheeduzzafar,(1990)“Influence of corrosion and cracking on bond behaviour and strength of reinforced concrete members” *ACI Structural Journal*, 87 (2), 220-231. ASTM G1. 1990.
4. Rodriguez J, Ortega L, Casal J. Load carrying capacity of concrete structures with corroded reinforcement. *Constr Build Mater*. 1997;11(4):239–48.
5. Chung L, Najm H, Balaguru P. Flexural behavior of concrete slabs with corroded bars. *Cem Concr Compos*. 2008;30(3):184–93.
6. Azad AK, Ahmad S, Azher SA. Residual strength of corrosion-damaged reinforced concrete beams. *ACI Mater J*. 2007;104(1).
7. Torres-Acosta AA, Navarro-Gutierrez S, Terán-Guillén J. Residual flexure capacity of corroded reinforced concrete beams. *Eng Struct*. 2007;29(6):1145–52.
8. Xia J, Jin W, Li L. Shear performance of reinforced concrete beams with corroded stirrups in chloride environment. *Corros Sci*. 2011;53(5):1794–805.
9. Wang X-H, Li B, Gao X-H, Liu X-L. Shear behaviour of RC beams with corrosion damaged partial length. *Mater Struct*. 2012;45(3):351–79.
10. Wang X-H, Gao X-H, Li B, Deng B-R. Effect of bond and corrosion within partial length on shear behaviour and load capacity of RC beam. *Constr Build Mater*. 2011;25(4):1812–23.
11. Zhu W, François R. Effect of corrosion pattern on the ductility of tensile reinforcement extracted from a 26-year-old corroded beam. *Adv Concr Constr*. 2013;1(2):121–37.
12. Khan I, François R, Castel A. Experimental and analytical study of corroded shear-critical reinforced concrete beams. *Mater Struct* 2014;47:1467–81.
13. De Lorenzis L, Nanni A. Shear strengthening of reinforced concrete beams with near-surface mounted fiber-reinforced polymer rods. *ACI Struct J*. 2001;98(1).
14. Islam AA. Effects of NSM CFRP bars in shear strengthening of concrete members. *ASCE*; 2009. p. 1–14.
15. Rizzo A, De Lorenzis L. Behavior and capacity of RC beams strengthened in shear with NSM FRP reinforcement. *Constr Build Mater*. 2009;23(4):1555–67.

16. Dias SJ, Barros JA. Performance of reinforced concrete T beams strengthened in shear with NSM CFRP laminates. *Eng Struct.* 2010;32(2):373–84.
17. De Lorenzis L, Nanni A, La Tegola A. Flexural and shear strengthening of reinforced concrete structures with near surface mounted FRP rods. 2000. p. 521–8.
18. Barros JA, Baghi H, Dias SJ, Ventura-Gouveia A. A FEM-based model to predict the behaviour of RC beams shear strengthened according to the NSM technique. *Eng Struct.* 2013;56:1192–206.
19. Castel A, François R, Arliguie G. Mechanical behaviour of corroded reinforced concrete beams—Part 1: experimental study of corroded beams. *Mater Struct.* 2000;33(9):539–44.
20. Vidal T, Castel A, François R. Corrosion process and structural performance of a 17 year old reinforced concrete beam stored in chloride environment. *Cem Concr Res.* 2007;37(11):1551–61.
21. Dang VH, François R. Influence of long-term corrosion in chloride environment on mechanical behaviour of RC beam. *Eng Struct.* 2013;48:558–68.
22. Zhu W. Effect of corrosion on the mechanical properties of the corroded reinforcement and the residual structural performance of the corroded beams. PhD thesis at Univeristy of Toulouse. (2014).
23. Zhang RJ, Yang HL, L’Hostis V, Castel A, François R. Characterization of Steel/Concrete Interface for a Long-Term Corroded Beam Stored in Chloride Environment. *Adv Mater Res.* 2011;163:3415–20.
24. Poursaee A, Hansson C. Potential pitfalls in assessing chloride-induced corrosion of steel in concrete. *Cem Concr Res.* 2009;39(5):391–400.
25. Yuan Y, Ji Y, Shah SP. Comparison of two accelerated corrosion techniques for concrete structures. *ACI Struct J.* 2007;104(3).
26. Otieno M, Beushausen H, Alexander M. Prediction of corrosion rate in reinforced concrete structures—a critical review and preliminary results. *Mater Corros.* 2012;63(9):777–90.
27. French regulations for reinforced concrete structures. B.A.E.L. 1983.
28. Khan I, François R, Castel A. Structural performance of a 26-year-old corroded reinforced concrete beam. *Eur J Environ Civ Eng.* 2012;16(3-4):440–9.
29. EN 206-1. European standard, concrete – Part 1: specifications, performance, production and conformity. NF EN 206-1; April. 2004.
30. EN 12390–2, 3, 5. Essai pour béton durci: confection et conservation des éprouvettes pour essais de résistance, résistance à la compression des éprouvettes et résistance à la flexion des éprouvettes. Bruxelles: IBN; 2000.
31. Norme Europeenne NF EN 18-459: Porosity and density test.
32. Al-Mahmoud F, Castel A, François R, Tourneur C. Effect of surface pre-conditioning on bond of carbon fibre reinforced polymer rods to concrete. *Cem Concr Compos.* 2007;29(9):677–89.

33. Al-Mahmoud F, Castel A, François R, Tourneur C, Marchand J, Bissonnette B, et al. Anchorage and tension-stiffening effect between Near-Surface-Mounted Fiber Reinforced polymer rod and concrete. 2006.
34. Al-Mahmoud F, Castel A, François R, Tourneur C. Strengthening of RC members with near-surface mounted CFRP rods. *Compos Struct.* 2009;91(2):138–47.
35. François R, Khan I, Dang VH. Impact of corrosion on mechanical properties of steel embedded in 27-year-old corroded reinforced concrete beams. *Mater Struct.* 2013;46(6):899–910.
36. Dang VH. Initiation and propagation phases of re-bars corrosion in pre-cracked reinforced concrete exposed to carbonation or chloride environment. PhD thesis at l'Institut National des Sciences Appliquées de Toulouse, France. 2013.
37. Almusallam AA. Effect of degree of corrosion on the properties of reinforcing steel bars. *Constr Build Mater.* 2001;15(8):361–8.
38. Tahershamsi M, Zandi K, Lundgren K, Plos M. Anchorage of naturally corroded bars in reinforced concrete structures. 2014;
39. Hanjari KZ, Coronelli D, Lundgren K. Bond capacity of severely corroded bars with corroded stirrups. *Mag Concr Res.* 2011;63(12):953–68.
40. Cairns J, Plizzari GA, Du Y, Law DW, Franzoni C. Mechanical properties of corrosion-damaged reinforcement. *ACI Mater J.* 2005;102(4).
41. Basic facts concerning shear failure. ACI; 1966.
42. Kani G. How safe are our large reinforced concrete beams? ACI; 1967.
43. Higgins C, Farrow III WC. Tests of reinforced concrete beams with corrosion-damaged stirrups. *ACI Struct J.* 2006;103(1).
44. fib Bulletin No. 57. Shear and punching shear in RC and FRC elements. 2010. 268 p.

Conclusions

There was no important effect of the NSM as a shear repair on the load capacity of the corroded RC beams having shear span to effective depth (a/d) ratio values less than 2, as for the corroded shear-repaired RC beam A1CL3-SB which has a/d equals to 1.4, the ultimate load capacities of shear repaired corroded beam A1CL3-SB and the non-shear-repaired beam A1CL3-B were close to each other (367.8 kN and 373.3 kN respectively) which could be explained by the reduced importance of the bending effect of RC beams as the a/d values decreased. While for control beams, the shear repaired control beam A1T-SB failed at 414.6 kN. This was larger than the ultimate load capacity of control beam A1T-B not repaired for shear, which failed at 337.4 kN.

Repairing against shear with NSM CFRP rods changed the failure mode from shear cracking (for non-shear-repaired beams) to concrete crushing with a large flexural crack at the middle (for shear-repaired beams).

The NSM also reduced significantly the maximum slip of the tensile steel bars for control RC beams. Moreover, failure of control beam (A1T-B) was a consequence of the re-bar slipping on the support while for corroded edges less slipping occurred which could be reasoned for the confinement of the natural corrosion system for both the corroded stirrups and the reactive force on the support which increase the bond capacity between steel and concrete.

The (a/d) ratio is considered to be an important parameter for deep beams as the general trend found for such beams is far from the classical bending theory effect. By repairing with CFRP rods in shear, not only the bonding anchorage but also the yielding capacity of the whole beam was increased, for (a/d) ratios between (2.5-3) which is a transition zone between bending response and shear response, a change in the mechanical response in bending was noticed.

Chapter 3

Flexural strengthening of corroded RC beams with NSM CFRP rods, a finite element modelling part

Introduction

As the first two chapters presented the experimental results of the NSM repair response on both flexural and shear aspects of the corroded RC beams, chapter 3 presents numerical models aim at studying the flexural response of the NSM repair of the corroded RC beams presented in chapter 1. The numerical models are based on non-linear finite element method using two approaches, starting with a 2D models using FEMIX code and moving to a 3D using ABAQUS for a specific RC beam case.

This chapter studies the RC beams repaired in bending with NSM CFRP rods which were presented in the first chapter, two-dimensional FE models for five RC beams are shown in this chapter and were produced in the finite element computer code FEMIX , two of them were control beams: one repaired beam with NSM A1T-R and one non-repaired beam A2T, the other three beams were corroded: one repaired beam with NSM A1CL3-R and two non-repaired beams A2CL3 and A2CL1, an elasto-plastic multi-fixed smeared crack model implemented in FEMIX is presented here along with the uniaxial constitutive models for both corroded and non-corroded steel bars.

In order to check the validity of the FE models implemented by FEMIX, a comparison is presented between the experimental and the FE numerical results for all five RC beams in terms of moment-deflection curves and crack patterns.

More investigation is also presented throughout implementing three-dimensional FE models (for the corroded repaired beam A1CL3-R) using the commercial software ABAQUS in order to study the special failure mode obtained from the experimental results which happened by the separation of the concrete cover due to the corrosion cracks plane. The concrete as well as the steel bars properties used in the 3D model are shown.

Finally, a complete procedure of creating horizontal corrosion crack plane is described and the 3D failure pattern for the repaired RC beam A1CL3-R is presented and compared to the experimental one.

Behaviour of corroded Reinforced Concrete beams repaired with NSM CFRP rods, Experimental and Finite Element Study

Belal ALMASSRI (1), Firas AL MAHMOUD (2), Raoul FRANCOIS (1)

(1) *Université de Toulouse; UPS, INSA, LMDC (Laboratoire Matériaux et Durabilité des Constructions), Toulouse, France*

(2) *Institut Jean Lamour, UMR 7198, CNRS, Université de Lorraine, Nancy, France*

Keywords: corrosion, repair, RC beams, NSM rods, failure mode, FEM, FEMIX, ABAQUS

ABSTRACT

The near surface mounted reinforcement (NSM) technique is one of the promising techniques used nowadays to strengthen reinforced concrete RC structures. In the NSM technique, the Carbon Fibre Reinforced Polymer (CFRP) rods are placed inside pre-cut grooves and are bonded to the concrete with epoxy adhesive. This paper investigates corroded RC beams repaired with NSM CFRP rods and studies the failure mode of the repaired beam according to experimental and numerical modelling results. Experimental results and numerical modelling results of a 2D finite element (FE) model using the FEMIX computer code were obtained on five, 3-metre-long beams: three corroded RC beams that had been exposed to natural corrosion for 25 years and two control beams with no corrosion. Two beams, one corroded and one control (A1CL3-R and A1T-R) were each repaired in bending with one 6-mm-diameter NSM CFRP rod and were then tested in three-point bending up to failure. The corrosion of the tensile steel bars and steel stirrups was studied. Ultimate capacity, yielding capacity and failure modes are also discussed. The experimental results showed that the NSM technique increased the overall capacity (ultimate load capacity and yielding capacity) of control and corroded beams despite a non-classical mode of failure with separation of the concrete cover occurring in the corroded beam due to damage induced by corrosion. The FE numerical modelling results from FEMIX were compatible with the experimental ones except for the repaired corroded beam A1CL3-R, for which a three-dimensional model using the commercial software ABAQUS was required. Finally some comparisons were made between the experimental and FE numerical modelling results obtained using ABAQUS in order to study the specific mode of failure of the corroded beam, which occurred by the separation of concrete cover.

3.1 Introduction

Corrosion of reinforcing steel is still a very important area of study for reinforced concrete structures as the cost induced by repairs to corroded RC structures world-wide exceeds \$1.8 trillion per year (1). Much research has been conducted to assess the damage to corroded RC structures. (2–4) presented such damage, starting from the reduction of cross sectional area of the steel and reduction of its ductility and ending with cracking and bonding problems in the RC elements, which lead to the early failure of structures.

The near surface mounted reinforcement (NSM) technique is one of the most promising techniques used nowadays for strengthening deteriorated structures. In the NSM technique, the Carbon Fibre Reinforced Polymer (CFRP) rods are placed inside pre-cut grooves and are bonded to the concrete with epoxy adhesive. (5–8) have shown that the NSM strengthened members can be expected to be much more ductile than externally-bonded-laminate (EBR) strengthened members and fail at much higher strain levels. De Lorenzis and Teng (9) showed also some of the advantages of the NSM technique over the EBR strengthening technique: (1) the NSM installation process is less time consuming, (2) the NSM reinforcements are protected from natural and accidental damage and (3) the NSM technique has better bonding as the FRP rod is fully embedded in this case. In addition, Bilotta et al. (10) showed that the tensile strength of FRP material used in the NSM technique was well exploited and debonding was delayed compared to the EBR technique.

Kreit et al. (11) and Al-Mahmoud et al. (12) indicated that the use of NSM reinforcement could significantly improve the flexural performance of the RC beams by increasing their ultimate load-bearing capacity, and Almassri et al. (13) showed that the NSM technique also restored sufficient ductility (2.8 times that of the non-repaired corroded beams) despite the ductility loss of steel bars induced by corrosion.

The experimental data presented by Al-Mahmoud et al. (12) was used later by Hawileh (14), who presented an FE model that could predict the ultimate capacity of RC beams subjected to 4-point loading using the commercial FEM-based computer software ANSYS. It was found that the diameter of the FRP reinforcement rod had a crucial effect on the stiffness and the ultimate capacity of the RC beams strengthened with NSM, the use of 16-mm-diameter FRP rod increasing the ultimate capacity by 83.6% compared to that of a beam strengthened with a 6-mm-diameter rod.

The computer code FEMIX has been used by several researchers to simulate RC beams strengthened with NSM strips. Sena Cruz et al. (15) showed that the epoxy adhesive had a

negligible effect on the global behaviour and the crack pattern and load-deflection curves obtained numerically in this study matched the experimental results.

The FEM-based computer software ABAQUS has been used several times to simulate RC beams, as by Lundqvist et al. (16), who studied the anchorage length of CFRP rod needed to prevent premature failure, while Radfar et al. (17) used ABAQUS to study the peeling-off failure mode in beams strengthened with externally bonded FRP laminates. Another study Kang et al. (18) used ABAQUS in order to study the percentage increase of the load bearing capacity when using different groove depths of NSM FRP laminates as a strengthening technique. Few studies have used FE models to investigate the mechanical behaviour of corroded RC beams repaired with the NSM CFRP rod technique.

The present paper studies the performance of five RC beams: one corroded and one control (non-corroded) repaired in bending with the NSM CFRP rod technique, and three non-repaired corroded and control beams. All beams were tested statically in three-point loading up to failure. The failure modes, and the ultimate and the yield moment capacities for all beams were studied. An FE model for all RC beams was created using the computer code FEMIX, and the moment-deflection curves and the modes of failure were compared to the experimental results. A high degree of compatibility was found between experimental and FEM results even though the 2-D model in FEMIX was not able to capture all aspects of corroded repaired beam A1CL3-R (e.g. the sufficient deflection at failure). It was necessary to implant a 3-D model in order to investigate the specific mode of failure of RC beam A1CL3-R using the commercial software ABAQUS.

3.2 Experimental programme

An experimental programme was started at LMDC (Laboratory of Materials and Durability of Constructions) in 1984 with the aim of understanding the effects of steel corrosion on the structural behaviour of RC elements. Many experimental studies have been conducted on those beams to evaluate the development of corrosion cracking, to measure chloride content, and to analyse the change of mechanical behaviour (19,20). The natural aggressive environment system is presented in (11).

The five beams studied in this paper were of the same type (the same size and shape of reinforcement but different values of service loading). One corroded beam (A1CL3-R) and one control beam (A1T-R) were repaired with one 6-mm-diameter CFRP rod and tested in bending by (13). Long-term corroded beams A2CL1 and A2CL3, and control beam A2T tested by (21,22) but not repaired were also used here for comparison.

Two loading values were applied: $M_{ser1} = 13.5$ kN.m for beams referred to as A1 (A1CL3-R and A1T-R) and $M_{ser2} = 21.2$ kN.m for beams referred to as A2 (A2CL1, A2CL3 and A2T). The layout of the reinforcement is shown in Figure 3-1. For these beams, M_{ser} represented the maximum loading value versus durability in an aggressive environment (serviceability limit-state requirements in an aggressive environment).

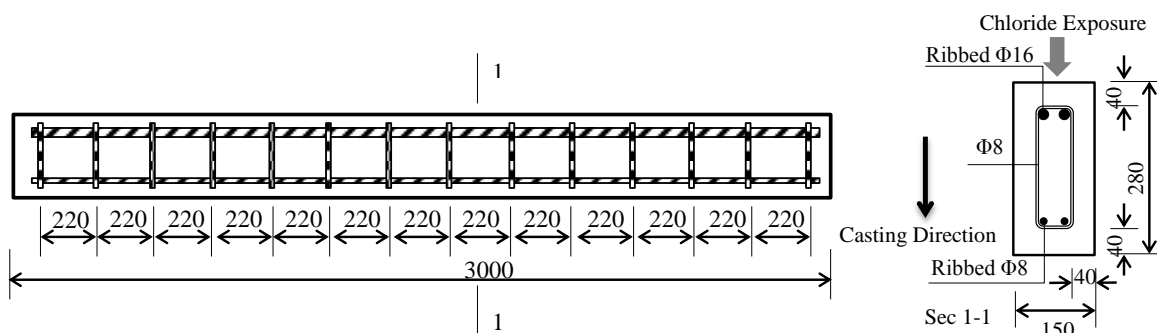


Figure 3 - 1 Reinforcement layout of type A beams. Dimensions are in mm

3.2.1 Material properties

3.2.1.1 Concrete properties

The average compression strength and the elastic modulus obtained on cylindrical specimens (11 cm diameter \times 22 cm height) were 45 MPa and 32 GPa respectively at 28 days. The tensile strength, measured using the splitting test, was 4.7 MPa. Water Porosity was 15.2%. To measure the present-day characteristics of the concrete, 70 \times 140 mm cylindrical cores were

drilled out of each beam and tested in both compression and tension. Table 3-1 shows the results of these core tests.

Table 3 - 1 Mechanical characteristics of the concrete at 27 years (average values of 3 tests)

Mechanical characteristics	A1CL3-R	A1T-R	A2T	A2CL3	A2CL1
Compression strength (MPa)	62.2	58.9	58.5	61.5	58.8
Tensile strength (MPa)	6.85	6	6	6.2	6
Elastic modulus (MPa)	34 000	30 000	32 000	32 000	32 000

3.2.1.2 Characterization of steel Bars, CFRP Bars and filling material

The ordinary ribbed reinforcing steel bars used were composed of natural S500 half-hard steels. The characteristics of the steel bars were measured after extracting the corroded bars from the corroded beam A1CL3-R and non-corroded bars from the control beam A1T-R. The specimens consisted of two corroded and two control steel bars of 400 mm length (the corroded steel bar specimens were extracted from the beam near the maximum corrosion pit found, as shown in figure 3-5) and their properties are presented in Table 3-2. The behaviour of corroded steel bars was the same as found by (23): the true yielding stress was the same for control and corroded specimens; the ultimate stress was higher for corroded than for control specimens as the brittle failure induced by corrosion strongly reduced the necking effect, which is not taken into account to calculate actual ultimate stress. The corrosion led to a brittle failure of bars in tension which was characterized by a strong reduction in ultimate elongation.

Table 3-3 shows the mechanical properties of the CFRP rods found in François' paper and the mechanical properties given by the manufacturer and by laboratory tests (24). In order to increase the bond between the CFRP rods and the filling material, the CFRP rods were coated with 0.2/0.3 mm of surface sanding material, which was sprinkled onto an epoxy resin applied to the surface of the rods. Table 3-4 shows the characteristics of the filling material (epoxy resin) after 7 days according to the manufacturer.

Table 3 - 2 Average values of steel bar properties

Specimen Type	Young's modulus (GPa)	Yield Strength (MPa)	Ultimate Strength (MPa)	Ultimate strain
Corroded specimen	200	550	604	4%
Non-corroded specimen	200	550	645	8%

Table 3 - 3 CFRP rod characteristics

Type of test	Ultimate strength (MPa)	Modulus of Elasticity (MPa)
Manufacturer's test	2300	150000
Laboratory test	1875	145900

Table 3 - 4 Filling material properties according to the manufacturer

Material	Compressive Strength (MPa)	Tensile Strength (MPa)	Elastic Modulus (MPa)
Epoxy	83	29.5	4900

Figure 3-2 shows the experimental tensile stress-strain curves for corroded steel bars, non-corroded steel bars and CFRP rods.

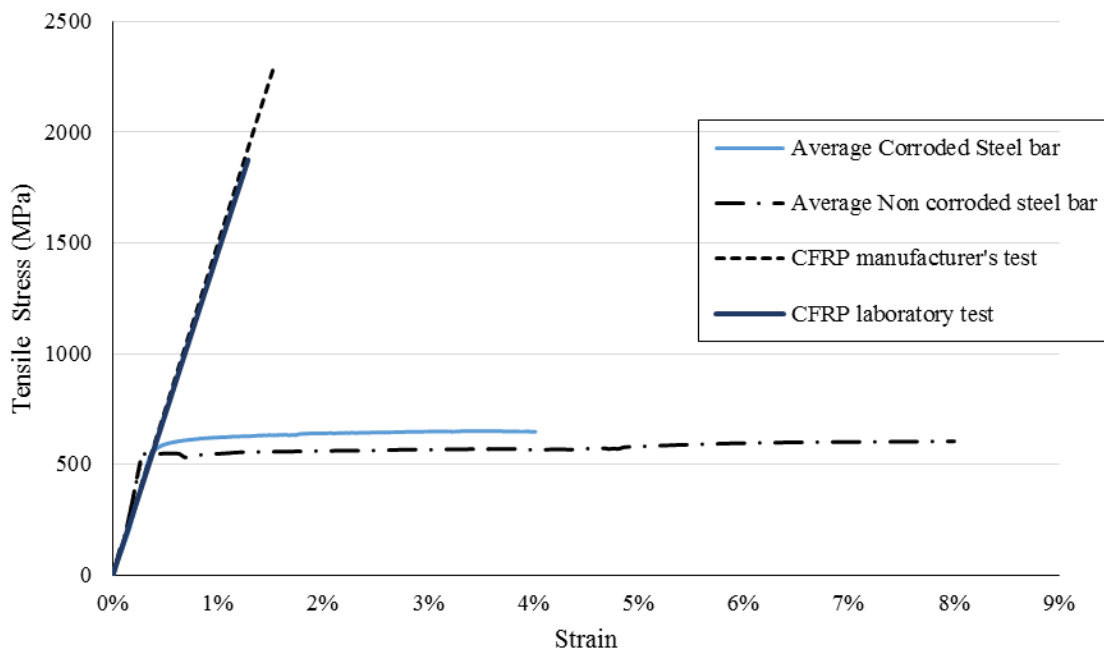


Figure 3 - 2 Tensile stress-strain curves for steel and CFRP rods (Corroded and control steel bar curves are average results of 2 tested specimens in each case)

3.2.2 NSM repair technique

The NSM CFRP rod was installed in the corroded beam A1CL3-R and in the control beam A1T-R by making two cuts in the concrete cover in the longitudinal direction at the tension side. A special concrete saw with a diamond blade was used. The groove was 15 mm deep (only 20 mm of concrete cover for beams) and 15 mm wide (around 2.5 times the rod diameter) (25). Figure 3-3 presents the main steps of this repair process while figure 3 shows the final shape of the repaired beams after their surfaces had been levelled.

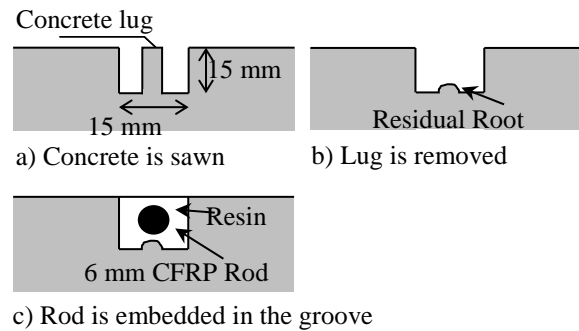


Figure 3 - 3 Installation of CFRP rod in concrete surface

The two beams were tested 1 week after the installation of the CFRP rod in order to ensure the maximum degree of adhesion between the concrete surface and the epoxy resin material. Figure 3-4 shows the concrete surfaces of the RC beams after the installation the CFRP rods.

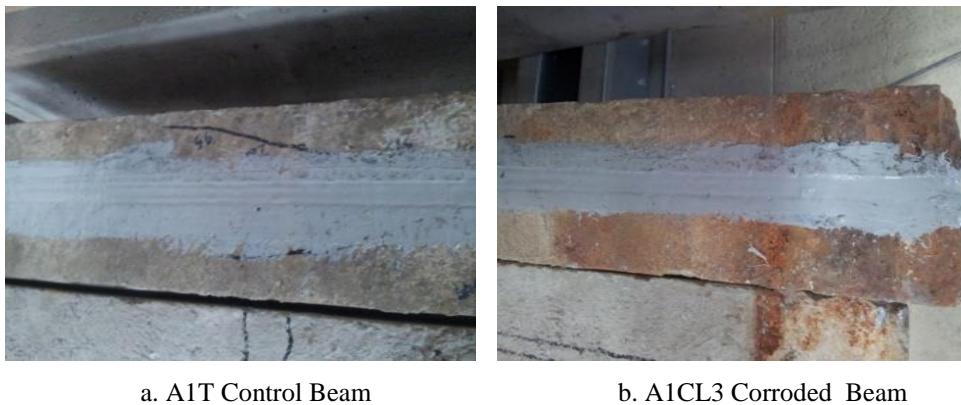


Figure 3 - 4 Concrete surfaces after installation of the CFRP rod.

3.3 Experimental results

3.3.1 Corrosion damage of the steel bars in corroded beam A1CL3-R

The values of the diameter losses were measured for both the Back Side (BS) and Front Side (FS) tensile steel bars which were extracted from the corroded beam A1CL3-R just after the bending test. The maximum diameter loss was found to be 38% at 120 cm from the left edge of the beam. The corrosion was found both at the top of the bars close to the surface cover, reflecting the classical result for natural corrosion (26), and at the bottom of the bars, reflecting the effect of casting direction and bar location at the top of the beam, known as “Top-bar effect” (27,28).

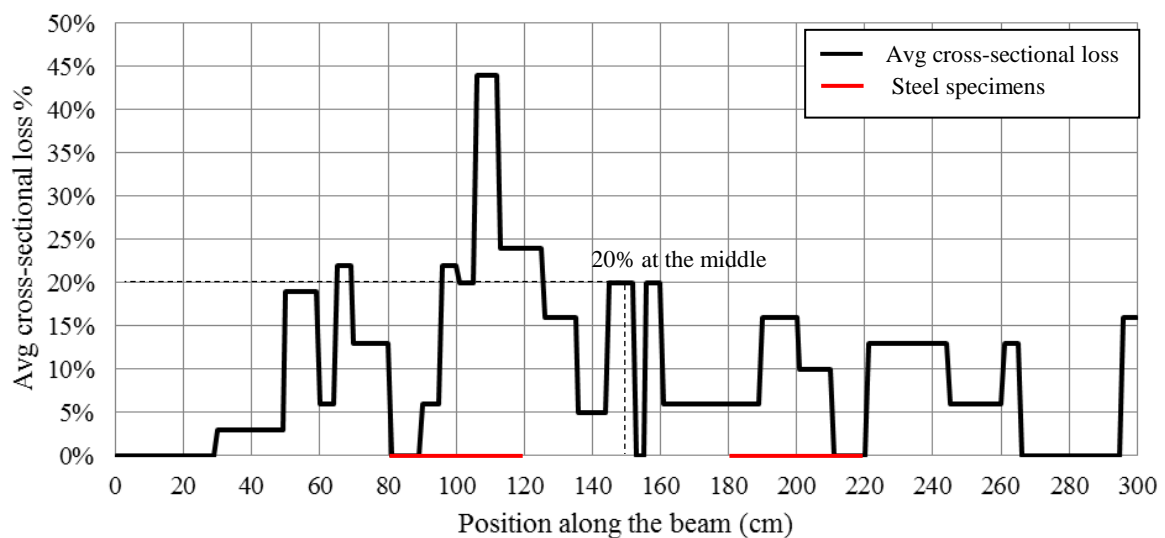


Figure 3 - 5 Average cross-section loss percentages in corroded beam A1CL3-R.

Figure 3-5 shows the average loss of cross-section along the beam calculated from both tensile bars. Despite the presence of a large local loss of steel cross-section at 110 cm from the beam end and 40 cm from the point load, the experimental results did not show any failure of steel re-bars during the bending test. It is therefore assumed that the yielding of steel during the loading occurred at mid-span, where the average loss of cross-section was 20%.

The steel stirrups were also measured for corrosion and it was found that stirrup corrosion was mostly located on the horizontal part of stirrups at the top of the beam according to the casting direction. This was related to the corrosion of tensile steel bars, while compressive steel bars showed corrosion pits only. It was assumed that stirrup corrosion did not influence the residual bending behaviour of corroded beams, so it was not taken into account in the modelling.

3.3.2 Response in bending for both corroded and non-corroded repaired beams

The two repaired beams A1CL3-R and A1T-R were tested with 3-point loading up to failure. More details of the experimental set-up can be found elsewhere (13). Figure 3-6 shows the bending moment versus the deflection for the two beams. The ultimate moment values were 52 kN.m and 66 kN.m respectively. Yielding and ultimate bending moment were reduced to similar extents: by 12 kN.m and 13.5 kN.m respectively. The ultimate elongation was reduced by 33%, which is quite considerable even though non-repaired corroded beams have exhibited more brittle behaviour (more than 50% of reduction) in previous studies (29).

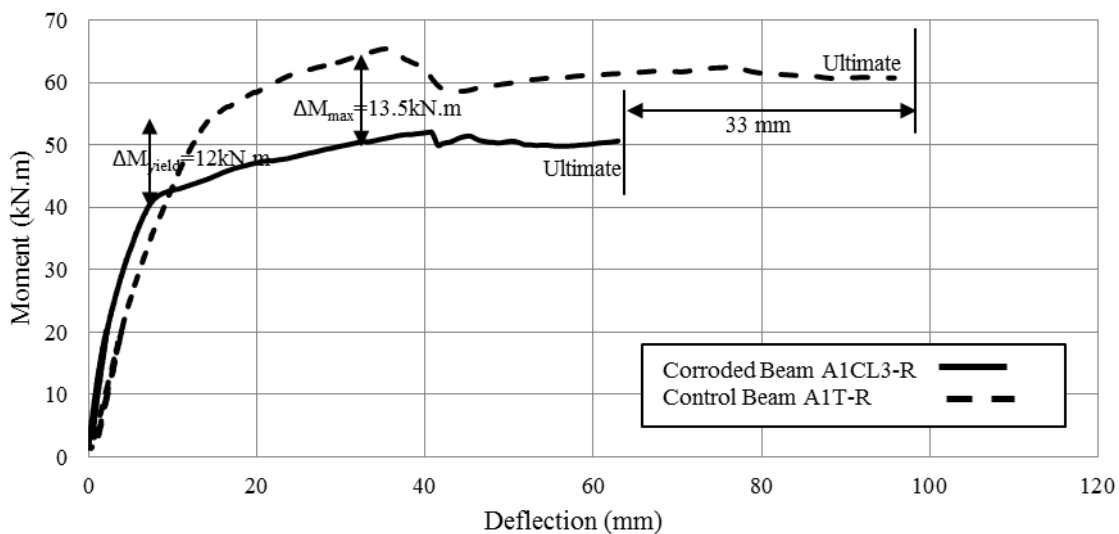


Figure 3 - 6 Moment-deflection curves for beams A1CL3-R and A1T-R tested experimentally

3.3.3 Failure modes

The failure mode of non-repaired type A beams is usually due to steel bar yielding followed by concrete crushing (21). After strengthening with NSM FRP rod, the RC beams may fail by concrete crushing, pull-out of the FRP rods or peeling-off as shown by (12). The failure of the repaired control beam A1T-R occurred by the crushing of compressed concrete while the failure mode observed for A1CL3-R was different from both the conventional and non-conventional failure modes found on non-corroded repaired beams. The failure of the repaired corroded beam A1CL3-R was due to the separation of the concrete cover as shown in Figure 3-7. It is also important to note that failure of the RC beams tested here was not due to brittle failure of the tensile corroded steel bars as usually found by previous studies on corroded RC beams (19–21,29).

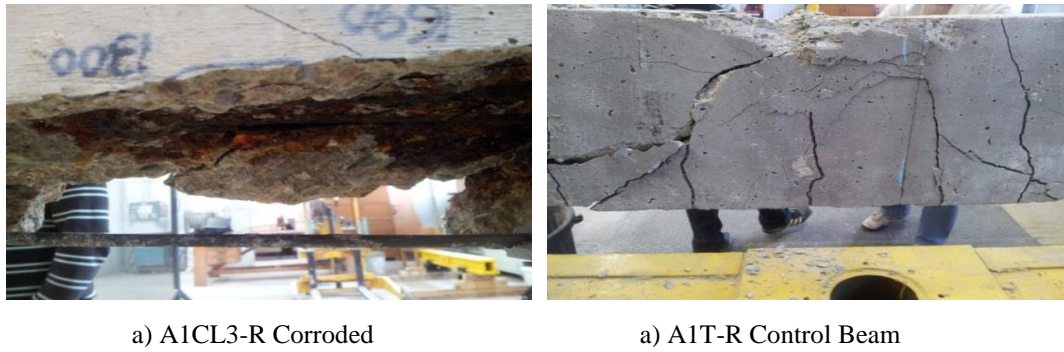


Figure 3 - 7 Experimental failure modes

3.4 Numerical modelling

FEMIX 4.0 is a computer code that has the ability to analyse structures by using the Finite Element Method (FEM). FEMIX code is integrated with GiD interface software which provides pre- and post-processing for numerical simulations analysis. FEMIX is based on the displacement method; it has a large number of types of finite elements inside, such as 3D frames and trusses, plane stress elements, flat or curved elements for shells, and 3D solid elements. Linear elements may have two or three nodes while plane stress elements may have 4, 8 or 9 nodes and 8 or 20 hexahedral nodes. Embedded line elements can be included in the analysis with the availability of static or dynamic tests using both linear and non-linear material configurations. Advanced numerical techniques are available, such as the Newton-Raphson method combined with arc-length techniques and path dependent or independent algorithms.

3.4.1 Concrete properties

An elasto-plastic multi-fixed smeared crack model was created on GiD FEMIX in order to define the concrete material (15). When the crack occurs in a sampling point, the total incremental strain becomes a sum of reversible elastic strain and irreversible plastic (crack) strain. The crack strain is controlled by the fracture parameters of the material. The Rankine criterion was used to define the concrete in tension and the Owen and Figueiras (30) yield surface was used to define the concrete in compression. The crack evolution in fracture mode was simulated using a tri-linear tension softening or stiffening diagram as shown in figure 3-8.

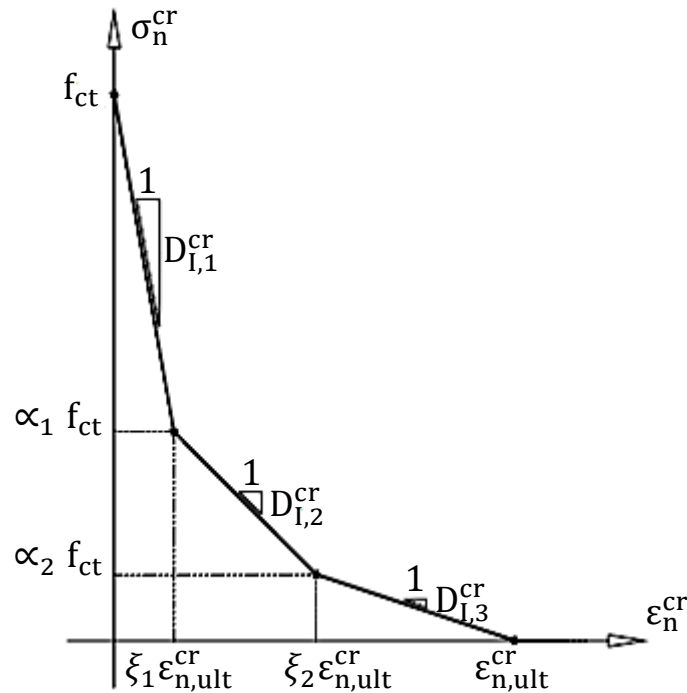


Figure 3 - 8 Tension softening diagram for concrete

Table 3-5 presents the concrete properties used in the numerical simulations. From the mean value of the experimentally obtained compressive strengths, all the other parameters were estimated. The post-cracking behaviour of the reinforced concrete was simulated using a tri-linear tensile-softening diagram.

Table 3 - 5 concrete properties used in FEMIX simulation analysis

Poisson's ratio	$\nu_c = 0.20$
Initial Young's modulus	$E_c = 30\,000\text{ N/mm}^2$
Compressive strength	$f_c = 60\text{ N/mm}^2$
Tri-linear tensile-softening diagram	$f_{ct} = 4.5\text{ N/mm}^2$, $G_f' = 0.09\text{ N/mm}$ $\xi_1 = 0.005$, $\alpha_1 = 0.5$, $\xi_2 = 0.3$, $\alpha_2 = 0.2$
Parameter defining the mode I fracture energy available to the new crack	$P_2 = 1$
Threshold angle	$\alpha_{th} = 30^\circ$

3.4.2 CFRP rods

The CFRP rod was modelled with an elastic stress-strain curve up to brittle failure in tension according to the manufacturer's criteria (tensile stress-strain curve is shown in Figure 3-2).

3.4.3 Steel reinforcement properties

The non-linear behaviour of the steel reinforcement bars was considered to be elastic-plastic. A Poisson's ratio of 0.3 was used, and the elastic modulus and yield strength values of the steel reinforcement bars and stirrups were as shown in Table 3-2. The post yielding hardening behaviour of the steel bars was modelled as shown in figure 3-10 (a) and (b). From the experimental tensile stress-strain results for steel bars (shown in figure 3-2), it was found that the ultimate strain value for the corroded steel bars was equal to half the ultimate strain value for non-corroded steel bars - the same result as obtained by Dang and François (31). The average ductility factor ($\epsilon_{u\text{-corroded}} / \epsilon_u$) was reduced to 0.5 for RC beams having cross-sectional loss of over 15% in the tensile steel bars, as shown in figure 3-9.

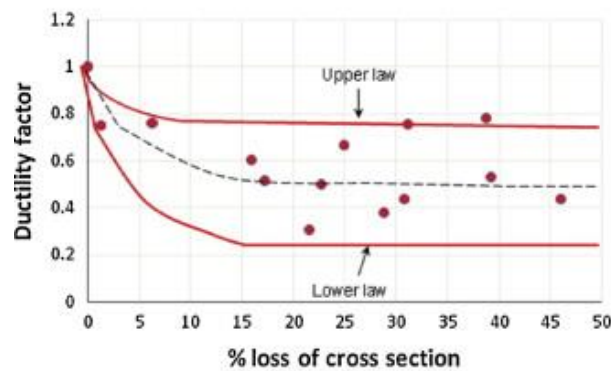


Figure 3 - 9 Ductility factor ($\epsilon_{u\text{corroded}}/\epsilon_u$) for steel bars versus corrosion, from Dang & Francois (31)

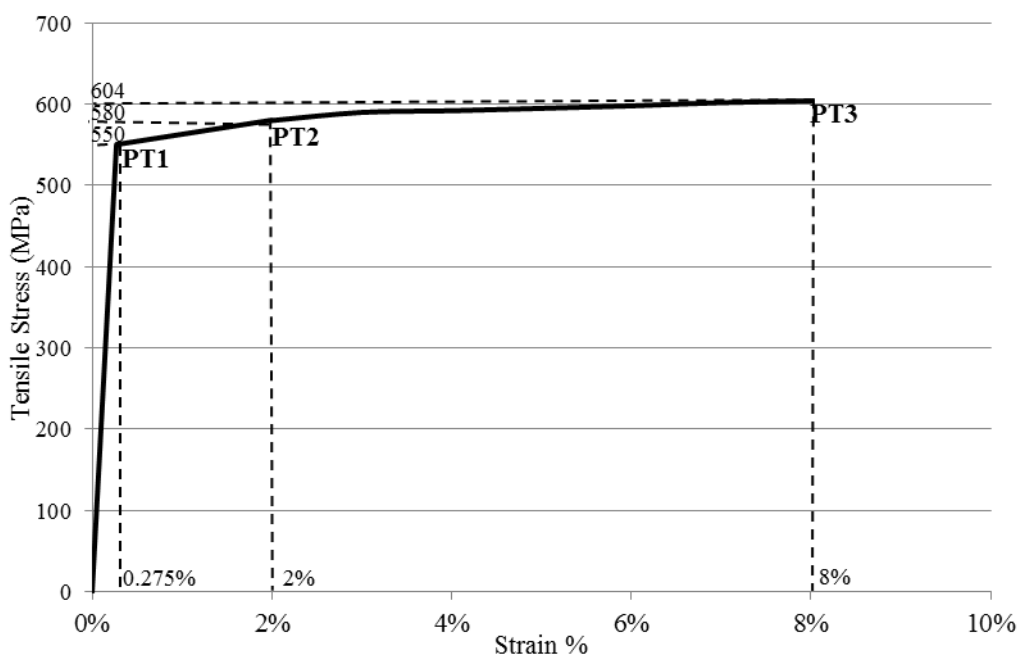


Figure 3 - 10 (a) uniaxial constitutive model for non-corroded rebar

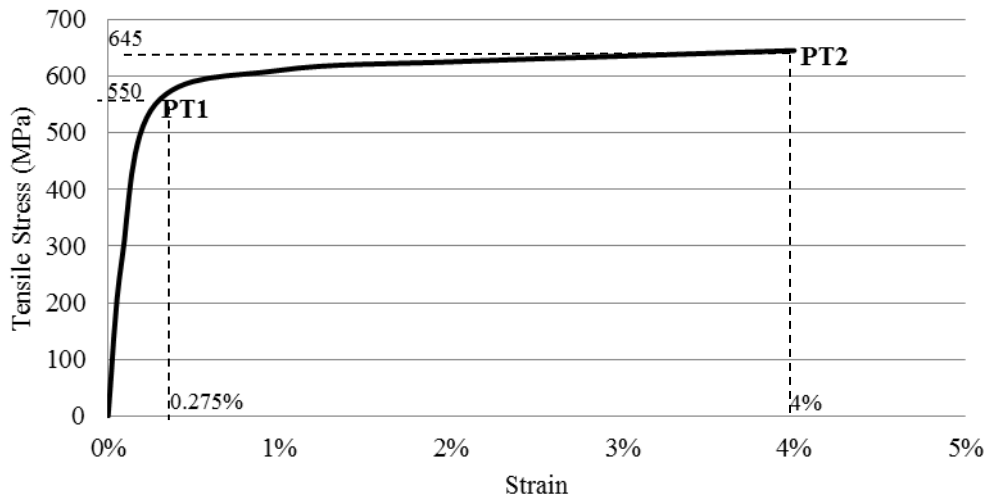


Figure 3 – 10 (b) uniaxial constitutive model for corroded rebar

3.4.4 Modelling of RC beams

The objective of this part is to create a reliable numerical model that can simulate and predict the global behaviour of five RC beams and analyse the NSM strengthening effect in bending. Two of the beams were control beams: A1T-R, A2T and the other three were corroded: A1CL3-R, A2CL3 and A2CL1 (A1T-R and A1CL3-R were RC beams strengthened with NSM CFRP rod in bending). To simulate the concrete in the beams, 8-node plane stress elements with 3×3 Gauss-Legendre integration were used. The steel bars and stirrup reinforcements, and the CFRP rods, were simulated using 3-node quadratic embedded cable elements with two Gauss-Legendre integration points. For this point, the steel bars and stirrups, as well as the CFRP rods, were assumed to be fully bonded with the concrete. Figures 3-11 and 3-12 show the geometry, elements mesh, loading and support configuration.

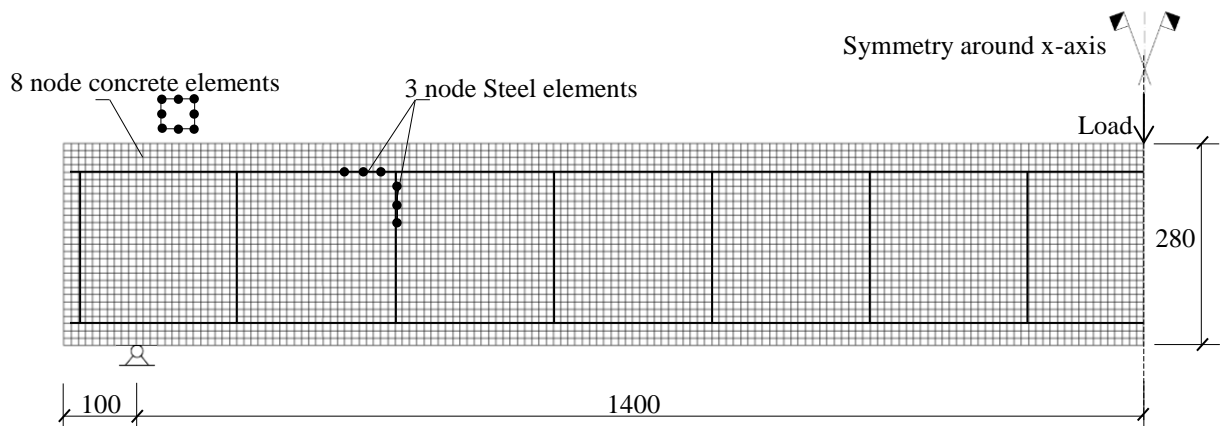


Figure 3 - 11 Geometry in (mm), mesh, loading and support conditions for non-strengthened beams with NSM CFRP

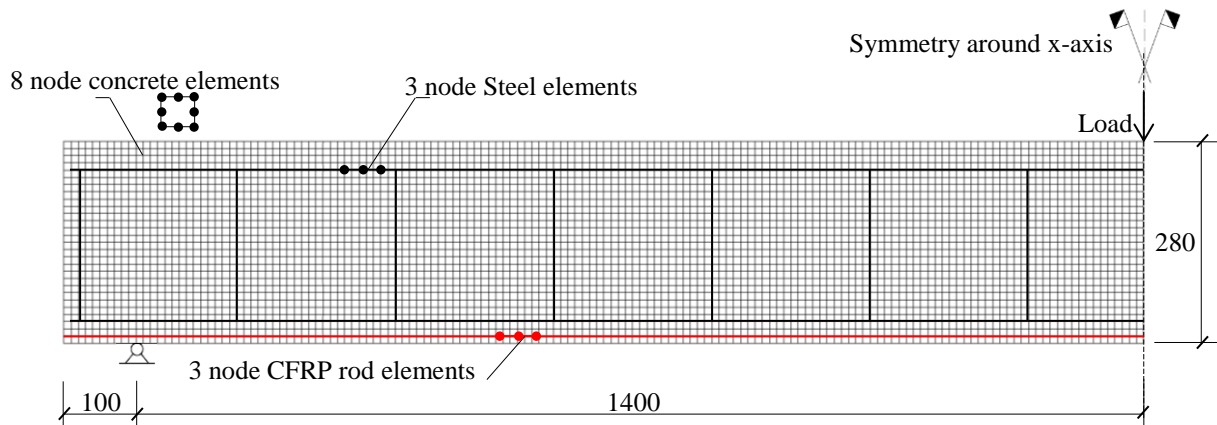


Figure 3 - 12 Geometry, mesh, loading and support conditions for strengthened beams with NSM CFRP

3.4.4.1 Corroded RC beams

The main goals of the numerical modelling were to capture the changes in yielding capacity, ultimate capacity and ultimate deflection values of the RC beams due to the corrosion of the reinforcing steel bars. As a result, the residual re-bar cross-section at the failure location was used here for all corroded RC beams that failed due to the failure of corroded tensile steel bars. The residual re-bar cross section was assumed to be constant all along the reinforced concrete beams. For RC beams that did not fail by brittle failure of corroded tensile steel bars, the residual steel cross-section at mid span was used as the constant cross section all along the beam. Moreover a perfect bond was assumed between the re-bars and the concrete, even in cases of corrosion of the reinforcement. This assumption did not allow the change in bending stiffness due to corrosion to be modelled. Both the decrease in the steel-concrete bond and the variability in the change of steel-cross section induced by corrosion along the beams have an influence of the load-deflection response of corroded beams.

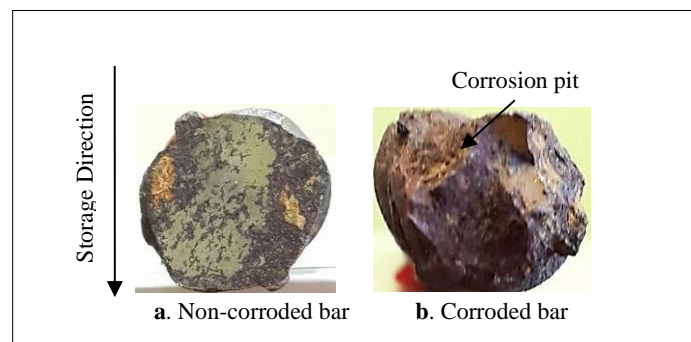


Figure 3 - 13 corrosion pits in tensile steel bars of corroded RC beam

A reduction of 20 % of the steel cross-section was considered for the repaired RC beam A1CL3-R (13), while the percentage values for beams A2CL3 and A2CL1 were considered to be 21.5 % and 30 % respectively (21). The reduction of the tensile steel bar diameters was not uniform in shape due to the existence of corrosion pits (shown in figure 3-13). The corrosion in steel stirrups was not considered in this model as it would have no effect on the flexural behaviour of the RC beams.

3.4.4.2 Results for all beams

Figure 3-14 shows the load-deflection curves for all beams tested experimentally, together with the numerical modelling results from 2-D FE modelling using the FEMIX computer code.

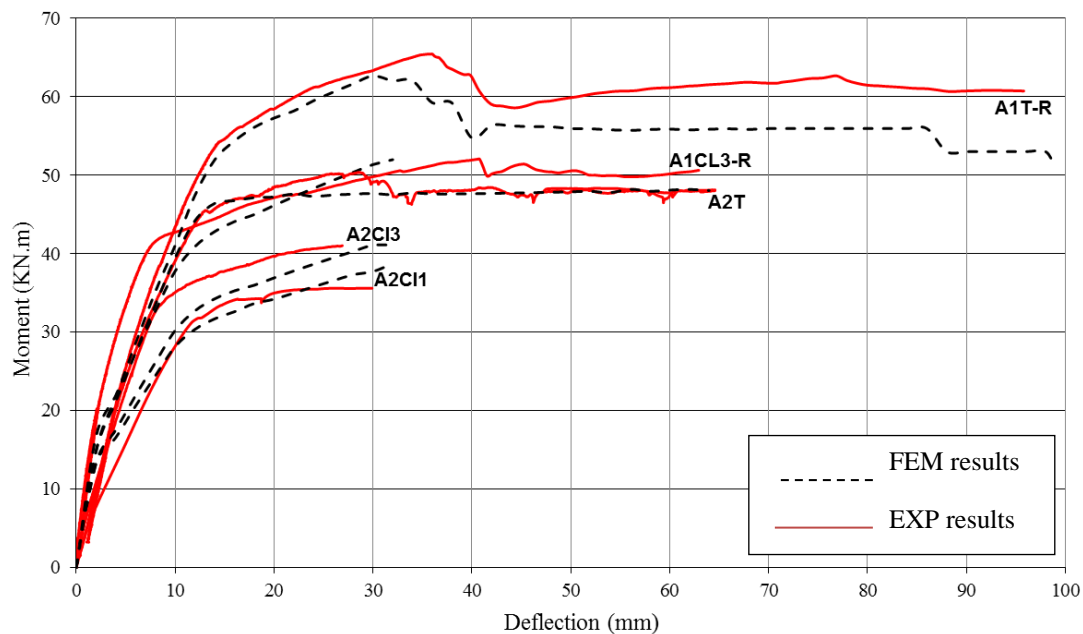


Figure 3 - 14 Load Deflection curves for all beams using FEMIX

The start of yielding of the steel reinforcements and the ultimate load carrying capacity were well predicted by the numerical models for all beams. The reduction in ultimate deflection of corroded beams was also well predicted by the model as the change in steel ultimate elongation induced by corrosion which was implemented in the modelling.

The post-yielding behaviour of corroded beams appeared to be stiffer than that of control beams due to a harder post-yielding behaviour of corroded steel bars than of controls (as shown in figure 3-10)

The only exception occurred in beam A1CL3-R, where the predicted ultimate deflection appeared to be half the experimental value. Moreover, it was the only beam with corroded

steel that did not collapse by brittle failure of the tensile steel bars, so modelling would be expected to predict a higher deflection. Thus it seems that the 2D model approach implemented could not model the behaviour of corroded RC beams repaired with NSM rods. Moreover, corroded repaired beam showed a non-classical mode of failure with separation of the concrete cover. Thus, the need for a 3D model to investigate this special mode of failure was highly evident for this point. Figure 3-15 presents a sample of the classical crack failure pattern that occurred for all beams, with large flexural cracks at the middle along with crushing of the concrete.

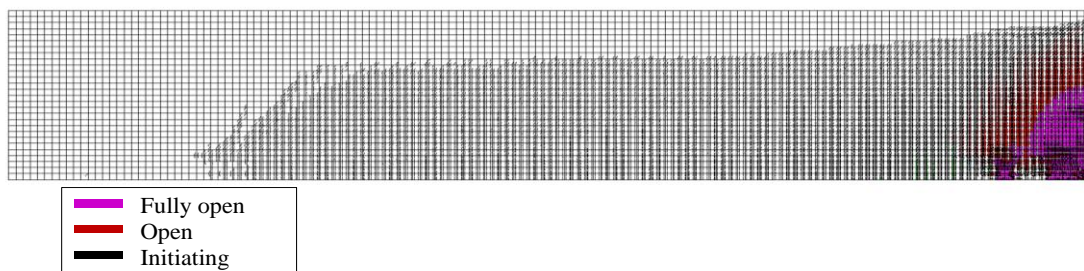


Figure 3 - 15: 2D crack failure pattern using FEMIX

3.4.5 Three-dimensional model for RC beam A1CL3-R

The objective of this part was to create a 3-D model that could accurately predict the moment deflection curve, the global behaviour and the mode of failure for the corroded RC beam repaired with NSM CFRP rod in bending (A1CL3-R), using the commercial software ABAQUS. In this 3-D model, the concrete material and the filling material (epoxy resin) were simulated using an ABAQUS 3-D deformable solid structural element while a 3-D deformable wire was used to simulate the steel bars, the steel stirrups and the CFRP NSM rod reinforcement using a truss element. The steel loading plate and the steel supports were simulated using a 3-D deformable solid element and they were given higher yield values than the steel bars and stirrups in order to prevent early yielding.

3.4.5.1 Concrete properties

The mechanical behaviour of concrete is difficult to simulate because of its complexity in traction and compression and its brittle cracking. Nowadays, many models can simulate concrete material using different approaches, such as the concrete smeared cracking approach (32,33), the concrete damaged plasticity approach (16,34) and the discrete cracking approach (35).

In this part, the mechanical properties of concrete found experimentally and listed in Table 3-1 were used in ABAQUS to define the characteristics of concrete material with a Poisson's

ratio of 0.2. The plastic behaviour of concrete in compression was defined using the Drucker-Prager yield function, which is controlled by the Drucker-Prager hardening variables in tension and compression. The Drucker-Prager criterion is a smooth approximation of the Mohr-Coulomb yield surface and it is controlled with two parameters: cohesion, C , and internal angle of friction, ϕ . It can be expressed using equation (1):

$$f(I_1, J_2) = \alpha I_1 + \sqrt{J_2} - k = 0 \quad \text{Eq.(1)}$$

Where α, k are Drucker-Prager material constants, I_1 is the first invariant of the effective stress tensor and J_2 is the second invariant of the stress deviator tensor. In cases where the Drucker-Prager passed the inner cone of the tension meridian of the Mohr-Coulomb hexagon, the Drucker-Prager constants were expressed using equations (2):

$$\alpha = \frac{2 \sin \phi}{\sqrt{3}(3 + \sin \phi)}, k = \frac{6c \cos \phi}{\sqrt{3}(3 + \sin \phi)} \quad \text{Eq.(2)}$$

The two parameters, cohesion C and internal angle of friction ϕ , were assumed to be $C = 2.8$ MPa and $\phi = 32^\circ$ as recommended by (36). The results of the experimental concrete specimens tested in compression were used in ABAQUS to fill in the Drucker-Prager hardening values and the Young's moduli of concrete beams shown in Table 3-1 were used. The same modulus of elasticity and Poisson's ratio were used here with the same tensile strength values obtained by the uniaxial traction tests as shown in Table 3-1. Figures 3-16 and 3-17 show the Drucker-Prager failure criterion and the tension softening of the concrete respectively.

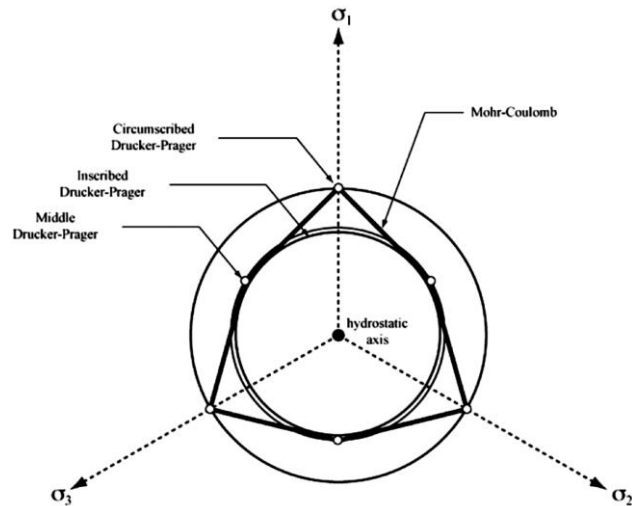


Figure 3 - 16 Drucker-Prager failure criterion in stress space (32)

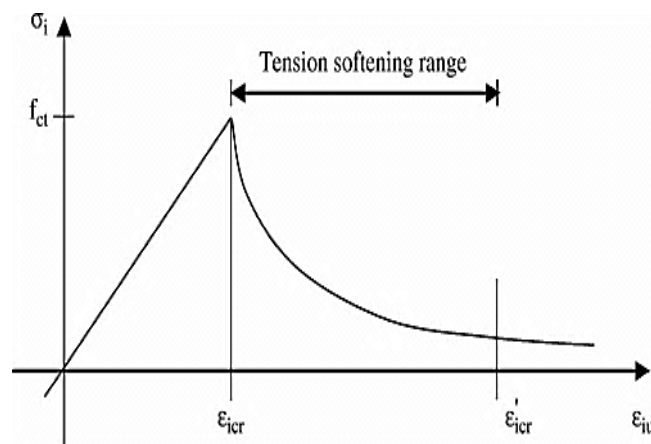


Figure 3 - 17 Tension softening of concrete

3.4.5.2 Steel properties

The steel reinforcement bars and stirrups were considered to have linear elastic-plastic behaviour. The post yielding hardening behaviour used in FEMIX and shown in figure 3-10 (b) was used again in ABAQUS for the corroded steel bars. The reduction in ultimate elongation induced by corrosion was also the same in ABAQUS as it was in FEMIX.

3.4.5.3 CFRP rods and filling material

The mechanical properties of the epoxy resin material and the CFRP rods used in this model were exactly the same as those found in the experimental tests and given in Tables 3-3 and 3-4. The filling material was modelled as a 3-D solid element while the cracking model of concrete was also used here in order to simulate the plastic behaviour of epoxy material. The CFRP rod was modelled by an elastic stress-strain curve up to brittle failure in tension and zero strength in compression, a method already used in a previous study (14).

3.4.5.4 Simulation of corrosion cracks

The corrosion cracks shown in figure 3-18 were considered to be the main reason why the separation of concrete cover was the mode of failure for the repaired corroded beam. This plane of cracks was simulated using a crack tool in the interaction section in ABAQUS as shown in figure 3-19. The cross-sectional area of the tensile steel bars of corroded beam A1CL3-R was reduced due to the corrosion and they were given an average corrosion value (20% for tensile steel bars) at the middle of the beam.

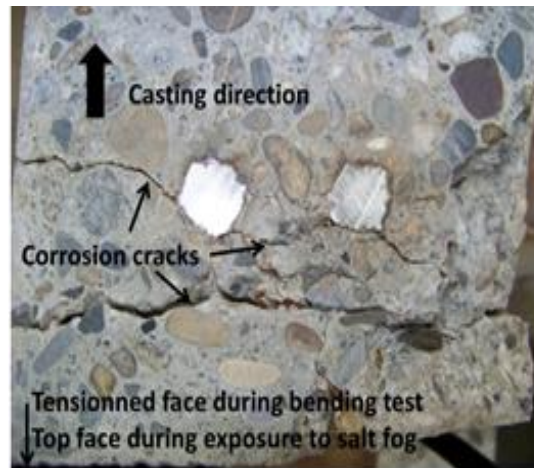


Figure 3 - 18 Corrosion-induced cracks appear in the concrete cover from the steel part closest to the tensioned surface exposed to chloride for type "A" beams (Almassri et al.(13))

In order to define the crack lines along the concrete cover of the corroded RC beam A1CL3-R2 FEM, several steps were employed (ABAQUS/CAE User's Manual):

1. Several partitions were drawn just where the cracks appeared in the concrete cover as shown in figure 3-19.
2. The crack line was defined using a crack tool from the interaction module in ABAQUS by selecting element edges of the partitioned parts that formed continuous lines.
3. The crack extension direction was defined normal to the crack plane (across the beam width) in order to simulate the corrosion cracks described in figure 3-18.
4. Finally, a seam crack was defined along the crack plane edges. This crack was defined by ABAQUS as an edge or a face in the model, which was originally closed but could open during the analysis.

The existing vertical flexural cracks were also added in order to simulate the real state of pre-loading of the corroded beam.

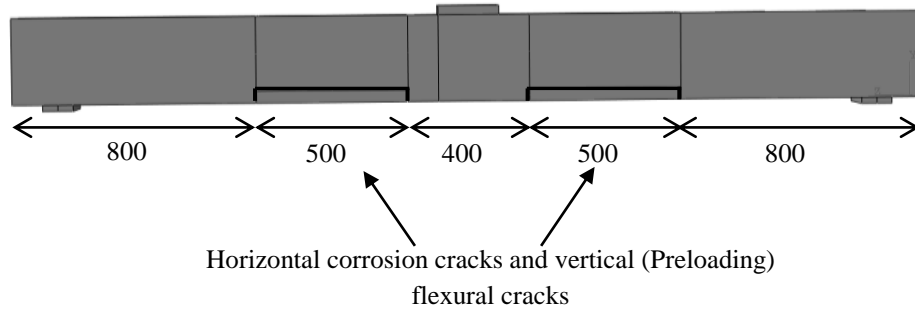


Figure 3 - 19 Cracks created at concrete cover plane of corroded beam in (mm)

3.4.6 FEM numerical model

3.4.6.1 General description

A 3-D finite element model was created with the commercial FEM software ABAQUS, which uses a non-linear static procedure with a classical Full-Newton solving method. In this study, the full beam was modelled using suitable boundary conditions as shown in figure 3-20, all the material discussed previously being inserted.

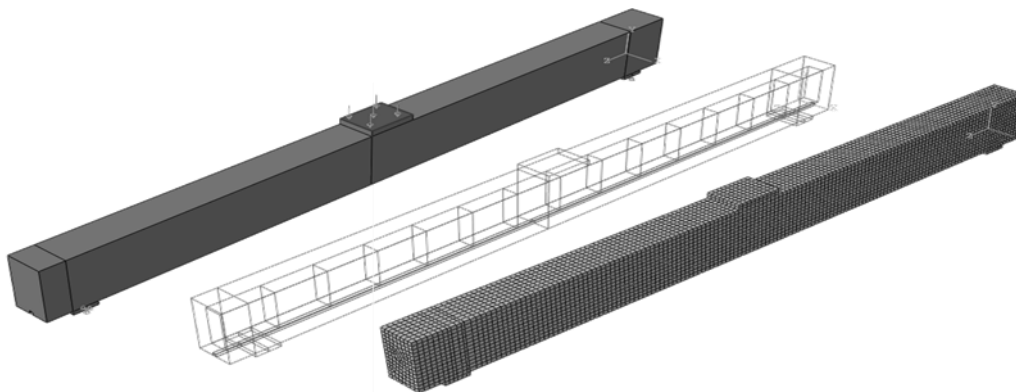


Figure 3 - 20 Boundary conditions, steel skeleton and meshing of beam model

As the main objective here is to discuss the failure mode in which there is separation of the concrete cover, a full bond was assumed between FRP and concrete and also between steel reinforcement rebars and concrete material as assumed by Radfar et al. (17) to model a non-conventional failure mode (peeling-off).

3.4.6.2 Meshing and step size increments

The meshing edge size of 10 mm was used for concrete elements; In order to ensure the maximum degree of accuracy in ABAQUS, a large value was entered as the maximum number of increments (100,000 increments) while a small value (1E-08) was entered for the minimum increment size.

3.4.7 FEM results of 3D model

3.4.7.1 Ultimate load capacity and failure mode of RC beam A1CL3-R

Two FEM models were created in ABAQUS. The first one dealt with the repaired corroded RC beam without considering any corrosion cracks (FEM A1CL3-R1) while the other (FEM A1CL3-R2) took the corrosion cracks of the corroded RC beam into account. The moment-deflection curves for both models were drawn at the mid-span point for comparison with the experimental results as shown in figure 3-21. From simulation results of the RC beam A1CL3-R1, it can be concluded that the 3-D model implemented in ABAQUS captures the recovery in ultimate deflection that is provided by the NSM rod. This was not the case for the 2-D model in FEMIX.

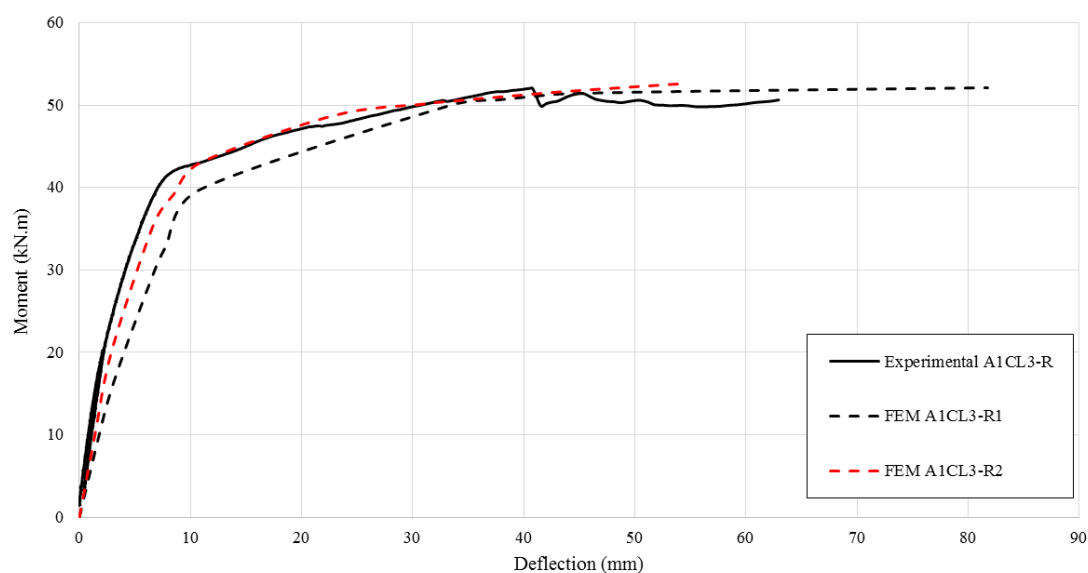


Figure 3 - 21 Experimental curves vs. 3D FE Model moment-deflection curves obtained with Abaqus for RC beam A1CL3-R

Nevertheless, the results show that the corroded, non-cracked beam FEM A1CL3-R1 gave higher deflection values than the experimental corroded beam (with 22 mm difference) whereas, when the corrosion crack line was defined in order to simulate premature failure (FEM A1CL3-R2), it gave lower deflection values than the non-cracked beam and results were closer to the experimental ones. Table 3-6 presents a comparison between experimental and 3-D FEM results for each model in terms of yielding moment, ultimate moment and ultimate deflection.

Table 3 - 6 FEM vs. Experimental results for A1CL3-R using Abaqus

Beam	Yielding moment (kN.m)	Ultimate moment (kN.m)	Ultimate deflection (mm)
Experimental A1CL3-R	42.3	52	63
FEM A1CL3-R1	39.7	52.2	85

FEM A1CL3-R2	43	52.6	55
--------------	----	------	----

The 3D model implanted in ABAQUS captured the failure occurring by the separation of concrete cover near the middle of the beam as shown in figure 3-22.

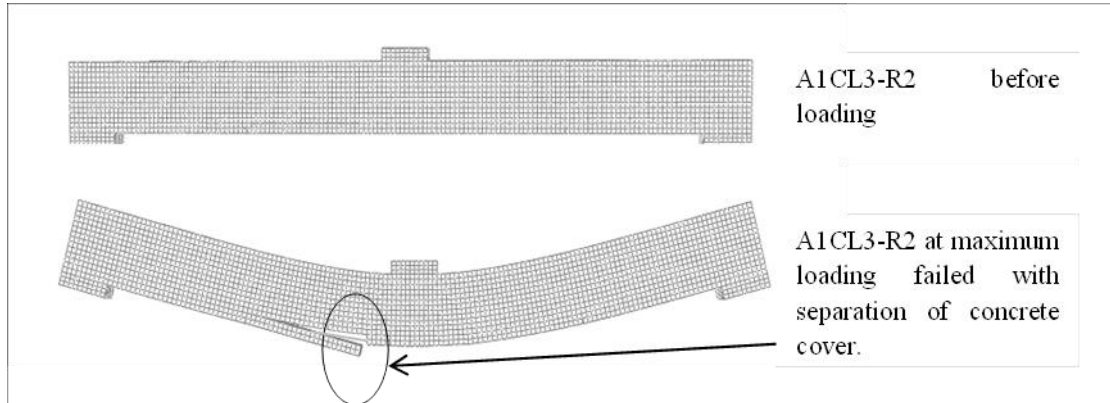


Figure 3 - 22 Mode of failure obtained for corroded RC beam A1CL3-R by 3D FE model using Abaqus

3.5 Conclusions

According to the results found in this work, the following conclusions can be drawn:

1. The NSM technique, which was used to repair corroded RC elements, restored significant ductility by avoiding premature failure of tensile bars at pit locations. However, the presence of cracks induced by corrosion coincident with the tensile reinforcement induced a new premature failure mode.
2. The two-dimensional FEM analysis using FEMIX captured the main aspects observed in the experimental tests, such as yield initiation of the steel bars and load carrying capacity for both repaired and non-repaired corroded and control beams.
3. The two-dimensional FEM analysis using FEMIX captured the reduction of ultimate deflection of non-repaired beams due to the more brittle behaviour of corroded steel in tension but could not capture the ductility recovery induced by the repair with NSM rod.
4. The damage induced by corrosion modifies the flexural response of repaired corroded beams and leads to a new, non-conventional failure mode by separation of concrete cover in the plane defined by the corrosion cracks.
5. Three-dimensional FEM analysis using ABAQUS was able to predict both load-bearing capacity and ultimate deflection reduction due to corrosion if the crack plane induced by corrosion was taken into account in the model.

3.6 Acknowledgements

The authors wish to acknowledge the support provided by Professor Joaquim Barros and his structural composites group in the civil engineering department of the University of Minho, Guimaraes, Portugal.

3.7 References

1. Schmitt G. Global needs for knowledge dissemination, research, and development in materials deterioration and corrosion control. *World Corros Organ N Y*. 2009.
2. Al-Sulaimani G, Kaleemullah M, Basunbul I. Rasheeduzzafar,(1990)“Influence of corrosion and cracking on bond behaviour and strength of reinforced concrete members” *ACI Structural Journal*, 87 (2), 220-231. ASTM G1. 1990.
3. Andrade C, Alonso C, Garcia D, Rodriguez J. Remaining lifetime of reinforced concrete structures: effect of corrosion on the mechanical properties of the steel. In: *Proceedings of the international conference on life prediction of corrodible structures*. National Association of Corrosion Engineers, Cambridge, UK, 23–26 September; 1991. p. 12/1–11.
4. Cairns J, Plizzari GA, Du Y, Law DW, Franzoni C. Mechanical properties of corrosion-damaged reinforcement. *ACI Mater J*. 2005;102(4).
5. Hassan T, Rizkalla S. Investigation of bond in concrete structures strengthened with near surface mounted carbon fiber reinforced polymer strips. *J Compos Constr*. 2003;7(3):248–57.
6. Täljsten B, Carolin A, Nordin H. Concrete structures strengthened with near surface mounted reinforcement of CFRP. *Adv Struct Eng*. 2003;6(3):201–13.
7. Barros JA, Fortes A. Flexural strengthening of concrete beams with CFRP laminates bonded into slits. *Cem Concr Compos*. 2005;27(4):471–80.
8. Barros JA, Ferreira DR, Fortes AS, Dias SJ. Assessing the effectiveness of embedding CFRP laminates in the near surface for structural strengthening. *Constr Build Mater*. 2006;20(7):478–91.
9. De Lorenzis L, Teng J. Near-surface mounted FRP reinforcement: An emerging technique for strengthening structures. *Compos Part B Eng*. 2007;38(2):119–43.
10. Bilotta A, Ceroni F, Di Ludovico M, Nigro E, Pecce M, Manfredi G. Bond efficiency of EBR and NSM FRP systems for strengthening concrete members. *J Compos Constr*. 2011;15(5):757–72.
11. Kreit A, Al-Mahmoud F, Castel A, François R. Repairing corroded RC beam with near-surface mounted CFRP rods. *Mater Struct*. 2011;44(7):1205–17.

12. Al-Mahmoud F, Castel A, François R, Tourneur C. Strengthening of RC members with near-surface mounted CFRP rods. *Compos Struct.* 2009;91(2):138–47.
13. Almassri B, Kreit A, Al Mahmoud F, François R. Mechanical behaviour of corroded RC beams strengthened by NSM CFRP rods. *Compos Part B Eng.* 2014;64:97–107.
14. Hawileh RA. Nonlinear finite element modeling of RC beams strengthened with NSM FRP rods. *Constr Build Mater.* 2012;27(1):461–71.
15. Sena Cruz JM, Barros JA, Gettu R, Azevedo ÁF. Bond behavior of near-surface mounted CFRP laminate strips under monotonic and cyclic loading. *J Compos Constr.* 2006;10(4):295–303.
16. Lundqvist J, Nordin H, Täljsten B, Olofsson T. Numerical analysis of concrete beams strengthened with CFRP-A study of anchorage lengths. 2005. p. 247–54.
17. Radfar S, Foret G, Saeedi N, Sab K. Simulation of concrete cover separation failure in FRP plated RC beams. *Constr Build Mater.* 2012;37:791–800.
18. Kang J-Y, Park Y-H, Park J-S, You Y-J, Jung W-T. Analytical evaluation of RC beams strengthened with near surface mounted CFRP laminates. *ACI Spec Publ.* 2005;230.
19. Castel A, François R, Arliguie G. Mechanical behaviour of corroded reinforced concrete beams—Part 1: experimental study of corroded beams. *Mater Struct.* 2000;33(9):539–44.
20. Vidal T, Castel A, François R. Corrosion process and structural performance of a 17 year old reinforced concrete beam stored in chloride environment. *Cem Concr Res.* 2007;37(11):1551–61.
21. Khan I, François R, Castel A. Structural performance of a 26-year-old corroded reinforced concrete beam. *Eur J Environ Civ Eng.* 2012;16(3-4):440–9.
22. Dang VH, François R. Influence of long-term corrosion in chloride environment on mechanical behaviour of RC beam. *Eng Struct.* 2013;48:558–68.
23. François R, Khan I, Dang VH. Impact of corrosion on mechanical properties of steel embedded in 27-year-old corroded reinforced concrete beams. *Mater Struct.* 2013;46(6):899–910.
24. Al-Mahmoud F, Castel A, François R, Tourneur C. Effect of surface pre-conditioning on bond of carbon fibre reinforced polymer rods to concrete. *Cem Concr Compos.* 2007;29(9):677–89.
25. Al-Mahmoud F, Castel A, François R, Tourneur C, Marchand J, Bissonnette B, et al. Anchorage and tension-stiffening effect between Near-Surface-Mounted Fiber Reinforced polymer rod and concrete. 2006.
26. Yuan Y, Ji Y, Shah SP. Comparison of two accelerated corrosion techniques for concrete structures. *ACI Struct J.* 2007;104(3).
27. Horne A, Richardson I, Brydson R. Quantitative analysis of the microstructure of interfaces in steel reinforced concrete. *Cem Concr Res.* 2007;37(12):1613–23.

28. Soylev T, François R. Quality of steel–concrete interface and corrosion of reinforcing steel. *Cem Concr Res.* 2003;33(9):1407–15.
29. Dang VH, François R. Influence of long-term corrosion in chloride environment on mechanical behaviour of RC beam. *Eng Struct.* 2013;48:558–68.
30. Owen D, Figueiras J. Anisotropic elasto-plastic finite element analysis of thick and thin plates and shells. *Int J Numer Methods Eng.* 1983;19(4):541–66.
31. Dang VH, François R. Prediction of ductility factor of corroded reinforced concrete beams exposed to long term aging in chloride environment. *Cem Concr Compos.* 2014;53:136–47.
32. Chaudhari S, Chakrabarti M. Modeling of concrete for nonlinear analysis Using Finite Element Code ABAQUS. *Int J Comput Appl.* 2012;44.
33. Si-Larbi A, Agbossou A, Ferrier E, Michel L. Strengthening RC beams with composite fiber cement plate reinforced by prestressed FRP rods: Experimental and numerical analysis. *Compos Struct.* 2012;94(3):830–8.
34. Abdullah R, Mokhatar SN. Computational analysis of reinforced concrete slabs subjected to impact loads. *Int J Integr Eng.* 2012;4(2):70–6.
35. Yang Z, Chen J, Proverbs D. Finite element modelling of concrete cover separation failure in FRP plated RC beams. *Constr Build Mater.* 2003;17(1):3–13.
36. Lubliner J, Oliver J, Oller S, Oñate E. A plastic-damage model for concrete. *Int J Solids Struct.* 1989;25(3):299–326.

Conclusions

The two-dimensional FE modelling using the FEMIX computer code well predicted the start of steel yielding and the ultimate bending moment capacity for the control repaired beam A1T-R, the control non-repaired beam A2T and the corroded non-repaired beams A2CL3, A2CL1. While for the corroded repaired beam with NSM A1CL3-R, the FE modelling results did not match the experimental results as it was the only corroded beam to not fail with the brittle failure of the tensile steel bars. Moreover, the reduction in the ultimate deflection of the corroded RC beams was well captured by the 2-D models by FEMIX as the non-linear constitutive model of the corroded steel bars took into account the reduction in the ultimate elongation induced by steel corrosion.

A three-dimensional FE model (FEM A1CL3-R1) was created using the commercial software ABAQUS for the corroded repaired beam with NSM CFRP rods A1CL3-R, the FE results for this model gave higher ultimate deflection values than the experimental one (22 mm difference).

Finally, both vertical flexural cracks and horizontal corrosion cracks were implemented in another 3-D model (FEM A1CL3-R2) using ABAQUS, which enabled the numerical model to predict the experimental load-bearing capacity, the ultimate deflection reduction and the failure pattern which occurred by the separation of the concrete cover. Moreover, the FEM A1CL3-R2 gave lower ultimate deflection value than the non-cracked beam FEM A1CL3-R1 (55 mm and 85 mm respectively).

Chapter 4

Shear strengthening of corroded RC beams with NSM CFRP rods, a finite element modelling part

Introduction

The FE modelling study conducted in chapter 3 presented a satisfactory level of accuracy to model the flexural response of the corroded RC beams repaired in bending with NSM CFRP rods.

Despite the fact that the shear behavior of the RC beams is more complex area of study than the flexural one, this chapter aims at presenting numerical models based on non-linear finite element method for short span RC beams repaired with NSM CFRP rods in shear based on the experimental results of the short beams studied in chapter 2.

The finite element computer code FEMIX was used to produce 3D numerical models that can study the shear response of the repaired RC beams with NSM, numerical FE models for five short span RC beams are presented in this chapter, two of them are shear repaired with NSM technique using four CFRP rods installed on each face; the two shear repaired RC beams were one control beam A1T-SB and one corroded beam A1CL3-SB, while the other three RC beams were non-shear-repaired; one control beam A1T-B and two corroded beams A1CL3-B and A2CL2-A.

A multi-directional fixed smeared crack model is presented here in this chapter, two fracture models of concrete were taken into account; the first one presents the tri-linear tension softening and the second one presents the linear shear softening of the concrete. The reduction of the cross-sectional area of the tensile steel bars and steel stirrups due to corrosion was taken into account in the constitutive model of the steel bars. The numerical model also deals with two different constitutive steel models (one for corroded beams and one for non-corroded (control) beams).

Moreover, it compares the experimental results (the load-deflection curves and the modes of failure) with FE results obtained for repaired and non-repaired RC beams with NSM in shear. Finally, three-dimensional failure/cracks patterns are presented for short span beams failed by specific mode of failure and these results were compared to previous analytical results.

A FEM-based model to study the behaviour of corroded RC beams shear repaired by NSM CFRP rods technique

Belal ALMASSRI (1), Joaquim A.O. BARROS (2), Firas AL MAHMOUD (3), Raoul FRANCOIS (1)

(1) *Université de Toulouse; UPS, INSA, LMDC (Laboratoire Matériaux et Durabilité des Constructions), Toulouse, France*

(2) *ISISE, Dep. Civil Eng., Minho University, Guimarães, Portugal*

(3) *Institut Jean Lamour, UMR 7198, CNRS, Université de Lorraine, Nancy, France*

Keywords: corrosion, repair, RC beams, NSM CFRP rods, FEM, shear.

ABSTRACT

This paper presents the main features of a finite element FE numerical model developed using the computer code FEMIX to predict the contribution of near-surface mounted (NSM) carbon-fibre-reinforced polymer (CFRP) rods to the shear repair of corroded reinforced concrete RC beams. In the RC beams repaired in shear with the NSM technique, the CFRP rods are placed inside grooves pre-cut into the concrete cover of the RC beam's lateral faces and are bonded to the concrete with high performance epoxy adhesive. Experimental and 3D numerical modelling results are presented here in terms of load-deflection curves and failure modes for 4 short corroded beams: two corroded beams (A1CL3-B and A1CL3-SB) and two control beams (A1T-B and A1T-SB), the beams noted B were repaired in bending only with NSM CFRP rods while those noted SB were repaired in both bending and shear with the NSM technique. The corrosion of the tensile steel bars and its effect on the shear capacity of the RC beams is discussed. Results show that the FE model is able to capture the main aspects of the experimental load-deflection curves of the RC beams. They also present the experimental failure modes and FE numerical modelling crack patterns, both of which gave similar results for non-shear repaired beams, which showed a diagonal tension mode of failure, and for shear-repaired beams, which failed due to a large flexural crack in the middle of the beams, along with the concrete crushing. Three-dimensional crack patterns were produced for shear-repaired beams in order to investigate the splitting cracks occurring at the middle of the beams and near the support.

4.1 Introduction

The deterioration of reinforced concrete (RC) structures is a serious issue for many nations, as it could put public safety in jeopardy and the escalating repair cost could directly burden the future economy (1). The corrosion of steel reinforcement is still one of the major concerns as it may lead to significant reduction in terms of ultimate capacity and serviceability of RC structures (2,3). Many studies have presented the effect of steel corrosion on the flexural behaviour of RC structures (4–7) but very few show the effect of corrosion on the shear capacity of such structures. Moreover, most of the available literature (8–10) studies the effect of corrosion on the shear behaviour of RC beams by using impressed current to induce corrosion of the steel bars. These accelerated systems do not represent the real state of corroded structures but very few studies have aimed to study naturally corroded structures. The studies of this type that exist were based on long-term natural corrosion systems (11,12) in which the RC beams were stored in a chloride environment under service loads.

Near surface mounting of CFRP rods is a promising strengthening technique to increase the shear resistance of RC beams that have some risk of collapsing in a brittle shear failure mode. Shear strengthening of RC beams by NSM CFRP rods consists of fixing the CFRP rods, by means of a high performance epoxy adhesive, into thin grooves cut onto the concrete cover of the RC beams' lateral faces. Several experiment-based studies have investigated the efficiency of using the NSM CFRP rods technique in the shear strengthening of RC beams (13–15). Other studies have used NSM CFRP laminates (strips), instead of round bars, to study the effect of the NSM technique on the shear capacity of RC beams (16,17). Nanni et al. (18) predicted the contribution of NSM systems to the shear resistance of RC beams but this prediction was based on the assumption that laminate debonding was the dominant mode of failure. The separation of the concrete cover containing the laminates is always more frequently reported in relevant studies (15,19). Bianco et al. (20) have produced an analytical model that is able to predict the contribution of NSM CFRP laminates to shear strength on the basis of various possible modes of failure: debonding; concrete semi-conical tensile fracture; mixed shallow-semi-cone-plus-debonding; and strip tensile fracture.

The NSM technique to repair corroded RC beams has hardly been studied. Bending strengthening is mainly concerned and only a very recent paper (21) has studied the NSM effect on the experimental shear behaviour of corroded RC beams.

The available research shows that the predictive performance of computer programs based on the finite element method (FEM) for the non-linear analysis of RC structures failing in shear is closely related to the constitutive model used to simulate shear stress transfer in cracked concrete (22,23). Suryanto et al. (23) mention the significant requirement that the shear stress-strain softening law for concrete should be taken into account in order to capture the real damage that occurs in concrete during the cracking process. There are some studies available (24–26) that use FE modelling programs to study the effect of applying the NSM technique to the shear strengthening of RC beams: a multi-directional fixed smeared crack model was implemented by Barros et al. (26) to simulate the CFRP strengthened RC beams failing in shear and flexure, and Barros et al. (19) investigated the effectiveness limitations of the NSM CFRP laminates technique in shear strengthening of RC beams using the FEMIX computer code and recorded the failure of concrete volume including the CFRP laminates.

There are no numerical modelling studies available that were performed to investigate the mechanical behaviour and failure modes of corroded RC beams repaired in shear with NSM CFRP rods. The present paper implements an FE model using the FEMIX computer code to study the performance of corroded short-span reinforced concrete beams repaired with the NSM FRP technique. Some of the beams were repaired in bending only and the others were repaired in bending and shear. All beams were tested experimentally in three-point loading up to failure. The FE model investigated the failure modes and the shear capacities for all RC beams, and the shear capacity of the short-span corroded beams repaired in shear and bending was compared to that of non-repaired similar beams.

4.2 Experimental programme

4.2.1 Experimental procedure

An experimental programme aimed at understanding the effects of steel corrosion on the structural behaviour of RC elements was started at LMDC (Laboratory of Materials and Durability of Constructions) in 1984. Many experimental studies have since been conducted on those beams to evaluate the development of corrosion cracking, to measure chloride content and to analyse changes in mechanical behaviour (27,28). Details of the natural aggressive environment system can be found elsewhere (29).

The four (80 cm) RC beams studied in this paper were cut from two long beams. Two short corroded beams were obtained from a long corroded RC beam (A1CL3-R) and two control beams were taken from the long control (non-corroded) RC beam (A1T-R). The two full span

length beams were repaired with one 6-mm-diameter CFRP rod in bending and tested in three point loading up to failure. More details of the long beams can be found elsewhere (30). Two short RC beams, one corroded (A1CL3-SB) and one control (A1T-SB), were shear repaired with NSM CFRP rods while two others; one corroded (A1CL3-B) and one control (A1T-B) were kept repaired in bending only. The reinforcement layout of the full length beams and the four short beams is shown in Figure 4-1.

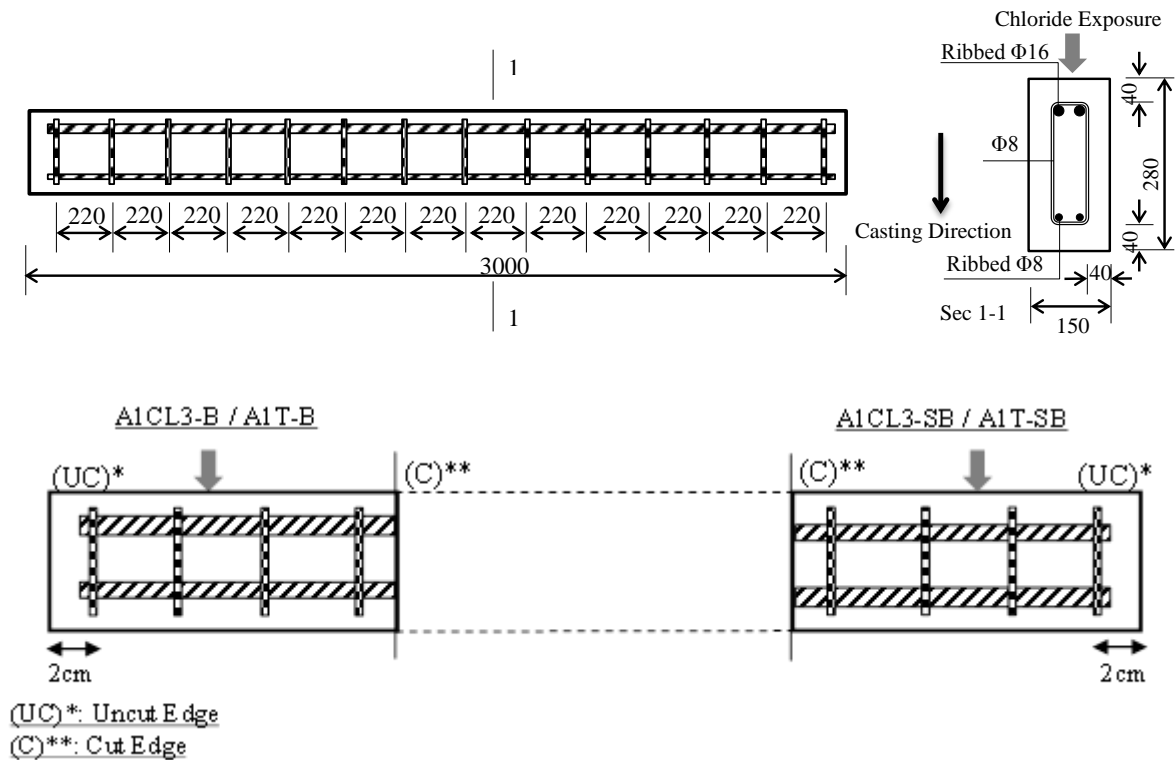


Figure 4 - 1 Reinforcement layout all beams. Dimensions are in mm

4.2.2 Main experimental results

4.2.2.1 Corrosion results

After the tensile steel bars and steel stirrups had been extracted from the two corroded beams and cleaned with Clark's solution ANSI/ASTM G1-72, the diameter loss was calculated with a weight loss method because the high scatter in the corrosion shape did not allow it to be measured directly using a Vernier calliper. According to the corrosion pattern, short pieces of corroded steel bars were cut and weighed to measure the loss of mass due to corrosion. Figure 4-2 shows that the maximum diameter loss found in the beam A1CL3-B was 18% while, for A1CL3-SB, it was 9%.

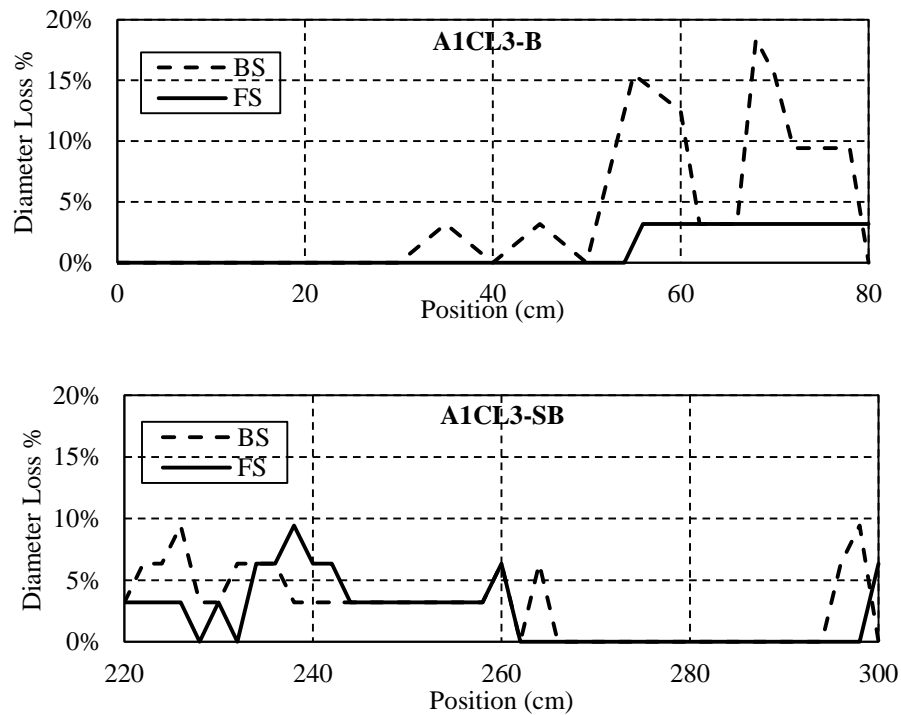


Figure 4 - 2 Diameter loss percentages of longitudinal tensile steel bars for corroded beams

For the corroded beam A1CL3-R, the steel stirrups were numbered to indicate the part of the beam they came from and their position in that part (the first number representing the part of the beam and the second number being the number of the stirrup) as shown in Figure 4-3, which also presents the stirrup numbers of the non-repaired corroded RC beam A2CL2-A studied by Dang et al. (31) that will be used here for comparison:

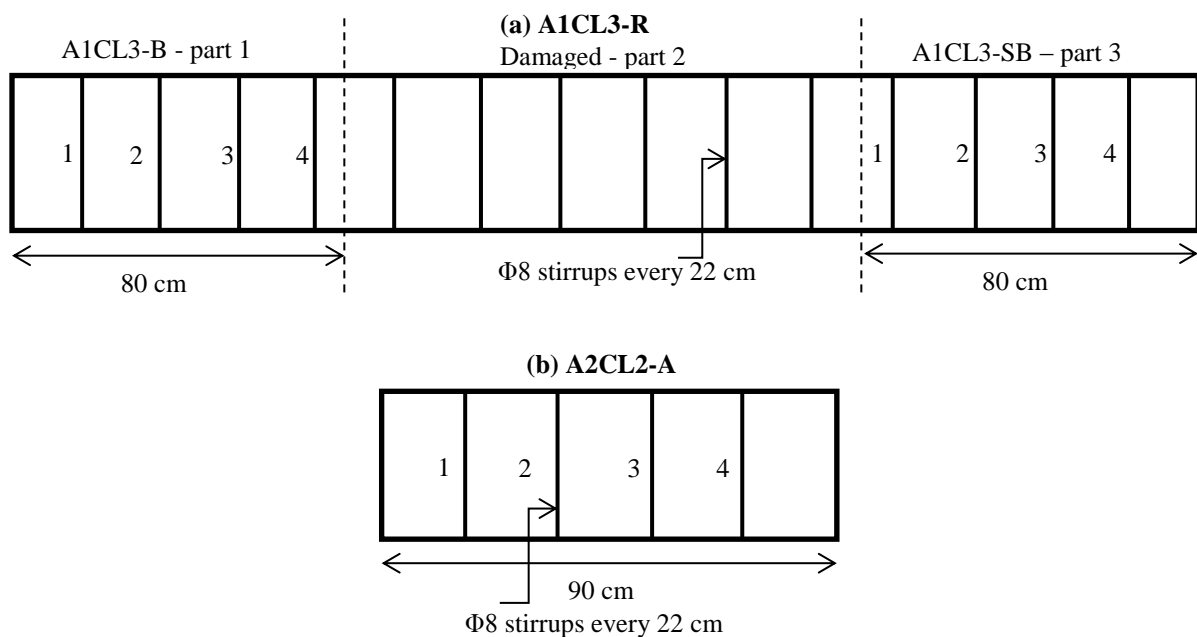


Figure 4 - 3 Stirrups numbers of corroded beams (a) A1CL3-R (b) A2CL2-A

Figure 4-4 (a) shows the locations of corrosion in the steel stirrups and the diameter values for the corroded beam A1CL3-R. No corrosion was found at stirrups 1-1 and 1-2. The maximum diameter loss found in beam A1CL3-B was 63 % at stirrup 1-4 (at the far edge of the diagonal shear crack) while the maximum loss in A1CL3-SB was 38 % at stirrup 3-1. Figure 4-4 also shows the corrosion map (% diameter loss) for corroded beam A2CL2-A. The maximum diameter loss found was 77% (1.84 mm) at the edge where the diagonal shear crack occurred.

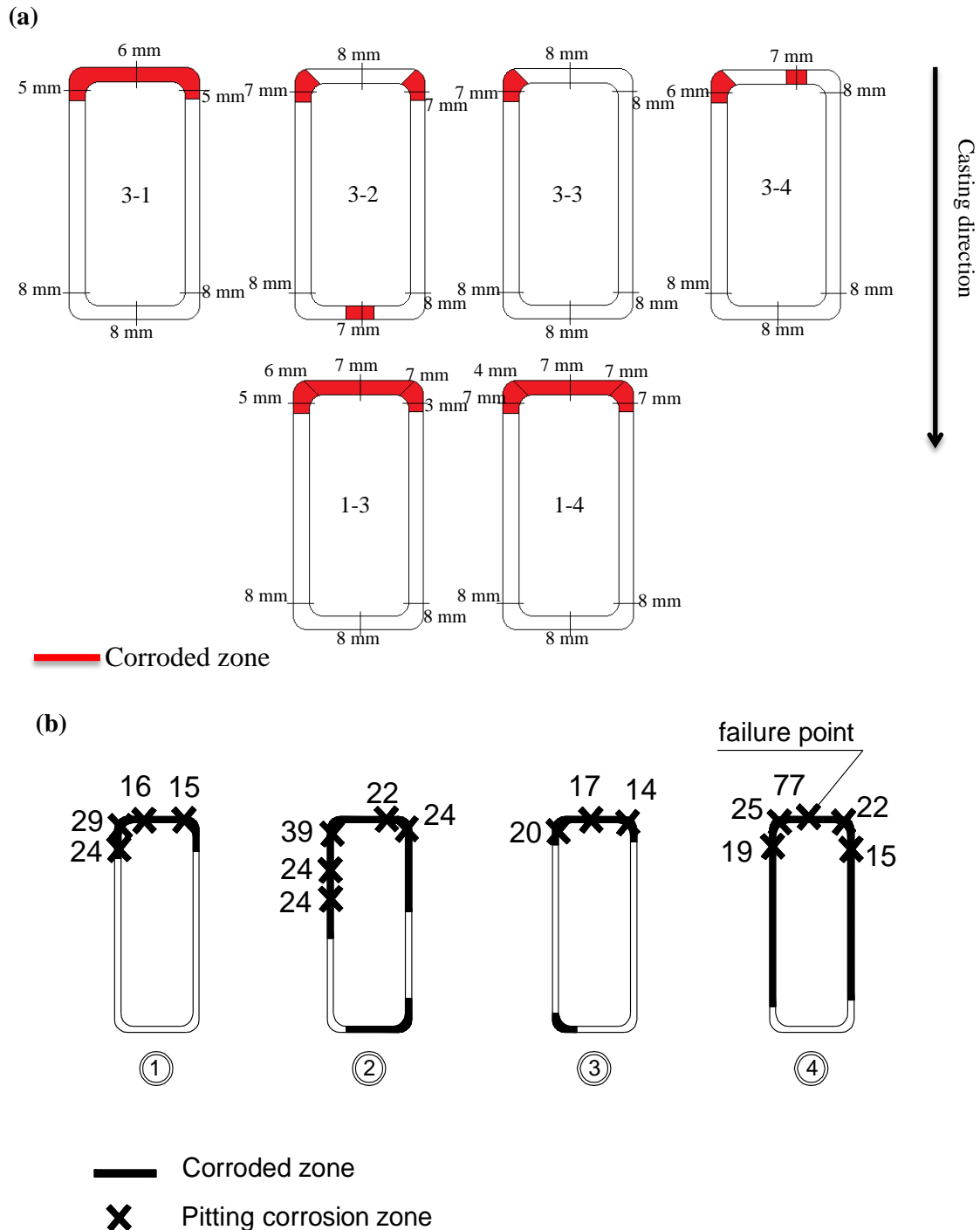


Figure 4 - 4 Stirrups corrosion maps (a) diameter in mm for A1CL3-R (b) diameter loss % in A2CL2-A

4.2.2.2 Ultimate load capacity and modes of failure

The four RC beams tested were compared with two other beams: the corroded beam A2CL2-A and the control tested by Dang et al. (31). Figure 4-5 shows the load-deflection curves for all short beams tested experimentally. The shear strengthening increased the shear capacity of the control beams, while the shear strengthening response of the corroded beams depended on the pattern and the intensity of steel corrosion.

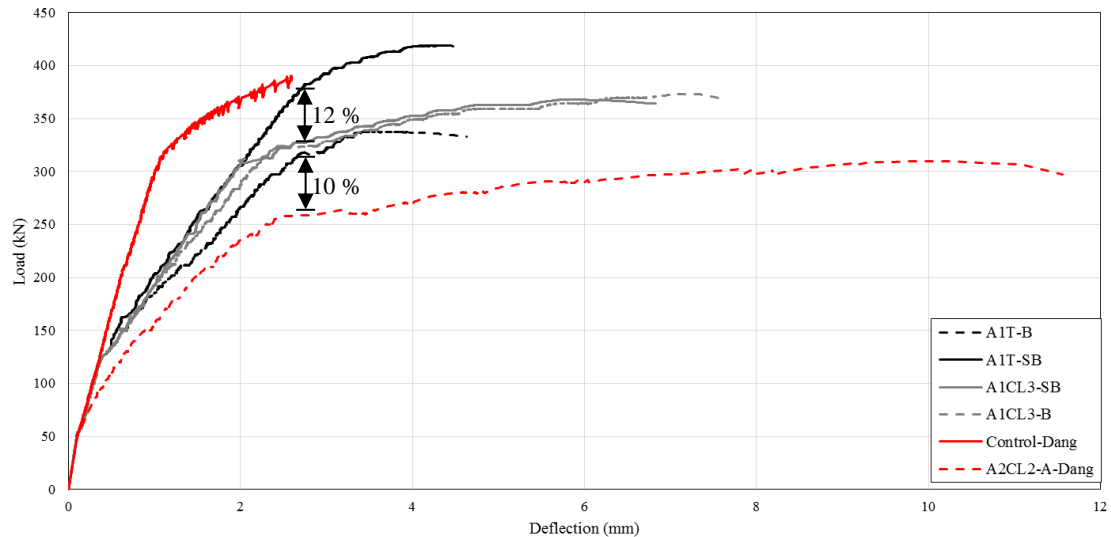


Figure 4 - 5 Load-deflection curves for all beams

The difference in the yielding capacity of the shear-repaired control beam A1T-SB and the shear-repaired corroded beam A1CL3-SB is associated with the 12% loss in cross section found at the middle of the corroded beam A1CL3-SB (the load-induced crack occurs at mid-span), while the decrease in the yielding capacity for non-shear repaired corroded beam A2CL2-A in comparison with non-shear repaired beams (Control, A1T-B and A1CL3-B) is associated with the 10% loss in cross section found at the edge of the corroded beam A2CL2-A (the same edge as the diagonal shear crack) (31).

Experimental results also showed that shear strengthening with NSM CFRP rods changed the mode of failure from diagonal crack failure close to the support due to slipping of the tensile re-bars at anchorage (for non-shear-repaired beams A1T-B and A1CL3-B), to failure by a large flexural crack at mid span followed by concrete crushing (for shear-repaired beams A1T-SB and A1CL3-SB) as shown in Figure 4-6.

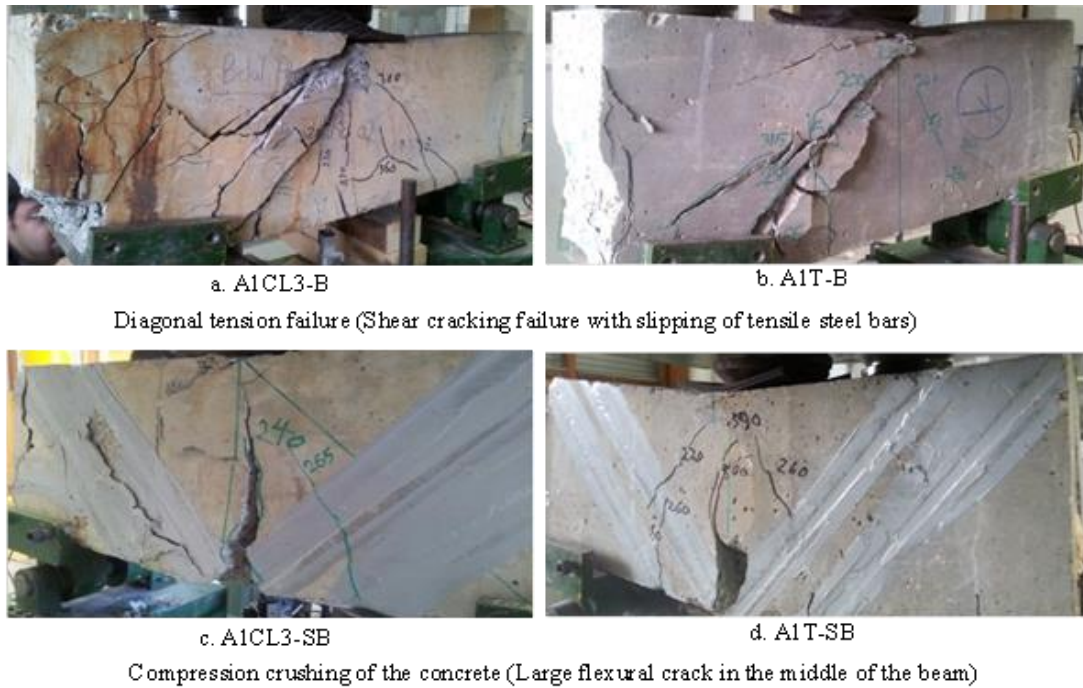


Figure 4 - 6 Experimental modes of failure for all tested beams

It is also noteworthy that, for shear-repaired beams A1T-SB and A1CL3-SB, many splitting cracks occurred mid-way through the beam's width as shown in Figure 4-7. These splitting cracks were easy to see at the bottom of the beam and at the beam edges near the supports. More details of the experimental programme for the short beams can be found elsewhere (21), together with the experimental results.

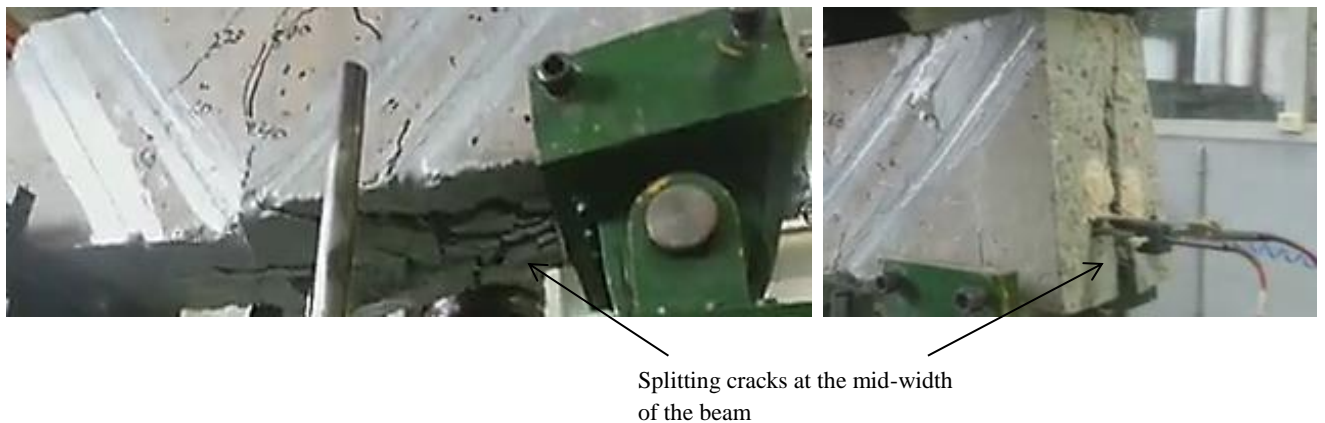


Figure 4 - 7 Tensile steel bars slip occurred in non-shear repaired beams A1T-SB and A1CL3-SB

4.3 Numerical model

In this study, a multi-directional fixed smeared crack model was used to simulate the RC beams failing in shear. The most important aspect of this constitutive model is that it uses concrete fracture modes I & II by using a softening diagram in order to simulate the crack shear stress vs. crack shear sliding in the context of a smeared approach. The description of the formulation of the multi-directional fixed smeared crack model is restricted to the case of cracked concrete here. This model is described in greater detail elsewhere (19).

4.3.1 Concrete Properties

Three-dimensional 20-node (quadratic) solid elements were used to simulate the concrete material in this numerical model. The concrete properties used are shown in Table 4-1.

Table 4 - 1 Concrete properties

Poisson's ratio	$\nu_c = 0.20$
Initial Young's modulus	$E_c = 30\,000 \text{ N/mm}^2$
Compressive strength	$f_c = 60 \text{ N/mm}^2$
Tri-linear tensile-softening diagram	$f_{ct} = 4.5 \text{ N/mm}^2$, $G_f^I = 0.05 \text{ N/mm}$ $\xi_1 = 0.005$, $\alpha_1 = 0.5$, $\xi_2 = 0.3$, $\alpha_2 = 0.2$
Parameter defining the mode I fracture energy available to the new crack	$P_2 = 1$
Shear softening parameters	$\tau_{t,p}^{cr} = 3 \text{ N/mm}^2$, $G_{f,s} = 0.1 \text{ N/mm}$, $\beta = 0.1$
Threshold angle	$\alpha_{th} = 30^\circ$
Maximum number of cracks per integration points	2

4.3.1.1 Fracture mode I for concrete “tension softening of concrete”

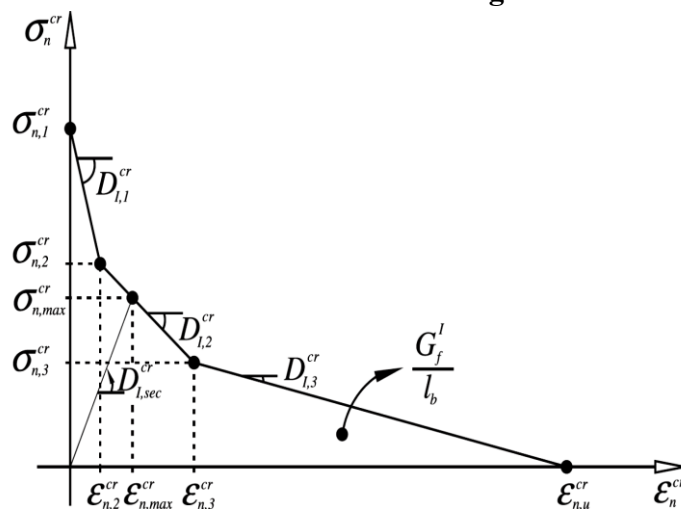


Figure 4 - 8 RC fracture mode I “tri-linear tension softening diagram”

The crack evolution in fracture mode I was simulated using a tri-linear tension softening or stiffening diagram as shown in Figure 4-8. In structures controlled by flexural modes of failure, there would be no need to adopt a softening crack shear stress vs. crack shear strain relationship in the numerical model.

4.3.1.2 Fracture mode II for concrete “Shear softening of concrete”

Suryanto et al. (23) showed that taking the shear softening law into account when modelling the shear stress transfer in cracked concrete was fundamental in order to better simulate the behaviour of engineered cement composite (ECC) beams failing in shear. Therefore, in this paper, a linear shear softening law (shown in Figure 4-9) for modelling fracture mode II of cement based materials is used.

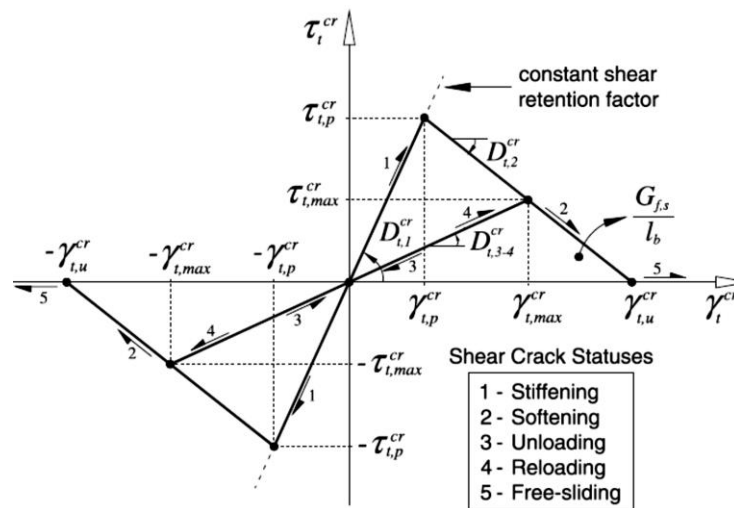


Figure 4 - 9 RC fracture mode II “linear shear softening diagram”

4.3.2 Steel properties

The steel reinforcement bars were implemented in this model as elastic-plastic behaviour. A Poisson’s ratio of 0.3 was used and the elastic modulus and yield strength values of steel reinforcement bars and stirrups were as in Table 4-2 for both control and corroded steel bars. The post yielding hardening behaviour of control and corroded steel bars and steel stirrups was modelled as shown in Figures 4-10 and 4-11 respectively. Corrosion did not modify the actual yield strength and hardly modified the actual ultimate strength (32,33) but it strongly decreased the ultimate elongation (34–37).

Table 4 - 2 Average values of steel bars properties

Specimen Type	Young's modulus (GPa)	Yield Strength (MPa)	Ultimate Strength (MPa)	Ultimate Strain
Non-corroded steel specimen	200	550	604	0.08
Corroded steel specimen	200	550	645	0.04

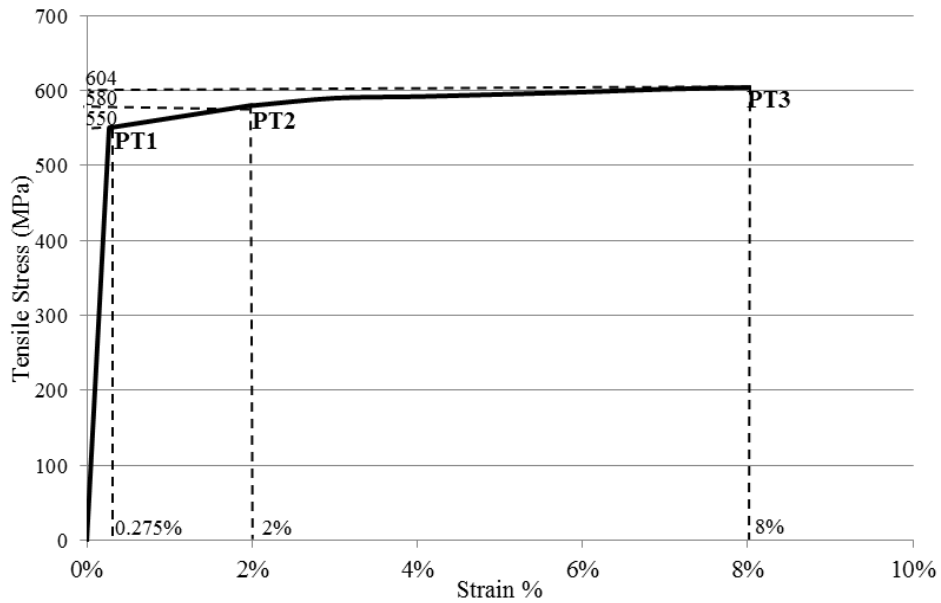


Figure 4 - 10 uniaxial constitutive model of non-corroded steel bars

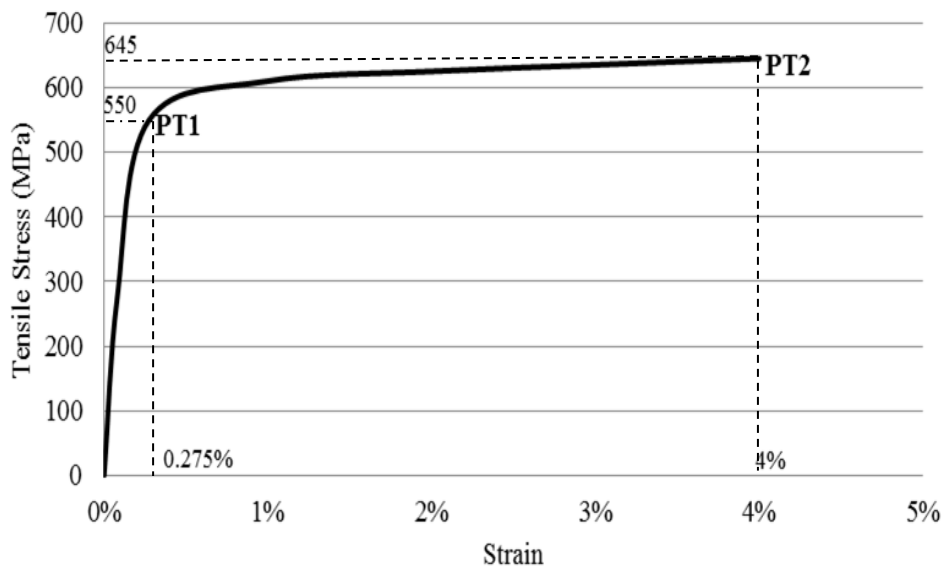


Figure 4 - 11 uniaxial constitutive model of corroded steel bars

4.3.3 CFRP properties

To model the NSM CFRP rods, a linear elastic stress–strain relationship was implemented. Table 4-3 presents the values used in the constitutive model for CFRP rods according to the manufacturer’s specifications.

Table 4 - 3 CFRP rods characteristics.

Type of test	Ultimate strength (MPa)	Modulus of Elasticity (MPa)
Manufacturer’s test	2300	150000

4.3.4 Modelling of RC beams bending and shear repaired with NSM CFRP rods (A1CL3-SB and A1T-SB)

The main objective of this part of the work was to create a reliable numerical model that could simulate and predict the global behaviour (load-deflection curves and modes of failure) of two RC beams repaired in shear with NSM CFRP rods (corroded beam A1CL3-SB and control beam A1T-SB). Both beams had already been repaired with NSM CFRP rod in bending as they were taken from full length beams A1CL3-R and A1T-R, two long beams that had already been tested (30). To simulate the concrete in the beams, three-dimensional solid 20-node elements with 3×3 Gauss-Legendre integration were used. The steel bar and stirrup reinforcements, and the CFRP rods, were simulated using 3-node quadratic three-dimensional embedded cable elements with two Gauss-Legendre integration points. The epoxy adhesive material was not represented in this model as a previous study (24) had shown that the epoxy adhesive had a negligible effect on the global behaviour of the RC beams. Figures 4-12 and 4-13 show the geometry, elements mesh, loading and support configuration.

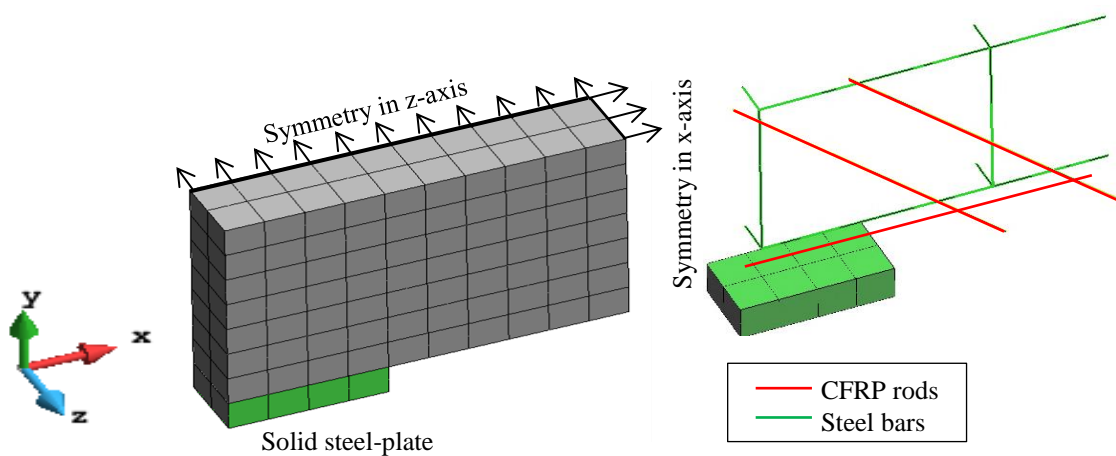


Figure 4 - 12 The boundary conditions of the 3D model in an isometric plane in GiD-FEMIX

In order to avoid the distortion of elements that could occur as a result of the point load in the FE numerical model, an edge load was implemented in this model as shown in Figure 4-13. Moreover, in all numerical models, the edge load was applied by direct displacement-control at the point located in the lower right corner of the mesh.

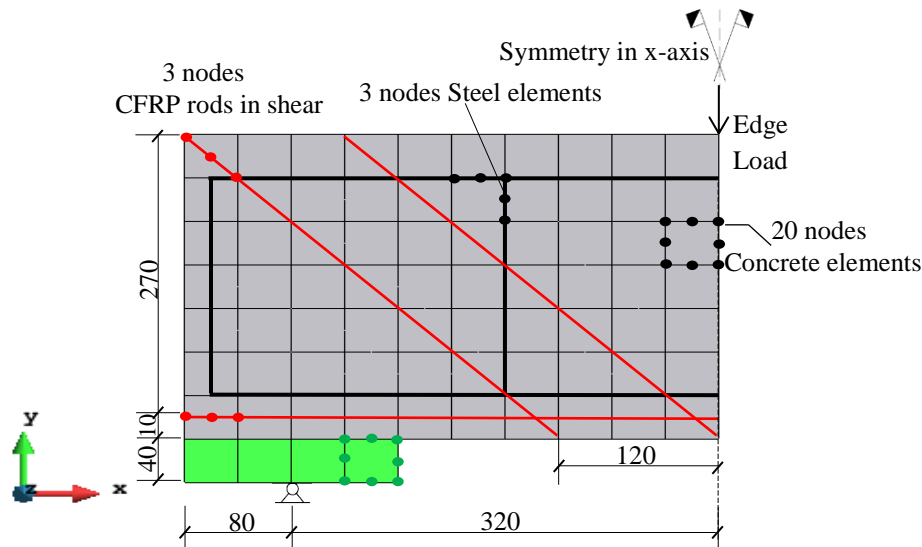


Figure 4 - 13 Geometry in (mm), mesh, loading and support conditions in x-y plane for shear repaired beams with NSM CFRP rods

4.3.4.1 Modelling of corroded RC beam A1CL3-SB

In this numerical model, the diameter loss at the middle of the beam (6%) found in tensile steel bars of the corroded beam A1CL3-SB (see Figure 4-2) was used as a constant residual re-bar cross section all along the RC beam. The reduced cross-sectional area at the mid-span point was used as the failure mode recorded experimentally for this beam was due to large crack at the middle of the beam.

4.3.5 Modelling of RC beams non-shear repaired with NSM CFRP rods (A1CL3-B, A2CL2-A and A1T-B)

One FEM model was implemented for the beams with NSM CFRP rods that were not repaired in shear. The model took account of the cross sectional area reduction due to steel corrosion for both tensile steel bars and steel stirrups at the failure location. The same numerical modelling properties of the fracture mode parameters for the concrete were used here and the FE model took two different constitutive steel models into account (one for corroded beams and one for control beams). Figure 4-14 shows the geometry, element mesh, loading and support configuration for the three beams not shear-repaired with NSM CFRP rods A1CL3-B, A1T-B and A2CL2-A.

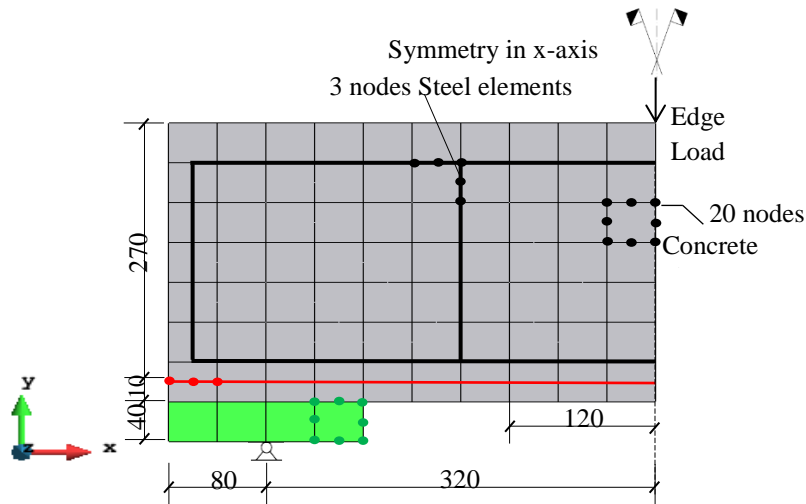


Figure 4 - 14 Geometry (in mm), mesh, loading and support conditions in x-y plane for non-shear-repaired beams with NSM CFRP rods

4.4 Numerical modelling results

4.4.1 Load-deflection curves and failure modes for RC beams non-shear repaired with NSM CFRP rods (A1CL3-B, A2CL2-A and A1T-B)

One FE model was used for beams A1CL3-B and A1T-B as no noteworthy steel corrosion (either in tensile steel bars or in steel stirrups) was found at the edge of the corroded beam A1CL3-B (the same diagonal shear crack edge). The FE model was used again for the corroded beam A2CL2-A (tested experimentally by Dang et al. (31)) using the 10% loss of tensile steel bar cross section, due to corrosion, which was found at the edge of the beam (the same diagonal shear crack edge) as a constant residual re-bar cross section all along the RC beam. The diameter found for the steel stirrups at the failure point of the corroded beam A2CL2-A, which was 1.84 mm (77% of diameter loss shown in Figure 4-4(b)), was used in this model as a constant residual cross section for all of the steel stirrups in the RC beam. For A2CL2-A modelling, the uniaxial constitutive law of corroded steel (shown in Figure 4-11) was used. The load-deflection curves for the FE numerical model for the three non-shear-repaired beams A1CL3-B, A1T-B and A2CL2-A were drawn with the experimental load-deflection curves in Figure 4-15.

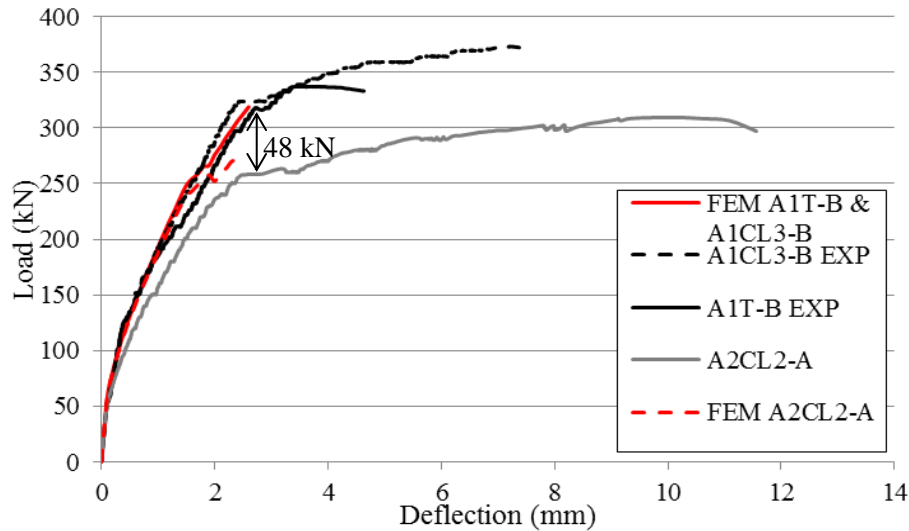


Figure 4 - 15 Experimental vs FE numerical model load-deflection curves for non-shear-repaired beams A1CL3-B , A2CL2-A and A1T-B

Figure 4-15 shows good agreement between FE numerical models and experimental results for the load-deflection behaviour. Although full numerical convergence was not obtained and capturing the post-yielding behaviour for RC beams failing in shear was difficult to achieve for this point since several new cracks formed and, at the same time, the old existing cracks changed their status. Figure 4-15 also shows that considering the steel corrosion for both tensile steel bars and steel stirrups in the FE numerical models led to a reduction of 48 kN in the yielding-moment capacity of the corroded RC beam A2CL2-A (56 kN loss of yielding-moment capacity was found experimentally). The same yielding capacity was obtained for beams A1T-B and A1CL3-B as the corroded beam A1CL3-B had no corrosion at the edge where the shear failure occurred. The crack pattern of the non-shear-repaired beams was obtained using FEMIX code and it is presented in Figure 4-16.

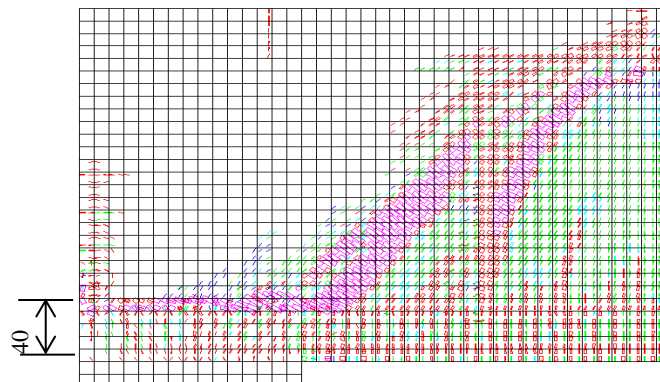


Figure 4 - 16 FE crack pattern of the non-shear-repaired beams (in pink colour: crack completely open; in red colour: crack in the opening process; in cyan colour: crack in the reopening process; green colour: crack in the closing process; in blue colour: closed crack).

The open diagonal shear cracks shown in Figure 4-16 present the modes of failure for both beams not shear-repaired with NSM obtained by the FE numerical model, which coincide with what was found experimentally (see Figure 4-6). The diagonal cracks remained horizontal near the support at the location of the tensile steel bars (40 mm from the surface).

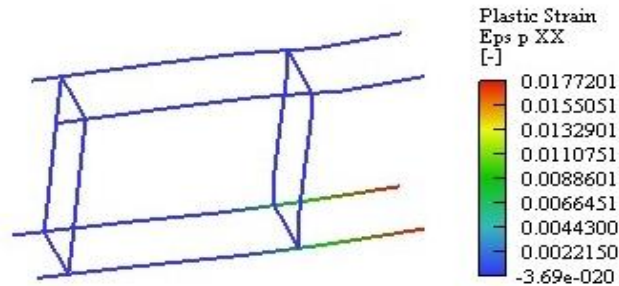


Figure 4 - 17 maximum strain values in the steel bars for the non-shear repaired beam A1CL3-B

The numerical FE model showed that the maximum strain value reached in the tensile bars of the corroded beam A1CL3-B was 0.02 (shown in Figure 4-17) which is still less than the 0.04 ultimate reduced strain value of the corroded steel bars. So, for this point, the steel corrosion did not lead to brittle failure of the steel bars either experimentally or in the numerical model, which is different from the behaviour of corroded RC beams in bending.

4.4.2 Load-deflection curves and failure modes for RC beams shear repaired with NSM CFRP rods (A1CL3-SB and A1T-SB)

Figure 4-18 shows the FE numerical load-deflection curves for both models created for beams repaired in shear with NSM and for the experimental beams. The results show good agreement among the behaviours of the four curves in terms of yielding capacity difference due to the corrosion found at the middle of the beam. This represented 12% of loss of cross section and led to 12% loss in yielding capacity, even though full convergence was not achieved for the two models due to the formation of new cracks and the simultaneous change of status of old cracks (i.e. reopening or reclosing of cracks).

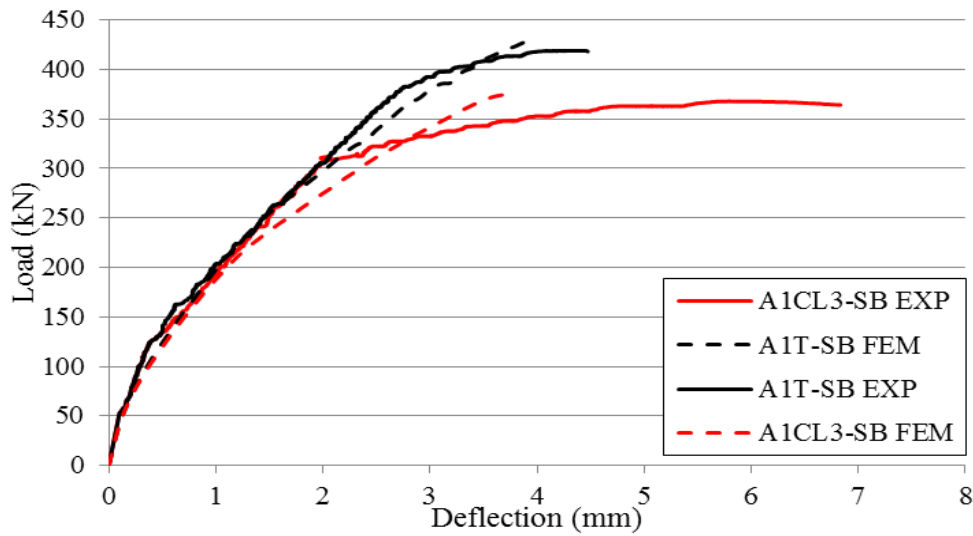


Figure 4 - 18 Experimental vs FE numerical model load-deflection curves for shear-repaired beams A1CL3-SB and A1T-SB

The crack patterns of the FE numerical model were obtained for planes in three perpendicular directions. The x-y plane in Figure 4-19 shows a large open crack (purple) occurring at the middle of the beam. The same effect of shear strengthening with NSM CFRP rods was captured in the FE numerical model. For non-shear repaired beam the model failed in a diagonal tension mode of failure with large shear cracks while, for the shear-repaired beam, the mode of failure changed to large flexural cracks at the middle of the beam as shown in Figure 4-19.

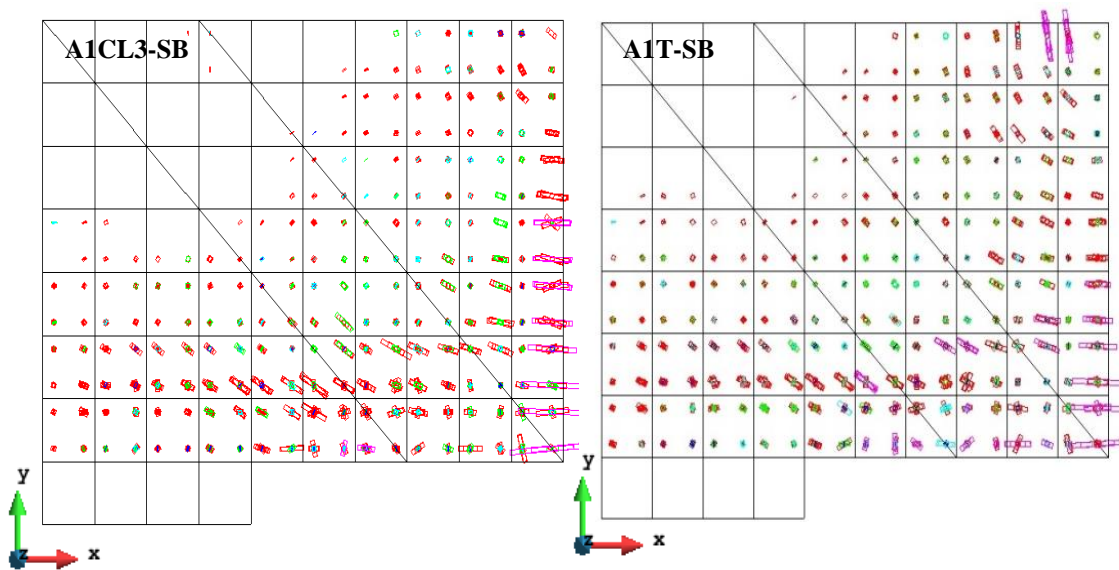


Figure 4 - 19 FE crack patterns of the shear repaired beams in x-y plane (in pink colour: crack completely open; in red colour: crack in the opening process; in cyan colour: crack in the reopening process; green colour: crack in the closing process; in blue colour: closed crack).

For the crack patterns in the x-z and y-z planes shown in Figure 4-20, some open cracks were observed at the middle and bottom of the beams while other open cracks were located at the bottom of the beams near the support.

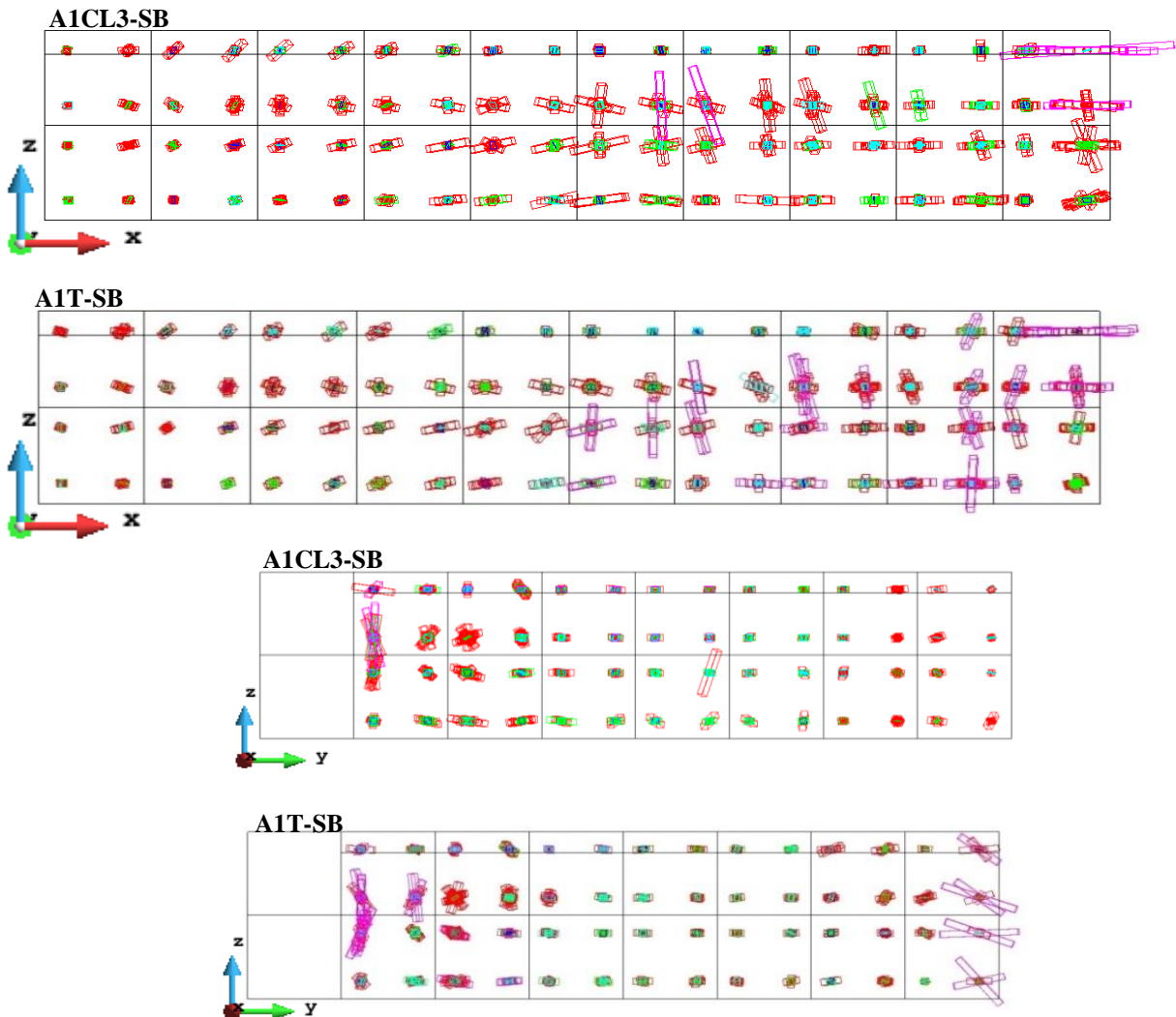


Figure 4 - 20 FE crack patterns of the shear repaired beams in x-z & y-z planes (in pink colour: crack completely open; in red colour: crack in the opening process; in cyan colour: crack in the reopening process; green colour: crack in the closing process; in blue colour: closed crack).

The contribution to the shear strength of an RC beam provided by a system of NSM FRP strips was evaluated throughout the loading process by fulfilling the equilibrium, kinematic compatibility, and constitutive laws of both the materials composing the model and the bond between those materials (38,39). Bianco et al. (20) proposed a predictive model to investigate the NSM shear strengthening contribution, and found that the contribution of the NSM laminates was limited by concrete tensile fracture along their available bond length. It was also found that the concrete around each NSM CFRP strip was not necessarily capable of

carrying the stresses transferred to it, and could thus fracture in a semi-conical surface. If the laminate spacing was reduced, the semi-conical surfaces overlapped (shown in Figure 4-21 (a)), which allowed the interaction between laminates to be easily taken into account and the resulting concrete failure surface was almost parallel to the web face of the beam. The same crack patterns were found for the beams shear-repaired with NSM CFRP rods studied in this paper (A1T-SB and A1CL3-SB). At the bottom and the edge of the beams, there were visible splitting cracks (separation of the concrete sides including the NSM CFRP rods) which matched the predictive model proposed by Bianco et al. (20).

Figure 4-21 (a) shows a section parallel to the shear crack plane, presenting the semi-conical fracture surfaces of concrete due to excessive stresses of the approach proposed by Bianco et al. (20). Figure 4-21 (b) and (c) presents the splitting cracks that occurred at the bottom and the edge of the shear-repaired beams A1T-SB and A1CL3-SB.

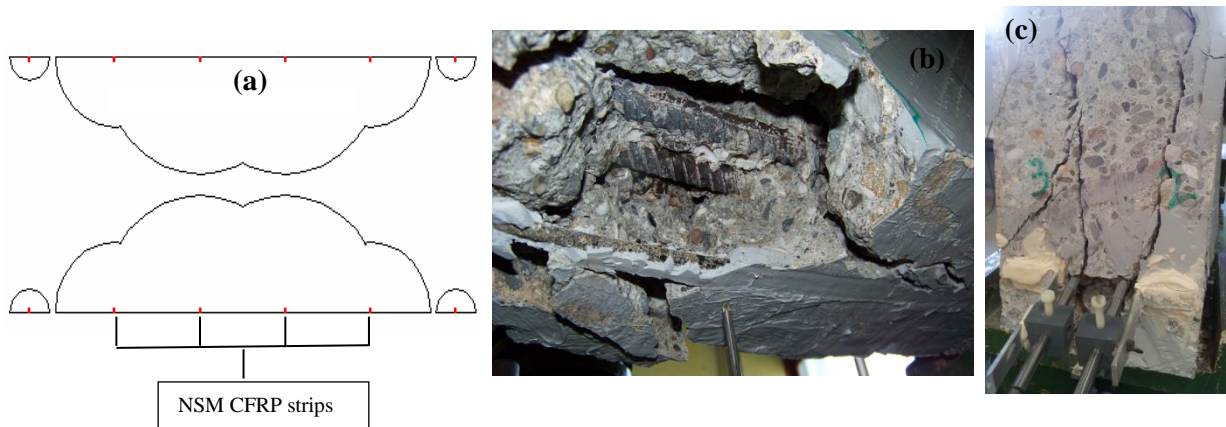


Figure 4 - 21 (a) Section parallel to the crack plane for the theory of the failure mode proposed by Bianco et al. 24. (b) Splitting cracks at the bottom of the shear repaired beams A1CL3-SB and A1T-SB. (c) Splitting cracks at the edge of the shear repaired beams A1CL3-SB and A1T-SB

4.5 Conclusions

According to the results found in this paper, the following conclusions can be drawn:

1. The comparison between the FE numerical predictions and the experimental results showed a satisfactory level of accuracy of the proposed model in terms of capturing the load-deflection curves and the crack patterns.
2. The loss of cross section of steel bars was well captured by the FE numerical models, which reproduced the same reduction of the yielding capacity as found experimentally.

3. The effectiveness of the NSM technique was limited by the semi-conical effect of each NSM CFRP rod contribution and the non-repaired mid span point of the SB beams, which led to the appearance of splitting cracks at the middle of the RC beams strengthened in shear.
4. A FE numerical model taking account of both the interaction between the NSM CFRP rods and the concrete, and the bond-slip relationship between concrete and corroded steel bars is required in the future.

4.6 References

1. Tayeh BA, Abu Bakar B, Megat Johari M, Voo YL. Mechanical and permeability properties of the interface between normal concrete substrate and ultra high performance fiber concrete overlay. *Constr Build Mater.* 2012;36:538–48.
2. Andrade C, Alonso C, Garcia D, Rodriguez J. Remaining lifetime of reinforced concrete structures: Effect of corrosion on the mechanical properties of the steel. *International conference on life prediction of corrodible structures, NACE Cambridge, UK, 1991; 546-557.*
3. Al-Sulaimani G, Kaleemullah M, Basunbul I. Rasheeduzzafar,(1990)“Influence of corrosion and cracking on bond behaviour and strength of reinforced concrete members” *ACI Structural Journal*, 87 (2), 220-231. ASTM G1. 1990;
4. Rodriguez J, Ortega L, Casal J. Load carrying capacity of concrete structures with corroded reinforcement. *Constr Build Mater.* 1997;11(4):239–48.
5. Chung L, Najm H, Balaguru P. Flexural behavior of concrete slabs with corroded bars. *Cem Concr Compos.* 2008;30(3):184–93.
6. Azad AK, Ahmad S, Azher SA. Residual strength of corrosion-damaged reinforced concrete beams. *ACI Mater J.* 2007;104(1).
7. Torres-Acosta AA, Navarro-Gutierrez S, Terán-Guillén J. Residual flexure capacity of corroded reinforced concrete beams. *Eng Struct.* 2007;29(6):1145–52.
8. Xia J, Jin W, Li L. Shear performance of reinforced concrete beams with corroded stirrups in chloride environment. *Corros Sci.* 2011;53(5):1794–805.
9. Wang X-H, Li B, Gao X-H, Liu X-L. Shear behaviour of RC beams with corrosion damaged partial length. *Mater Struct.* 2012;45(3):351–79.
10. Wang X-H, Gao X-H, Li B, Deng B-R. Effect of bond and corrosion within partial length on shear behaviour and load capacity of RC beam. *Constr Build Mater.* 2011;25(4):1812–23.
11. Zhu W, François R, Coronelli D, Cleland D. Effect of corrosion of reinforcement on the mechanical behaviour of highly corroded RC beams. *Eng Struct.* 2013;56:544–54.
12. Khan I, François R, Castel A. Experimental and analytical study of corroded shear-critical reinforced concrete beams. *Mater Struct.* 2014;1–15.
13. De Lorenzis L, Nanni A. Shear strengthening of reinforced concrete beams with near-surface mounted fiber-reinforced polymer rods. *ACI Struct J.* 2001;98(1).
14. Islam AA. Effects of NSM CFRP bars in shear strengthening of concrete members. *ASCE*; 2009. p. 1–14.
15. Rizzo A, De Lorenzis L. Behavior and capacity of RC beams strengthened in shear with NSM FRP reinforcement. *Constr Build Mater.* 2009;23(4):1555–67.

16. Dias SJ, Barros JA. Performance of reinforced concrete T beams strengthened in shear with NSM CFRP laminates. *Eng Struct.* 2010;32(2):373–84.
17. Omran HY, El-Hacha R. Nonlinear 3D finite element modeling of RC beams strengthened with prestressed NSM-CFRP strips. *Constr Build Mater.* 2012;31:74–85.
18. Nanni A, Di Ludovico M, Parretti R. Shear strengthening of a PC bridge girder with NSM CFRP rectangular bars. *Adv Struct Eng.* 2004;7(4):297–309.
19. Barros JA, Baghi H, Dias SJ, Ventura-Gouveia A. A FEM-based model to predict the behaviour of RC beams shear strengthened according to the NSM technique. *Eng Struct.* 2013;56:1192–206.
20. Bianco V, Barros JA, Monti G. A new approach for modelling the NSM shear strengthening contribution in reinforced concrete beams. *J Compos Constr.* 2007;
21. Almassri B, Kreit A, Al Mahmoud F, François R. Behaviour of corroded shear-critical reinforced concrete beams repaired with NSM CFRP rods. *Composite Structures* 2015; 123:204-215.
22. Rots JG, De Borst R. Analysis of mixed-mode fracture in concrete. *J Eng Mech.* 1987;113(11):1739–58.
23. Suryanto B, Nagai K, Maekawa K. Modeling and analysis of shear-critical ECC members with anisotropic stress and strain fields. *J Adv Concr Technol.* 2010;8(2):239–58.
24. Sena Cruz JM, Barros JA, Gettu R, Azevedo ÁF. Bond behavior of near-surface mounted CFRP laminate strips under monotonic and cyclic loading. *J Compos Constr.* 2006;10(4):295–303.
25. Barros JAO, Baghi H, Dias SJE, Ventura-Gouveia A. A FEM-based model to predict the behaviour of RC beams shear strengthened according to the NSM technique. *Eng Struct.* 2013 Nov;56(0):1192–206.
26. Barros JA, Costa IG, Ventura-Gouveia A. CFRP flexural and shear strengthening technique for RC beams: experimental and numerical research. *Adv Struct Eng.* 2011;14(3):551–71.
27. Castel A, François R, Arliguie G. Mechanical behaviour of corroded reinforced concrete beams—Part 1: experimental study of corroded beams. *Mater Struct.* 2000;33(9):539–44.
28. Vidal T, Castel A, François R. Corrosion process and structural performance of a 17 year old reinforced concrete beam stored in chloride environment. *Cem Concr Res.* 2007;37(11):1551–61.
29. Kreit A, Al-Mahmoud F, Castel A, François R. Repairing corroded RC beam with near-surface mounted CFRP rods. *Mater Struct.* 2011;44(7):1205–17.
30. Almassri B, Kreit A, Mahmoud FA, François R. Mechanical behaviour of corroded RC beams strengthened by NSM CFRP rods. *Compos Part B Eng.* 2014;64:97–107.

31. Dang VH, François R., Coronelli D., Shear behaviour and load capacity of short reinforced concrete beams exposed to chloride environment, *European Journal of Environmental and Civil Engineering*, to be published 2015.
32. François R, Khan I, Dang VH. Impact of corrosion on mechanical properties of steel embedded in 27-year-old corroded reinforced concrete beams. *Mater Struct.* 2013;46(6):899–910.
33. Zhu W, François R. Effect of corrosion pattern on the ductility of tensile reinforcement extracted from a 26-year-old corroded beam. *Adv Concr Constr.* 2013;1(2):121–37.
34. Apostolopoulos C, Papadakis V. Consequences of steel corrosion on the ductility properties of reinforcement bar. *Constr Build Mater.* 2008;22(12):2316–24.
35. Cairns J, Plizzari GA, Du Y, Law DW, Franzoni C. Mechanical properties of corrosion-damaged reinforcement. *ACI Mater J.* 2005;102(4).
36. Almusallam AA. Effect of degree of corrosion on the properties of reinforcing steel bars. *Constr Build Mater.* 2001;15(8):361–8.
37. Du Y, Clark L, Chan A. Residual capacity of corroded reinforcing bars. *Mag Concr Res.* 2005;57(3):135–47.
38. Bianco, V. “Shear strengthening of RC beams by means of NSM FRP strips: Experimental evidence and analytical modeling.” Ph.D. thesis, Dept. of Structural Engrg. and Geotechnics, Sapienza Univ. of Rome, Italy. 2008.
39. Bianco V, Barros JA, Monti G. Bond model of NSM-FRP strips in the context of the shear strengthening of RC beams. *J Struct Eng.* 2009;135(6):619–31.

Conclusions

The FE modelling results using the FEMIX computer code showed a good agreement in terms of the load-deflection curves compared to the experimental results for the non-shear-repaired beams A1CL3-B, A2CL2-A and A1T-B. While full FE numerical convergence was not achieved at this point as several new cracks were appearing at the same time of old cracks changing their status.

The failure/cracks pattern obtained from FEMIX for the non-shear-repaired beams A1CL3-B, A2CL2-A and A1T-B matched the experimental mode of failure which occurred by the diagonal tension failure with large diagonal open shear cracks which extended from the top of the beam till the support near the concrete cover. Moreover, the numerical model could capture the corrosion effect in tensile steel bars and steel stirrups on the yielding-moment capacity of the corroded RC beams.

The results showed also a good agreement for shear-repaired beams A1CL3-SB and A1T-SB between the experimental and FE modelling load-deflection curves. The yielding capacity difference between the two beams (12%) induced by steel corrosion was well captured as well.

The three-dimensional cracks patterns x-z and y-z planes for both shear repaired beams A1T-SB and A1CL3-SB presented some specific splitting cracks which were observed at the middle and bottom of the beams while other open cracks located at the bottom of the beams near the support, these splitting cracks were discussed in a previous analytical research was made to study the shear strengthening contribution of the NSM CFRP strips, this specific mode of failure was reasoned for the concrete around each NSM CFRP strip was not necessarily capable of carrying the stresses transferred to it.

Using transversal strengthening for shear-repaired RC beams in order to prevent these early splitting cracks from happening could be an option while more investigation are needed in this area of study in order to provide safe design provisions.

General Conclusion

The first objective of this thesis was to study the effectiveness of the NSM CFRP rods technique on the mechanical performance of the naturally corroded RC beams in both shear and bending. For this purpose, one corroded and one control RC beams (3-meters-long) were repaired or strengthened in bending with NSM CFRP (6 mm diameter) rod and were tested in three-point loading tests up to failure. The results were compared to similar non-repaired RC beams, it was found that the NSM technique is able to increase the ultimate load capacity of a corroded beam that has suffered considerable damage and can allow it to reach to the ultimate capacity of the control beam, as well as the NSM technique slightly increases the stiffness of both repaired corroded and strengthened control beams, it also restores a sufficient ductility lost due to steel corrosion (almost 2.8 times that of the non-repaired corroded beams), moreover the NSM technique increases the ultimate deflection for both repaired corroded and strengthened control beams. Finally, the efficiency of using the NSM as a repair technique for the corroded RC beams could be limited by the appearance of a new non-conventional failure mode which occurred by the separation of the concrete cover.

Later two edges (80-cm-long) of the two full beams were repaired with NSM in shear (4 inclined CFRP rods with 45 degrees were fixed on each face of the RC beams) while the other two edges were left repaired in bending only, all of the short beams were tested in three-point loading tests up to failure and they were compared to other non-repaired short beams. Repairing against shear with NSM CFRP rods changed the failure mode from shear cracking (for non-shear-repaired beams) to concrete crushing with a large flexural crack at the middle (for shear-repaired beams), the NSM technique also reduced significantly the maximum slip of the tensile steel bars for control RC beams. It was found also that the NSM technique had no effect on the load-capacity of the corroded beams having shear span to effective depth (a/d) ratio values less than 2, the (a/d) ratio is considered to be an important parameter for deep beams as the general trend found for such beams is far from the classical bending theory effect. By repairing in shear with CFRP rods, not only the bonding anchorage but also the yielding capacity of the whole beam was increased, for (a/d) ratios between (2.5-3) which is a transition zone between bending response and shear response, a change in the mechanical response in bending was noticed.

The second objective of this thesis was to implement numerical models based on the FEM analysis, in order to simulate the non-linear behavior of the corroded RC structures repaired

with NSM CFRP rods in both bending and shear, For those beams repaired with NSM CFRP rods in bending, results of 2D FEM using the FEMIX computer code were obtained on five, (3-metre-long) beams: three corroded RC beams and two control beams with no corrosion. Two beams, one corroded and one control were each repaired or strengthened in bending with one 6-mm-diameter NSM CFRP rod, the yielding of the steel bars and the ultimate load carrying capacity were well predicted by the 2D numerical models for all beams, the reduction in ultimate deflection of corroded beams was also well predicted by the model as the change in steel ultimate elongation induced by corrosion which was taken into account in the modelling. Only, the behaviour of the corroded RC beam repaired with NSM technique which failed experimentally by a non-conventional failure mode due to the separation of the concrete cover couldn't be well predicted by the 2D modelling, so for this point it was highly required to implement 3D FE model using ABAQUS software in order to investigate this special case. The results showed that the 3D FEM analysis using ABAQUS was able to predict both load-bearing capacity and ultimate deflection reduction due to corrosion if the crack plane induced by corrosion was taken into account in the model.

Finally, for short RC beams shear-repaired with NSM technique, the computer code FEMIX was used to implement 3D FEM analysis in order to predict the behaviour of four short RC beams (80-cm-long), two corroded and two control beams, while one corroded and one control beams were shear-repaired with NSM technique, one more non-shear-repaired corroded beam was studied also. The results showed a satisfactory level of agreement between the experimental and the FEM results in terms of load-deflection curves and failure modes (crack patterns), the numerical models well captured the change in failure mode before and after shear-repairing with NSM CFRP rods, the numerical models showed also that the effectiveness of the NSM technique in shear-repairing could be limited by the semi conical effect of each NSM CFRP rod contribution (based on previous analytical study by Bianco et al.) which led to splitting cracks happened at the middle of the RC beams strengthened or repaired in shear.

The NSM technique could be a promising technique for repairing the naturally corroded RC beams. Nevertheless, the appearance of new non-conventional failure modes needs more investigation to propose a relevant method of design furnishing safe design provisions. More investigations are also required in the FE modelling field regarding the numerical modelling simulation which takes into account both the cross sectional reduction of corroded steel bars and the bond-slip relationship between concrete and corroded steel bars.

Scientific Production

Papers in international Journals:

Almassri B, Kreit A, Al Mahmoud F, François R. Mechanical behaviour of corroded RC beams strengthened by NSM CFRP rods. *Composites Part B Eng.* 2014; 64:97–107.

Almassri B, Kreit A, Al Mahmoud F, François R. Behaviour of corroded shear-critical reinforced concrete beams repaired with NSM CFRP rods. *Composite Structures* 2015; 123:204-215.

Almassri B, Mahmoud FA, Francois R, Behaviour of corroded Reinforced Concrete beams repaired with NSM CFRP rods, Experimental and Finite Element Study, *Composites Part B*, doi: 10.1016/j.compositesb.2015.01.022.

Almassri B, Barros JA. Al-Mahmoud F, François R, A FEM-based model to study the behaviour of corroded RC beams shear repaired by NSM CFRP rods technique; *Composite Structures*, (Under review by *Composite Structures*), 2015.

Papers in international conferences:

Almassri B, Kreit A, Al Mahmoud F, François R. Study on behaviour of corroded RC beams repaired in shear with NSM CFRP rods. *Chemistry and Materials Research* 5 (2013): 57-63. Special Issue for International Congress on Materials & Structural Stability, Rabat, Morocco, 27-30th of November 2013.

Almassri B, Kreit A, Al Mahmoud F, François R. Study on behaviour of corroded RC beams strengthened with NSM CFRP rods – an experimental and finite element modeling study. *Structural Faults and Repair Conference*, London, UK, 8-10th of July 2014.

Almassri B, Kreit A, Al Mahmoud F, François R. Mechanical Behavior of Corroded RC Beams Strengthened by NSM CFRP Rods. *ICSE 2015: XIII International Conference on Structural Engineering*, Rome, Italy, 04/2015

Almassri B, Barros JA. Al-Mahmoud F, François R, A FEM-based model to study the behaviour of corroded RC beams shear repaired by NSM CFRP rods technique; *International Conference on Advances in Composite Materials and Structures*, Istanbul, Turkey; 04/2015.

Almassri B, Barros JA. Al-Mahmoud F, François R, Etude du comportement mécanique des poutres corrodées réparées à l'effort tranchant par l'insertion des joncs de carbone.; *Regroupement Francophone pour la Recherche et la Formation sur le Béton, RF2B*, Lausanne, Switzerland; 07/2015.

References

Note: (All the references used in each chapter are listed here in an alphabetical order)

- Abdullah R, Mokhatar SN. Computational analysis of reinforced concrete slabs subjected to impact loads. *Int J Integr Eng.* 2012;4(2):70–6.
- ACI, Guide for the Design and Construction of Externally Bonded FRP Systems for Strengthening Concrete Structures, 440.2R 02 American Concrete Institute ACI, committee 440, 2002, 45 pp.
- Al-Mahmoud F, Castel A, François R, Tourneur C. RC beams strengthened with NSM CFRP rods and modeling of peeling-off failure. *Compos Struct.* 2010;92(8):1920–30.
- Al-Mahmoud F, Castel A, François R. Failure modes and failure mechanisms of RC members strengthened by NSM CFRP composites—Analysis of pull-out failure mode. *Compos Part B Eng.* 2012;43(4):1893–901.
- Al-Mahmoud F, Castel A, François R, Tourneur C. Effect of surface pre-conditioning on bond of carbon fibre reinforced polymer rods to concrete. *Cem Concr Compos.* 2007; 29(9):677–89.
- Al-Mahmoud F, Castel A, François R, Tourneur C, Marchand J, Bissonnette B, et al. Anchorage and tension-stiffening effect between Near-Surface-Mounted Fiber Reinforced polymer rod and concrete. 2006.
- Al-Mahmoud F, Castel A, François R, Tourneur C. Strengthening of RC members with near-surface mounted CFRP rods. *Compos Struct.* 2009;91(2):138–47.
- Almassri B, Kreit A, Al Mahmoud F, François R. Mechanical behaviour of corroded RC beams strengthened by NSM CFRP rods. *Compos Part B Eng.* 2014; 64:97–107.
- Almassri B, Kreit A, Al Mahmoud F, François R. Behaviour of corroded shear-critical reinforced concrete beams repaired with NSM CFRP rods. *Composite Structures* 2015; 123:204-215.
- Almusallam AA. Effect of degree of corrosion on the properties of reinforcing steel bars. *Constr Build Mater.* 2001;15(8):361–8.
- Al-Sulaimani G, Kaleemullah M, Basunbul I. Rasheeduzzafar,(1990)“Influence of corrosion and cracking on bond behaviour and strength of reinforced concrete members” *ACI Structural Journal*, 87 (2), 220-231. ASTM G1. 1990.
- Andrade C, Alonso C, Garcia D, Rodriguez J. Remaining lifetime of reinforced concrete structures: effect of corrosion on the mechanical properties of the steel. In: *Proceedings of the international conference on life prediction of corrodible structures.* National Association of Corrosion Engineers, Cambridge, UK, 23–26 September; 1991. p. 12/1–11.
- Apostolopoulos C, Papadakis V. Consequences of steel corrosion on the ductility properties of reinforcement bar. *Constr Build Mater.* 2008;22(12):2316–24.

- Azad AK, Ahmad S, Azher SA. Residual strength of corrosion-damaged reinforced concrete beams. *ACI Mater J*. 2007;104(1).
- Badawi M, Soudki K. Flexural strengthening of RC beams with prestressed NSM CFRP rods—experimental and analytical investigation. *Constr Build Mater*. 2009;23(10):3292–300.
- Barros JA, Costa IG, Ventura-Gouveia A. CFRP flexural and shear strengthening technique for RC beams: experimental and numerical research. *Adv Struct Eng*. 2011;14(3):551–71.
- Barros JA, Fortes A. Flexural strengthening of concrete beams with CFRP laminates bonded into slits. *Cem Concr Compos*. 2005;27(4):471–80.
- Barros JA, Ferreira DR, Fortes AS, Dias SJ. Assessing the effectiveness of embedding CFRP laminates in the near surface for structural strengthening. *Constr Build Mater*. 2006;20(7):478–91.
- Barros JA, Baghi H, Dias SJ, Ventura-Gouveia A. A FEM-based model to predict the behaviour of RC beams shear strengthened according to the NSM technique. *Eng Struct*. 2013;56:1192–206.
- Basic facts concerning shear failure. *ACI*; 1966.
- Beeby A. *Concrete in the oceans: cracking and corrosion*. Cement and Concrete Association; 1978.
- Bianco, V. “Shear strengthening of RC beams by means of NSM FRP strips: Experimental evidence and analytical modeling.” Ph.D. thesis, Dept. of Structural Engrg. and Geotechnics, Sapienza Univ. of Rome, Italy. 2008.
- Bianco V, Barros JA, Monti G. Bond model of NSM-FRP strips in the context of the shear strengthening of RC beams. *J Struct Eng*. 2009;135(6):619–31.
- Bianco V, Barros JA, Monti G. A new approach for modeling the NSM shear strengthening contribution in reinforced concrete beams. *FRPRCS-8*, Univ. Patras, Greece, 16-18 July 2007, ID 8-12.
- Bilotta A, Ceroni F, Di Ludovico M, Nigro E, Pecce M, Manfredi G. Bond efficiency of EBR and NSM FRP systems for strengthening concrete members. *J Compos Constr*. 2011;15(5):757–72.
- Cairns J, Plizzari GA, Du Y, Law DW, Franzoni C. Mechanical properties of corrosion-damaged reinforcement. *ACI Mater J*. 2005;102(4).
- Castel A, François R, Arliguie G. Mechanical behaviour of corroded reinforced concrete beams—Part 1: experimental study of corroded beams. *Mater Struct*. 2000;33(9):539–44.
- Chaudhari S, Chakrabarti M. Modeling of concrete for nonlinear analysis Using Finite Element Code ABAQUS. *Int J Comput Appl*. 2012;44.
- Chung L, Najm H, Balaguru P. Flexural behavior of concrete slabs with corroded bars. *Cem Concr Compos*. 2008;30(3):184–93.

- Dang VH, François R. Influence of long-term corrosion in chloride environment on mechanical behaviour of RC beam. *Eng Struct.* 2013;48:558–68.
- Dang VH, François R. Prediction of ductility factor of corroded reinforced concrete beams exposed to long term aging in chloride environment. *Cem Concr Compos.* 2014;53:136–47.
- Dang VH, François R., Coronelli D., Shear behaviour and load capacity of short reinforced concrete beams exposed to chloride environment, *European Journal of Environmental and Civil Engineering*, to be published 2015.
- Dang VH. Initiation and propagation phases of re-bars corrosion in pre-cracked reinforced concrete exposed to caronation or chloride environment. PhD thesis at l’Institut National des Sciences Appliquées de Toulouse, France. 2013.
- De Lorenzis L, Teng J. Near-surface mounted FRP reinforcement: An emerging technique for strengthening structures. *Compos Part B Eng.* 2007;38(2):119–43.
- De Lorenzis L, Micelli F, La Tegola A. Passive and active near surface mounted FRP rods for flexural strengthening of RC beams. 2002.
- De Lorenzis L, Nanni A. Bond between near-surface mounted fiber-reinforced polymer rods and concrete in structural strengthening. *ACI Struct J.* 2002;99(2).
- De Lorenzis L, Nanni A, La Tegola A. Flexural and shear strengthening of reinforced concrete structures with near surface mounted FRP rods. 2000. p. 521–8.
- De Lorenzis L, Nanni A. Shear strengthening of reinforced concrete beams with near-surface mounted fiber-reinforced polymer rods. *ACI Struct J.* 2001;98(1).
- Dias SJ, Barros JA. Performance of reinforced concrete T beams strengthened in shear with NSM CFRP laminates. *Eng Struct.* 2010;32(2):373–84.
- Du Y, Clark LA, Chan AH. Impact of reinforcement corrosion on ductile behavior of reinforced concrete beams. *ACI Struct J.* 2007;104(3).
- Du Y, Clark L, Chan A. Residual capacity of corroded reinforcing bars. *Mag Concr Res.* 2005;57(3):135–47.
- EN 206-1. European standard, concrete – Part 1: specifications, performance, production and conformity. NF EN 206-1; April. 2004.
- EN 12390–2, 3, 5. Essai pour béton durci: confection et conservation des éprouvettes pour essais de résistance, résistance à la compression des éprouvettes et résistance à la flexion des éprouvettes. Bruxelles: IBN; 2000.
- FIB, technical report bulletin 14, “Externally bonded FRP reinforcement for RC structures”, The international federation for structural concrete FIB, published in Europe (fib, CEB-FIP, 2001).
- FIB Bulletin No. 57. Shear and punching shear in RC and FRC elements. 2010. 268 p.

- François R, Castel A, Vidal T, Vu N.-A. Long term corrosion behavior of reinforced concrete structures in chloride environment. *J Phys IV Fr.* 2006 Nov;136:285–93.
- François R, Khan I, Dang VH. Impact of corrosion on mechanical properties of steel embedded in 27-year-old corroded reinforced concrete beams. *Mater Struct.* 2013;46(6):899–910.
- French regulations for reinforced concrete structures. B.A.E.L. 1983.
- Hanjari KZ, Coronelli D, Lundgren K. Bond capacity of severely corroded bars with corroded stirrups. *Mag Concr Res.* 2011;63(12):953–68.
- Hassan T, Rizkalla S. Investigation of bond in concrete structures strengthened with near surface mounted carbon fiber reinforced polymer strips. *J Compos Constr.* 2003;7(3):248–57.
- Hawileh RA. Nonlinear finite element modeling of RC beams strengthened with NSM FRP rods. *Constr Build Mater.* 2012;27(1):461–71.
- Higgins C, Farrow III WC. Tests of reinforced concrete beams with corrosion-damaged stirrups. *ACI Struct J.* 2006;103(1).
- Horne A, Richardson I, Brydson R. Quantitative analysis of the microstructure of interfaces in steel reinforced concrete. *Cem Concr Res.* 2007;37(12):1613–23.
- Islam AA. Effects of NSM CFRP bars in shear strengthening of concrete members. *ASCE*; 2009. p. 1–14.
- Kani G. How safe are our large reinforced concrete beams? *ACI*; 1967.
- Kang J-Y, Park Y-H, Park J-S, You Y-J, Jung W-T. Analytical evaluation of RC beams strengthened with near surface mounted CFRP laminates. *ACI Spec Publ.* 2005;230.
- Khan I, François R, Castel A. Structural performance of a 26-year-old corroded reinforced concrete beam. *Eur J Environ Civ Eng.* 2012;16(3-4):440–9.
- Khan I, François R, Castel A. Experimental and analytical study of corroded shear-critical reinforced concrete beams. *Mater Struct* 2014;47:1467–81.
- Kreit A, Al-Mahmoud F, Castel A, François R. Repairing corroded RC beam with near-surface mounted CFRP rods. *Mater Struct.* 2011;44(7):1205–17.
- Kreit A. Prolongation de la durée de vie des hôpitaux, PhD thesis at l'Institut National des Sciences Appliquées de Toulouse, France. 2012.
- Lublinter J, Oliver J, Oller S, Oñate E. A plastic-damage model for concrete. *Int J Solids Struct.* 1989;25(3):299–326.
- Lundqvist J, Nordin H, Täljsten B, Olofsson T. Numerical analysis of concrete beams strengthened with CFRP-A study of anchorage lengths. 2005. p. 247–54.

- Malumbela G, Moyo P, Alexander M. A step towards standardising accelerated corrosion tests on laboratory reinforced concrete specimens. *J South Afr Inst Civ Eng.* 2012;54(2):78–85.
- Nanni A, Di Ludovico M, Parretti R. Shear strengthening of a PC bridge girder with NSM CFRP rectangular bars. *Adv Struct Eng.* 2004;7(4):297–309.
- Nguyen DM, Chan TK, Cheong HK. Brittle failure and bond development length of CFRP-concrete beams. *J Compos Constr.* 2001;5(1):12–7.
- Norme Europeenne NF EN 18-459: Porosity and density test.
- Omran HY, El-Hacha R. Nonlinear 3D finite element modeling of RC beams strengthened with prestressed NSM-CFRP strips. *Constr Build Mater.* 2012;31:74–85.
- Otieno M, Beushausen H, Alexander M. Prediction of corrosion rate in reinforced concrete structures—a critical review and preliminary results. *Mater Corros.* 2012;63(9):777–90.
- Owen D, Figueiras J. Anisotropic elasto-plastic finite element analysis of thick and thin plates and shells. *Int J Numer Methods Eng.* 1983;19(4):541–66.
- Poursaee A, Hansson C. Potential pitfalls in assessing chloride-induced corrosion of steel in concrete. *Cem Concr Res.* 2009;39(5):391–400.
- Radfar S, Foret G, Saeedi N, Sab K. Simulation of concrete cover separation failure in FRP plated RC beams. *Constr Build Mater.* 2012;37:791–800.
- Rizzo A, De Lorenzis L. Behavior and capacity of RC beams strengthened in shear with NSM FRP reinforcement. *Constr Build Mater.* 2009;23(4):1555–67.
- Rodriguez J, Ortega L, Casal J. Load carrying capacity of concrete structures with corroded reinforcement. *Constr Build Mater.* 1997;11(4):239–48.
- Rots JG, De Borst R. Analysis of mixed-mode fracture in concrete. *J Eng Mech.* 1987;113(11):1739–58.
- Schmitt G. Global needs for knowledge dissemination, research, and development in materials deterioration and corrosion control. *World Corros Organ N Y.* 2009.
- Sena Cruz JM, Barros JA, Gettu R, Azevedo ÁF. Bond behavior of near-surface mounted CFRP laminate strips under monotonic and cyclic loading. *J Compos Constr.* 2006;10(4):295–303.
- Sherwood E, Soudki K. Confinement of Corrosion Cracking in Reinforced Concrete Beams Using Carbon Fiber Reinforced Polymer Laminates. *ACI Spec Publ.* 1999;188.
- Si-Larbi A, Agbossou A, Ferrier E, Michel L. Strengthening RC beams with composite fiber cement plate reinforced by prestressed FRP rods: Experimental and numerical analysis. *Compos Struct.* 2012;94(3):830–8.

- Soudki KA, Sherwood TG. Behaviour of reinforced concrete beams strengthened with carbon fibre reinforced polymer laminates subjected to corrosion damage. *Can J Civ Eng.* 2000;27(5):1005–10.
- Soudki K. FRP Repair of Corrosion-damaged Concrete Beams — Waterloo Experience. In: Pandey M, Xie W-C, Xu L, editors. *Advances in Engineering Structures, Mechanics & Construction* [Internet]. Springer Netherlands; 2006. p. 165–73. Available from: http://dx.doi.org/10.1007/1-4020-4891-2_14
- Soylev T, François R. Quality of steel–concrete interface and corrosion of reinforcing steel. *Cem Concr Res.* 2003;33(9):1407–15.
- Steiner W. Strengthening of structures with CFRP strips. Canadian Society for Civil Engineers, Montreal, Quebec, Canada; 1996. p. 407–19.
- Suryanto B, Nagai K, Maekawa K. Modeling and analysis of shear-critical ECC members with anisotropic stress and strain fields. *J Adv Concr Technol.* 2010;8(2):239–58.
- Tahershamsi M, Zandi K, Lundgren K, Plos M. Anchorage of naturally corroded bars in reinforced concrete structures. 2014.
- Täljsten B, Carolin A, Nordin H. Concrete structures strengthened with near surface mounted reinforcement of CFRP. *Adv Struct Eng.* 2003;6(3):201–13.
- Tayeh BA, Abu Bakar B, Megat Johari M, Voo YL. Mechanical and permeability properties of the interface between normal concrete substrate and ultra high performance fiber concrete overlay. *Constr Build Mater.* 2012;36:538–48.
- Torres-Acosta AA, Navarro-Gutierrez S, Terán-Guillén J. Residual flexure capacity of corroded reinforced concrete beams. *Eng Struct.* 2007;29(6):1145–52.
- Vidal T, Castel A, François R. Corrosion process and structural performance of a 17 year old reinforced concrete beam stored in chloride environment. *Cem Concr Res.* 2007;37(11):1551–61.
- Wang X-H, Li B, Gao X-H, Liu X-L. Shear behaviour of RC beams with corrosion damaged partial length. *Mater Struct.* 2012;45(3):351–79.
- Wang X-H, Gao X-H, Li B, Deng B-R. Effect of bond and corrosion within partial length on shear behaviour and load capacity of RC beam. *Constr Build Mater.* 2011;25(4):1812–23.
- Xia J, Jin W, Li L. Shear performance of reinforced concrete beams with corroded stirrups in chloride environment. *Corros Sci.* 2011;53(5):1794–805.
- Yang Z, Chen J, Proverbs D. Finite element modelling of concrete cover separation failure in FRP plated RC beams. *Constr Build Mater.* 2003;17(1):3–13.
- Yuan Y, Ji Y, Shah SP. Comparison of two accelerated corrosion techniques for concrete structures. *ACI Struct J.* 2007;104(3).

- Zhu W, François R. Corrosion of the reinforcement and its influence on the residual structural performance of a 26-year-old corroded RC beam. *Constr Build Mater.* 2014;51:461–72.
- Zhu W, François R, Coronelli D, Cleland D. Effect of corrosion of reinforcement on the mechanical behaviour of highly corroded RC beams. *Eng Struct.* 2013;56:544–54.
- Zhu W, François R. Effect of corrosion pattern on the ductility of tensile reinforcement extracted from a 26-year-old corroded beam. *Adv Concr Constr.* 2013;1(2):121–37.
- Zhu W. Effect of corrosion on the mechanical properties of the corroded reinforcement and the residual structural performance of the corroded beams. PhD thesis at Univeristy of Toulouse. (2014).
- Zhang RJ, Yang HL, L'Hostis V, Castel A, François R. Characterization of Steel/Concrete Interface for a Long-Term Corroded Beam Stored in Chloride Environment. *Adv Mater Res.* 2011;163:3415–20.